**DTU Library**

# Progress and Perspectives of Electrochemical CO2 Reduction on Copper in Aqueous Electrolyte

Nitopi, Stephanie A.; Bertheussen, Erlend; Scott, Søren Bertelsen; Liu, Xinyan; Engstfeld, Albert Kilian; Horch, Sebastian; Seger, Brian; Stephens, Ifan; Chan, Karen; Hahn, Christopher

# Progress and Perspectives of Electrochemical $CO_2$ Reduction on Copper in Aqueous Electrolyte

Stephanie Nitopi,[†,#] Erlend Bertheussen,[‡,#] Soren B. Scott,[‡] Xinyan Liu,[†] Albert K. Engstfeld,[‡,§] Sebastian Horch,[‡] Brian Seger,[‡] Ifan E. L. Stephens,[‡,⊥] Karen Chan,[†,‖] Christopher Hahn,[†,‖] Jens K. Nørskov,*,[†,‡,‖] Thomas F. Jaramillo,*,[†,‖] and Ib Chorkendorff*,[‡]

[†]SUNCAT Center for Interface Science and Catalysis, Department of Chemical Engineering, Stanford University, Stanford, California 94305, United States

[‡]Section for Surface Physics and Catalysis, Department of Physics, Technical University of Denmark, 2800 Kgs. Lyngby, Denmark
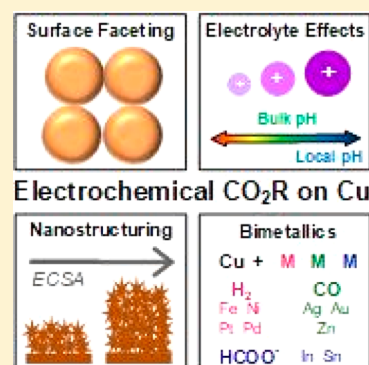
[§]Institute of Surface Chemistry and Catalysis, Ulm University, D-89069 Ulm, Germany

[‖]SUNCAT Center for Interface Science and Catalysis, SLAC National Accelerator Laboratory, Menlo Park, California 94025, United States

[⊥]Department of Materials, Imperial College London, Royal School of Mines, London SW7 2AZ, United Kingdom

**S** *Supporting Information*

**ABSTRACT:** To date, copper is the only heterogeneous catalyst that has shown a propensity to produce valuable hydrocarbons and alcohols, such as ethylene and ethanol, from electrochemical $CO_2$ reduction ($CO_2R$). There are variety of factors that impact $CO_2R$ activity and selectivity, including the catalyst surface structure, morphology, composition, the choice of electrolyte ions and pH, and the electrochemical cell design. Many of these factors are often intertwined, which can complicate catalyst discovery and design efforts. Here we take a broad and historical view of these different aspects and their complex interplay in $CO_2R$ catalysis on Cu, with the purpose of providing new insights, critical evaluations, and guidance to the field with regard to research directions and best practices. First, we describe the various experimental probes and complementary theoretical methods that have been used to discern the mechanisms by which products are formed, and next we present our current understanding of the complex reaction networks for $CO_2R$ on Cu. We then analyze two key methods that have been used in attempts to alter the activity and selectivity of Cu: nanostructuring and the formation of bimetallic electrodes. Finally, we offer some perspectives on the future outlook for electrochemical $CO_2R$.

## CONTENTS

# 1. INTRODUCTION

There is a pressing need to advance the development of $CO_2$ utilization technologies such as electrochemical $CO_2$ reduction ($CO_2R$); as a result, this has been a rapidly expanding field of research in recent years. In particular, there is a large body of work on copper (Cu) materials for this reaction, since Cu is, as of yet, unique in its ability to catalyze the electrochemical conversion of $CO_2$ to valuable fuels and chemicals. While many a great review and perspective articles have been published in this area, they have typically had a more narrow

focus in terms of either timespan or topics covered.[1−21] Here we aim to provide an organized and comprehensive review of $CO_2R$ on copper and the multitude of approaches that have been used to tune its catalytic activity and selectivity. The scope strives to include all studies of electrochemical $CO_2R$ in aqueous electrolytes on Cu-based catalysts, beginning with many of the early works in the 1980s−1990s through those published in 2018, and it takes into consideration both experimental and theoretical methods, planar and nano-structured Cu, and Cu modified with other elements. This work is also a perspective in which we critically analyze the literature in attempts to normalize/compare the various results and show general trends throughout the field. Additionally, we suggest several techniques and protocols that can allow for more reliable comparisons, enable a more fundamental understanding of the catalysis, and help drive this technology toward commercialization. This section first provides a broad context by summarizing anthropogenic carbon streams, comparing different strategies to recycle $CO_2$, and touching upon the economics of electrochemical $CO_2$ conversion. Then, planar polycrystalline copper is introduced as a unique electrocatalyst for this reaction, which will serve as the basis for all the discussions that follow.

## 1.1. Motivation for $CO_2$ Recycling

At the core of biological metabolism is the ability to convert carbon between different oxidation states in order to store and release energy, as well as to synthesize functional molecules. Likewise, the oxidation of carbon is at the center of human civilization's collective "industrial metabolism" consisting of our energy infrastructure and chemical industry. Whereas in biological metabolism, reduction of $CO_2$ in photosynthesis balances the oxidation of carbon in cellular respiration, carbon reduction is as of yet a missing piece of humanity's industrial metabolism. This imbalance has become a significant perturbation to Earth's natural carbon cycle, as indicated in the top two sections of Table 1. The resulting accumulation of the greenhouse gas $CO_2$ in the atmosphere is the primary driver of today's climate change.[22] While the Paris Climate Accord commits signatories to the goal of achieving "a balance between anthropogenic emissions by sources and removals by sinks of greenhouse gases in the second half of this century",[23] it leaves it to individual nations to volunteer the specifics of how to achieve this goal. The problem is urgent: net $CO_2$ emissions need to decrease rapidly and cross zero around the year 2050 if global warming is to be limited to the relatively safe level of 1.5 °C above preindustrial levels.[24] Strategies to reduce net $CO_2$ emissions fall under three categories: decarbonization, carbon sequestration, and carbon recycling, all three of which will most likely need to play a role. This Review will focus in-depth on the scientific progress and challenges of carbon recycling based on electrochemical $CO_2$ reduction on Cu catalysts. For context, we will first briefly comment on decarbonization and carbon sequestration, as well as the other major $CO_2$ recycling strategies.

**1.1.1. Closing the Carbon Cycle.** Significant progress is presently being made in decarbonization. Economic growth is increasingly decoupled from energy consumption and from $CO_2$ emissions (Figure 1),[25−27] electricity from renewable sources such as wind turbines and photovoltaics is increasing in volume and decreasing in price,[28] private investment in renewable energy is outpacing investment in fossil fuels,[29] and global annual $CO_2$ emissions are plateauing.[25] However,

**Table 1. Global Carbon Fluxes[c]**

| Carbon flux[a] | Amount/[GtC/yr] | Year[citation] |
|---|---|---|
| Carbon Cycle Overview | | |
| Air−land natural exchange | 120 | 2007[38] |
| Air−ocean natural exchange | 90 | 2007[38] |
| Anthropogenic carbon emissions | 11 | 2014[39] |
| Total anthropogenic GHG emissions by $CO_2$ equivalent | 13 | 2010[22] |
| Fate of Anthropogenic Emissions | | |
| Net ocean uptake | 4 | 2014[39] |
| Net land uptake | 3 | 2014[39] |
| Accumulated in atmosphere | 4 | 2014[39] |
| Anthropogenic Emissions by Sector (100% = 13 GtC/yr) | | |
| Electricity generation | 3.3 (25%) | 2010[22] |
| Agriculture and land-use change (deforestation) | 3.2 (24%) | 2010[22] |
| Industry (excluding electricity) | 2.8 (21%) | 2010[22] |
| Transportation | 1.9 (14%) | 2010[22] |
| Buildings | 0.9 (6%) | 2010[22] |
| Other | 1.4 (10%) | 2010[22] |
| Carbon in Industrial Reactions, $CO_2$ as Ultimate Byproduct[b] | | |
| Cement (calcination): $CaCO_3 \rightarrow CaO + CO_2$ | 0.59 | 2017[33] |
| Steel (via CO): $2Fe_2O_3 + 6C + 3O_2 \rightarrow 4Fe + 6CO_2$ | 0.38 | 2017[34] |
| Plastic (disposal): $(CH_2)_{2n} + 3nO_2 \rightarrow 2nH_2O + 2nCO_2$ | 0.26 | 2015[35] |
| Ammonia (via $H_2$): $3CH_4 + 6H_2O + 4N_2 \rightarrow 8NH_3 + 3CO_2$ | 0.045 | 2016[36] |
| Aluminum (carbon anode): $2Al_2O_3 + 3C \rightarrow 4Al + 3CO_2$ | 0.019 | 2016[37] |
| Total nonfuel carbon as industrial reactant | 1.28 | |

[a]Some of the carbon fluxes have been converted from carbon dioxide flux emissions to molecular mass (1 GtC/yr is equivalent to 3.66 $GtCO_2$/yr). The data from ref 22 are reported, not in terms of carbon or carbon dioxide flux, but by total greenhouse gas emissions converted to the equivalent mass of $CO_2$ emissions based on the green house gas's global warming potential. These data were converted to carbon flux as if they were $CO_2$ emissions. [b]The bottom section of the table shows the minimum nonenergy carbon usage of the most important carbon-using industrial processes, calculated based on global production and the stoichiometry of the simplified reaction shown. Figures for steel and plastic exclude recycling. For plastic, we write the combustion reaction to represent the stoichiometric amount of $CO_2$, even though most plastic today is not incinerated but ends up in landfills or the environment after use.[35] [c]For more details, see section 2 of the Supporting Information (SI).
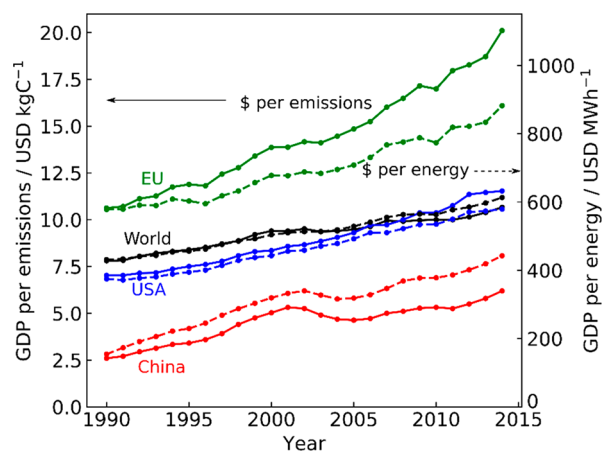


**Figure 1.** World GDP (purchasing power parity, 2011 dollars) is growing relative to energy consumption and $CO_2$ emissions. Data obtained from The World Bank.[27]

significant challenges remain for full decarbonization.[30] First, renewable energy sources such as wind and solar are variable and produce electrical power, which has to be utilized immediately or stored. While a number of energy storage technologies exist, including pumped hydro, compressed air, batteries, redox flow batteries, and flywheels, they all have limitations in terms of scalability, versatility, and/or maximum storage time.[31,32] As of yet there is no technology in use that could feasibly store enough renewable electricity to power society through a cloudy and windless day. Second, not all

energy is easily electrifiable. In transport, especially, which accounts for 14% of global $CO_2$ emissions[22] (middle portion of Table 1), there are clear advantages to energy in the form of liquid fuel. Finally, not all $CO_2$ emissions are due to energy use. The bottom section of Table 1 shows a lower-bound estimation to the direct nonenergy carbon use in industry, calculated as the stoichiometric amount of carbon used or released globally in the production of several key products: cement,[33] steel,[34] plastic,[35] ammonia,[36] and aluminum.[37] Together, these products involve as much carbon as 12% of global carbon emissions. Increased recycling can help to lower this number, and decarbonization may be possible, if difficult, in some of these industries.[30] However, it is clear that industry would continue to have an appetite for carbon even if energy were to be fully decarbonized.

In contrast to decarbonization, carbon sequestration is a strategy that accepts some continued net production of $CO_2$ but aims to prevent its release to the atmosphere.[24,40] There are at present 18 large-scale carbon capture and storage (CCS) projects in operation worldwide, separating about 40 megatonnes of $CO_2$ per year (9.6 MtC/yr), from industrial point sources and storing it underground.[41] This is just under 0.1% of global carbon emissions, but this could in principle be scaled up indefinitely as there are suitable geological formations for the storage of hundreds of years of $CO_2$ at the present emissions rate.[42] In particular, if the carbon stored underground originates from the atmosphere rather than from fossil fuels, as in the case when $CO_2$ resulting from the combustion of biomass is stored, the result is net-negative emissions. This strategy, bioenergy with carbon capture and

storage (BECCS), can provide electricity at the same time as net-negative emissions, and will be necessary for stabilizing the climate in all but the most optimistic projections, but is as of yet largely unused.[24] Unfortunately for net $CO_2$ emissions, most existing and planned projects for CCS fall under the category of enhanced oil recovery (EOR), whereby $CO_2$ is pumped underground to aid in the extraction of additional fossil fuels.[41] This highlights one of the main challenges with carbon sequestration: the lack of a viable business case. $CO_2$ separation from a power plant, for example, costs on the order of $60 to $100 USD per ton $CO_2$ (approximately $200 to $350 USD/tC),[40] and together with transportation and storage costs, this results in a total increase of more than 25% in the cost of the electricity generated by a power plant utilizing CCS.[43] Under existing policies and economics, carbon sequestration is thus rarely economically viable without EOR, which in effect adds value to the $CO_2$ by using it to facilitate the extraction of additional fossil fuels. The immense potential of CCS, and in particular BECCS, for reducing net carbon emissions will only be realized once regulations make the cost of emitting $CO_2$ higher than the costs of separation and storage.[40]

The limitations to full implementation of decarbonization and carbon sequestration outlined above all point to a common missing piece of human civilization's collective "industrial metabolism", namely, carbon recycling based on the conversion of $CO_2$ to more reduced products. $CO_2$ recycling can enable the storage of renewable electricity from intermittent sources in a dense and versatile form, provide a renewable carbon feedstock to chemical industries, and add value to $CO_2$ captured at industrial point sources or directly from the air.

**1.1.2. Strategies for CO$_2$ Recycling.** $CO_2$ is the most oxidized form of carbon, together with carbonate minerals, with a formal oxidation state of +4. As a result, conversion of $CO_2$ into a more energetic product involves transfer of electrons to carbon, reducing its oxidation state. The family of reactions by which $CO_2$ is converted to a more reduced product is most often called *CO$_2$ reduction*. These reactions are also often referred to as *CO$_2$ hydrogenation* for thermally driven processes involving reaction with hydrogen (H$_2$) or *CO$_2$ fixation* in natural photosynthesis and bioinspired catalysis.[44]

In order for the production and ultimate combustion of $CO_2$ reduction/hydrogenation products to represent a closed cycle, the ultimate source of electrons and protons for the reduction of $CO_2$ must be water (H$_2$O), as combustion of a hydrogenated carbon product releases H$_2$O. $CO_2$ reduction/hydrogenation/fixation thus follows the overall formula:

$$x CO_2 + y H_2O \rightarrow \text{product} + z O_2 \quad \text{CO$_2$ recycling reaction}$$
$$(1)$$
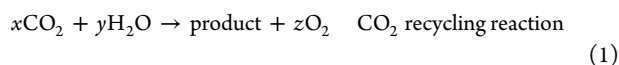
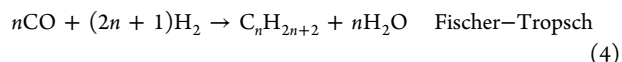Natural photosynthesis by plants and other phototrophs fixates a much larger amount of carbon globally than human activity releases (Table 1),[38,39] so using biomass as a carbon source is an obvious carbon recycling strategy. However, the utility of biobased carbon is limited by the amount of land required. Well-intended markets for transportation biofuels such as ethanol and biodiesel need energy-intensive care (e.g., fertilizers, pesticides, etc.) and have led to deforestation in some cases, thus greatly mitigating or even eliminating any potential $CO_2$ emissions savings.[45,46] As mentioned earlier, biomass energy with carbon capture and storage (BECCS) has the potential of achieving net negative emissions; however, the

land requirement is immense. Near-term availability of biomass for BECCS in the US, for example, corresponds at most to about 370 $MtCO_2$/yr (0.1 GtC/yr), less than 10% of US emissions.[47] The picture is similar on a global scale.[48] High-yield biomass such as short-rotation forestry can yield up to about 800 tC/km$^2$/yr,[49] meaning that it would require about 14 million square kilometers to offset the present global carbon emissions of 11 GtC/yr. Repurposing this amount of land, about the same area as is used globally for food crop production,[22] is clearly not feasible. Thus, while important, harnessing the power of natural photosynthesis can only play a limited role in reaching net-zero emissions, leaving room for other $CO_2$ recycling strategies.

There are pathways in the traditional chemical industry, all thermally activated, that could be used for $CO_2$ hydrogenation, using H$_2$ as the reductant.[50,51] $CO_2$ can be reduced to carbon monoxide (CO) by the reverse water gas shift reaction:

$$CO_2 + H_2 \rightarrow CO + H_2O \quad \text{Reverse water} - \text{gas shift}$$
$$(2)$$
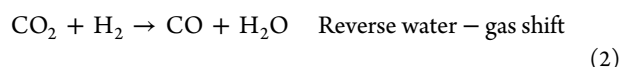
If an excess of H$_2$ is used and the water is condensed out, the product gas is a mixture of H$_2$ and CO, which is called synthesis gas or syngas. Syngas can be used as the precursor to methane on a Ni catalyst,[52] to multicarbon hydrocarbons on an Fe or Co catalyst,[53] or to methanol on a Cu/ZnO catalyst.[54,55] These reactions are called methanation, the Fischer–Tropsch reaction, and methanol synthesis, respectively.

$$CO + 3H_2 \rightarrow CH_4 + H_2O \quad \text{Methanation} \qquad (3)$$

$$n CO + (2n + 1)H_2 \rightarrow C_nH_{2n+2} + n H_2O \quad \text{Fischer–Tropsch}$$
$$(4)$$

In methanol synthesis, some $CO_2$ is required in the syngas stream because $CO_2$ is actually the immediate reactant.[56] The role of CO is to react with the water released by $CO_2$ hydrogenation and generate more $CO_2$ via the water–gas shift (reverse of Reaction 2). The net reaction is

$$CO + 2H_2 \rightarrow CH_3OH \quad \text{Water–gas shift plus methanol synthesis}$$
$$(5)$$
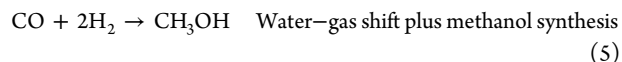
All of these processes run at high pressures and temperatures; for example, ~100 bar and 250 °C are typical conditions for methanol synthesis, the mildest of the three reactions.[51]

In order for $CO_2$ hydrogenation by the above reactions to be a renewable process, the hydrogen must come from water splitting using renewable energy:

$$2H_2O \rightarrow O_2 + 2H_2 \quad \text{Water splitting} \qquad (6)$$
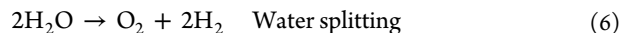
such that the combined reaction is in the form of Reaction 1 above. The water splitting would be driven electrochemically using electrical energy from renewable sources such as wind and solar,[30,57,58] according to the half-reactions

$$2H^+ + 2e^- \rightarrow H_2 \quad \text{H$_2$ Evolution Reaction (HER) at the cathode}$$
$$(7)$$

$$2H_2O \rightarrow O_2 + 4H^+ + 4e^- \quad \text{O$_2$ Evolution Reaction (OER) at the anode}$$
$$(8)$$
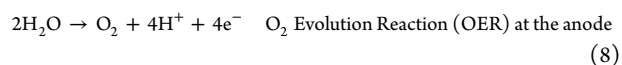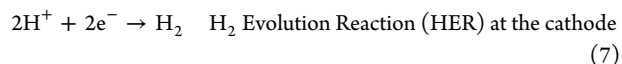
Compared to hydrogen, carbon-based fuels have the advantages of higher volumetric energy density and greater ease of integration in the present infrastructure (drop-in fuels). Furthermore, carbon-based chemicals will still be needed regardless of energy decarbonization.[59]

**Table 2. Electrochemical Reactions with Equilibrium Potentials**

| Reaction | $E^0$/[V vs RHE] | (Product) Name, abbreviation |
|---|---|---|
| $2H_2O \rightarrow O_2 + 4H^+ + 4e^-$ | 1.23 | Oxygen Evolution Reaction, OER |
| $2H^+ + 2e^- \rightarrow H_2$ | 0 | Hydrogen Evolution Reaction, HER |
| $xCO_2 + nH^+ + ne^- \rightarrow product + yH_2O$ | | *$CO_2$ Reduction, $CO_2R$* |
| $CO_2 + 2H^+ + 2e^- \rightarrow HCOOH_{(aq)}$ | −0.12 | Formic acid |
| $CO_2 + 2H^+ + 2e^- \rightarrow CO_{(g)} + H_2O$ | −0.10 | Carbon monoxide |
| $CO_2 + 6H^+ + 6e^- \rightarrow CH_3OH_{(aq)} + H_2O$ | 0.03 | Methanol, MeOH |
| $CO_2 + 4H^+ + 4e^- \rightarrow C_{(s)} + 2H_2O$ | 0.21 | Graphite |
| $CO_2 + 8H^+ + 8e^- \rightarrow CH_{4(g)} + 2H_2O$ | 0.17 | Methane |
| $2CO_2 + 2H^+ + 2e^- \rightarrow (COOH)_{2(s)}$ | −0.47 | Oxalic acid |
| $2CO_2 + 8H^+ + 8e^- \rightarrow CH_3COOH_{(aq)} + 2H_2O$ | 0.11 | Acetic acid |
| $2CO_2 + 10H^+ + 10e^- \rightarrow CH_3CHO_{(aq)} + 3H_2O$ | 0.06 | Acetaldehyde |
| $2CO_2 + 12H^+ + 12e^- \rightarrow C_2H_5OH_{(aq)} + 3H_2O$ | 0.09 | Ethanol, EtOH |
| $2CO_2 + 12H^+ + 12e^- \rightarrow C_2H_{4(g)} + 4H_2O$ | 0.08 | Ethylene |
| $2CO_2 + 14H^+ + 14e^- \rightarrow C_2H_{6(g)} + 4H_2O$ | 0.14 | Ethane |
| $3CO_2 + 16H^+ + 16e^- \rightarrow C_2H_5CHO_{(aq)} + 5H_2O$ | 0.09 | Propionaldehyde |
| $3CO_2 + 18H^+ + 18e^- \rightarrow C_3H_7OH_{(aq)} + 5H_2O$ | 0.10 | Propanol, PrOH |
| $xCO + nH^+ + ne^- \rightarrow product + yH_2O$ | | *CO Reduction, COR* |
| $CO + 6H^+ + 6e^- \rightarrow CH_{4(g)} + H_2O$ | 0.26 | Methane |
| $2CO + 8H^+ + 8e^- \rightarrow CH_3CH_2OH_{(aq)} + H_2O$ | 0.19 | Ethanol, EtOH |
| $2CO + 8H^+ + 8e^- \rightarrow C_2H_{4(g)} + 2H_2O$ | 0.17 | Ethylene |

An alternative to CO production by the reverse water−gas shift (Reaction 2) is electrochemical reduction of $CO_2$ to CO:

$$CO_2 + 2H^+ + 2e^- \rightarrow CO + H_2O \quad \text{Electrochemical CO production} \quad (9)$$
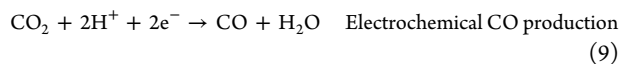
balanced by the OER (Reaction 8). The electrochemically produced CO can then be reacted further as described above to form hydrocarbons or alcohols from $CO_2$. This combined approach using electroreduction of $CO_2$ in a high-temperature solid-oxide electrolysis cell and subsequent thermal hydrogenation proved especially promising in an analysis of $CO_2$ recycling strategies.[60]

However, direct electrochemical reduction of $CO_2$ can have a number of advantages compared to hydrogenation of $CO_2$ or CO by electrochemically produced $H_2$:[2,61] it (1) combines the electrochemical water splitting and subsequent thermal hydrogenation into a single electrochemical process, (2) enables products that cannot easily be prepared by thermally driven processes, and (3) can often run at or near room temperature and ambient pressure. These features imply that processes based on electrochemical $CO_2$ reduction are more suitable to decentralization than the thermal counterparts, and that electrochemical $CO_2$ reduction processes can be designed to enable relatively quick adjustment of production in order to match the overproduction of electricity from intermittent renewable sources.[62]

## 1.2. Electrochemical $CO_2$ Reduction

In electrochemical $CO_2$ reduction, the cathodic reaction is of the general form

$$xCO_2 + nH^+ + ne^- \rightarrow product + yH_2O \quad \text{$CO_2$ reduction ($CO_2R$)} \quad (9a)$$
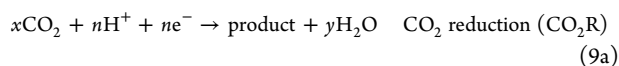
Like in water splitting, the anodic reaction in electrochemical $CO_2R$ must be the oxygen evolution reaction (OER, Reaction 8) in order to sum to the overall reaction given by

Reaction 1 above. In other words, water is the only renewable and scalable source of electrons and protons.[63] In this section, we first discuss the carbon dioxide reduction reaction in general, with a focus on the thermodynamics and economics of reducing $CO_2$ to various products. We then summarize the actual $CO_2R$ activity and selectivity of metal electrodes, highlighting the unique ability of copper to reduce $CO_2$ to hydrocarbons and alcohols.

**1.2.1. Desired Products: Thermodynamics and Economics.** Table 2 lists the equilibrium potentials for $CO_2R$ to commonly reported electrochemical products. All of the $CO_2R$ standard potentials here are calculated via the Gibbs free energy of reaction using gas-phase thermochemistry data and, for aqueous products, Henry's Law data, from NIST.[64] $CO_2$ is always considered a gas, water a liquid, and the state of the product is gas or aqueous as indicated. Regardless of which $CO_2R$ product is formed at the cathode, the fact that the $CO_2R$ reaction together with OER (Reaction 8) must add to an overall reaction of the form of Reaction 1 means that the stoichiometric coefficients for electrons and protons in a sustained $CO_2$ reduction reaction must be equal. Acidic products are therefore considered in the fully protonated form. Similar tables and lists provided in previous $CO_2R$ reviews,[1,2,15,16,44] studies of $CO_2R$ electrocatalysis,[65] and process/economic analyses for electrochemical $CO_2$ conversion[66−69] all show some variation due to the use of different potential scales, deprotonated products, and/or different standard states (for instance liquid instead of aqueous).

As described in detail in subsequent sections of this Review, CO is an important intermediate in $CO_2R$ to hydrocarbons, aldehydes, and alcohols on Cu, and a promising approach to $CO_2R$ is a stepwise one via CO, in which CO reduction (COR) is an important reaction in its own right.[70] The equilibrium potentials for CO reduction to a few products are therefore also included in this table, and an equation relating

CO reduction equilibrium potential to $CO_2$ reduction equilibrium potential is given in section 1 of the Supporting Information (SI).

We recommend reporting and using potentials on the thermodynamically relevant and pH-independent RHE scale for all calculations of overpotential and energetic efficiency. For more discussion of thermodynamics and equilibrium potentials, please see section 1 of the SI.

While the equilibrium potentials of $CO_2$ reduction to hydrocarbons, aldehydes, and alcohols are slightly positive of RHE, their direct electrochemical production still requires significant energy input, as the minimum possible potential to drive the overall reaction (i.e., the difference between the $CO_2$R equilibrium potential and the equilibrium potential of OER) is larger than 1 V. Furthermore, both the OER and $CO_2$R currently require large overpotentials, meaning that a $CO_2$R device will run at a larger cell potential than this thermodynamic potential. Nonetheless, the thermodynamic cell potential indicates the minimum energy requirement for a given product, and thus, given a cost of energy, provides a means to estimate the economic viability of a product. More thorough techno-economic analyses have also been performed, which include capital and operational costs as well as assumptions about the overpotential and Faradaic efficiency of the desired $CO_2$ reduction reaction.[66,68,69,71]

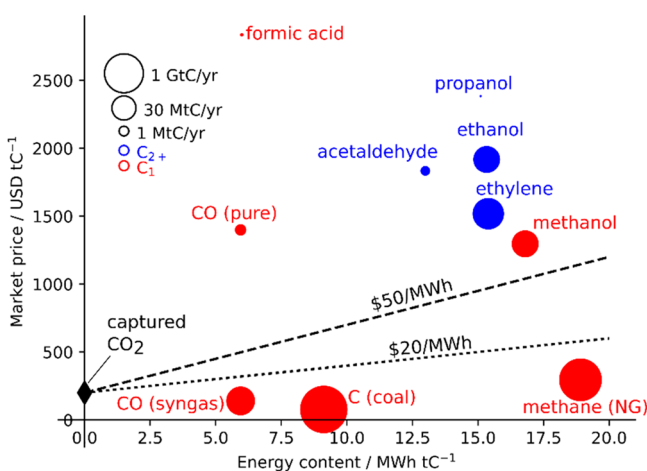Figure 2 shows a simple mapping of the economics and energetics of possible $CO_2$ reduction products. The approx-



**Figure 2.** Market price of select $CO_2$ recycling products as a function of energy content. Lines represent minimum energy and $CO_2$ costs. Capital costs are not considered.

imate market price of selected possible $CO_2$ reduction products are plotted against the minimum energy needed for their production by $CO_2$R balanced with OER. The marker size indicates the (logarithmic) size of the global market, which spans more than 4 orders of magnitude. All economic quantities are normalized to the mass of carbon. The dashed and dotted lines indicate the minimum cost of production given a captured $CO_2$ price of \$200/tC and an electricity price of \$50/MWh or \$20/MWh, respectively. \$200/tC is a representative price for carbon captured from a power plant.[40] \$50/MWh is representative of recent solar installations.[29] Current record lows for solar installation are around \$20/MWh, which will likely become more common in the future. Products above the line for a given $CO_2$ capture cost and electricity cost may be economically feasible depending on

capital and other costs, which are not considered here, but are in other analyses. Products below the line are not economically feasible. Direct air capture is estimated to cost \$2000/tC with current technologies,[40] which would push the lines up above nearly all products, though this will likely come down in the future. Taxes on carbon emissions push the effective price of captured $CO_2$ down, since capturing $CO_2$ avoids the tax. The raw data, sources, and calculations are given in section 2 of the SI. For a more full picture, we refer the reader to techno-economic analyses of $CO_2$ reduction in the literature.[66,68,69,71]

Despite its simplicity, Figure 2 captures a widely shared conclusion:[28,40,68,69,72,73] $CO_2$ reduction to specialty chemicals such as formic acid (0.2 MtC/yr[74]) and propanol (0.1 MtC/yr[69]) give a better chance of near-term economic feasibility, whereas making an impact on the GtC/year scale relevant for global climate change will likely require renewable production of fuels competitive with the likes of coal (4 GtC/yr[22]) and natural gas (1.4 GtC/yr[75]). This is not feasible in the near term, as coal and natural gas are cheaper than the minimum energy required to synthesize them from $CO_2$ even at \$20/MWh.

Ethylene (120 MtC/yr[76]) and ethanol (40 MtC/yr[69]) represent promising compromises between profitable niche market and impactful mass market for $CO_2$ reduction. Ethylene is produced on a large scale as a precursor for plastics and ethylene glycol in a highly energy-demanding and unselective process involving repeated cycles of steam cracking at 750−950 °C followed by quenching, distillation, and recompression.[77,78] At an electricity price of \$50 USD/MWh, it is worth about twice as much as the minimum energy input, with a global market about 100 times larger than the specialty chemicals. Ethanol is a fuel with high volumetric energy density that can be substituted for fossil fuels in the transport industry with minimal modifications, and thus represents a market with high growth potential.[79] Ethanol is produced primarily as a biofuel today, and is sold for a price much higher than the minimum energy required for its production by $CO_2$R at \$50/MWh. Ethylene and ethanol are both major products in $CO_2$ and CO electroreduction on copper, as described below.

**1.2.2. Copper as a Unique Electrocatalyst.** Studies of electrochemical $CO_2$ reduction date back to at least the 1950s.[80] The first study to quantify both gaseous and liquid products, and thus account for 100% of Faradaic efficiency, was reported by Yoshio Hori and co-workers in 1985.[81] In this study, constant-current electrolysis of $CO_2$-saturated 0.5 M $KHCO_3$ at 5 mA cm$^{-2}$ (geometric) was performed for up to an hour as a batch experiment on a number of polycrystalline metal electrodes. This and subsequent studies utilizing basically the same methods[82−85] led to a classification of metal electrodes into four groups:[1] Pb, Hg, Tl, In, Sn, Cd, and Bi produce primarily formate ($HCOO^-$); Au, Ag, Zn, Pd, and Ga produce primarily carbon monoxide (CO); Ni, Fe, Pt, and Ti reduce very little $CO_2$ and instead almost exclusively reduce water to $H_2$; and Cu stands out in uniquely producing a number of hydrocarbons, aldehydes, and alcohols. Cu is thus the only pure metal that reduces $CO_2$ to products requiring more than two electrons transfers (collectively referred to as "further reduced products" or ">2e$^-$ products") with substantial Faradaic efficiencies. These results are summarized in Table 3, adapted from Hori's 2008 review of $CO_2$ reduction on metal electrodes.[1]

**Table 3. Faradaic Efficiencies of CO$_2$ Reduction Products on Metal Electrodes in CO$_2$-Saturated 0.1 M KHCO$_3$ (pH = 6.8)$^a$**

| Metal | E [V vs RHE] | J$_{total}$ [mA/cm$^2$ geo] | CH$_4$ [%] | C$_2$H$_4$ [%] | EtOH [%] | PrOH [%] | CO [%] | HCOO$^-$ [%] | H$_2$ [%] | Total [%] |
|---|---|---|---|---|---|---|---|---|---|---|
| Pb | −1.24 | −5.0 | 0 | 0 | 0 | 0 | 0 | 97.4 | 5.0 | 102.4 |
| Hg | −1.12 | −0.5 | 0 | 0 | 0 | 0 | 0 | 99.5 | 0 | 99.5 |
| Tl | −1.21 | −5.0 | 0 | 0 | 0 | 0 | 0 | 95.1 | 6.2 | 101.3 |
| In | −1.16 | −5.0 | 0 | 0 | 0 | 0 | 2.1 | 94.9 | 3.3 | 100.3 |
| Sn | −1.09 | −5.0 | 0 | 0 | 0 | 0 | 7.1 | 88.4 | 4.6 | 100.1 |
| Cd | −1.24 | −5.0 | 1.3 | 0 | 0 | 0 | 13.9 | 78.4 | 9.4 | 103.0 |
| Au | −0.65 | −5.0 | 0 | 0 | 0 | 0 | 87.1 | 0.7 | 10.2 | 98.0 |
| Ag | −0.98 | −5.0 | 0 | 0 | 0 | 0 | 81.5 | 0.6 | 12.4 | 94.6 |
| Zn | −1.15 | −5.0 | 0 | 0 | 0 | 0 | 79.4 | 6.1 | 9.9 | 95.4 |
| Pd | −0.81 | −5.0 | 2.9 | 0 | 0 | 0 | 28.3 | 2.8 | 26.2 | 60.2 |
| Ga | −0.85 | −5.0 | 0 | 0 | 0 | 0 | 23.2 | 0 | 79.0 | 102.0 |
| Cu | −1.05 | −5.0 | 33.3 | 25.5 | 5.7 | 3.0 | 1.3 | 9.4 | 20.5 | 103.5 |
| Ni | −1.09 | −5.0 | 1.8 | 0.1 | 0 | 0 | 0 | 1.4 | 88.9 | 92.4 |
| Fe | −0.52 | −5.0 | 0 | 0 | 0 | 0 | 0 | 0 | 94.8 | 94.8 |
| Pt | −0.68 | −5.0 | 0 | 0 | 0 | 0 | 0 | 0.1 | 95.7 | 95.8 |
| Ti | −1.21 | −5.0 | 0 | 0 | 0 | 0 | tr. | 0 | 99.7 | 99.7 |

$^a$The potential has been converted from the reported SHE potential to the RHE scale [T=18.5 °C, pH=6.8] by adding $(RT/F)\ln(10)$pH = 0.39 V. Adapted with permission from Hori.[1] Copyright 2008, Springer Science Business Media, LLC.

Note that in all cases, a significant overpotential is required to reach the specified current density, usually −5 mA/cm$^2$. The largest overpotentials are required by the formate-producing metals, which also typically show very high CO$_2$R Faradaic efficiencies (for example, 97% of −5 mA/cm$^2$ for Pb at −1.23 V vs RHE, an overpotential of 1.1 V) due to very low HER activity. The smallest overpotential for CO$_2$R is achieved by Au, which produces CO with high Faradaic efficiency, 87% of −5 mA/cm$^2$ at −0.7 V vs RHE, an overpotential of 0.6 V. Copper uniquely produces a variety of hydrocarbon and oxygenated products at an intermediate potential −1.04 V vs RHE (e.g., an overpotential of 0.9 V for CO$_2$R to CO and an overpotential of 1.2 V for CO$_2$R to methane). Note also that these results, by measuring CO$_2$ reduction selectivity for each electrode at only one current density, effectively provide only a snapshot, as CO$_2$ reduction selectivity can change with conditions and electrode potential.

The splitting of the metals into these four groups based on their selectivity has been explained as the result of their binding energy to key CO$_2$R and HER intermediates, including *H, *OCHO (bound to the surface through O), *COOH (bound to the surface through C), and *CO.[86] The unique ability of Cu to reduce CO$_2$ to >2e$^-$ products may be due to the fact that it is the only metal that has a negative adsorption energy for *CO but a positive adsorption energy for *H, as shown in Figure 3.

After the previously mentioned constant-current electrolysis experiments to compare different metal electrodes, Hori and co-workers also performed constant-potential electrolysis experiments on Cu in CO$_2$-saturated 0.1 M KHCO$_3$ (pH = 6.8), the most common electrolyte for CO$_2$ reduction studies, to characterize the CO$_2$R product distribution as a function of potential.[85] The results, shown in Figure 4 (hollow markers) span a potential range of −0.8 to −1.45 V vs NHE, or approximately −0.4 to −1.05 V vs RHE. In order of least cathodic to most cathodic onset potential (which loosely refers to the potential closest to the equilibrium potential at which a product is produced in detectable quantities), the major CO$_2$ reduction products are CO, HCOO$^-$, C$_2$H$_4$, and CH$_4$. CO and HCOO$^-$ pass through potentials of maximum Faradaic efficiency, and the Faradaic efficiency toward C$_2$H$_4$ reaches a
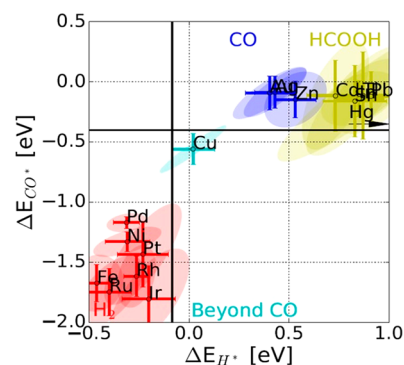


**Figure 3.** CO$_2$ reduction metal classification. Reproduced with permission from Bagger et al.[86] Copyright 2017, John Wiley and Sons.

plateau by about −1.0 V vs RHE. Similar conclusions were reached years later by Kuhl et al.;[65] electrolysis experiments were performed at potentials between −0.6 and −1.2 V vs RHE and, using more sensitive product detection techniques for liquid products, a total of 16 products were observed. These results are coplotted with Hori's in Figure 4 (filled markers).

The ability to reduce CO$_2$ to valuable hydrocarbons, aldehydes, and alcohols is of great interest; as a result, there has been much work done in the field to better understand the reactivity of Cu and how it can be tuned to achieve greater selectivity, stability, and efficiency. Thus, the remainder of this work will focus exclusively on Cu and Cu-based electrocatalysts. In the sections that follow, we will discuss experimental probes used to identify CO$_2$R reaction mechanisms on Cu and the complementary theoretical methods and descriptions of CO$_2$R. We will then discuss two materials classes that have been studied in attempts to alter the reactivity of planar polycrystalline Cu (nanostructured Cu and bimetallics with Cu). Finally, we will provide some overall perspectives and an outlook for the future of CO$_2$R.
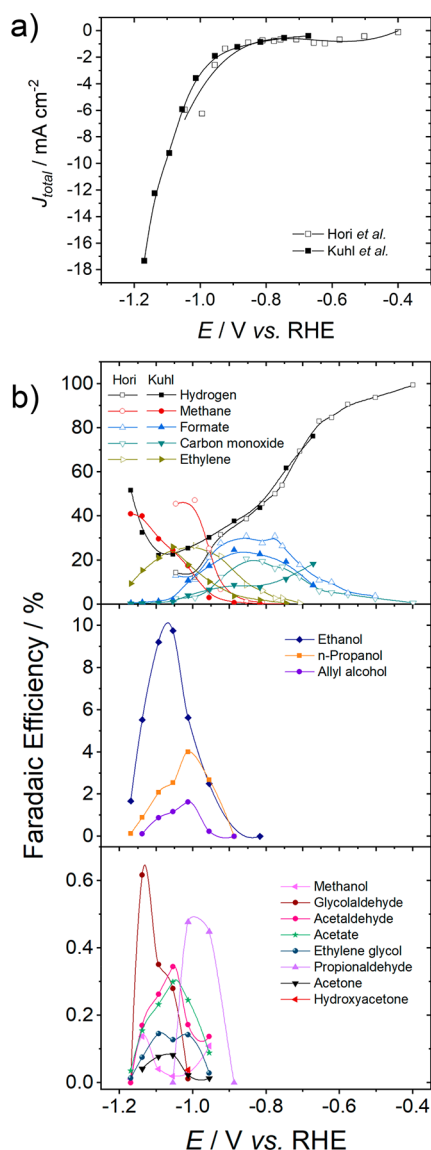
**Figure 4.** $CO_2R$ activity and selectivity on polycrystalline copper in $CO_2$-saturated 0.1 M $KHCO_3$ (pH = 6.8): (a) total current density and (b) product Faradaic efficiencies; data obtained from Hori et al.[85] (hollow) and Kuhl et al.[65] (filled).

## 2. CONSIDERATIONS FOR CONDUCTING AND COMPARING ELECTROCHEMICAL CO₂ REDUCTION EXPERIMENTS

Before diving into the results in subsequent sections, we would like to set the stage by discussing some of the difficulties encountered when trying to reliably compare the electrocatalytic behavior of Cu between different electrochemical cells and conditions. For more detailed discussions of these challenges in an objective evaluation of $CO_2R$ performance, we direct the reader to recent perspective articles, which also provide recommendations to help standardize methods for measuring and reporting $CO_2R$ data.[87,88]

### 2.1. Reporting Data

First, we would briefly like to discuss the metrics by which electrocatalytic activity and selectivity are reported. The selectivity is most often described in terms of *Faradaic efficiency*, which is the portion of the electrical current going to a specific product in steady-state electrolysis. The activity for

$CO_2R$ to a specific product is described in terms of the *overpotential*, which is the absolute difference between the actual potential needed to make a product and the thermodynamic potential, or in terms of the *partial current density* at a given potential, which is the total current times the Faradaic efficiency. A more active catalyst is one that achieves a given partial current density at a lower overpotential, and/or provides a larger partial current density at a given overpotential. A major goal of applied electrocatalysis research is the development of electrode materials and conditions that are selective and active (as well as cheap and stable) for production of desired products. However, understanding the fundamentals of electrocatalysis on simple materials and model systems facilitates the design of better electrodes,[57] and the trade-off between practical application and fundamental insight is important to keep in mind when comparing different works in the field.

An essential consideration is how the measured activity is normalized. The geometric area of the electrode is most commonly used to report the current density. While useful for assessing the overall electrode performance, this metric is inherently dependent on the catalyst loading or surface area. Thus, it is also important to consider the current normalized by the electrochemically active surface area (ECSA) of the electrode. This facilitates activity comparisons between catalysts with different roughness factors (RF, defined here as the ratio of ECSA/geometric electrode area), allowing one to determine if higher catalytic activity results from a higher average turnover frequency or simply from an increased number of active sites. There exist a variety of methods in electrocatalysis for determining the ECSA based on capacitance, underpotential deposition (UPD), CO stripping, and redox features that can be employed depending on the surface chemistry and morphology, and the best method varies based on the material studied. So far, only capacitance has found wide use for estimating the ECSA of nanostructured polycrystalline copper electrodes.[89−95] We emphasize that on any nonplanar surface, the measurement of the ECSA is at best an approximation; consequently, we recommend that researchers take the limitations of each method of determining the ECSA into account when analyzing their data. Furthermore, we would also like to highlight the need for all future work, particularly on nanostructured electrodes, to report the ECSA whenever possible. It is only possible to evaluate whether a novel catalyst represents an improvement in intrinsic activity compared to state-of-the-art materials if the ECSA-normalized activity can be compared with the literature. As will be shown in subsection 6.2.4 and section 7.4, much of the suggested activity improvements in the field can attributed to increased surface area.

### 2.2. Intrinsic Kinetics vs Mass Transport Effects

As a consequence of the HER and $CO_2R$, which deplete protons or (equivalently) produce hydroxide ions, a pH gradient can develop at the electrode surface. This high local pH has several competing effects on these reactions due to a complicated interplay between mass transport, buffer equilibria, and pH, which will be discussed in more detail in subsection 3.3.1. Notably, in the $CO_2$/bicarbonate system, $CO_2$ is both a reactant and a buffer, which means that changes in pH near the cathode surface can cause the concentration of dissolved $CO_2$ to deviate from the concentration in the bulk electrolyte. For planar polycrystalline Cu, it was found that the

reported activity at potentials more cathodic than −1 V vs RHE is strongly influenced by concentration polarization and thus does not represent its true intrinsic activity under bulk pH 6.8 conditions.[96] However, this cannot be used as a universal rule of thumb, as the hydrodynamics of the electrochemical cell and the morphology of the catalyst itself can both impact the extent of concentration polarization at a given potential.

Ultimately, since both the HER and $CO_2R$ produce 1 equivalent of $OH^-$ for each $e^-$ transfer (with the exception of the organic anions formate and acetate, for which one less $OH^-$ is released than electron transferred), changes in interfacial concentrations are primarily a function of the electrolyte and the total geometric current density. This means that nanostructured catalysts with high surface areas will be more susceptible to concentration polarization at lower overpotentials due to the increased activity on a geometric area basis and increased transport requirements within a porous catalyst compared to a planar electrode.[97,98] Therefore, caution must be taken when comparing $CO_2R$ performance between catalysts with very different roughness factors since they will reach mass transport limitations at different rates.

In general, it is critical to ensure sufficient supply of $CO_2$ to the electrode surface. In aqueous systems, this is accomplished by diffusion of $CO_2$ through the electrolyte, so it is important that the electrochemical cell is well-mixed in order to maximize the potential window where the reaction is governed by intrinsic reaction kinetics. As one would expect for a diffusion-limited process, it has been shown that the maximum *rate* of $CO_2R$ increases with increased mixing due to a decrease in the boundary layer thickness.[99−102] Thus, the hydrodynamics of an electrochemical cell will also have a direct effect on the local pH change at the electrode surface. We therefore recommend that researchers quantify the boundary layer thickness, for example, by measuring the diffusion-limited current density for a facile, outer sphere redox reaction such as ferricyanide reduction.[87] This will allow for better comparisons between different electrochemical cells and mass transport conditions. Still, as described further in subsection 3.3.1, correcting for mass transport effects in aqueous systems is extremely difficult. As a result, we strongly recommend that conclusions about intrinsic activity and selectivity only be drawn from data that is not impacted by significant concentration polarization so as not to convolute effects of the catalyst properties and the effects of mass transport.

## 2.3. Deactivation of Cu Electrodes

It has been demonstrated that the activity and selectivity of polycrystalline and single crystalline Cu electrodes toward $CO_2R$ and COR decays over time, although the details vary.[103−117] The changes in activity can be tentatively attributed to (i) poisoning by impurities from the experimental setup, (ii) poisoning of the surface with reaction intermediates, and/or (iii) restructuring of the surface under reaction conditions. The latter will be discussed in subsection 3.1.3, as it has been observed with *in situ/operando* methods that the Cu surface structure is dynamic and can reconstruct under reaction conditions. More often, the deactivation is attributed either to deposition of metal contaminants from the electrolyte,[111,113] $CO_2$ stream,[112] glassware,[114] or counter electrode,[118] including Fe,[111,112] Zn,[111,113] Pb,[113] Si,[114] and Pt;[118] or to poisoning or coking of the surface by (decomposition of) reaction intermediates.[103−110,117] Authors have recommended using the highest-purity reagents,[111,112]

pre-electrolyzing the electrolyte solution,[111] and/or removing impurities from the electrolyte with a bed of chelating agent before use[113] to minimize the impact of contaminants on the reaction. Additionally, in light of the observation that Pt from the counter electrode can deposit on the working electrode despite separation by an anion exchange membrane, the use of alternate counter electrodes has also been suggested.[87,118] Deactivation does not seem to play as much of a role in high surface area electrodes (this has mechanistic implications that will be discussed in section 5).[87,109,114]

Finally, it is worth mentioning another technique that has been used to prevent deactivation and/or restore activity for $CO_2R$ on Cu, namely, anodic pulses or sweeps.[104,108,110,117,119] Pulsed electrolysis may allow for anodic stripping of poisoning species from the electrode surface.[110] Anodic pulses or sweeps will also likely cause roughening of the electrode and/or oxidation of the Cu surface.[108,117,119,120] Gupta et al. modeled the effect of pulsed electroreduction and showed that pulsing causes corresponding swings in local pH and $CO_2$ concentrations.[99] While we cannot say with certainty which of these factors are responsible, it is clear that pulsing or sweeping to anodic potentials has a beneficial impact on maintaining and/ or restoring $CO_2R$ activity on Cu. There have also been several other interesting observations noted when using potential pulsing/sweeping techniques, such as the formation of methanol[121] and increased selectivity for the production of $C_{2+}$ compounds.[100,119,122] These results have been attributed to transient changes in the local chemical conditions such as an increased coverage of *OH and an accumulation of CO near the Cu surface, respectively. On the other hand, studies using applied voltage pulses in the millisecond time regime demonstrated that the selectivity on polycrystalline Cu could be shifted entirely to syngas ($H_2$ and CO), with the ratio of these two products changing with the length of the pulses,[120] or to strongly favor CO or $CH_4$ production.[123] Since these pulsed-bias methods have yielded increased selectivities for desirable products in addition to helping prevent deactivation, further work should be done to better understand the mechanisms at play and how they can best be utilized to enhance $CO_2R$ catalysis.

## 2.4. Deconvolution of Various Effects in Complex Catalysts

In addition to the deactivation mechanisms just discussed, there are a number of other factors that can lead to discrepancies in the catalytic performance of Cu between electrochemical systems. For example, as we will discuss in section 3.3, the choice of electrolyte anions, cations, and pH can have a significant influence on the catalyst performance, so ideally, direct comparisons should only be made between catalysts tested in the same electrolyte. Ultimately, the entire electrochemical system (including catalyst, electrolyte composition and concentration, electrochemical cell geometry and hydrodynamics, membrane composition, and operating conditions) needs to be considered in order to determine if the measured activity and selectivity can be confidently attributed to the properties of the catalyst itself. To ensure that experimental conditions are satisfactory, researchers should benchmark their electrochemical setup by making sure that literature results using a standard electrode material, such as planar polycrystalline Cu, can be reproduced (within the variation typical of the field, as indicated by Figure 4). If this is not the case, any results obtained from more advanced

materials are not meaningful, as other factors could be impacting the catalysis.

As will be discussed further in sections 6 and 7, different preparation methods can also yield very different $CO_2R$ performance for seemingly similar catalysts. Unfortunately, many advanced catalyst designs such as nanostructured and/or bimetallic electrodes are ill-defined, which can make it extremely challenging to deconvolute the influence of different morphological factors that can cause changes in behavior (such as surface faceting, composition, oxidation state, strain, grain boundaries, porosity, etc.). Complex catalysts should preferably be characterized to the greatest extent possible. In general, however, planar and/or well-defined electrodes are best for systematic studies that seek to draw fundamental relationships between activity/selectivity and structure/composition of catalysts. Furthermore, detailed studies as a function of voltage are needed to properly identify when novel catalysts are limited by their intrinsic kinetics rather than a convolution of kinetic and mass transport effects; only reporting data at one potential gives an incomplete picture of the catalyst behavior and can complicate comparisons between different catalysts and/or electrochemical systems.

Another key challenge in this area is the disconnect between *ex situ* characterization and how catalysts function *in situ.* This is especially challenging for a highly mobile and readily oxidized material such as Cu. We caution against drawing conclusions about the catalyst under reaction conditions using *ex situ* measurements alone, since the electrolyte and negative polarization of the cathode can have a significant influence on the catalyst properties. We also urge the continued development of *in situ/operando* spectroscopic techniques in order to elucidate the true chemical state and structure of active sites during electrochemical $CO_2R$. Not only will this aid in the search for more active and selective catalysts, but this can also provide more useful insights into the reaction mechanisms occurring on the surface on an atomic-scale level.

## 3. EXPERIMENTAL PROBES OF $CO_2$ REDUCTION MECHANISMS

In section 1.2 we discussed how a large number of >2e$^-$ products are formed during $CO_2R$ on polycrystalline Cu electrodes. Steering selectivity toward certain products instead of others is therefore an important challenge, and could potentially be done by stabilizing/destabilizing key intermediates, making the pathway of the desired product(s) energetically more favorable. Thus, comprehensive mechanistic understanding of $CO_2R$ is crucial in order to design more selective catalysts. In this section, various experimental studies aiming to provide mechanistic insight about $CO_2R$ on Cu electrodes are presented. This includes measurements on single crystals, further reduction of possible intermediates, and measurements probing the impact of the electrolyte and electrochemical conditions. The key findings will furthermore be the basis of the theoretical descriptions of the processes occurring on Cu surfaces, which will be discussed in detail in section 4. Then, section 5 will bring together the key conclusions from these experimental and theoretical studies and present our current understanding of the complex reaction networks for electrochemical $CO_2R$ on Cu.

We would first like to acknowledge a growing area of research that underpins much of the gains in mechanistic understanding: *in situ/operando* spectroscopies. Development of spectroanalytic techniques, such as X-ray absorption spectroscopy (XAS),[124−127] Raman spectroscopy,[95,128−136] and various forms of infrared (IR) spectroscopy,[118,133,136−149] has become increasingly important for discerning the catalyst surface structure, composition, and oxidation state under *in situ/operando* conditions, as well for detecting the presence of adsorbed intermediates during electrochemical $CO_2R$. Therefore, we will highlight relevant studies where they have contributed to mechanistic understanding throughout the different sections of this work.

### 3.1. Influence of Surface Facet on $CO_2$ and CO Reduction

It is complicated, if not impossible, to derive unambiguously which structural elements present on a polycrystalline catalyst surface are contributing to the observed catalytic activity, since the measured catalytic activity is always a sum of activities resulting from different structures. In a simplified picture, a catalyst surface can consist of planar areas with single crystal orientations and various step and kink sites with low coordination. Further, complex atomic structures could be present at the interface between different grains that are typically observed in polycrystalline materials and/or nanostructured surfaces. Cu single crystal electrodes with preferential orientation are possible model catalysts to investigate the first two of the mentioned structural properties. This includes planar surfaces, such as Cu(111), Cu(100), and Cu(110), as well as higher-index surfaces which can be described as a low-index surface with a certain density of step sites. Single crystal electrodes are ideal systems to draw comparisons with theoretical calculations because methods such as density functional theory (DFT) only probe local phenomena, which should be equally distributed on these atomically flat catalysts. Further, single crystals are also quite useful for studying the influence of other $CO_2R$ rate-determining factors such as electrolyte pH, cations, and anions since they provide a well-defined surface structure. Note, however, that single crystals themselves are not viable catalysts for practical applications, due to their low geometric surface area, and the resulting low geometric current densities. Therefore, several groups have synthesized nanostructured materials with preferential faceting and high dispersion, which will be discussed further in section 6. In this section, we describe experimental findings obtained on single-crystal model systems, describe surface reconstructions on Cu, discuss the mechanistic interpretations, and suggest focus areas for future studies.

#### 3.1.1. Influence of Various Cu(hkl) Surfaces on Product Distribution. The electrochemical reduction of $CO_2$ on Cu single crystals has been studied by a variety of methods, including voltammetry (linear potential sweeps),[150−155] chronoamperometry (constant potential),[154,156,157] and chronopotentiometry (constant current).[150−153,158] The choice of electrochemical technique depends on the method employed to characterize liquid and gaseous products. For instance, *in situ* techniques that can monitor the evolution of products in real time, such as differential electrochemical mass spectrometry (DEMS), can be coupled with cyclic voltammetry (CV) or other scanning techniques. However, *ex situ* bulk product analysis, such as chromatography techniques and NMR spectroscopy, need to be coupled with chronoamperometry and/or chronopotentiometry. The choice of technique also depends on whether quantitative information, such as the concentrations of

**Table 4. Product Distribution in $CO_2$ Reduction at a Series of Copper Single-Crystal Electrodes, Cu(S)−[n(100) × (111)] and Cu(S)−[n(100) × (110)][a]**

| Crystal orientation | Potential/V vs SHE | Potential/V vs RHE | Faradaic efficiency/% | | | | | | | | $C_2H_4/CH_4$ |
|---|---|---|---|---|---|---|---|---|---|---|---|
| | | | $CH_4$ | $C_2H_4$ | CO | Alc. | Ald. | HCOOH | $H_2$ | |
| | | | Cu(S)−[n(100) × (111)] | | | | | | | | |
| (100) | −1.40 | −1.00 | 30.4 | 40.4 | 0.9 | 12.0 | 4.4 | 3.0 | 6.8 | 1.3 |
| (11 1 1) | −1.37 | −0.97 | 8.9 | 50.2 | 1.8 | 17.7 | 4.4 | 3.2 | 8.8 | 5.8 |
| (711) | −1.34 | −0.94 | 5.0 | 50.0 | 1.1 | 14.2 | 6.4 | 4.6 | 15.6 | 10.0 |
| (311) | −1.37 | −0.97 | 36.0 | 23.8 | 2.6 | 5.2 | 3.4 | 14.0 | 13.3 | 0.7 |
| (111) | −1.55 | −1.15 | 46.3 | 8.3 | 6.4 | 3.3 | 2.7 | 11.5 | 16.3 | 0.2 |
| | | | Cu(S)-[n(100) × (110)] | | | | | | | | |
| (810) | −1.38 | −0.98 | 6.4 | 45.1 | 1.4 | 28.8 | 2.0 | 1.5 | 8.7 | 7.0 |
| (610) | −1.37 | −0.97 | 7.6 | 44.7 | 0.9 | 29.3 | 2.7 | 1.4 | 9.0 | 5.9 |
| (510) | −1.38 | −0.98 | 8.1 | 42.3 | 2.1 | 29.5 | 5.6 | 2.9 | 10.5 | 5.2 |
| (210) | −1.52 | −1.12 | 64.0 | 13.4 | 2.2 | 7.3 | 1.5 | 5.5 | 7.0 | 0.2 |
| (110) | −1.55 | −1.15 | 49.5 | 15.1 | 0 | 7.4 | 3.1 | 6.6 | 18.8 | 0.3 |

[a]The measurements were performed by chronopotentiometriy at 5 mA cm$^{-2}$ in 0.1 M $KHCO_3$. The potentials vs RHE were calculated from the potentials vs SHE using the Nernst equation, assuming a pH of 6.8 and temperature of 25 °C. Adapted with permission from Hori.[1] Copyright 2008, Springer Science Business Media, LLC. The data for Cu(110) is from Hori, 1995.[150]

products formed, is of interest, or if it is sufficient to identify trends between electrodes.

Early chronopotentiometric measurements by Frese indicated that, among the three low-index Cu single crystal facets, i.e., Cu(111), Cu(110), and Cu(100), the Cu(111) surface yields the highest $CH_4$ rate and Cu(100) the lowest.[158] Further measurements by Hori et al. indicated that Cu(100) surfaces primarily form $C_2H_4$ and a somewhat smaller amount of $CH_4$, while Cu(110) and Cu(111) surfaces preferentially form $CH_4$ with very small amounts of $C_2H_4$.[150] This was later confirmed in follow-up measurements by Hori et al.,[151−153] as well as other research groups.[154,155] In a study showing the product distribution over a range of potentials, $C_2H_4$ formation set in at a similar or lower overpotential than $CH_4$ formation for all investigated single crystal electrodes.[155] At higher overpotentials, the formation of $CH_4$ becomes the dominant process.[155] This is similar to the trend observed for polycrystalline Cu, as shown in Figure 4 of subsection 1.2.2, for which $CH_4$ formation reaches maximum selectivity at around −1.1 V to −1.2 V vs RHE, where $CO_2R$ activity starts becoming mass transport limited on planar electrodes.[65,96,155]

Liquid, oxygenated compounds are interesting products as well, due to their aforementioned high energy density and moderate to high value. In the previously described studies by Hori et al., several liquid compounds were detected, of which alcohols and carboxylates were the most significant, as shown in Table 4.[151−153] Around −1.0 V vs RHE, Cu(100) surfaces preferentially formed alcohols compared to formic acid, while the opposite could be observed for Cu(111). Cu(110) surfaces yielded similar selectivity toward alcohols and carboxylates. Huang et al. recently showed a similar trend as Hori et al. around −1.0 V vs RHE, and at less cathodic potentials, the main liquid product observed was formate.[155] At potentials more negative than −1.0 V vs RHE, where the formation of $C_2H_4$ reached a maximum on all single crystal surfaces, Huang et al. observed formation of ethanol with significant Faradaic efficiency. A similar trend was observed on polycrystalline Cu, suggesting that the two products are formed through a partially shared pathway.

In order to elucidate the influence of undercoordinated sites on the product distribution, Hori et al. also performed a series of $CO_2$ reduction studies on stepped Cu single crystal

surfaces.[151−153] The distribution of gaseous and liquid products is summarized in Table 4. The presence of (111) or (110) steps on Cu(100) surfaces led to significantly enhanced Faradaic efficiency toward alcohols. Their data also indicated that a number of stepped surfaces exist that yield higher $C_2H_4/CH_4$ ratios compared to the Cu(100) surface, which is the most selective low-index crystal facet for the formation of $C_2H_4$, as described above. In Figure 5, the $C_2H_4/$
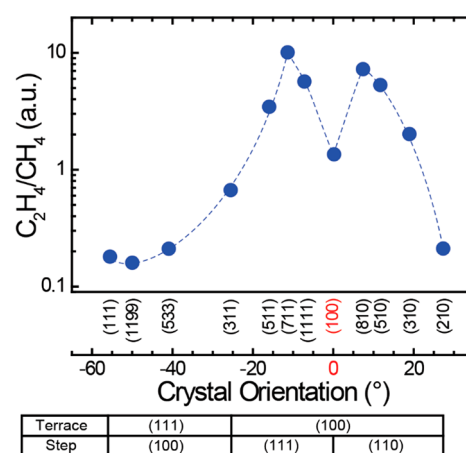


**Figure 5.** Variation of $\log(C_2H_4/CH_4)$ in terms of the current efficiency and the electrode potential with the angle of the crystal orientation with reference of Cu(100). The data for the figure were obtained from Hori et al.[153]

$CH_4$ ratio is plotted as a function of crystal orientation, clearly illustrating the notion that steps can further enhance the selectivity to $C_2H_4$ formation compared to the planar single crystals. Thus, it seems that one approach to improve the selectivity toward $C_2H_4$ is to engineer Cu electrodes with an increased occurrence of (100) surfaces and optimal occurrence of steps. Indeed, this has been seen in epitaxially grown copper films with a high degree of preferential surface orientation, where films with a preferentially (751)-oriented surface rich in steps with highly undercoordinated sites show high selectivity to $C_{2+}$ products and especially oxygenated products.[157]

Additional efforts following this direction will be discussed in more detail in section 6.

As discussed later in subsections 3.2.1 and 4.2.2, CO has been identified as a key intermediate in the reduction of $CO_2$ to >$2e^-$ products.[85,103,159−161] Thus, to obtain further mechanistic insight about the formation of these compounds, COR has been studied on Cu single crystals.[162−166] None of these studies quantified the various products formed, making it hard to draw conclusions about Faradaic efficiencies and partial current densities. However, studying the onset potentials for the various products can give an indication of the selectivity toward the different compounds in various potential ranges. In DEMS measurements of various single crystals in phosphate buffer at pH 7, Cu(100) exhibited an earlier onset than Cu(111) and Cu(110) for $C_2H_4$.[166] Further, Cu(100) facilitated little to no $CH_4$ formation at the measured potentials, while Cu(111) gave a similar onset for $C_2H_4$ and $CH_4$. Cu(911), which was shown by Hori et al. to be particularly selective toward $C_2H_4$, behaves similarly to Cu(100) in this study. In order to gain more conclusive insights about COR on various single crystalline surfaces, further systematic investigations with complete product quantification are required, similar to what has been demonstrated by Hori et al. for $CO_2$ reduction.

Based on the discussion above, it is clear that $CO_2R$ measurements on single crystals can yield important information about which surface sites are responsible for the formation of key products. Increasing our understanding of the active surface can aid in the development of highly selective catalyst materials. However, based on the measurements described in the previous paragraphs, it seems clear that more work performing thorough and complete product analysis is necessary before conclusions can be drawn about specific trends. In addition, the reports on nonplanar surfaces indicate that engineering of materials to achieve presence of well-defined steps on the surface can be a valuable design principle for improving selectivity toward $C_{2+}$ products such as $C_2H_4$ and alcohols.

**3.1.2. Influence of Various Cu(hkl) Surfaces on Activity.** As will be discussed in section 4, theoretical studies predict vastly different *activity* for different crystal facets, rather than just the *selectivity* differences described so far. In order to be able to evaluate $CO_2R$ activity experimentally, thorough, quantitative product analysis is needed. Additionally, the catalyst needs to be studied while under activation control, i.e., not experiencing mass transport limitations, as discussed in detail in section 2.2. As a result, only a few of the reports mentioned in the previous subsection can be used to draw conclusions about trends in activity. These studies[153,155,157] do show slight variations in both overall and $CO_2R$ activity depending on orientation, but nothing comparable to the magnitude expected based on computational studies. For example, the study on epitaxially grown Cu thin films reported ~1 order of magnitude higher activity toward C−C coupled products for the highly stepped Cu(751)-oriented surface as compared to the planar Cu(111)-oriented surface.[157] These results are illustrated in Figure 6. Note that while these electrodes exhibit preferential orientation, they are not truly single crystalline, meaning that they have a certain occurrence of grain boundaries and other undercoordinated defects on the surface. This could explain why the activity of these and other well-defined surfaces do not show as much difference as predicted by theory. Step sites have been identified as the main
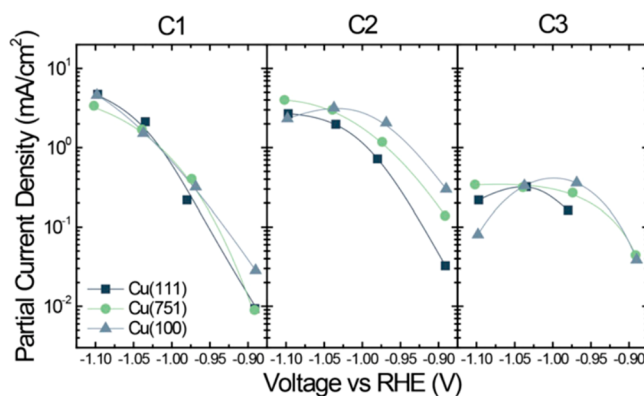


**Figure 6.** $CO_2R$ on epitaxially grown Cu films oriented in the (111), (751), and (100) directions. The graphs show partial current density toward $C_1$ (left), $C_2$ (middle), and $C_3$ (right) products. Reprinted with permission from Hahn et al.[157]

contributor to the activity of various catalytic systems. For instance, it has been seen in the field of thermally activated catalysis that blocking step sites can have a drastic impact; experiments where the steps of Ru single crystals (~1% of the surface) were blocked led to a reduction in $N_2$ dissociation activity by more than 9 orders of magnitude.[167] Similarly, a small fraction of step sites have also been suggested to dominate the overall electrochemical $CO_2$/CO reduction activity.[168] Thus, even a small quantity of existing defects or step sites formed *in situ* (*vide infra*) could be dominating the activity of these otherwise single crystalline electrodes.

**3.1.3. Restructuring and Other Challenges Regarding Single Crystal Measurements.** As described above, single crystal measurements can be highly useful to study the $CO_2R$ activity and selectivity of various structures. However, one must be cautious because the quality and consistency of single crystal studies are sensitive to a number of factors, discussed herein. Hori et al. described in detail how the reproducibility of $CO_2R$ measurements on Cu(110) and Cu(111) single crystals strongly depends on the pretreatment of the electrodes.[152] Although the structural properties of the bulk are well-defined, the homogeneity of the surface can vary depending on the pretreatment. One possible factor could be the formation of oxides during the preparation and transfer to the electrochemical cell. A partially oxidized surface, which is reduced in the actual electrochemical cell, could lead to an irreversible reconstruction of the Cu surface, a phenomenon that for example has been shown in detail for Pt electrodes.[169,170] This effect has also been intentionally exploited to prepare nanostructured electrodes in a number of studies, as discussed in subsection 6.2.1. As a result of the oxidation occurring upon exposure to ambient air, Hori and co-workers do not rule out that the final electrodes might be textured with defect sites, which could have a large influence on the measured electrocatalytic activity of the electrodes, as we just discussed. However, they probed the surface structure only by the use of CV, which can give indicative but not conclusive evidence.

Surface probe techniques, such as scanning tunneling microscopy (STM), can image the surface with excellent resolution to evaluate whether defect sites are present. It is important to keep in mind that only small fractions of the electrode surface are probed with this type of technique, so the resulting image may therefore not provide a representative indication of the whole surface. Nonetheless, STM can give a

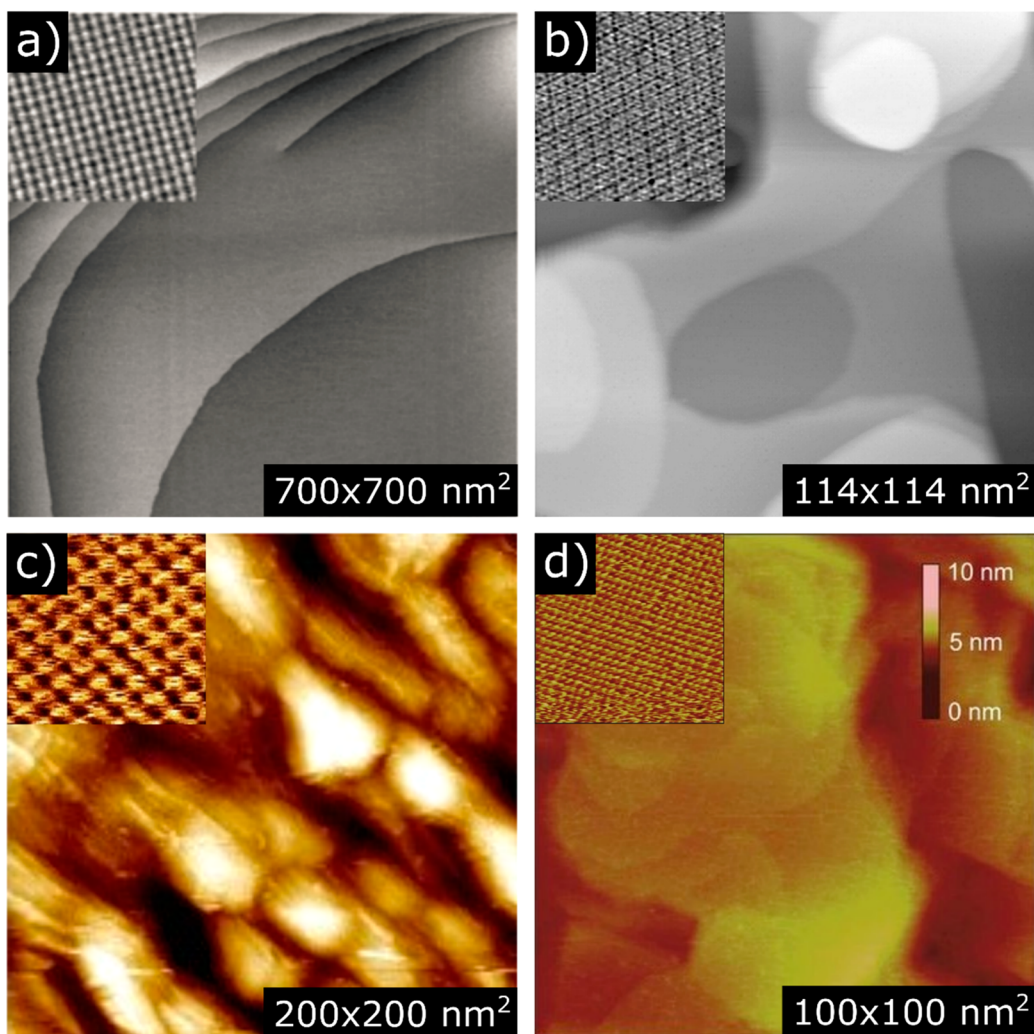**Figure 7.** STM images of various oriented surfaces. (a) 700 nm × 700 nm STM image of ultrahigh vacuum prepared Cu(100) single crystal. Inset: 4 nm × 4 nm image of the same surface. Reproduced with permission from Engstfeld et al.[171] Copyright 2018, John Wiley and Sons. (b) 114 nm × 114 nm *in situ* STM image of electropolished Cu(111) single crystal at −0.6 V (vs pseudoreference) in PO₄ buffer. Inset: 9.5 nm × 9.5 nm image of the same surface. Reprinted with permission from Schlaup et al.[172] Copyright 2012, Elsevier B.V. (c) 200 nm × 200 nm *in situ* STM image of electropolished Cu(100) single crystal at −0.9 V vs SHE. Inset: 2 nm × 2 nm image of the same surface. Adapted with permission from Kim et al.[173] Copyright 2016, Springer Science Business Media New York. (d) 100 nm × 100 nm *in situ* STM image of epitaxially grown Cu(100) film at −0.24 V vs RHE in 0.1 M HClO₄. Inset: 5 nm × 5 nm image of the same surface. Reprinted with permission from Hahn et al.[157]

good impression of the defect density for various types of electrodes. In Figure 7, STM images are shown from 4 different preferentially oriented electrodes, spanning 3 preparation procedures and 4 measurement conditions. Figure 7a shows an STM image of a Cu(100) single crystal that was prepared by annealing under ultrahigh vacuum (UHV) and transferred to the characterization chamber without being exposed to oxygen. The crystal exhibits large terraces and a relatively small amount of defects on the surface. In comparison, *in situ* STM images of electropolished Cu(111) (Figure 7b) and Cu(100) (Figure 7c) show significant occurrence of steps and other defects. An example of *in situ* STM images from an epitaxially grown Cu(100)-oriented film are shown in Figure 7d, which also displays a significant occurrence of defects since this preparation procedure does not lead to truly single crystalline electrodes.

In addition to the influence of pretreatment, there is the possibility that Cu surface restructuring under reaction conditions can lead to changes in activity and selectivity.

Earlier reports indicated that Cu(111) restructures to a highly textured surface when exposed to even small CO partial pressures in vacuum,[174] and recent experimental spectroscopic[133] and computational[175] studies have also indicated that the presence of CO increases the density of highly active, undercoordinated step sites on polycrystalline Cu. Furthermore, restructuring promoted by CO was also observed using *operando* grazing incidence X-ray diffraction (GIXRD) on polycrystalline copper thin films.[176] Thus, since there is typically a significant coverage of CO under CO₂R conditions,[177] it is possible that reconstruction and the formation of step sites on otherwise defect-free single crystalline surfaces during reaction could explain why there are only moderate differences in CO₂R activity on different facets, as mentioned above.

Various studies employing *in situ* electrochemical scanning tunneling microscopy (ECSTM) have also reported reconstruction of Cu surfaces under applied potentials while not in the presence of CO₂/CO.[172,173,178−181] For example, it has

been demonstrated that at a potential of −0.9 V vs SHE in both argon-purged 0.1 M KOH and 0.1 M KHCO$_3$, a polycrystalline Cu surface gradually forms Cu(111) facets on a time scale of 30 min, which subsequently transform into Cu(100) facets after another 30 min.[178,181] The Cu(110) surface undergoes a similar restructuring compared to the polycrystalline Cu electrodes; the topmost planes of a Cu(110) surface transformed over time into a disordered Cu(110), then into a disordered mixed Cu(110)−Cu(111), and finally into an ordered Cu(110)−Cu(100) plane.[180] In contrast, no reconstruction was observed on single crystal Cu(111) or Cu(100) surfaces under the same conditions,[180] nor for epitaxially grown Cu(111) and Cu(100) films at −0.24 V vs RHE in 0.1 M HClO$_4$.[157] While it is somewhat unclear what drives the (in)stability of these different systems, it is likely that it has to do with the comparative adhesions of various surfaces in contact with each other.[180] Another possibility could be due to other factors from the local reaction environment (i.e., electrolyte and/or potential-dependent effects). However, more work needs to be done to better understand how and why Cu restructuring occurs under reaction conditions.

Another important point for Cu is that, compared to other monometallic catalyst systems,[169] few thorough benchmarking studies on the electrochemical properties of Cu single crystal surfaces have been reported. Such data could be used to determine the properties of electrodes used for a particular study, which is standard practice for other electrode materials, such as Pt.[182] For example, CVs of single crystal electrodes recorded in alkaline solutions at potentials where only OH adsorption on the surface occurs (−0.2 to 0.5 V vs RHE) and no bulk oxide formation is expected exhibit different redox features for different reports in the literature, which should not be the case for truly single crystal electrodes.[155,164,179,183−186] Further, a recent study on the electrochemical properties of polycrystalline Cu and Cu(100) electrodes, including samples prepared under UHV conditions to avoid surface contamination of oxygen, clearly suggests that the features observed in the CV strongly depend on the pretreatment of the electrodes.[171] This is illustrated in Figure 8, where the CV of a Cu electrode prepared under UHV conditions is plotted vs the CVs obtained for samples exposed to different pretreatments under laboratory conditions.[171] The authors ascribed the features in the CV between 0.30 and 0.45 V to different sites than the Cu(100) planes, indicating that all electrodes except for that prepared under UHV conditions contain a significant amount of defect sites on the surface. Other approaches to assess the consistency of Cu electrodes could include comparing key values for the HER, which so far has only been reported in a few studies on polycrystalline Cu electrodes in alkaline[187−189] or acidic[190] solutions, or investigating the distinct features obtained from lead[190,191] or thallium[192] underpotential deposition (UPD) on single crystal electrodes.

Better insight about the fundamental electrochemical properties of Cu single crystal electrodes would be valuable in order to better compare results among different research groups within the field of CO$_2$R. In addition, it would be useful to elucidate the influence of higher overpotentials and different electrolytes and pH ranges. For example, it was shown by CV that new sites are formed on the surface of polycrystalline Cu electrodes exposed to −0.5 V or −0.6 V vs RHE in 1 M NaOH at 60 °C for 3 h.[193] Cathodic corrosion, hydrogen embrittlement, or hydride formation can also play a crucial
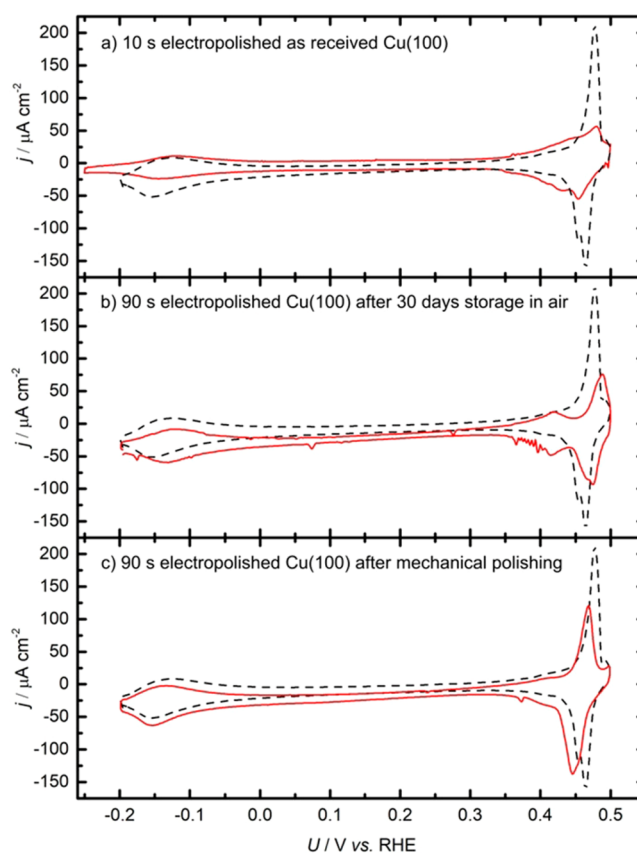


**Figure 8.** Comparison of the CV recorded on a Cu(100) electrode prepared under UHV conditions (dashed line) with (a) an electropolished as received Cu(100) electrode from the supplier, (b) 90 s electropolished Cu(100) electrode after storage in air for 30 days, and (c) an electropolished Cu(100) electrode after mechanical polishing (0.1 μm alumina powder for 10 min and further 10 min with 0.05 μm alumina powder). All CVs were recorded in 0.1 M KOH and at a scan rate of 50 mV·s$^{-1}$. Reprinted with permission from Engstfeld et al.[171] Copyright 2018, John Wiley and Sons.

role at such potentials.[194,195] These effects have received little attention in relation to CO$_2$R as of yet, but could influence activity and stability. Furthermore, such insights could also be highly useful for other processes where the electrochemical/electrocatalytic properties of Cu are important, such as nitrate reduction or studies related to the initial oxidation of Cu single crystal electrodes in aqueous environment.[196−199]

### 3.2. Reduction of Possible Intermediates

In the previous section, we outlined the facet-dependent activity and selectivity of Cu and saw how tunable the reaction is on the atomic scale. Here we will discuss some of the key intermediate species and how probing their reactivity has helped shed light on CO$_2$ reduction pathways.

**3.2.1. CO as a Crucial Intermediate.** Carbon monoxide (CO) and formate (HCOO$^-$) are the 2e$^-$ products formed from CO$_2$R, and as discussed in subsection 1.2.2, there are classes of metals that yield each of these products with high selectivity. Early experimental work found that the reduction of CO on Cu leads to a similar product distribution as CO$_2$R on Cu, suggesting that CO is a key reaction intermediate.[85,103,159−161] Subsequent detailed studies of CO reduction (COR) on Cu have provided further support for this claim,[114,159,200] in addition to the spectroscopic observation of surface adsorbed CO under CO$_2$R conditions.[132−134,144−147]

Consequently, several studies proposed that the binding energy of adsorbed CO (*CO) is a key descriptor for reduction activity to >2e⁻ products.[201−203] Metals that bind CO too strongly will be poisoned by this intermediate, whereas metals that bind CO too weakly will desorb it from the surface before it can react further. Thus, well-aligned with the Sabatier principle,[204] the intermediate binding energy for CO on Cu is a key reason for its ability to catalyze $CO_2R$ to products further reduced than CO. In addition, studies have shown that CO adsorption on Cu suppresses the competing hydrogen evolution reaction (HER) due to site blocking effects and/or changes in *H binding energy.[85,177,201,205] The coverage of CO on Cu is typically very high,[177] at least until there are mass transport limitations (*vide infra*). Thus, CO poisoning of the HER is an important mechanism by which Cu maintains a high Faradaic efficiency for $CO_2R$ in aqueous electrolytes.[205]

Ever since the determination of CO as a key intermediate in the reduction of $CO_2$ to hydrocarbons and alcohols, there has been increasing interest in studying COR as a proxy for understanding trends in $CO_2R$. This has several advantages including fewer reaction steps/intermediates to consider and avoiding the complication of the reactant being part of the buffer (as is the case for $CO_2R$ in bicarbonate solutions). The latter, in turn, allows for a wider range of pH conditions to be examined, in addition to allowing for direct comparison with blank measurements where the electrolyte is purged with an inert gas. Another motivation for better understanding COR catalysis is that this could provide an alternate route for $CO_2R$ that can potentially overcome scaling relations by splitting the reaction into two separate steps: (1) $CO_2$ reduction to CO, then (2) CO reduction to the desired product(s). Thus, we will discuss insights gained from experimental and computational COR studies where appropriate in the sections that follow, and we also recommend continued development of viable COR catalysts for potential tandem systems.

**3.2.2. Reduction of Oxygenated $C_1$ and $C_2$ Species.** The discovery of at least 16 distinct products formed from $CO_2R$ on Cu highlights the complexity of this reaction.[65] Besides the dominant hydrocarbons, methane and ethylene, this includes a broad mix of aldehydes, ketones, carboxylic acids, and alcohols, the majority of which are multicarbon compounds. As a result, probing the reduction activity of small oxygenated species has been used as a technique to help elucidate mechanistic pathways; here we will briefly describe the key findings from these studies.

Unlike CO, it has been shown that another 2e⁻ reduction product, formate/formic acid, does not typically undergo further reduction on Cu under reductive conditions;[85] however, with very high concentrations, high cathodic bias, and highly acidic or basic electrolytes, trace amounts of methane have been reported.[103,206] Formaldehyde ($CH_2O$) reduction has been shown to produce mainly methanol,[107,112,159] although small amounts of methane have also been reported.[103,107,112,159,206] Finally, reduction of methanol (or methoxide, which is methanol deprotonated under high pH) has been shown to yield no products.[103,112,206] These results strongly suggest that formate and methanol are terminal products for electrochemical $CO_2R$, and intermediate(s) related to formaldehyde (such as adsorbed formyl, *CHO) may be on the pathway to methanol and methane.

The presence of hydroxyl and/or carbonyl moieties in many of the multicarbon products suggests that the C−C bond is formed early in the reaction, at least before one of the two carbon−oxygen bonds in $CO_2$ is broken.[65] Accordingly, it has been suggested that enol-like species may be intermediates to multicarbon products,[65] such as an enediol or enediolate.[112] The observation that reduction of ethylene oxide produces ethylene indicates that a strongly adsorbed epoxide in the form of an oxametallacycle is another possible intermediate in ethylene formation.[112] Ethylene glycol and oxalic acid reduction did not lead to any reduction products, suggesting that these are not intermediates in $CO_2R$.[112] This is curious given that ethylene glycol has been detected as a minor product,[65] so a recent theoretical study suggested that the reason why this species is not further reduced is due to its OH groups being repelled by the surface, making its readsorption endergonic.[207] Finally, both glyoxal[112,208] and glycolaldehyde[112] reduction have been shown to produce acetaldehyde and ethanol but not ethylene. This suggests that these minor products are intermediates on the pathway to acetaldehyde and ethanol.[207]

It has long been thought that aldehydes are key intermediates to alcohols after Hori and co-workers observed that acetaldehyde and propionaldehyde were easily reduced to ethanol and *n*-propanol, respectively.[159] Further support for this has been provided by several COR studies that have noted aldehyde production at lower overpotentials than alcohols that decreases with increasing overpotential where alcohols become dominant,[114,200] as well as recent demonstrations of direct acetaldehyde reduction to ethanol.[90,209] Another study employed a DEMS setup where the catalyst was coated directly onto the pervaporation membrane used to transfer volatile species into the mass spectrometer in order to detect species directly from the electrode−electrolyte interface.[100] Through this method, it was observed that acetaldehyde and propionaldehyde are produced in 2−4 times higher abundance than ethanol or propanol compared to sampling from the bulk electrolyte, where they are typically only observed as minor products.[100] Thus, the authors suggest that these aldehydes are transiently produced and relatively abundant within the local reaction environment, but are typically reduced further to the corresponding alcohols before diffusing into the bulk electrolyte. Interestingly, it was also found that ethanol production increased at the expense of propionaldehyde at more cathodic potentials, suggesting that ethanol and propionaldehyde may share a common intermediate such as acetaldehyde.[100]

Finally, it is worth highlighting a recent study that has led to significant new insights on the role of water in the formation of $C_{2+}$ oxygenated products.[210] By carrying out $C^{16}O$ reduction in $H_2^{18}O$ electrolyte and quantifying the isotopic composition of the products using gas chromatography−mass spectrometry (GC-MS), Lum et al. determined that the majority of ethanol, acetate, and 1-propanol formed were ¹⁸O enriched, meaning that they incorporated oxygen from the solvent water. Allyl alcohol and methanol were not enriched with ¹⁸O, which suggests different mechanisms for their formation. Importantly, water has not previously been considered as a dominant O source in the formation of oxygenated products, so the researchers then investigated how this could be the case using quantum mechanics-based metadynamics calculations. This led to the identification of a new mechanism for (¹⁸O)ethanol formation, which was termed as Grotthuss chain ethynyl concerted hydrolysis (GECH).[210] The mechanistic pathways and intermediate branch points for formation of ethylene, (¹⁸O)ethanol, and (¹⁶O)ethanol were then elucidated; these $C_2$ reaction networks are shown in purple in Figure 18. It is

important to keep in mind that Cannizzaro-type disproportionation reactions could also occur in the electrolyte, especially at high pH, converting an aldehyde (acetaldehyde) into the corresponding alcohol (ethanol) and carboxylate (acetate).[211] Thus, this is another possible mechanism by which $^{18}O$ could be incorporated into the products. Lum et al. performed control experiments that indicate this is not the main mechanism by which these products are formed,[210] but researchers should still keep the possibility of these reactions in mind when working under strongly alkaline conditions, especially when a high concentration of aldehydes are formed.

## 3.3. Electrolyte Effects

The choice of electrolyte can have a huge impact on $CO_2R$ performance. There are a number of factors that have complex relations with the local reaction environment; the composition and concentration of anions and cations can cause changes in the electrostatic interactions, buffer capacity, pH, and availability of proton donors. These changes are not always straightforward to map due to intertwining effects. In this section we will discuss the major variables within the electrolyte (pH, cations, anions) and their impacts on $CO_2R$ catalysis.

**3.3.1. pH Effects.** Studying the effect of pH on $CO_2R$ comes with several challenges. Given that $CO_2$ forms bicarbonate and carbonate when it is purged through alkaline solutions, electrolytes for $CO_2R$ are generally limited to neutral and acidic pH conditions. However, by using CO reduction (COR) as a proxy, mechanistic insights about the pathway to further reduced products can be obtained. Pioneering work of this nature by Hori et al. first revealed that the selectivity between $CH_4$ and $C_2H_4$ is impacted by pH.[85,159,160] By studying COR on Cu, the production rates for each product could be compared in buffer solutions spanning a bulk pH of 6 to 12.[159] When the measurements of partial current density toward $C_2H_4$ (or $C_2H_5OH$) are included on a single Tafel plot on the SHE scale (Figure 9a), a straight line emerges. Thus,
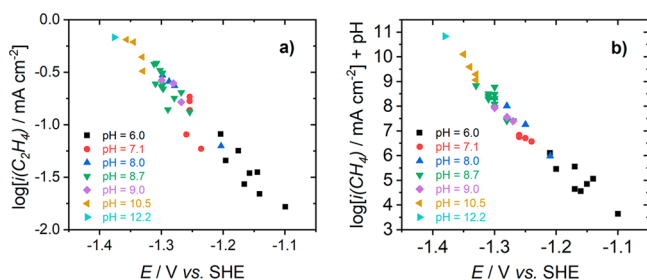
**Figure 9.** Tafel plots from COR measurements that were made over a pH range of 6 to 12. (a) plots the logarithm of the partial current density going toward ethylene against applied potential on the SHE scale; (b) plots the logarithm of the partial current density going toward methane, plus the pH, against applied potential on the SHE scale. Adapted from Hori et al.[159] Copyright 1997, American Chemical Society.

the rate-determining step on the pathway to $C_{2+}$ products such as $C_2H_4$ is independent of pH on an absolute potential scale (SHE), and thus will shift on the RHE scale to more positive potential (decreasing overpotential) by 59 mV per unit increase in pH. For $CH_4$, on the other hand, the Tafel plot was widely scattered unless only measurements at the same pH were included, indicating that the rate-determining step for the $C_1$ pathway involves proton transfer and is thus dependent on

pH. Hori et al. explained this pH dependence in terms of the Tafel equation where the partial current for $CH_4$ is proportional to the proton activity; indeed, by plotting the logarithm of the $CH_4$ partial current density plus pH (Figure 9b), a straight line emerges. From these plots, transfer coefficients of $\alpha$ = 0.35 and $\alpha$ = 1.33 were extracted for $C_2H_4$ and $CH_4$, respectively.[159] This led Hori et al. to propose that the reaction paths for $CH_4$ and $C_2H_4$ formation do not share rate-determining steps and thus have mechanisms that are separated at early stages of CO reduction. Further evidence for this notion was provided in a series of studies on single crystal electrodes by the group of Marc Koper,[163,165,166] which revealed that there are two possible pathways to $C_2H_4$ depending on the pH, surface structure, and overpotential. These mechanisms will be discussed further in sections 4 and 5.

Recent work comparing $CO_2R$ and COR on planar polycrystalline Cu in pH 6.8 and 13, respectively, has led to increased mechanistic understanding of the role of pH.[200] The partial current densities for $CO_2R$ and COR products plotted on both the RHE and SHE scale illustrates the overall effect of pH (Figure 10). The $C_{2+}$ product overpotentials display a pH
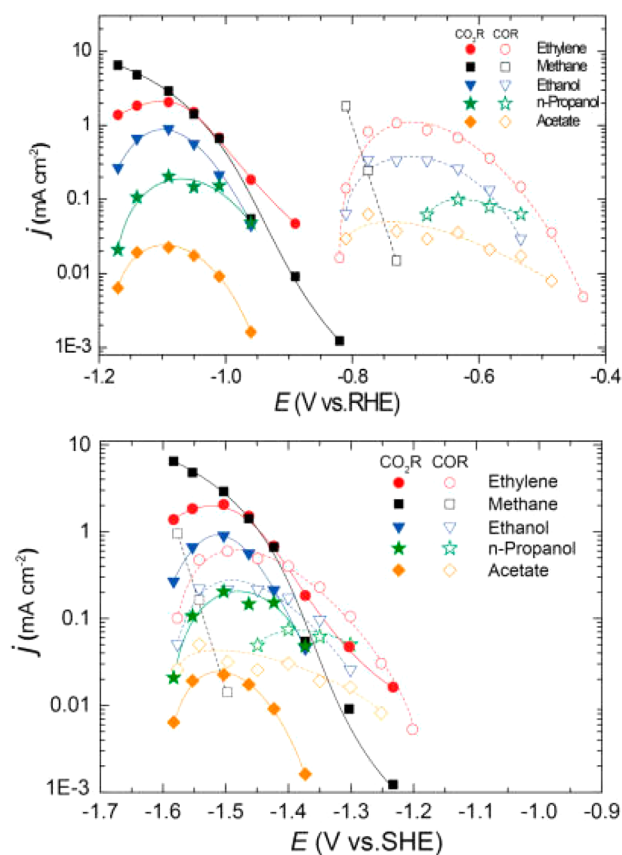
**Figure 10.** $CO_2R$ (filled) and COR (hollow) partial current densities on the RHE scale (top) and the SHE scale (bottom). Reprinted from Wang et al.[200] Copyright 2018, American Chemical Society.

independence on the SHE scale, essentially overlapping for $CO_2R$ and COR, which corresponds to a positive ∼0.36 V shift on the RHE scale from pH 6.8 to pH 13 (or ∼59 mV per pH unit, as expected). On the other hand, the $C_1$ product ($CH_4$) overpotential shows a pH dependence on the SHE scale, leading to a much smaller shift on the RHE scale of ∼0.15 V. It

was concluded that both field stabilization of a rate-limiting chemical reaction (i.e., CO dimerization) or proton–electron transfer from water during the rate-limiting step are plausible explanations for the pH independence of the $C_{2+}$ pathway on the SHE scale. Then, the complex pH dependence for $CH_4$ was rationalized by a kinetic analysis, which suggested that this pathway is limited by a later proton–electron transfer.[200,212] These findings, which will be discussed in more detail in section 4.2, are in good agreement with Hori's observations (also see section 1 of the SI for a derivation of the RHE-scale pH dependence from Figure 9b). Notably, because the overpotential for $C_{2+}$ products is greatly reduced on the RHE scale, this means that operating in basic electrolytes can lead to a major improvement in energy efficiency for the production of multicarbon compounds from $CO_2R/COR$. Consequently, KOH electrolytes are increasingly being explored as a means to achieve higher selectivity and energy efficiency for $C_{2+}$ products, particularly in vapor-fed systems where $CO_2$ is directly delivered in the gas-phase rather than solubilized in the aqueous electrolyte and diffused to the cathode. These efforts are described in more detail in section 6.3.

While $CO_2R$ has not typically been conducted in aqueous electrolytes with high pH due to the buffering capacity of $CO_2$, understanding the impacts of pH has still been a major area of study due to the dynamic reaction environment at the electrode surface. As discussed in section 2.2, a local pH gradient can develop at the cathode surface due to depletion of protons/production of hydroxide ions from the HER and $CO_2R$. In the $CO_2$/bicarbonate system, $CO_2$ is both a reactant and a buffer, so an increased pH near the cathode surface can cause the concentration of dissolved $CO_2$ to deviate (decrease) from that in the bulk electrolyte. The key equilibria reactions for this system are[2,99,213]

$$CO_{2(g)} \leftrightarrow CO_{2(aq)} \quad K_S = 30 \text{ mM/bar} \tag{10}$$

$$CO_{2(aq)} + H_2O \leftrightarrow H_2CO_3 \quad K_{eq} = 1.7 \times 10^{-3} \tag{11.1}$$

$$H_2CO_3 \leftrightarrow HCO_3^- + H^+ \quad pK_a = 3.6 \tag{11.2}$$

$$CO_{2(aq)} + H_2O \leftrightarrow HCO_3^- + H^+ \quad pK_a = 6.4 \tag{11 = 11.1 + 11.2}$$

$$HCO_3^- \leftrightarrow CO_3^{2-} + H^+ \quad pK_a = 10.3 \tag{12}$$
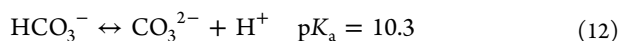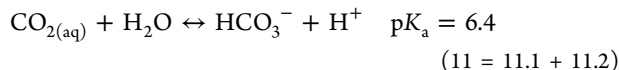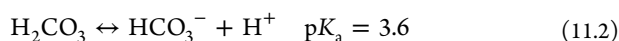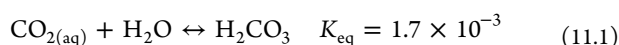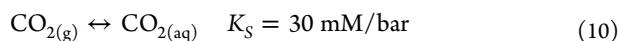
Or in alkaline solutions, these can be written as

$$CO_2 + OH^- \leftrightarrow HCO_3^- \tag{11a}$$

$$HCO_3^- + OH^- \leftrightarrow CO_3^{2-} + H_2O \tag{12a}$$

Reactions 10, 11, and 12 result in $CO_2$ saturated solutions having bulk pH values from around pH 6–8 for bicarbonate concentrations of 0.05–2 M, respectively.[2] The kinetics of $CO_2$ hydration (Reaction 11.1) are slow, and the equilibrium concentration of $H_2CO_3$ is very low.[2,99] However, the nucleophilic attack of dissolved $CO_2$ by $OH^-$ is faster, such that Reaction 11a dominates over Reaction 11 (11 = 11.1 + 11.2) when pH >10.[213] The kinetics for the protonation/deprotonation Reactions 11.2, 12, and 12a are all quite fast, and it can be assumed that $HCO_3^-$ is in equilibrium with $CO_3^{2-}$ at all times.[99] Mathematical models have been us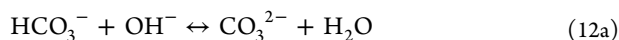ed to solve the relevant diffusion equations, along with the reaction equations for $CO_2$ electroreduction with a given selectivity and

geometric current density, to estimate the interfacial pH and concentrations, many of which are based on the seminal work by Gupta et al. (ref 99).[85,96–99,109,214–217] It has been shown that even modest current densities can cause the interfacial pH to vary significantly from that in the bulk electrolyte, perturbing the reaction thermodynamics and kinetics in several ways.

First, it is worth taking a moment to briefly discuss the impact of pH on the HER. At higher pH where the proton concentration is low, water reduction is expected to dominate over proton reduction. From a thermodynamics standpoint, hydrogen evolution is independent of pH on the RHE scale, and it is irrelevant whether this reaction proceeds via proton or water reduction; in principle, any Brønsted acid can act as a proton donor.[205] However, this can have a huge impact on the kinetics of the HER, as demonstrated by Strmcnik et al. for noble-metal electrodes.[218,219] Furthermore, Grozovski et al. distinguished $H^+$ reduction from $H_2O$ reduction and found their corresponding kinetic parameters using a combination of RDE experiments and modeling.[220] It is expected that the HER proceeds primarily via water reduction under $CO_2R$ conditions.[205] It is also possible that the electrolyte buffer can act as a proton donor, depending on its $pK_a$ value, concentration, and mass transport/availability; this will be discussed in more detail in subsection 3.3.3. While the explicit impact of pH on the HER is still an ongoing area of research, it has been thought that increasing local pH helps favor $CO_2R$ over HER, mainly due to the decreasing overpotential for the formation of $C_{2+}$ products, as discussed earlier. On the other hand, a high local pH shifts equilibria of the acid–base reactions toward (bi)carbonates, which can reduce the concentration of $CO_2$ near the surface, decreasing selectivity toward $CO_2R$ and favoring the HER instead.[96,214]

These contradictory consequences have led to some debate over whether a high local pH is beneficial or detrimental for $CO_2R$ catalysis. Several researchers have proposed that $CO_2$ is still likely to be present under a nonequilibrium high pH owing to its slow hydration kinetics.[85,138,149,221,222] This of course is very dependent on the sufficient transport of $CO_2$ to the surface. However, with this in mind, it seems likely that there is an optimum pH that balances the benefits of increased pH with the slow, disadvantageous decline in $CO_2$ concentration. Indeed, recent modeling studies have found such a volcano-type dependence on pH for $CO_2R$ selectivity (particularly to $C_{2+}$ products) and proposed an optimal local pH range of 9–10.[97,98] At higher pHs, the HER becomes dominant due to mass transport limitations of $CO_2$. Interestingly, in this mass transport limited regime, the activity and selectivity for $C_{2+}$ products plateau and eventually decline, while $CH_4$ production generally increases.[65,96,200] Thus, one can identify when the reaction is limited by $CO_2$ mass transport by observing when the $C_{2+}$ activity plateaus[200] or by increasing mixing at a given potential to see if the $C_{2+}$ selectivity is altered.[208] An example of the latter approach is shown in Figure 11. While it remains unclear how pH itself affects the adsorption energies and coverages of reaction intermediates, especially since these are all also a strong function of potential, it seems likely that *H coverage increases at the expense of *CO in this mass transport limited regime, providing a stronger driving force for hydrogenation of CO to $CH_4$ and a decreased probability of CO coupling to $C_{2+}$ products.[65,215] This hypothesis was further supported by a recent study incorporating microkinetic modeling, which revealed that *CO coverage is gradually
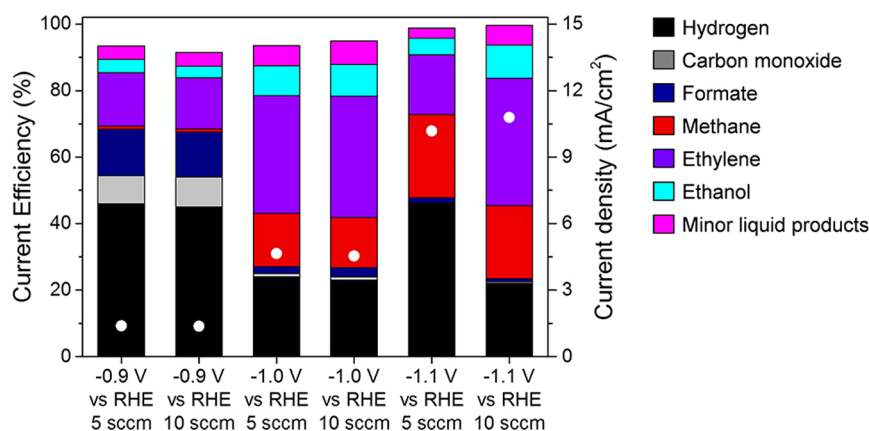
**Figure 11.** Current efficiency (bars) and total current density (dots) for $CO_2$ reduction over Cu(100) at different flow rates of $CO_2$. Under mass transport limited conditions, increased reactant availability will affect the product distribution; thus, this was used to identify under what potentials the reaction is governed by the intrinsic kinetics. Reprinted from Resasco et al.[208] Copyright 2017, American Chemical Society.

depleted as its reduction becomes increasingly favorable with decreasing (more cathodic) potential, and formation rates of $C_{2+}$ products are more drastically impacted due to their second-order dependence on *CO coverage.[212]

Potential-dependent trends can be difficult to discuss in the context of the pH effect. First of all, it is important to realize that if the RHE potential is considered with respect to the bulk pH, then the catalytic overpotential is overestimated under mass transport limited conditions due to the local pH gradient, which can cause errors in mechanistic interpretations.[109,149,205] This has led some researchers to report results on a "corrected RHE" scale that uses the local pH as estimated from mathematical modeling.[217] This has also motivated experimental measurement of the pH at the electrode/electrolyte interface under $CO_2R$ conditions. While this has remained a difficult challenge, there are two recent reports that have attempted to do so using attenuated total reflectance surface-enhanced infrared absorption spectroscopy (ATR-SEIRAS) to measure and correlate the relative intensities of species involved in the buffer equilibria reactions with the local pH near the electrode surface.[148,149] There are a few discrepancies between these studies, as this is an active area of method development, and more work should be done to validate and further advance these techniques.

Second, as discussed in section 2.2, it is also important to keep in mind that the extent of OH⁻ concentration polarization and thus local pH at a given applied potential will differ between catalysts and electrochemical cells. Catalysts with high surface areas will be more susceptible to OH⁻ concentration polarization at lower overpotentials. On the plus side, this likely explains the $CH_4$ suppression and enhanced selectivity to $C_{2+}$ products typically observed on high surface area catalysts, which will be discussed in more detail in section 6. This can also lead to HER suppression by local depletion of buffer species that act as competent proton donors,[221,223] as discussed in subsection 3.3.3. Unfortunately this also causes difficulties comparing potential-dependent $CO_2R$ performance between catalysts with very different roughness factors. This is not only an issue for high surface area catalysts though; even planar catalysts can exhibit different activity and selectivity if evaluated in electrochemical cells with different hydrodynamic boundary layer thicknesses.[100] Therefore, it is important to keep all of these factors in mind when drawing conclusions about potential-dependent activity and selectivity.

Finally, it is worth noting that a gas diffusion electrode (GDE), while not suited for fundamental studies due to a complex interface, can in principle combine the best of both worlds, enabling both high pH conditions and sufficient mass transport of $CO_2$ even with high surface area catalysts. See section 6.3 for further discussion of these vapor-fed systems.

**3.3.2. Cation Effects.** It has been well documented in the literature that electrochemical $CO_2R$ activity and selectivity is influenced by the alkali metal cation in the electrolyte. Initial work by Hori and Murata showed that the selectivity of $CO_2$ and CO reduction on polycrystalline Cu was strongly influenced by cation size, with larger cations increasing the selectivity toward formation of $C_{2+}$ species and decreasing the selectivity for the HER.[224] Since then, a number of reports have confirmed and expanded on these experimental observations.[97,208,214,225,226] While the experimental trends are largely in agreement, there has been some disagreement over the explanation for this effect. Hori and Murata rationalized the change in selectivity with cation size by the difference of outer Helmholtz plane (OHP) potential, based on Frumkin's theory,[227] whereby the OHP potential will shift to more positive values with the degree of specific adsorption, which increases with cation size due to their lower hydration numbers.[224] Recent theoretical work, however, has suggested that specific adsorption of alkali cations is not applicable to the conditions of $CO_2R$,[214] in part due to the very negative reduction potentials of alkali ions calculated on transition metal electrodes.[228] In addition, oxygen reduction studies have shown that alkali cations primarily interact noncovalently, with surface X-ray scattering data suggesting that the cations are not adsorbed and remain partially solvated at the interface.[229,230] DFT calculations demonstrate that solvation increases the favorability of specific adsorption and suggest a low coverage of partially hydrated $K^+$ is thermodynamically favorable under high cathodic potentials and pH conditions.[231] Due to the complex nature of the electrochemical interface, it is difficult to say with certainty to what extent alkali cations interact with the electrode surface. Experimental identification of the mechanism(s) by which cations affect surface electrochemical processes (i.e., via specific adsorption and/or nonspecific interactions) is extremely challenging and remains an open question. We will not distinguish that here and instead simply focus on the potential impacts that cations on/near the surface could have on $CO_2R$.

Electrochemical $CO_2$ reduction potentials are typically more negative than the potential of zero charge (PZC) on low-index facets of Cu (~0.7 V vs SHE),[190] so solvated cations should accumulate on/near the surface of the electrode during reaction. This can block active sites on the surface, alter the binding energy or coverage of reaction intermediates, and/or influence the barriers of elementary steps.[231] The presence of the cation near the metal surface also gives rise to high electric fields of roughly −1 V/Å in the vicinity of the ion (within 5 Å).[232,233] While cations in the bulk of the electrolyte are stable to hydrolysis, electrostatic interactions between the solvated cation and cathode lower the $pK_a$ in the vicinity of the electrode; the magnitude of this decrease in $pK_a$ increases with larger alkali cation size and larger cathodic potentials.[214] Thus, it was proposed that this allows larger cations to act as a pH buffer, offsetting the increase in local pH induced by concentration polarization and restoring the local $CO_2$ concentration closer to the bulk value.[214] This theoretical model matched their experimental measurements, but it must be noted that the experiments were performed under strong mass transport limitations. Thus, this model does not explain the fact that increasing activity and selectivity to $C_{2+}$ products are observed both at lower overpotentials when not in a concentration polarized regime, as well as during COR, which does not have the same dependence of reactant concentration on pH.[208,226]

Two recent studies have instead suggested that the primary role of the cation is to act as a promoter, stabilizing certain $CO_2R$/COR intermediates on the surface that have favorable electrostatic interactions with solvated cations.[208,226] Specifically, cation-created electrostatic field stabilization decreases the energy for $*CO_2$ adsorption, the precursor to $2e^-$ products, and C−C coupling to form $*OCCO$ or $*OCCHO$, possible precursors to $C_{2+}$ products.[208] This explains the trends observed not only for Cu, but is also consistent with $CO_2R$ selectivity enhancements to $2e^-$ products observed on Ag[208,214,234] and Sn.[208] This alone, however, does not explain the observed trend with cation size. For that, DFT calculations by Resasco et al. revealed that larger hydrated cations are more energetically favored at the outer Helmholtz plane than smaller ones, which suggests that a higher concentration of cations will accumulate with increasing cation size leading to a larger local electric field.[208] The same researchers then provided support for this hypothesis by conducting experiments in mixed electrolytes, which showed that only a small percentage of the larger cations is needed to observe their influence on the intrinsic rates of formation of certain reaction products (e.g., ≤1 order of magnitude increase in partial current densities for $C_2H_4$, $C_2H_5OH$).[208] A recent study using attenuated-total internal reflection Fourier-transform infrared (ATR-FTIR) spectroscopy has provided further evidence for this cation promotion effect, as it was found that with increasing cation size, surface-adsorbed CO molecules experience a greater interfacial electrostatic field that accelerates its reduction kinetics and acts to shift the C≡O stretch frequency to lower energies.[137]

Future work in this area could expand on the findings for these monovalent alkali cations by investigating the impacts of divalent or trivalent cations. For example, $CO_2R$ rate increases have been observed over a Cu−Sn−Pb alloy cathode as the size and surface charge of the cation in the supporting electrolyte increases from $Na^+$ to $La^{3+}$.[235] There has also been some interest in the use of ionic liquids for $CO_2R$ after initial

reports showed increased selectivity to CO at low over-potentials on Ag, $MoS_2$, and Pt electrodes.[236−238] It has been hypothesized that the presence of ionic liquids can stabilize reaction intermediates, help bind the $CO_2$ molecule, and/or suppress the HER by blocking active sites on the surface. While this could be a promising avenue to explore, we offer a word of caution, as it has also been found that the ionic liquids break down during $CO_2R$,[239,240] which can cause difficulties with product detection and limit its practicality for (re)use at scale. Finally, in moving toward practical $CO_2$/CO electro-lyzers, which will likely be vapor-fed reactors that employ GDEs, we will need to carefully consider how to engineer the ionomer/membrane moieties to promote stabilization of intermediates in a similar manner to the cation effects discussed here.

**3.3.3. Anion Effects.** The vast majority of $CO_2$ reduction catalysis has been studied in $KHCO_3$ electrolytes due to the $CO_2$-(bi)carbonate-water equilibrium, which helps maintain a neutral bulk pH. As a result, the impacts of the electrolyte anion have been studied to a lesser extent. Hori and co-workers presented results for constant current electrolysis in various electrolyte solutions, which showed that hydrocarbons and alcohols are the preferred products in KCl, $KClO_4$, $K_2SO_4$, and dilute $KHCO_3$ solutions, while $H_2$ formation dominates in $K_2HPO_4$ solutions.[83,85] These findings were explained in terms of a nonequilibrium local region of high pH close to the electrode. As discussed earlier, $OH^-$ ions are released during electroreduction, which can be neutralized by $HCO_3^-$ or $H_2PO_4^-$. Thus, in the nonbuffering electrolytes or in dilute $KHCO_3$, there is likely insufficient neutralization leading to a rise in pH, which favors $CO_2R$ over HER and $C_{2+}$ over $C_1$ products.[83,85] Other studies on the impact of $KHCO_3$ concentration have mirrored these trends, showing that with increasing anion concentration the rates of hydrogen evolution and methane production increase, again pointing to local pH effects as the cause.[109,241]

A recent report, however, found that the changes in pH near the electrode surface were insufficient to explain differences in activity and selectivity observed with changes in anion buffering capacity; instead, it was proposed that these differences result from the ability of buffering anions to donate hydrogen directly to the electrode surface.[217] While water is expected to be the proton source under $CO_2R$ conditions, it is possible that buffering anions can serve as proton donors given the lower $pK_a$ values compared to water. Thus, products where the rate-limiting step involves a proton transfer ($H_2$ and $CH_4$) will be impacted by changes in the hydrogen source. Accordingly, it was found that $H_2$ and $CH_4$ activity increased (≤1 order of magnitude) with decreasing $pK_a$ of the buffering anion and were not impacted by nonbuffering anions, while formation of CO, $HCOO^-$, and $C_{2+}$ products were insensitive to anion identity.[217] This suggests that the buffering anions can serve as competent proton donors, with their effectiveness increasing with decreasing $pK_a$. The impact was less pronounced once the local pH (as determined by mathematical modeling) was taken into account by plotting the activities on a calculated RHE scale; future studies should seek to test these effects over a wider range of potentials in case transport effects were also playing a role. Interestingly, this could still shed some light on one mechanism by which $H_2$ evolution may be suppressed during $CO_2R$; depletion of $HCO_3^-$ under basic conditions could impose mass transport limitations for the HER and limit the ability for this buffer to serve as a proton

donor.[221,223] Especially for mesoporous electrodes with high RFs and inhibited diffusion, this could serve to slow the rate of HER until sufficient overpotential to drive the sluggish water reduction kinetics is achieved.

In addition to bicarbonate serving as a pH buffer and proton source, recent studies have also discussed the possibility of bicarbonate serving as a $CO_2$ source.[118,138,139] Using a combination of in situ spectroscopic analysis (ATR-SEIRAS) and isotopic labeling, along with mass spectroscopy (MS) or potential stepping techniques, two reports proposed that the $CO_2$ source during $CO_2R$ is $CO_2$ in equilibrium with bicarbonate anions instead of free $CO_2$ molecules supplied to the solution.[118,139] This hypothesis, however, relies on the critical assumption of fast equilibrium between $CO_2$ and bicarbonate, which may not be the case since rate constants for the other equilibrium reactions are several orders of magnitude larger.[138] With the increasing trend of in situ spectroscopic analysis during $CO_2R$, the role of bicarbonate is an active area of research; thus, continued work should be done to further elucidate the $CO_2R$ reaction mechanisms in bicarbonate electrolytes.

Finally, it is also worth noting that there have been various studies on the influence of halide ions on Cu electrochemistry.[94,95,116,242−249] Some reports suggest that there will be specific adsorption of these anions on the Cu surface, which could alter the charge density and selectivity for $CO_2R$ products, as well as aid in suppression of the HER.[243−248] However, many studies show that the presence of halide ions primarily leads to changes in the Cu surface structure and morphology; in particular, oxidation−reduction cycles in the presence of halide ions has been one strategy used to increase selectivity to $C_{2+}$ products, such as $C_2H_4$ (see section 6 for further discussion).[94,95,116,242,243,248,249] Thus, it is currently unclear what the dominating effect(s) of employing halides are, so this represents another area for future studies aimed at better understanding ionic interactions during $CO_2R$ catalysis.

## 3.4. Electrochemical Conditions

In addition to electrolyte effects, several studies outline the importance of the electrochemical cell design, components, and operating conditions.[87,96,250] While an in-depth discussion of these topics is outside the scope of this Review, there are a few considerations and trends that we will touch upon here. Most $CO_2R$ studies to date have been conducted under ambient temperature and pressure, but these factors have also been explored to manipulate the local reaction conditions. Here we will briefly discuss some of the trends observed under nonambient environments.

### 3.4.1. Temperature and Pressure.
From Henry's Law and the acid/base buffer equilibria ($CO_2/HCO_3^-/CO_3^{2-}$), it is understood that increasing the concentration of dissolved $CO_2$ in the electrolyte can be achieved by decreasing temperature or increasing pressure (see Figure 12).[2,101,102,109,251−254] As a result, several studies have looked at varying the temperature[82,101,103,161,251−254] and pressure[101,102,109,200,225] during $CO_2R/COR$. In general, it is difficult to draw direct comparisons between these limited studies due to the use of different electrolytes, applied voltages, techniques (galvanostatic vs potentiostatic), and temperature/pressure ranges. However, a few high level trends can be extracted from their findings. Across the board, decreasing temperature was found to increase selectivity to $CH_4$.[82,101,103,161,251−254] Trends for the other products are not as clear, although some results do
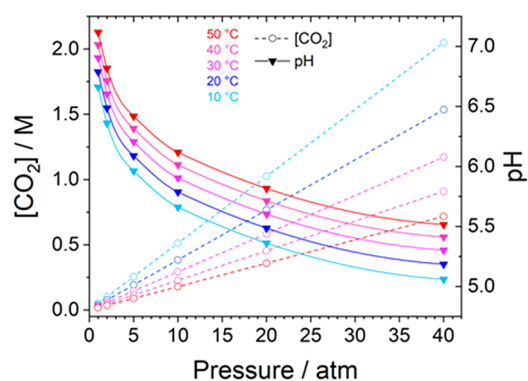
**Figure 12.** Effect of pressure and temperature on the pH and concentration of dissolved $CO_2$ in 0.1 M $KHCO_3$ electrolyte; based on work by T. Hatsukade.[255]

show an increased production rate of $C_2H_4$[82,103] and/or $CO$[82,254] at higher temperatures. The rate of $H_2$ evolution was found to be suppressed at lower temperatures and greatly enhanced at higher temperatures.[82,101,251,252,254] The overall rate of $CO_2R$ was impacted by temperature to a lesser degree,[101] with some studies finding minimal changes in the total partial current density for $CO_2R$ below room temperature[4,103,104] and modest increases in reaction rate above room temperature.[103,254] This leads to overall higher selectivity for $CO_2R$ at lower temperatures, and lower selectivity at higher temperatures where the HER becomes dominant. The reasons for these temperature effects are not entirely clear; changes in temperature affect the $CO_2$ solubility, thermal diffusion rates, pH, and solution resistance, and may also alter adsorption equilibria. More detailed studies are needed to better understand the impact of temperature on $CO_2R$ product selectivity over a broader range of potentials.

As $CO_2$ or CO pressure decreases below 1 atm, the HER is dominant and minimal $CO_2R/COR$ is detected.[200,225] Meanwhile, with increased pressures, the total $CO_2R$ current generally increases (with the exception of the highest pressures in Hara et al.,[102] where there is significant missing Faradaic efficiency in their galvanostatic experiments at 40 and 60 atm).[101,102,109] These trends are likely due in large part to the changes in dissolved concentration of $CO_2$ with pressure. Interestingly, one study found that $C_2H_4$ selectivity increased with increased pressure, which was attributed to an increase in local CO concentration and surface coverage.[109] Again, more systematic studies are needed to better understand the impact of pressure over a broader range of potentials and conditions. While operation of $CO_2R$ under ambient temperature and pressure has been discussed as a potential advantage of electrochemical $CO_2$ recycling compared to other processes, we should not limit the scope of study to ambient conditions. Altering temperature and pressure remain areas ripe for further investigation, both to gain increased mechanistic understanding of electrochemical vs chemical steps and for identifying operating conditions that achieve optimal activity and selectivity for $CO_2R$ to desired product(s).

## 3.5. Summary

Electrochemical $CO_2$ reduction on copper is a complex reaction involving multiple steps, intermediates, and reaction pathways. It is also highly sensitive to many factors from the atomic scale to the reactor scale including the electrode surface structure and morphology, electrolyte pH and identity/

quantity of ions present, degree of mass transport, temperature, pressure, etc.

Single crystals and oriented surfaces represent useful tools to study the impact of crystal facet on $CO_2R$ performance of Cu electrodes. In particular, interesting trends in product distribution have been reported as a function of surface structure. Among the planar surfaces, Cu(100) was shown to yield a particularly high ethylene/methane ratio, and the selectivity toward ethylene could be further improved by adding steps to the surface.[151−153,158] These findings can help provide design principles to steer the selectivity of catalyst materials toward important products. On the other hand, no significant trends in activity have been reported. This could be due to defects or step sites existing on the surface and/or formed *in situ*, leading to similar overall activity on all the Cu single crystal surfaces investigated. We would like to emphasize the need for more quantitative data from oriented surfaces, preferably of single crystal quality, as a function of potential. This is vital in order to obtain further mechanistic information, which can lead to identification of key parameters that can be optimized to steer selectivity and activity toward desired products.

At the same time, it is also important to keep in mind that the crystallographic orientation of the surface of single crystal electrodes can differ from their bulk orientation. Some reports indicated that the surface structure of the electrodes was strongly dependent on the choice of pretreatment procedure,[152,171] while others showed that certain electrodes tended to restructure under reaction conditions.[172,173,178−181] While the causes for restructuring require further investigation, some likely reasons include effects from the presence of CO, the negative applied potentials, or other factors from the local reaction environment, such as electrolyte effects. We emphasize that phenomena exhibited by crystals or films oriented in a specific direction may not originate from the bulk orientation, but rather from the defects present at the surface, as illustrated in Figure 7; as such, scientists should be cautious in making direct comparisons between the results from experiments on single crystals to DFT-based models. In addition, due to the complications we discussed above, we strongly recommend that future studies of single crystals and other oriented systems investigate the structural properties the electrodes *in situ/operando* whenever possible.

The electrolyte presents several variables that can be used to tune $CO_2R$ activity and selectivity. In particular, the impact of pH is a complex subject that causes several competing effects on the local reaction environment. A high interfacial pH is beneficial for increasing selectivity toward $CO_2R$ and reducing the overpotential required to form desirable $C_{2+}$ products on an RHE scale; it becomes a detriment, however, when there is insufficient mass transport of $CO_2$, and the acid−base equilibrium between $CO_2$, $HCO_3^−$, $CO_3^{2−}$, and $OH^−$ causes a significant decrease in the local $CO_2$ concentration. The extent of concentration polarization is determined by the overall flux of species both to and from the electrode surface. This depends not only on the degree of mixing within an electrochemical cell, which impacts the hydrodynamic boundary layer thickness, but also the overall reaction rate (current density), which is impacted by the surface area of the catalyst. We strongly recommend that conclusions about intrinsic activity and selectivity only be drawn from data that is not significantly impacted by mass transport effects.

The electrolyte cation and anion also play important roles in the catalysis. Experimental trends for $CO_2R$ on Cu have consistently demonstrated increased activity and selectivity for $C_{2+}$ products with increasing alkali cation size, although the hypotheses behind these effects have evolved over time.[97,208,214,224−226] By combining theoretical and experimental methods, greater mechanistic insights have been obtained. While the extent and mechanism of alkali cation interaction with the surface is still an open question, the localized electrostatic fields they create is proving to be a critical factor impacting $CO_2R$ activity and selectivity. Indeed, DFT calculations reveal that cation-created field effects are crucial for $CO_2$ activation on weak binding surfaces[232] and CO dimerization on Cu at room temperature.[233] Anion effects have often been discussed in relation to the local pH at the electrode surface,[83,85,109,241] but it has also been proposed that buffering anions can donate hydrogen directly to the electrode surface, which increases the rates of $H_2$ and $CH_4$ formation.[217] Recent studies have additionally discussed the possibility of bicarbonate serving as a $CO_2$ source, but further work is needed to determine the extent to which this may occur. Finally, temperature and pressure represent additional levers by which to tune the catalysis since the concentration of $CO_2$ in the electrolyte can be increased via increasing pressure or decreasing temperature; in addition, these electrochemical conditions may also alter adsorption equilibria and diffusion rates. While some trends in product selectivity have been observed, this remains an area in need of further systematic investigations.

In summary, in this section we discussed how a variety of different experimental factors can impact $CO_2R$ on Cu, the mechanistic insights that have been gained from studying them, and how they can be tailored to optimize activity and selectivity to desired product(s), including areas for future study. In the next section we will build upon these experimental findings and take a more in-depth look at the complementary theoretical descriptions of $CO_2R$ on Cu and how these methods have helped shape our mechanistic understanding of the factors governing $CO_2R$ activity and selectivity.

## 4. THEORETICAL STUDIES ON COPPER

In recent years, developments in *ab initio* methods for the simulation of surface and electrochemical reactions have enabled theoretical mechanistic investigations and theory-guided catalyst design.[57] Electrochemical $CO_2$ reduction is particularly challenging due to the complex reaction networks and the importance of activation energies and cation effects.[168,232] In what follows, we provide an introduction to state-of-the-art modeling approaches for electrochemical processes and discuss the major conclusions, controversies, and open challenges in recent work.

### 4.1. Introduction to Theoretical Approaches

Modeling electrochemical interfaces from an atomistic perspective presents many open challenges. In general, the thermodynamics for electrochemical reactions are relatively simple to obtain with the computational hydrogen electrode model,[256] which relies on calculations of adsorption energies and a $H_2$ gas reference to account for the free energy of proton−electron pairs, i.e., $\mu(H^+) + \mu(e) = \frac{1}{2}\mu(H_2) - eU$, where $U$ is the potential vs the reversible hydrogen electrode

(RHE). For a proton−electron transfer to *CO to form *CHO, for instance, the corresponding free energy change is

$$\Delta G = \mu(CHO^*) - \mu(CO^*) - \left[\frac{1}{2}\mu(H_2) - eU\right] + \Delta G_{solv}$$
$$+ \Delta G_{field} \quad (13)$$

where $\Delta G_{solv}$ and $\Delta G_{field}$ refer to contributions of solvation and field.[257,258] For a given reaction step, a thermodynamic limiting potential $U_L$ can be determined, which is defined as the potential at which a reaction step becomes exergonic, where $\Delta G = 0$. For a reaction pathway, the corresponding limiting potential is given by that of the step with the highest reaction free energy. This approach has been applied to a mechanistic analysis of CO₂R pathways toward C₁ products on stepped Cu(211), and $U_L$ for various products have been shown to be correlated with experimental onset potentials on polycrystalline copper.[201] Likewise, the onset potentials for $CH_4$ or $CH_3OH$ across polycrystalline transition metals have been shown to follow trends in the corresponding $U_L$.[57]

While a thermodynamic analysis using the limiting potential $U_L$ as a key metric has shown mechanistic insight and correlation with experimental data on transition metals, this presents only a necessary but insufficient criterion for activity. Determination of activation energies allows for turnover frequencies to be evaluated as a function of potential. Surface hydrogenation barriers (i.e., Langmuir−Hinshelwood type) through an adsorbed *H, where electron transfer has already occurred, are easy to determine in vacuum, but electrochemical barriers (sometimes referred to as Eley−Rideal[259] type) are considerably more challenging. In addition, as discussed in section 3.3, ion and solvent effects have been shown to be important factors determining activity and selectivity toward various products. The investigation of electrochemical activation energies and the resultant kinetics and selectivities require models that explicitly account for the potential, solvent, and ions, where much method development is ongoing and where considerable variations exist in the energetics for similar processes determined using different approaches. In recent years, CO₂R energetics have been studied theoretically using implicit solvent models that include a continuum description of the ions,[260,261] explicit solvent models where water and ions are considered atomistically,[168,259] and also a H-shuttling approach[261−263] where a water molecule shuttles protons from the surface and back. We will first briefly summarize these different theoretical approaches.

**4.1.1. Implicit Models.** In general, the inclusion of solvent molecules and ions adds many extra degrees of freedom and computational time relative to vacuum|metal calculations for determination of activation barriers. Implicit solvent models apply a continuum model of the electrolyte, which corresponds to a negligible increase in computational time. The charge at the interface can be varied continuously, such that the potential is easily tuned. While simple and computationally cheap, these models present several challenges. One of the most widely used implementations of the implicit method makes use of a simple linearized Poisson−Boltzmann distribution of the ions,[264] which does not account for effects of finite ion size and has been suggested in classical models to lead to unphysical interfacial capacitances.[265] The potential of zero charge (PZC) has been proposed as a benchmark for these methods;[260,266] however, since PZCs and metal work functions are correlated,[265] the agreement between exper-

imental and theoretical PZC may reflect the accuracy of generalized gradient approximation (GGA) functionals in the determination of metal work functions more than the description of the solvent. Such a benchmark also does not evaluate the accuracy of the reaction energetics, where solvation or cation interactions can have a significant effect. Finally, a fundamental challenge associated with implicit solvent simulations at constant potential is that the ions are modeled to adiabatically follow the shifts in dipoles associated with a reaction event. These two processes, however, occur on very different time scales.[267,268] The effect of such an assumption on the energetics has not been evaluated against explicit models.

**4.1.2. Explicit Models.** Explicit solvent methods allow for an atomistic level picture of solvation and cation effects, but at the expense of significantly increased computational cost and the introduction of other challenges. Since ions are modeled explicitly and within finite-sized unit cells, the potential is not continuously variable. Proton−electron transfer processes modeled in finite-sized unit cells also give rise to significant shifts in the potential along the reaction pathway. These issues can be mitigated using a capacitor model of the interface, which allows for the extrapolation of calculated barriers to the limit of infinite cell sizes, corresponding to the constant-potential limit.[269,270] State of the art GGA-level functionals predict a poor band alignment of solvent HOMO, LUMO with the metal Fermi level, which can give rise to artificial charge transfer across the interface and corresponding effects on the reaction energetics.[271] Unrelated to band alignment is the partial charge of hydronium ions at the Helmholtz plane arising from overlap of solvent and metal charge, which affect the reaction energetics.[272] Transition states have been determined using either nudged elastic band (NEB)[168,273] or metadynamics and potential of mean force;[259,274] the latter method includes entropic contributions from solvent reorganization, but at an increased computational cost.

**4.1.3. H-Shuttling Model.** An alternative to full explicit solvent models has been put forth by Janik et al.[262,263,275] In this approach, a water molecule is used to shuttle an adsorbed *H from the surface to the adsorbate (Figure 13). This shuttling process is considered to provide an estimate of the associated proton−electron transfer barrier. The potential vs RHE for the process is assumed to correspond to that where *H in the initial state is equilibrated with a proton−electron pair, as determined using the computational hydrogen
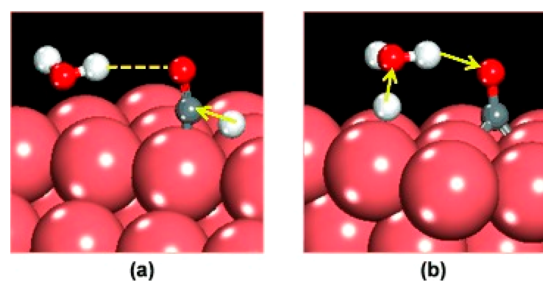


**Figure 13.** Water shuttling model for proton−electron transfer to *CO to form (a) *CHO and (b) *COH. A single water molecule is included to shuttle an adsorbed *H and mimic proton−electron transfer from solution. It was found that *CHO formation occurs through direct transfer of *H to the *CO. Reprinted with permission from Janik et al.[263] Copyright 2013, John Wiley and Sons.
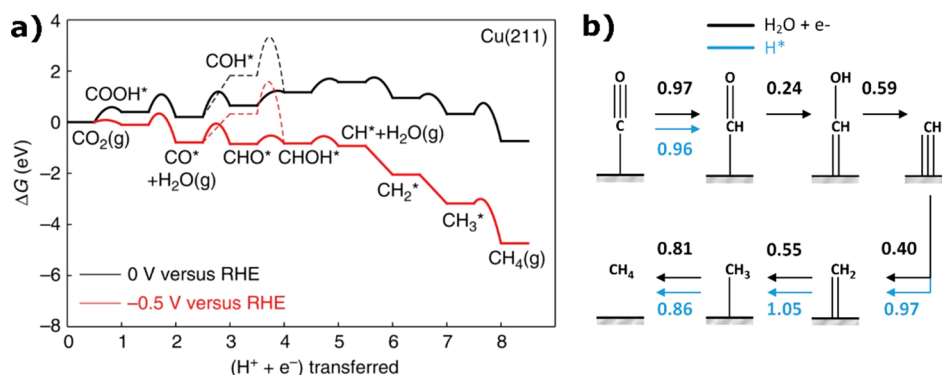
**Figure 14.** (a) Free energy diagram of $CO_2R$ to $CH_4$ on Cu(211), model system for Cu steps. Reprinted from Liu et al.[168] This work is licensed under a Creative Commons Attribution 4.0 International License (https://creativecommons.org/licenses/by/4.0/). (b) Reaction intermediates toward $CH_4$ determined on Cu(100). Reprinted with permission from Cheng et al.[259]

electrode. In contrast to explicit solvent calculations, potential shifts along the reaction pathway arising from shifts in charge are not considered. The transfer coefficient is assumed to be 0.5 plus a correction determined by shifts in the dipoles of the adsorbates. While the simplicity of this approach is compelling, the assumptions should be evaluated with more detailed models.

## 4.2. Theoretical Insights

In general, thermodynamic analyses in the current literature have been performed using the computational hydrogen electrode model. The choice of functional, pseudopotentials, and the treatment of solvation should all affect the energies, but resultant trends and energies reported by different groups do not differ significantly (e.g., the similarity in trends in energetics of Cu(111) intermediates from refs 262,276). Theoretical electrochemical activation energies, on the other hand, widely differ with approach, due to the differences in the simplifying assumptions made in modeling the electrochemical interface. Tables S2, S3, and S4 summarize, respectively, the activation energies for key $CO_2R$ to CO, initial CO reduction, and C–C coupling steps determined using various methods, and, where available, their transfer coefficient $\beta$ and the barrier for the corresponding surface hydrogenation process. These tables can be found in section 3 of the Supporting Information (SI). In this Review, we assume the criterion for facile kinetics to be a turnover frequency of 1/s per site, which corresponds to approximately a 0.75 eV barrier at room temperature,[277] and we have reported the barriers at 0 V vs RHE wherever possible. In reporting barriers determined with H-shuttling, we considered the transfer of *H through $H_2O$ to be classified as electrochemical (i.e., involving electron transfer) and a direct transfer of *H as a surface hydrogenation. Overall, the differences in energetics and resultant mechanisms reported point to the importance of evaluating the assumptions made in the models of the electrochemical interface. In what follows, we discuss general insights and controversies in current theoretical investigations of $CO_2R$ on Cu.

### 4.2.1. Trends in Electrochemical Barriers. One of the general insights from existing theoretical investigations is the trends in activation energies for proton–electron transfer toward different intermediates, which, given the complexity of $CO_2R$ pathways toward the many possible products (as shown later in section 5, Figure 18), provides some qualitative guidance in the search for rate-determining steps. Using an explicit solvent model and NEB barrier calculations on various

transition metals, proton–electron transfers to oxygen ends of reaction intermediates were found to be in general facile, while those to carbon or those involving C–O bond scission are more difficult.[273] Similarly, metadynamics[259] with explicit solvent and H-shuttling[263,275] barrier calculations found that oxygen atoms are hydrogenated primarily through electrochemical vs direct *H transfer steps.

### 4.2.2. CO as a Crucial Intermediate. The pathway toward CO has been analyzed with several methods, as tabulated in Table S2. On Cu(111), both explicit solvent with NEB transition state search[168] and H-shuttling methods[262,263] find the activation energies for $CO_2$ reduction to *CO to require low overpotentials to reach the 0.75 eV threshold for facile kinetics. On Cu(100), H-shuttling models[275] report less surmountable barriers than explicit solvent with metadynamics,[278] which give a net barrier of 0.8 eV for $CO_{2(g)}$ to *COOH at −0.4 V vs RHE; the reason for this discrepancy may be differences in solvation or the simplifying assumptions behind the H-shuttling model. Overall, a facile path toward CO is consistent with experimental reports that both CO and $CO_2$ reduction give similar product distributions, suggesting CO to be a key reaction intermediate in $CO_2$ reduction, as discussed earlier in subsection 3.2.1. Formate, on the other hand, was shown to be a dead end, given that the free energy difference from *OCHO to *$OCH_2O$ is 1.6 eV.[201] This theoretical result is consistent with experiments using $HCOO^-$ as a feedstock, which gave no detectable products.[85]

### 4.2.3. Pathway toward Methane. Using explicit water models, barriers determined using NEB and metadynamics suggest identical reaction intermediates from CO to $CH_4$ on stepped Cu(211)[168] and Cu(100)[259] at pH 7, respectively. The free energy diagram for Cu(211) is shown in Figure 14a, and the reaction species determined on Cu(100) are shown in Figure 14b. In this pathway, *CO to *CHO is the rate-determining step, which is followed by a series of proton–electron transfers to form *CHOH, *CH, *$CH_2$, *$CH_3$, and $CH_4$. In contrast to a purely thermochemical analysis,[201] *$CH_3O$ is not found to be an intermediate toward $CH_4$ due to the insurmountable barrier for proton–electron transfer to *$CH_3O$ to form $CH_4$ + *O.[263,273] It must be noted that crucial differences exist between pathways determined by explicit and H-shuttling models. Whereas explicit methods[168,259] suggest that all steps following *CO are proton–electron transfers on Cu(211) and Cu(100), H-shuttling calculations suggest that *CHO is formed through a direct transfer of *H on both Cu(100) and Cu(111).[262,279] On Cu(111), H-shuttling in

conjunction with implicit solvent[261] and explicit water[168] methods suggest a *COH and *CHO intermediate, respectively. (Note: Goddard et al. consider the surface hydrogenation to *CO to form *CHO to be favored vs the associated proton transfer, and report barriers of 0.96 and 0.97 eV (at −0.59 V vs RHE) respectively. However, the latter electrochemical barrier would go down substantially with decreasing potential, assuming a usual $\beta \sim 0.5$.)

**4.2.4. CO Dimerization.** Pathways toward $C_{2+}$ products are considerably more complex and present more controversy among theoretical studies. Adding to this complexity is that certain $C_{2+}$ intermediates with large dipole moments are dramatically affected by the fields induced by cations at the interface, which add additional degrees of freedom affecting the energetics (see Figure 15). Both vibrational spec-
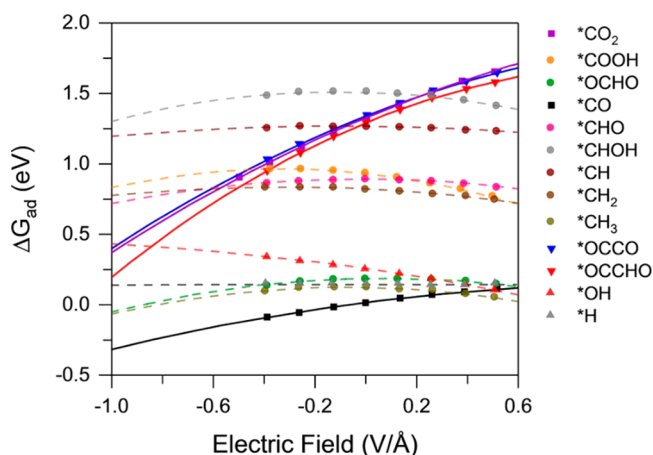


**Figure 15.** Field effects on various $CO_2R$ intermediates on Cu(111). The energy of each adsorbate as a function of field strength is obtained by applying a uniform electric field oriented perpendicular to the slab. Adsorbates that are most stabilized by field are *$CO_2$, *OCCO, *OCCHO. Reprinted from Resasco et al.[208] Copyright 2017, American Chemical Society.

tra[133,144−147] and kinetic models[168,260] suggest *CO to be present on Cu under $CO_2$ and CO reduction conditions, and the coupling of 2 *CO to form a *OCCO dimer has been studied using several approaches. It was found that *OCCO on Cu(100), (111), and (211) have insurmountable dimerization

barriers (>1 eV) in vacuum, but water solvation and cation effects together stabilize the *OCCO relative to 2 *CO such that dimerization becomes facile.[233,280−282] Further, it was found that Cu(100) and stepped (211) exhibit lower barriers than Cu(111).[282] Implicit solvent models with a continuum ion distribution should also provide a field-induced stabilization, though the charge and field distribution would not be as localized as in the case of an explicit cation; Head-Gordon et al. report a dimerization barrier of only 0.53 eV at 0 V vs RHE on Cu(100) in the presence of a continuum distribution of charge in the solvent.[260] Overall, the sensitivity of the energetics of this step to water solvation and cation-induced fields likely contributes to the tremendous variation in reported CO dimerization barriers on Cu facets: 0.53 to 1.3 eV on Cu(100), and 0.89 to 1.7 eV on Cu(111) (see Table S3 in SI).

**4.2.5. $C_2$ Pathways.** Beyond *OCCO, the determination of $C_2$ mechanistic pathways and their facet dependence presents an open challenge, with different methods reporting different mechanisms. These differences point to the importance of method development and benchmarking efforts in *ab initio* simulations of the electrochemical interface. Vacuum calculations on Cu(211) suggest that coupling barriers tend to decrease with increasing hydrogenation of the coupling species,[280] and that the pathway to acetaldehyde and ethanol is thermodynamically downhill from *OCCHO.[90] With vacuum|metal calculations on Cu(100), a *OCCOH to *OCC pathway was found to be thermodynamically favored after *CO dimerization.[283] Likewise, this pathway was found to be dominant in an *ab initio*, explicit solvent study on Cu(211), despite the difference in the treatment of the interface and in the facet.[212] An analysis with the H-shuttling model suggests that pure Cu(100) facets do not have facile barriers to form $C_2$ products, and it is concluded that reconstruction of the surface is required for C−C coupling.[275] However, these calculations were performed without cations and a full solvent layer, both of which can stabilize some crucial intermediates in the processes considered. An implicit solvent study on Cu(100) found *OCCHO to be a critical intermediate toward $C_{2+}$ products, with *OCHCHO found to be the precursor to acetaldehyde and ethanol, and *COCHOH the precursor to ethylene.[207] The former is in line with experimental observation that OCHCHO (glyoxal) can be reduced to acetaldehyde and ethanol.[112,208] Finally,
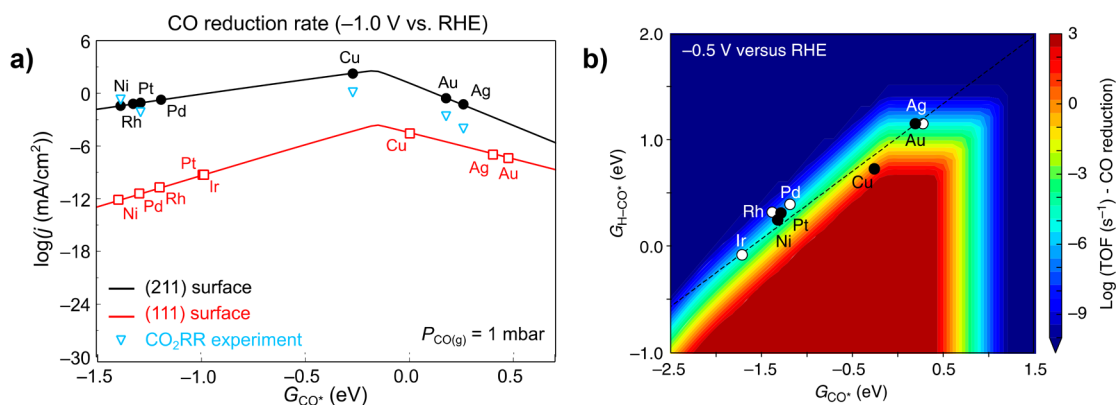


**Figure 16.** (a) Kinetic volcano for CO reduction to $CH_4$ on transition metals. $CO_2R$ Experiments from Kuhl et al.[203] A 1 mbar CO pressure was assumed in the kinetic model to compare CO and $CO_2R$ rates. (b) 2D volcano reflecting the dependence of activity on H−CO transition state and CO scaling. Both figures are reprinted from Liu et al.[168] This work is licensed under a Creative Commons Attribution 4.0 International License (https://creativecommons.org/licenses/by/4.0/).

explicit solvent simulations with metadynamics on Cu(100) suggest that, at low overpotentials, $C_{2+}$ products are formed through CO dimerization and subsequent proton–electron transfers toward *HOCCOH[259] (vs the *OCC intermediate proposed by ref 283). At high overpotentials, it is assumed that adsorbed *H saturates the surface such that *OCCHO is formed through 2 Eley–Rideal steps of $CO_{(g)}$ + *H → *CHO, then *CHO + $CO_{(g)}$ → *OCCHO.[259] We note, however, that the barrier reported for the first Eley–Rideal step is insurmountable at room temperature at 1.01 eV. Microkinetic models also suggest that at steady state the *CO coverage continues to dominate over *H, even down to −1 V,[168,260] and *CO has been observed with vibrational spectroscopy down to such potentials.[146]

**4.2.6. Kinetics.** Given the challenge of determining electrochemical activation energies, few mean-field kinetic models of CO reduction have been reported in the literature.[168,212,260] Kinetics provide insight into rates, selectivities, intermediate coverages, and competition among different pathways, all as a function of reaction conditions. However, since rates depend exponentially on energies (i.e., $r \sim \exp(-E_a/kT)$), large uncertainties are expected in predicted rates. For example, only a 0.1 eV uncertainty in a barrier translates to over an order of magnitude uncertainty in rate at room temperature. Trends in general are therefore considered to be more reliable than absolute rates.

Recently, a kinetic model for CO reduction to $CH_4$ on transition metals was developed.[168] Based on the reaction pathway on Cu(211) (Figure 14a), it was assumed that the proton–electron transfer from *CO to *CHO is the limiting step for CO reduction on all transition metals. Scaling relations for the H–CO transition state and the corresponding kinetic activity volcano for CO reduction to $CH_4$ were determined on (111) and (211) surfaces (see Figure 16). Adsorbate–adsorbate interactions, which come into play on metals that bind as strongly as Cu or more, were included with a first-order adsorbate interaction model.[284] The stepped facet was found to be considerably more favorable for *CO protonation than flat ones, owing to the ease of *CO rotation and also the accessibility of the C end to proton transfer from the solvent. Stepped facets were therefore predicted to give orders of magnitude higher rates than flat ones.[168] In fact, it is suggested that only a small fraction of stepped sites can account for the experimentally determined activity of polycrystalline transition metals,[203] which are overlaid in Figure 16a.[168] Cu already lies close to the peak of the activity volcano for materials that follow transition metal scaling, due to its intermediate *CO binding energy. Based on this analysis, two design criteria for active CO reduction catalysts were proposed: (i) stabilization of stepped sites and (ii) stabilization of the *H–CO intermediates for a given *CO binding energy.[168] The corresponding contour plot of activity based on *H–CO and *CO energies is given in Figure 16b. We note that the predicted significantly higher activity of steps has yet to be demonstrated experimentally, although studies of both single crystal[1] and epitaxial films[157] do suggest roughly an order of magnitude variation in activity among different facets. Step poisoning, undercoordinated surface defects, and/or surface reconstruction may contribute to this discrepancy between experimental and theoretical results, as discussed earlier in section 3.1.

The $C_2$ kinetic model of Head-Gordon et al.[260] considers the initial C–C coupling steps, with energetics determined through an implicit solvent model. The coupling barriers for CO dimerization were found to slightly increase with more cathodic potential, such that the dimerization pathway shuts down in favor of CO–CHO coupling at high overpotential. The resultant kinetics suggested a decrease in $C_{2+}$ products at moderate overpotentials, consistent with DEMS experiments on Cu(100).[163] This picture is in contrast with an atomistic picture, where cation concentrations, and therefore CO dimerization rates, should increase with decreasing potential. The physical origin of these effects and the differences between conclusions obtained through implicit and explicit approaches requires further evaluation.

**4.2.7. Rate-Limiting Electron Transfers.** Rate-limiting electron transfers in $CO_2$ reduction has been a recurrent and contentious theme in the current theoretical literature. In particular, CO dimerization has been postulated to have a rate-limiting electron transfer decoupled from proton transfer.[283] However, adsorbate states are strongly coupled to the metal surface, where electrons are readily available. Adsorbate-induced states have widths on the order of eV,[168,276] and the corresponding rate of electron jumps is then of the order $10^{15}$/s; therefore, the electrons respond adiabatically to the configurational changes of the reaction intermediates along the reaction pathway.[277]

One motivation for the hypothesis behind rate-limiting electron transfers is the experimental observation of a lower onset potential (vs RHE) for $C_{2+}$ products with increased pH,[163,285] which is consistent with the analysis of the pH independence of ethylene formation on the SHE scale in the seminal work by Hori.[159] The idea is that a rate-limiting electron transfer decoupled from proton transfer would show an absolute potential (e.g., vs SHE) dependence, which is invariant with pH since the chemical potential of protons is not involved. Absolute potential dependence then translates to more positive onsets on an RHE scale, which accounts for pH. However, dependence on the absolute potential can also arise from either proton–electron transfer from $H_2O$, which is the proton source in neutral to basic solution, or through field-stabilization of chemical steps with large dipoles. Indeed, hydrogen evolution current densities from metal surfaces have been observed to depend only on SHE potential under a range of pH from neutral to very alkaline conditions,[218] which also translates to earlier onsets as pH is increased.

The effects of pH on $C_2$ vs $C_1$ selectivity and activity for COR and $CO_2R$ on Cu(211) was examined in a kinetic model that was based on *ab initio* activation energies and mean-field adsorbate–adsorbate interactions.[212] In general, as discussed in subsection 3.3.1, the $C_{2+}$ activity is enhanced at high pH and only shows a dependence on the absolute potential, while the $C_1$ activity shows a lesser enhancement with increasing pH.[159,200] $H_2$ formation was shown to exhibit a similar SHE dependence to $C_2$ activity.[200] The kinetic model suggested that the pure SHE dependence of $C_2$ and $H_2$ activities was due to an early rate-determining proton–electron transfer (*OCCO to *OCCOH, and the Volmer step, respectively) while the mixed RHE/SHE dependence of $C_1$ activity was due to a later proton–electron transfer (*CHOH to *CH). The latter is in line with the hypotheses from Hori's original study.[159] Figure 17 shows the experimental[200] and theoretical[212] curves for CO reduction at pH 7 and 13.[212] Overall, the major qualitative features between experiment and theory are in agreement. The depletion of $C_2$ products at high overpotentials arises from a decreased CO coverage upon the onset of $C_1$ production; since
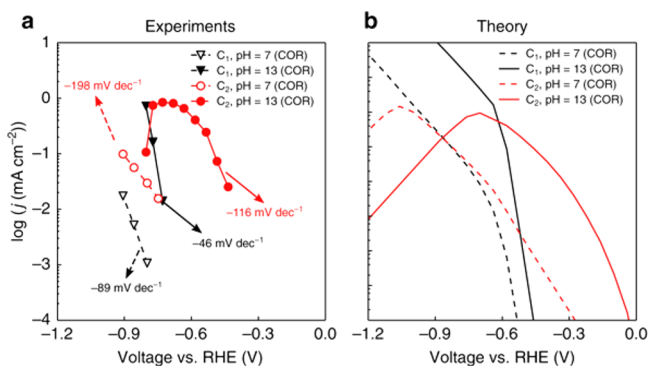
**Figure 17.** (a) Measured COR activities toward $C_1$ and $C_{2+}$ products on polycrystalline Cu at pH 7 and 13. Data from Wang et al.[200] (b) Predicted COR polarization curves from microkinetic model at pH = 7 and pH = 13. Reprinted from Liu et al.[212] This work is licensed under a Creative Commons Attribution 4.0 International License (https://creativecommons.org/licenses/by/4.0/).

$C_2$ production rates are second order in CO coverage, $C_2$ activity is affected significantly more than $C_1$ products by decreases in coverage. This effect is worsened with mass transport limitations. The branching out of the $C_1$ activity at high overpotentials is due to a transition to a regime where the *CO to *CHO electrochemical step is rate limiting, in line with the conclusions from Liu et al.[168]

Xiao et al. also investigated the energetics of reaction pathways on Cu(111) as a function of pH, using a hybrid of H-shuttling and implicit solvent models.[261] A pH dependence was added by correcting proton−electron transfer barriers with the shift in the chemical potential of a proton with pH, 0.059 eV/pH unit (some examples given in Table S3 in SI). However, as discussed above, under neutral and alkaline conditions, the source of protons is water, such that the electrochemical barriers would show an absolute (SHE) potential dependence, translating to lower activation energies at higher pH. As a result of the model's pH correction, under alkaline conditions, all H transfers are less favored relative to C−C coupling. The main conclusion from this analysis was a higher $C_2$ selectivity at high pH, in accordance with experiment, but the assumptions behind the model applied require further examination.

### 4.3. Summary

In recent years, developments in atomistic modeling of the electrochemical interface have made the analysis of $CO_2R$ pathways possible. Major advances in the field include the establishment of CO as a crucial reaction intermediate, investigations of cation promotion, the determination of the mechanism toward $CH_4$, where results from different explicit solvent methods appear to converge, and the establishment of design criteria for more active catalysts. On the other hand, there have thus far been little consensus in the theoretical literature regarding $C_2$ reaction pathways and their dependence on pH and facet termination, due to their inherent complexity, the sensitivity of the intermediates to the solvent and cation environment, and controversy regarding the origin of pH effects. Experimental evaluation of facet dependence is also challenging due to the possibility of surface reconstruction and defects in single crystal or epitaxial films, as discussed in section 3.1. We suggest that, while the analysis of onset potentials from reaction energetics can offer significant insight, kinetic modeling is required to elucidate the interplay between

coverage, potential dependence of activation energies, adsorbate−adsorbate interactions, and pH effects. Furthermore, we would like to highlight the need for development of multiscale models[286] that can help bridge quantum- and molecular-level dynamics with continuum models of reactant and product transport. Additional theoretical hurdles, not limited to investigations of $CO_2R$, are the reconciliation of differences in conclusions among existing theoretical approaches, the evaluation of the simplifying approximations made, and also development of new functionals for improved descriptions of charge at the interface, which would have major implications on the accuracy of the associated energetics.

## 5. ELECTROCHEMICAL $CO_2$ REDUCTION PATHWAYS ON CU

Ever since Hori's discovery in 1985 that $CO_2$ is reduced to hydrocarbons on Cu electrodes with relatively large Faradaic efficiencies,[81] many researchers have put a lot of effort into elucidating the reaction mechanisms of $CO_2R$ on Cu. However, after three decades of work, there is still little consensus. Understanding the mechanisms by which products are formed during $CO_2R$ is essential for the development of effective catalysts that can better meet our needs. Therefore, at this point, we would like to present our current state of understanding of the mechanistic pathways for $CO_2R$ on Cu (Figure 18), which takes into account a variety of both experimental and theoretical studies described in the previous two sections.

First, we will provide a few brief notes about the structure and flow of this figure. We have drawn the intermediates in a way that consistently gives each carbon atom a valency of 4, even though this sometimes differs slightly from the way the intermediate was drawn when proposed. The number on the horizontal axis is the number of carbons in an intermediate or product. The number on the vertical axis is the number of electrons transferred to the intermediate or product, which is four times the number of carbon atoms minus the total oxidation state of the species. The total oxidation state is taken to be the sum of the formal oxidation states of the carbon atoms plus the number of surface-oxygen bonds, representing the fact that bound oxygen has to be reductively cleared from the surface to complete a catalytic cycle.[201] The formal oxidation of each carbon atom is defined as the sum of the contributions from each of the four bonds: C−H bonds contribute −1 to the carbon atom's oxidation state, C−O bonds contribute +1, C−C bonds and C-surface bonds contribute 0, and an unbound electron pair contributes −1. A dotted bond contributes exactly half as much to the carbon atom's oxidation state as a full bond. Note that these rules are a formalism which actual charge distribution does not rigorously obey. When named, intermediates are generally referred to using the name of their desorbed state. For a bound intermediate to desorb, a pair of bonds to the surface are replaced by an additional bond in the molecule, enabling tautomerization if a C−C double bond is formed adjacent to an OH group.[65] If an intermediate with an odd total oxidation state were to desorb from the surface without an electron transfer, it would form a free radical.

Concerted proton−electron transfer (CPET) steps are represented by solid lines going down one level, while dashed lines involve no proton transfer, dash-dotted lines are coupling reactions involving neither proton nor electron transfer, and dotted lines involve multiple electron transfers. To simplify the
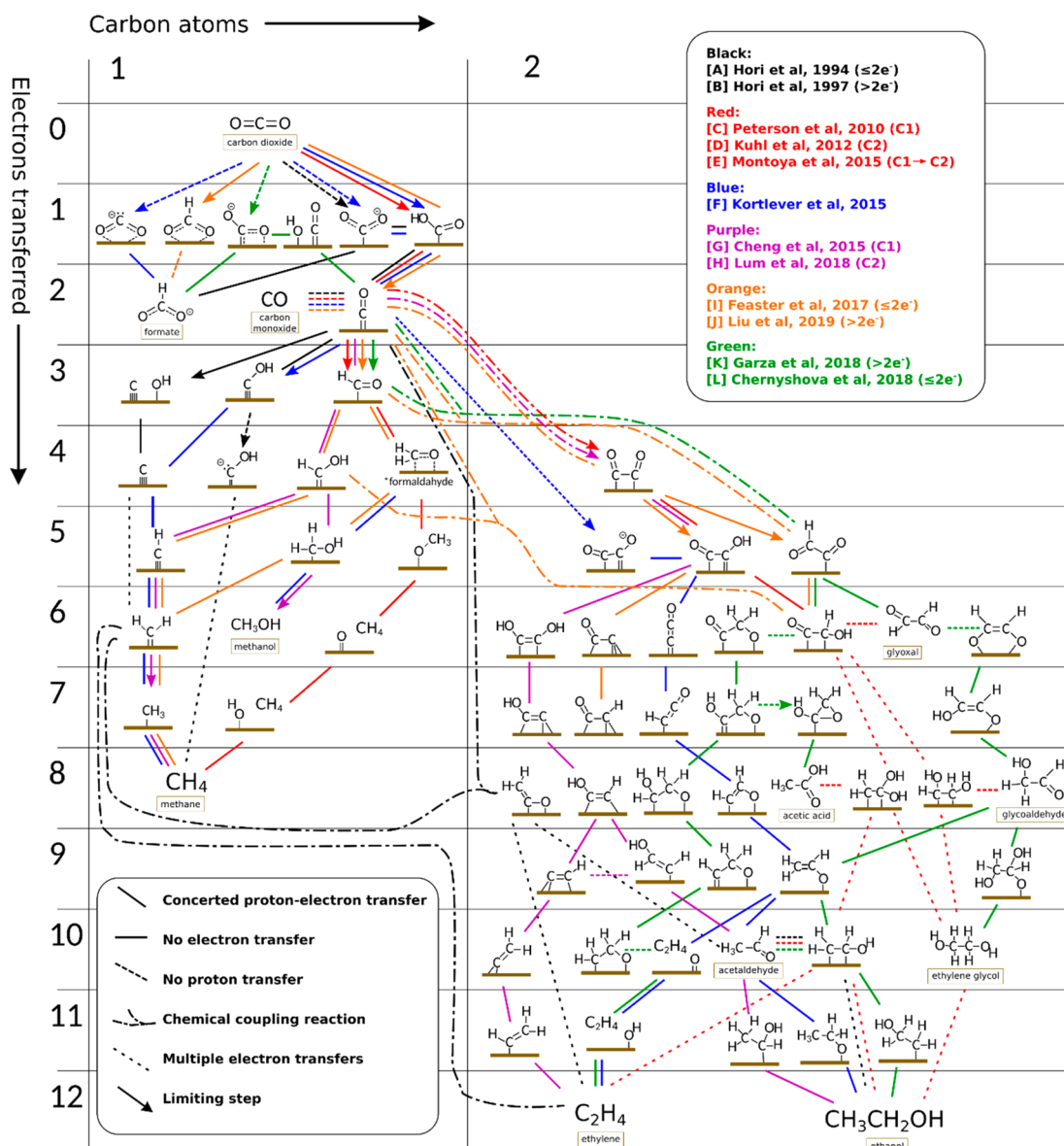
**Figure 18.** Possible mechanistic pathways of $CO_2$ reduction to $C_1$ and $C_2$ products on polycrystalline copper, grouped into different colored reaction schemes taken from the works in the top-right legend: [A] Hori et al.;[84] [B] Hori et al.;[159] [C] Peterson et al.;[201] [D] Kuhl et al.;[65] [E] Montoya et al.;[233] [F] Kortlever et al.;[16] [G] Cheng et al.;[274] [H] Lum et al.;[210] [I] Feaster et al.;[287] [J] Liu et al.;[212] [K] Garza et al.;[207] [L] Chernyshova et al.[134] The bottom-left legend states the meaning of the texture of the lines connecting intermediates. Expanded from the mechanistic compilation by S. Scott.[290]

figure, we have attempted to group mechanistic proposals that are consistent with each other, also considering which research groups have supported or contributed to each other's proposed mechanisms. The remainder of this section summarizes the key reasoning behind the proposed mechanisms based on the experimental and theoretical studies discussed in the previous two sections. In short, the mechanism in black was proposed by Hori based on his own and other early research in the field.[84,159] The mechanism in red includes a one-carbon ($C_1$) pathway[201] and initial C−C coupling mechanism[233] proposed based on DFT calculations by the group of Jens Nørskov, and a $C_2$ pathway based on experimental work from Thomas Jaramillo's group.[65] The mechanism in blue was proposed by the group of Marc Koper[16] based on a combination of their experimental observations[112] and theoretical calculations,[283] as well as much of the $C_1$ pathway suggested by the group of

Michael Janik.[263] The mechanisms in purple are works by the Goddard group.[210,274] The orange lines represent a mechanism combining 2e⁻ product pathways from a combined theory-experiment study,[287] and >2e⁻ $C_1$ and $C_2$ pathways determined from microkinetic modeling.[212] Finally, the green lines depict recent reports on 2e⁻ pathways[134] and $C_2$ pathways.[207] Keep in mind that the division of mechanistic proposals in Figure 18 is not absolute or complete. For example, there are many individual theoretical studies described in section 4 that only overlap with certain portions of more extensive mechanistic frameworks shown here. Furthermore, the field is developing quickly, with researchers often adding, removing, and adjusting proposed pathways. Thus, for clarity, the goal of this figure is not meant to be entirely exhaustive in representing *all* references and the divergences between them, but rather to show several schools

of thought that have evolved over time. It is also worth noting that a few other reports have similarly provided mechanistic overviews in recent years.[8,275,288,289]

In general, most mechanisms agree that the step in which $CO_2$ is adsorbed is the limiting step in $CO_2R$ to $2e^-$ products, but there is some uncertainty on whether this first intermediate is arrived at by CPET or a decoupled pathway through a charged intermediate.[16] Then, whether this intermediate binds through the carbon atom or oxygen atom(s) is thought to be a key distinction between the formate and CO pathways. A recent combined experimental and theoretical study found clear volcano trends for the *COOH binding energy and *OCHO binding energy for $CO_2R$ to CO and $HCOO^-$, respectively, indicating that these are likely the main intermediates for these products.[287] Alternatively, a recent report combining *operando* surface-enhanced Raman scattering (SERS) and DFT simulations provided evidence that the first intermediate to both $HCOO^-$ and CO on Cu electrodes is a carboxylate anion $*CO_2^-$.[134] However, rather than being bound through the carbon atom or the oxygen atoms, as shown above, the authors propose that carboxylate is coordinated to the surface through one of its C−O bonds, rigorously using isotope exchange and electrochemical Stark effects to verify the assignment of relevant SERS peaks. Then, DFT simulations suggest that this intermediate is converted into $HCOO^-$ and CO via activation of the Cu−C and C−O bonds and stabilization of the Cu−O bond, respectively, with increasing negative potential.[134] Thus, while different intermediates are proposed, evidently both the Cu−C and Cu−O bond strengths may still serve as key descriptors governing the selectivity of Cu to both CO and $HCOO^-$.

As discussed earlier, it is widely accepted that CO is the key intermediate to $>2e^-$ products. Beyond *CO, a significant distinguishing feature between the $C_1$ and $C_{2+}$ pathways is the observed sensitivity to pH. It has been shown that the ethylene formation pathway is independent of pH on the SHE scale, whereas the methane formation pathway is pH dependent on the SHE scale,[159,200] which leads to the experimental observation of a lower onset potential (vs RHE) for $C_{2+}$ products with increased pH. Accordingly, the limiting step in $C_1$ formation has been thought to be CO protonation either through a *COH or *CHO intermediate,[112,159,201,263,274,291] while the limiting step in $C_{2+}$ formation has generally been thought to be CO dimerization that is decoupled from proton transfer.[2,112,233,259,260,283] Theoretical calculations have differed in their view of *COH vs *CHO depending on the computational techniques and assumptions. A recent microkinetic model has suggested that this $C_1$ rate-limiting step actually changes under different applied potentials, with *CO → *CHO being limiting at high overpotentials and *CHO → *CHOH being limiting at low overpotentials.[212] Furthermore, contrary to the above, this microkinetic model has also suggested that the $C_{2+}$ pathway could indeed be limited by a CPET step, since the first proton−electron transfer from water to an adsorbate would yield a pure dependence on the absolute potential (i.e., it is independent of pH on the SHE scale).[212] However, it is equally suggested that this pH independence could also arise from field-stabilization of a limiting chemical reaction with large dipoles (i.e., CO dimerization), which is supported by studies investigating cation effects. This analysis highlights the need for future theoretical studies to consider not only thermodynamics but also reaction kinetics due to the complicated interplay between adsorbate coverages, adsorbate−adsorbate interactions, field effects, etc.

While CO dimerization has been widely suggested, there are many aspects to this step that are still up for debate, such as whether CO coupling is an electrochemical step (involving a rate-limiting electron transfer)[2,112,233,260,283] or is purely a chemical step (not involving a rate-limiting electron transfer)[233,260] and whether coupling occurs between two adsorbed CO molecules (*CO + *CO)[2,112,233,259,260] and/or an adsorbed and a free CO molecule (*CO + $CO_{(g)}$).[207,283] Additionally, some studies also include the possibility of coupling between species such as *CHO and *CO[260] or $CO_{(g)}$,[207,259] particularly at higher overpotentials. This partially stems from the notion that there are two possible pathways to ethylene depending on the surface structure and overpotential. A series of studies on Cu single crystals have noted a low overpotential pathway (CO dimerization) preferred on Cu(100) and a higher overpotential pathway shared with $CH_4$, likely through *CHO, that is preferred on Cu(111).[163,165,166] This is consistent with the higher selectivity for $C_2H_4$ observed on Cu(100) compared to Cu(111), as discussed in subsection 3.1.1. Furthermore, a recent study employing *in situ* Fourier-transform infrared spectroscopy (FTIR) observed a hydrogenated CO dimer intermediate at low overpotentials on the Cu(100) surface but not Cu(111), providing strong support for this mechanism.[140] While the authors assigned this species to be *COCOH based on their DFT calculations, another theoretical study[207] suggested that, since the vibrational frequencies of adsorbates depend strongly on their adsorption mode, their calculated *COCHO structure could also have signals in the same range. Thus, discussions continue as to whether the CO dimerization pathway proceeds through a *COCHO[207,233,260] or *COCOH[140,259,283] intermediate.

Finally, it is also worth mentioning that alternate $C_{2+}$ mechanisms have been proposed involving dimerization of $CH_2$ groups,[103,159,275,292] dimerization of $CH_3$ groups,[293] coupling of two hydrogenated CO species,[275,280] and a Fischer−Tropsch-like CO insertion mechanism of adsorbed $CH_2$ and CO.[129,159,292] While these may be thermodynamically feasible, it is suggested that the surface concentration of these intermediates is likely to be too low for them to be a major source of C−C bonds.[207] However, this could be highly dependent on the reaction conditions, and thus, these possible mechanisms cannot be conclusively ruled out.

Within the $C_1$ pathway, the selectivity between methane and methanol is of particular interest, as methanol is by far the more valuable product (Figure 2), but has proven elusive. As discussed earlier in subsection 3.2.2, species related to formaldehyde have been thought to serve as intermediates for methane and methanol formation. One plausible pathway is *CHO → $*CH_2O$ → $*CH_3O$ → $CH_3OH$ or $CH_4$.[201] The lack of reduction of methanol to methane[112] is one indicator that this may not be the most facile route to methane, although the reduction of formaldehyde primarily leads to methanol,[107,112,159] suggesting that this may be an intermediate on the route to methanol formation. Still, Kuhl et al. observed methane and methanol formation on a number of transition metals and saw that the onset potentials for methane and methanol formation are closely correlated, indicating a mechanism in which these products share a common limiting step.[203] Cheng et al. (purple $C_1$ lines in Figure 18) found that after subsequent protonation of *CHO, *CHOH is the likely

branch point between methanol (*CHOH → *CH$_2$OH → CH$_3$OH) and methane (*CHOH → *CH → *CH$_2$ → *CH$_3$ → CH$_4$), with the latter pathway being more favorable.[274] Thus, *CO protonation to *CHO could still apply to both pathways. Interestingly, Kuhl et al. found methanol but no detectable methane on Au (the least oxophilic metal studied) and methane but no detectable methanol on Fe (the most oxophilic metal studied), while the other 5 metals tested (Ag, Zn, Cu, Ni, Pt) produced both.[203] Thus, the oxophilicity of the surface may play an important role in determining the selectivity between these two products.

Interestingly, when the selectivity toward methane is increased, a deactivation effect occurs that is not present when ethylene is the major product.[109] This implies that large amounts of poisoning intermediates form on Cu in the C$_1$ pathway, and such intermediates may not take part in the C$_{2+}$ pathway. A likely culprit in this regard is graphitic carbon. Some reports suggest that graphitic carbon can serve as an intermediate in CO$_2$R,[106,263,294] and as shown above, a possible pathway to CH$_4$ could go through *COH → *C → subsequent hydrogenation to CH$_4$.[263] Buildup of graphitic carbon has been commonly suggested as a cause for deactivation though, so this could explain why deactivation is seen on Cu electrodes that more predominantly make CH$_4$. This could also explain why nanostructured Cu electrodes, which typically exhibit suppression of the CH$_4$ pathway, have demonstrated increased stability with minimal or no deactivation observed over long-term electrolysis.[89,107,115,116] In addition, the increased surface area of nanostructured electrodes can itself be a cause for their increased stability since the higher ratio of ECSA to electrolyte volume can reduce the impact of poisoning via other mechanisms, such as deposition of trace metal impurities in the electrolyte.[87,109,114] Furthermore, the surface area of Cu electrodes also plays a key role in determining selectivity, which will be addressed in the next section.

As can be seen in the right half of Figure 18 above, the proposed mechanisms for C$_2$ products diverge completely after the C−C coupling step, and we refer the reader to the original studies for the detailed reasoning behind each proposed mechanism.[16,65,159,207,210,212,233] In short, as discussed in subsection 3.2.2, the reduction of oxygenated species such as glyoxal, glycoaldehyde, acetaldehyde, propionaldehyde, etc. have led to identification of possible intermediates and pathways to alcohols. In addition, water has recently been shown to play an important role in the formation of certain oxygenated products.[210] Under strongly alkaline conditions, Cannizzaro-type disproportionation reactions in the electrolyte may also lead to the formation of alcohols and carboxylic acids from the corresponding aldehyde.[211] In terms of potential-dependent trends, some studies have demonstrated that oxygenates are preferred over hydrocarbons at lower over-potentials.[114,200] Overall, there is still much being learned about what dictates selectivity between the various C$_{2+}$ oxygenates and hydrocarbons. Through future work developing in situ/operando spectroscopies, isotope labeling experiments, and computational methods involving kinetic modeling, we may be able to ascertain the distinguishing features of the dominant pathway(s) in order to tailor CO$_2$R activity and selectivity toward the desired product(s).

This concludes our brief overview of reaction networks for CO$_2$R on Cu. In the sections that follow, we will expand on this framework and discuss deeper insights on activity and selectivity trends that have been gained from studying more advanced (nanostructured and bimetallic) Cu catalysts.

# 6. NANOSTRUCTURED COPPER

Nanostructuring of Cu electrodes has been widely applied in attempts to improve selectivity and energy efficiency for CO$_2$R. Nanostructuring of electrocatalyst materials leads to improved geometric activity (current density normalized to the geometric surface area of the electrode) due to an increase in the electrochemically active surface area (ECSA) compared to planar electrodes. In addition, it can oftentimes lead to altered electrocatalytic properties compared to those of planar electrodes. These differences can be caused by a number of effects, including, but not limited to, a higher occurrence of undercoordinated sites, preferential faceting, changes in the local pH, and readsorption of products.[295,296] In this work, we classify the Cu nanomaterials into two different types of systems: (supported) nanoparticles (section 6.1) and (unsupported) three-dimensionally interconnected electrodes (section 6.2). It is important to note that these two sections both address aqueous phase CO$_2$R, meaning that CO$_2$ is delivered to the electrode via diffusion through the aqueous electrolyte. Vapor-fed CO$_2$R systems, where the CO$_2$ is delivered directly to the electrode in the gas phase, will briefly be addressed in section 6.3. In this section we will only discuss pure Cu systems, in some cases on a support material; nanostructured bimetallic systems with Cu are covered in section 7.

## 6.1. Nanoparticles

Nanoparticles are individual particles with a diameter of 100 nm or less that are typically supported on a suitable material. Since all heterogeneous catalytic processes take place at the surface, the high surface area to volume ratio of nanoparticulate catalysts allows for greater utilization of a given material on a mass basis. This is an important concern for precious metal catalysts, but is less of an issue for Cu because of its natural abundancy.[297] An important motivating factor for studying nanoparticle catalysts is their high degree of compatibility to be incorporated into gas diffusion electrodes (GDEs) and membrane electrode assemblies (MEAs); these vapor-fed systems will be discussed in section 6.3. Here we will detail work that has been done to study the fundamental effects of nanoparticle size, shape, and loading on CO$_2$R performance in aqueous-phase reactors.[298−306]

**6.1.1. Nanoparticle Size Effects.** Particle size can have a direct influence on the reactivity of a catalyst material. This comes down to a number of possible effects, mainly related to a significant increase in the surface to bulk atom ratio as the size is decreased. First, as the size of a particle decreases the curvature of its surface becomes larger and the average coordination of the surface atoms is lowered, due to a higher occurrence of undercoordinated sites.[307] Decreasing the coordination number of catalytically active atoms leads to perturbed electronic structure and oftentimes increased reactivity. Furthermore, for very small particles, a significant amount of strain is induced on the surface atoms. This shifts the d-band and, again, influences reactivity.[308] Depending on the catalytic process and material, increased reactivity may improve or deteriorate activity. For simple 2e$^−$ processes, the effect of changes in reactivity can be predicted by determining the optimum binding energy of the key intermediate.[204] However, CO$_2$R pathways to >2e$^−$ products are inherently

much more complex (as shown in Figure 18) and involve many more proton–electron transfers and intermediate species. Therefore, it is hard to predict the effect of changes in the electronic structure on the catalyst performance, and both theory and experimental work are needed.

Based on the concepts outlined above, a few different groups have investigated size effects of Cu nanoparticles for $CO_2R$.[298–300] The results from various individual studies generally show different trends. Importantly, they all used different catalyst synthesis methods, which can lead to different nanoparticle size, morphology, and stability. If ligands are used during synthesis, they can bind to active sites and alter the activity if not completely removed before electrochemical testing. Furthermore, Cu is inherently mobile, in particular, in the presence of CO.[174] Thus, depending on the initial geometry, significant restructuring can take place under reaction conditions, which can cause changes in nanoparticle size, shape, and distribution.

Reske et al. synthesized various Cu nanoparticle electrodes of diameter 15 nm and smaller. A TEM image of a representative sample is displayed in Figure 19a. When
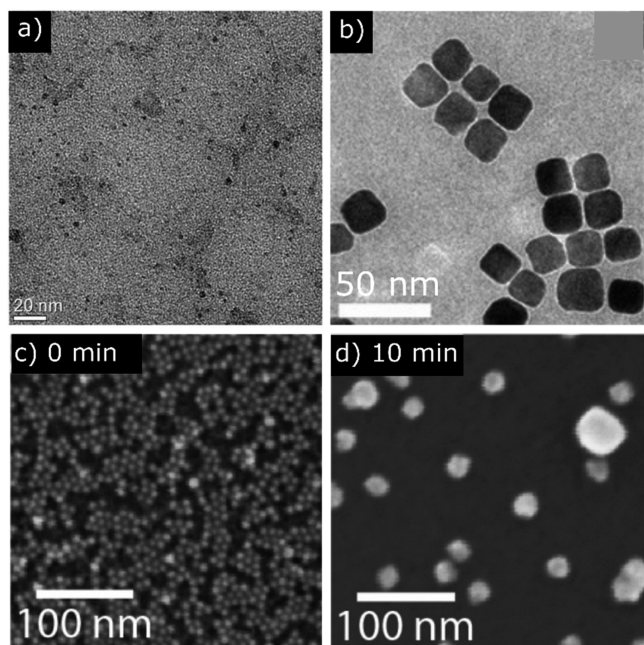
**Figure 19.** TEM images of Cu nanoparticles from various studies. (a) Spherical particles, 2.4 nm average diameter. Reprinted from Reske et al.[298] Copyright 2014, American Chemical Society. (b) Cubic particles, 24 nm average edge length, Reprinted with permission from Loiudice et al.[300] Copyright 2016, John Wiley and Sons. (c) and (d) Spherical particles as-prepared and after 10 min $CO_2R$ at −1.25 V vs RHE, respectively. Reprinted from Manthiram et al.[299] Copyright 2014, American Chemical Society.

measuring $CO_2R$, the authors observed that the samples exhibited lower $CO_2R$ Faradaic efficiency toward hydrocarbons and increased selectivity to the formation of CO and $H_2$ as compared to polycrystalline foils, as displayed in Figure 20b.[298] Furthermore, they showed that particles smaller than 5 nm gave rise to significantly increased current density at a fixed potential, which led to increased production rates for the various products as displayed in Figure 20a. Surprisingly, no clear trend in product distribution could be observed with changing particle size in this study. Manthiram et al., on the
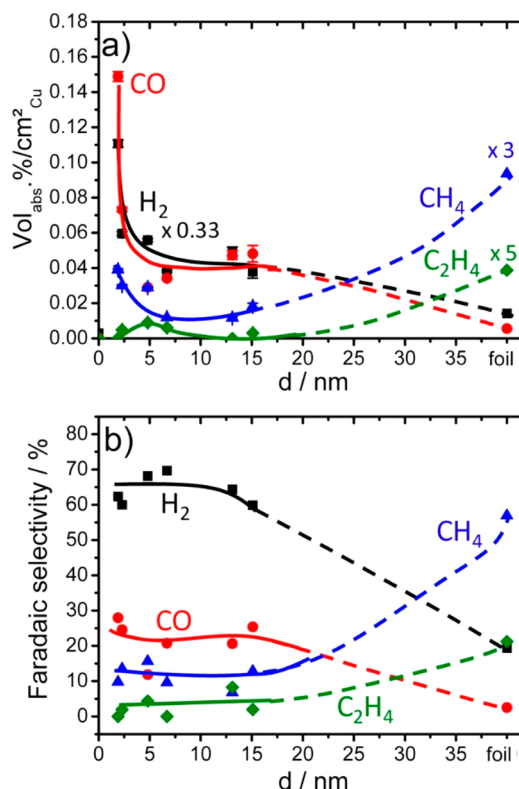
**Figure 20.** $CO_2$ reduction on Cu nanoparticles of different size at −1.1 V vs RHE. (a) Production rate of individual products. (b) Faradaic efficiency to individual products. Reprinted from Reske et al.[298] Copyright 2014, American Chemical Society.

other hand, reported enhanced methane production between −0.95 and −1.45 V vs RHE on Cu nanoparticles with an initial size of 7 nm, as compared to polycrystalline Cu.[299] These nanoparticles quickly sintered, as illustrated by the transformation over 10 min of $CO_2R$ shown in Figure 19c,d. Loiudice et al. synthesized larger, cube-shaped nanocrystals of 24−63 nm, with a TEM image of a 24 nm particle sample displayed in Figure 19b.[300] They showed an optimal $CO_2R$ Faradaic efficiency of around 80%, with high selectivity toward ethylene, for 44 nm particles at −1.1 V vs RHE. As mentioned above, the divergence between these three studies can have different reasons. Manthiram et al. showed that their 7 nm particles aggregated to form larger clusters with an average size of 23 nm shortly after introduction to the catalytic environment.[299] Furthermore, two of the studies used spherical particles,[298,299] while the third mainly studied cube-shaped particles.[300] As discussed in section 3.1, differences in surface structure can influence product distribution, and to some extent activity. Finally, different loadings were used, both between the different studies and within a single study. The effect of this will be discussed in the following subsection. Unfortunately, the diverging results make it difficult to draw clear conclusions about trends for different sizes of Cu nanoparticles.

**6.1.2. Loading/Interparticle Distance.** Another parameter that can influence the $CO_2R$ activity and selectivity of nanoparticles is the amount that is loaded onto the support.[301,302] Mistry et al. used inverse micelle encapsulation to synthesize nanoparticles with well-defined size and interparticle distance.[301] They found some variation in the product distribution with loading, depending on particle size,

but no clear trend, similarly to what was the case for the study of pure size effects, as discussed above. They attributed the effects to readsorption of products/intermediates and local pH effects. Kim et al. investigated three widely different loadings of 6.7 nm Cu particles on carbon paper.[302] The highest loading was studied further, leading to observations of a structural transition of nanoparticle ensembles into cube-shaped structures. This coincided with a shift in product distribution toward more $C_{2+}$ compounds and lower $H_2$ evolution, possibly caused by the exposure of different surface sites and/or local pH changes in the rough structure. The studies mentioned above should be followed up with further work regarding mass transport effects on $CO_2R$ activity and selectivity for Cu nanoparticle systems. Additional well-controlled studies using alternative synthesis techniques and three-dimensional support materials will help to elucidate some of these phenomena.

**6.1.3. Shape Effects.** As discussed in subsection 3.1.1, certain Cu single crystal facets exhibit improved selectivity to specific products. Cu(100) electrodes, and especially "miscut" Cu(100) electrodes with an optimal density of steps, have been shown to exhibit higher selectivity for C−C coupling than other planar surfaces.[153,157,163,166] Reports also suggest that the production of oxygenates is enhanced on certain crystals, including single crystals with (100) and (110) terraces and varying step density, as well as epitaxially grown Cu films with (751) orientation.[152,153,157] Motivated by the work on single crystals, some effort has gone into increasing the occurrence of certain facets by controlling nanoparticle shape. For instance, the surface of cubic structures should be dominated by (100) facets since Cu is a face-centered cubic (FCC) metal. In addition, unlike perfect single crystals, faceted nanoparticles also contain edge and corner sites, which could strongly affect the resulting activity. For instance, recent DFT results suggest that Cu(211), which exhibits a high density of surface step sites, yields several orders of magnitude higher activity than (100) and (111) surfaces for CO reduction to $CH_4$.[168]

Cubic Cu nanoparticles have been synthesized by different groups, as discussed in the previous two subsections.[300,302,309] A representative TEM image is shown in Figure 19b. These particles exhibit enhanced $C_{2+}$ product selectivity compared to polycrystalline Cu, possibly caused by increased occurrence of (100) facets. However, Grosse et al. reported drastic morphology changes occurring during $CO_2R$, including loss of the cubic shape.[309] Li et al. produced thin nanowires with well-defined 5-fold twinned edges, exhibiting high selectivity toward $CO_2R$, with $CH_4$ produced almost exclusively around −1.25 V vs RHE.[303] It is unclear, however, which facets are exposed on the terraces of the nanowires. It is also worth mentioning that −1.25 V is a large overpotential, where polycrystalline Cu also mainly produces methane from $CO_2R$.[65] Furthermore, at potentials more negative than −1.0 V vs RHE, polarization effects begin to impact $CO_2R$ catalysis on planar polycrystalline Cu,[96] meaning that these high surface area nanowire electrodes will likely experience mass transport limitations at even lower applied potentials. We would like to underline the importance of measuring novel catalyst materials at potentials where mass transport limitations are not prevalent in order to more directly investigate their intrinsic behavior; this issue was discussed in more detail in section 2.2.

The studies mentioned in the previous paragraph utilized bottom-up methods to obtain faceting of their particles. With a different, top-down approach, Wang et al. used chemical etching of cubic Cu nanoparticles with varying duration to

obtain different shapes, as shown in Figure 21.[304] The nanocrystals that were etched for 12 h or more (Figure 21c
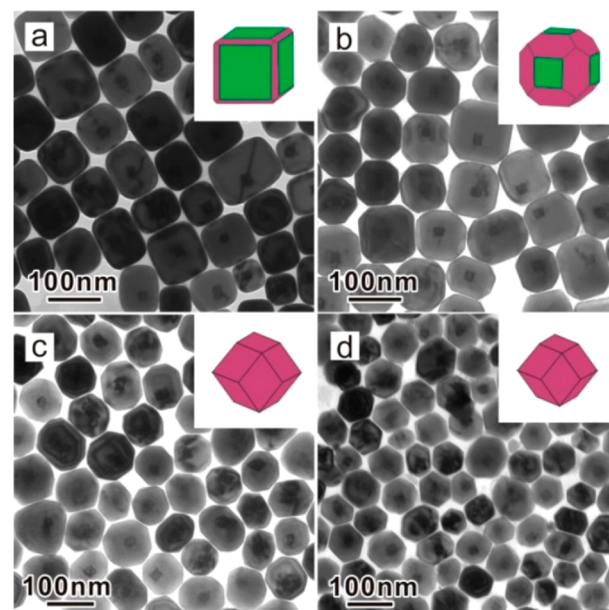


**Figure 21.** Cu nanoparticles prepared by etching cubic particles for different durations: (a) 4 h, (b) 8 h, (c) 12 h, and (d) 24 h. Reprinted from Wang et al.[304] Copyright 2016, American Chemical Society.

and d) exhibited a rhombic dodecahedral shape with preferential exposure of (110) facets. These particles exhibited enhanced selectivity to hydrocarbons and reduced CO production at around −0.8 V vs RHE. The authors did not, however, report any liquid products. As mentioned above, Hori et al. reported that single crystals with (110) orientation exhibit significantly enhanced production of oxygenates.[152] Therefore, it is likely that oxygenates were produced from these measurements as well. This emphasizes the importance of carrying out thorough product analysis, since this information can give significant fundamental insight.

An important point to consider when investigating shape effects is stability, in terms of both activity and retaining the synthesized shape. This is particularly important for Cu, where structural transformations are likely due to its high mobility. In an attempt to address this issue, Huang et al. studied the development of shape and $CO_2R$ activity of the cubic Cu nanoparticles shown in Figure 19b with electrolysis time. Using TEM, they performed *ex situ* monitoring of changes to the morphology of the nanoparticles after various durations of electrolysis up to 12 h, while also tracking activity and product distribution. They saw some changes with time; $H_2$ evolution activity increased and $CO_2R$ activity decreased with longer duration for most samples, and the nanoparticle shape became increasingly ill-defined. They attributed the changes to adsorbate-induced restructuring of the Cu catalyst, yielding useful information for further studies. However, they did not provide conclusive evidence that this is the only or main cause of the deactivation. Importantly, they did not provide evidence that their electrodes were not contaminated, which can be challenging to avoid for such long-term measurements due to the highly negative polarization of the electrode.[111,113,114] Furthermore, they only reported $CO_2R$ at −1.1 V vs RHE, which is in a potential region where nonplanar electrodes are

**Figure 22.** Transmission electron microscopy images of Cu nanoparticles on two different supports. (a) Carbon nanospikes. Reprinted with permission from Song et al.[311] Copyrigh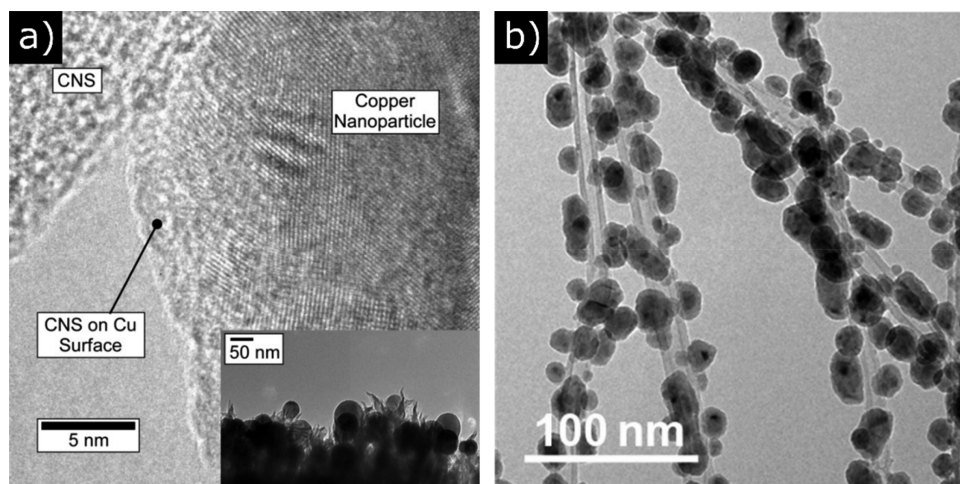t 2016, John Wiley and Sons. (b) Carbon nanotubes. Reprinted with permission from Feng et al.[315] Further permissions related to this material should be directed to the American Chemical Society.
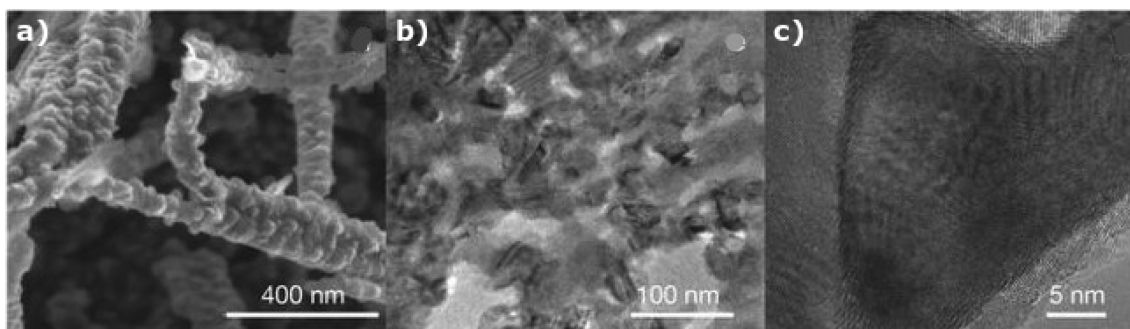


**Figure 23.** Electron microscopy images of calcined oxide-derived Cu electrodes. (a) and (b) SEM images. (c) TEM image. Reprinted with permission from Li et al.[70] Copyright 2014, Springer Nature.

likely in a mass transport limited regime. Thus, any trends in activity that are observed here might not be valid at lower overpotentials.

In general, more work on nanoparticles with preferential faceting would be welcome, in particular to elucidate the effect of particle shape in more detail, and to be able to decouple it from other parameters such as size, loading, support effects, etc. Further stability studies addressing the points raised in the previous paragraph would also be of value to the community.

**6.1.4. Effect of Support and Catalyst−Ionomer Interaction.** For any nanoparticle-based catalyst, a suitable support material is vital to ensure good dispersion and mechanical stability of the catalyst material. In addition, the interaction between support and nanoparticles can induce changes in the electronic structure of the catalyst and/or add interfacial sites, altering the performance of the catalyst. The support effect is utilized heavily in several industrial catalytic reactions, such as methanol synthesis on $Cu/ZnO/Al_2O_3$.[310] However, only a limited number of studies investigating support effects in $CO_2R$ have been reported to date. Song et al. showed that Cu nanoparticles supported on needle-shaped nitrogen-doped carbon exhibit high selectivity toward ethanol production at high overpotentials, with a maximum Faradaic efficiency of 63% at −1.2 V vs RHE.[311] They attributed the high selectivity to the interaction between the nanoparticles and the highly textured support material. Subsequently, a number of further studies on Cu nanoparticles on various

supports reported significant selectivity toward ethanol[312] or ethylene.[313,314]

Feng et al. synthesized Cu nanoparticles on graphene by physical vapor deposition, and observed a large number of grain boundaries.[315] From these nonequilibrium structures, they observe high selectivity toward ethanol and acetate from COR. Some works also report catalytic enhancement from metal−support interactions for $CO_2R$ on Au and Ag.[316,317] TEM images illustrating the geometry of these two studies are shown in Figure 22a and b, respectively.

In moving toward more practical device designs, such as vapor-fed systems (Section 6.3), understanding how the other components, including the support and ionomer materials, impact $CO_2R$ on Cu will become increasingly important. For example, it has previously been shown that an optimal ionomer loading exists for hydrogen oxidation electrocatalysts.[318] Gupta et al. tried to determine a similar ideal ionomer content for Cu nanoparticles, and found that optimal formate production occurs using 25% Nafion content in the catalyst ink.[306] We would like to highlight the need for more fundamental studies in these areas in order to help translate aqueous-phase $CO_2R$ catalysis to highly complex vapor-fed designs.

## 6.2. Three-Dimensionally Interconnected Catalyst Materials

Another approach to nanostructuring is the preparation of three-dimensionally interconnected (3-D) electrodes. In the following, we separate the discussion between oxide-derived
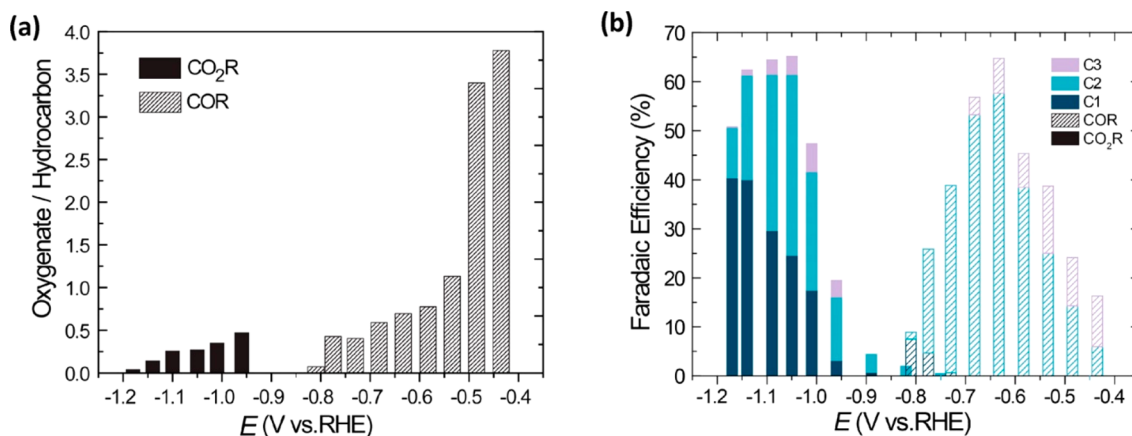
**Figure 24.** Potential-dependent selectivity of Cu toward $CO_2R$ and COR. (a) Oxygenate/hydrocarbon ratios of the reduction products as a function of potential, and (b) Faradaic efficiencies for $C_1$, $C_2$, and $C_3$ products, each as a function of potential. These potential-dependent selectivity trends reveal that the production of $C_{2+}$ oxygenates is increasingly favored over hydrocarbons at Reprinted from Wang et al.[200] Copyright 2018, American Chemical Society.

and non-oxide-derived electrodes and consider how the different pretreatments influence $CO_2R$ activity.

**6.2.1. Oxide-Derived Copper.** Rapid removal of oxygen during reduction of oxidized Cu is a straightforward means to achieve porous, inhomogeneous surfaces that exhibit altered $CO_2R$ performance. Hori et al. were the first, to the best of our knowledge, to report $CO_2R$ on this type of Cu electrode, which had significantly higher ECSA, as measured by the double-layer charging current.[159] Other early work by Karl W. Frese Jr. reported significant methanol production from $CO_2R$ on intentionally oxidized copper electrodes.[319] A large number of later works on similar catalysts have not reported methanol production; thus, it is still not clear how, if at all, methanol can be produced with significant selectivity from Cu electrodes. However, the preparation of nanostructured surfaces from oxidized precursors has still led to a number of interesting findings, which will be discussed subsequently. For ease of navigating the wide variety of materials that have been studied, we organize this subsection by the choice of synthesis method: thermal oxidation, anodic treatment, and other $Cu_2O$ film-derived electrodes.

*Thermal Oxidation.* Kanan and co-workers showed that calcination of planar Cu foils in air and subsequent electrochemical reduction resulted in high surface area 3-D electrodes.[89] An SEM image that illustrates the resulting surface structure can be seen in Figure 23a. When carrying out $CO_2R$ on these electrodes, the selectivity toward CO and formate was improved between −0.2 and −0.7 V vs RHE, compared to polycrystalline Cu foil. Similar studies have since been carried out using this thermal oxidation and electro-chemical reduction method to alter the $CO_2R$ activity of Cu electrodes, but a common approach has been to use a copper precursor material with a higher surface area than planar foils, such as Cu mesh, foam, and nanowire structures.[91−93,320,321] Some of these studies report enhanced production of CO and formate, and little to no formation of >2e⁻ products.[91−93] This corresponds well to the results by Kanan and co-workers.[89] On the other hand, two studies also showed enhanced selectivity for >2e⁻ products, such as hydrocarbons and alcohols, compared to polycrystalline Cu, which was not reported previously.[320,321] Notably, $CH_4$ production was suppressed in favor of C−C coupled products. Possible causes for the discrepancy between these studies on calcined oxide-derived

Cu electrodes could be inadequate product analysis in some of the studies and varying mass transport conditions within the different catalyst morphologies and electrochemical cells used by the different research groups.

Kanan and co-workers also conducted CO reduction (COR) studies on their oxide-derived Cu foils.[70] High COR selectivity was observed between −0.25 and −0.40 V vs RHE, mostly toward the $C_2$ compounds ethanol and acetate. At −0.3 V vs RHE, CO was reduced at a Faradaic efficiency of 57%, with an impressive 43% to ethanol production. Similarly high activity and selectivity toward COR was reported by Raciti et al. on Cu nanowires.[322] However, due to the poor solubility of carbon monoxide in aqueous solutions,[323] low maximum COR current densities were obtained in both of these studies. Nevertheless, such a high selectivity toward liquid products spurred much interest in this class of materials.[90,315,324,325]

In the aforementioned COR study by Kanan and co-workers, a large number of grain boundaries in the calcined oxide-derived Cu electrodes were found using transmission electron microscopy (TEM), as illustrated in Figure 23b and Figure 23c.[70] They hypothesized that the high selectivity could be caused by undercoordinated sites with special geometries that were stabilized by grain boundary surface terminations. By later studying nanoparticles with varying grain boundary density, they were able to correlate the COR performance to a high occurrence of grain boundaries.[315] Verdaguer-Casadevall et al. used CO temperature-programmed desorption (TPD) to probe the binding strength of CO on oxide-derived Cu foils.[324] A high temperature feature that was not present for planar polycrystalline Cu could be identified, suggesting the presence of strong-binding sites on the oxide-derived surface. The occurrence of these sites could be correlated with COR activity, supporting the notion that certain sites present on oxide-derived Cu are responsible for its excellent performance. However, the TPD in this study was complicated by gas-phase mass transport and CO readsorption in the pores of the oxide-derived copper, and modeling was required to decouple this effect from the binding strength of particular sites. The modeling suggested that the high temperature feature was entirely due to strong binding of CO, rather than mass transport, but there is still some uncertainty to this result due to the inhomogeneity of the material.
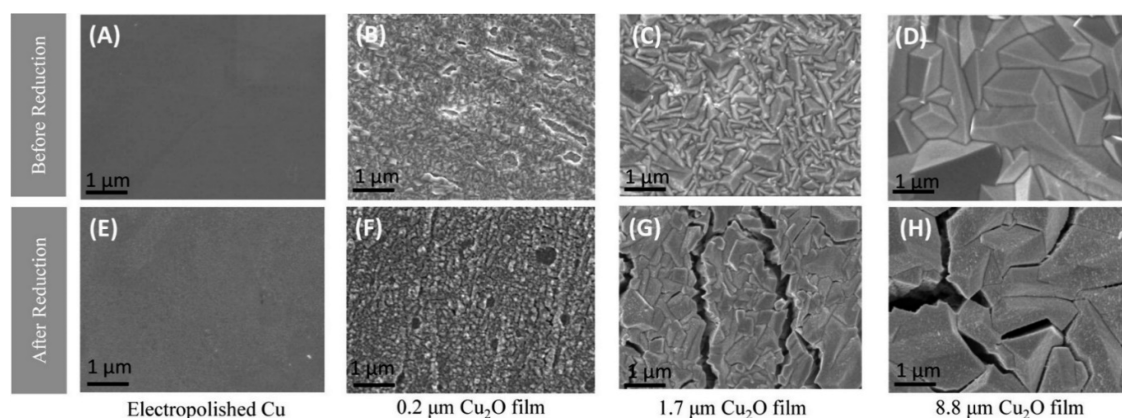
**Figure 25.** SEM micrographs of various $Cu_2O$ films prepared by electrodeposition. (a−d) As-deposited and (e−h) after $CO_2R$ at −0.99 V vs RHE. Reprinted from Ren et al.[128] Copyright 2015, American Chemical Society.

Rather than specific morphological features being responsible for the high COR activity and selectivity to oxygenated products, other studies have suggested that this has more to do with the increased surface area of these materials.[114,200] As shown in Figure 24, the production of both oxygenated and C−C coupled products are favored at lower overpotentials.[200] Thus, the performance of these very rough morphologies can be explained by their greater number of surface sites, which allow these electrodes to reach high geometric COR rates at more positive potentials where the production of $C_{2+}$ oxygenates is favored. Importantly, when normalized by the ECSA, planar $Cu^{200}$ and these state of the art Cu materials[70,322] exhibit very similar COR rates when compared at potentials that are free of diffusion limitations, suggesting that these potential-dependent selectivity trends are the key reason for the differing performance of these materials.[200]

*Anodic Treatment.* Another approach to prepare oxide-derived nanostructured electrocatalysts is *in situ* anodic treatments. Oxidation−reduction cycles result in the formation of nanostructures on the surface of polycrystalline Cu.[94,95,116,326] Similar to some studies on calcined oxide-derived Cu, the *in situ* electrochemical oxidation−reduction treatment resulted in suppressed $CH_4$ evolution and enhanced production of $C_2H_4$ compared to planar Cu. $C_2$ and $C_3$ oxygenates were later identified as important liquid products from anodically treated Cu foils by performing rigorous product analysis.[95,327] Roberts et al. followed up their $CO_2R$ work on copper nanocubes synthesized by potential cycling in the presence of $Cl^{-94}$ by also testing these anodically nanostructured catalysts for COR.[285] Ethylene formation was favored over methane on copper nanocubes compared to polycrystalline foils, confirming the trends they observed previously for $CO_2R$. In general, it seems that anodic nanostructuring of Cu surfaces favors production of $C_{2+}$ over $C_1$ compounds. Using a different approach, Roldan Cuenya and co-workers created a thick, amorphous oxide film on the surface of Cu foils by oxygen plasma treatment.[125,248,328] Depending on the exact pretreatment conditions, this material exhibited high selectivity toward ethylene formation; a maximum Faradaic efficiency of 62% was observed at around −0.9 V vs RHE.[125]

Different reasons for the high ethylene selectivity of these materials have been suggested. Kwon et al.[95] reiterated the explanation given by Kanan and co-workers for calcined oxide-derived copper, attributing it to the high occurrence of grain boundaries and/or other defects on the surface.[315] In the case of the copper nanocubes, it has been speculated that the high degree of (100) surface orientation of the electrodes could play a role, due to the cubic geometry of the surface crystallites and the large number of undercoordinated sites present.[94] Eilert et al. used X-ray absorption spectroscopy to study the properties of the Cu electrodes as they were undergoing redox cycling to produce the cube-shaped surfaces, showing that these nanostructures are derived from $Cu_2O$.[124] They also prepared a catalyst derived from a CuO precursor, exhibiting very similar $CO_2R$ performance, but these electrodes showed a disordered surface morphology without cubic geometries. This points toward other causes for the high $C_2H_4/CH_4$ ratio than the occurrence of cubic facets with preferential (100) orientation. The higher roughness factors (ECSA/geometric electrode area) of these nanostructured electrodes would lead to an elevated local pH close to the electrode surface, which has been shown to favor $C_2H_4$ over $CH_4$, so this is another likely reason for the altered product distribution compared to more planar electrodes.

*Other $Cu_2O$ Film-Derived Electrodes.* A third class of oxide-derived materials are electrodes derived from copper(I)oxide films, prepared by electrodeposition or hydrothermal synthesis onto a substrate.[115,128,215,329] A rough surface is again created after reduction of the oxide layer, although typically less rough than the calcined electrodes described above. Examples of such films of different thicknesses as-deposited and after reduction are shown in Figure 25, illustrating the change in morphology induced by removal of lattice oxygen. $CO_2R$ measurements on this class of materials resulted in suppression of methane and enhanced $C_2$ product formation, with ethylene, ethane, and ethanol being the main products. In the different studies, the effects of bulk crystal structure, film thickness and crystallite size were discussed, giving minor variations in product distribution. Interestingly, these methods for preparing oxide-derived, nanostructured electrodes overall yield similar results to the anodic treatments discussed above with regard to methane suppression and higher selectivity to $C_{2+}$ products. On the other hand, some of the calcined oxide-derived copper electrodes were highly selective toward CO and $HCOO^-$ at low overpotential, but exhibited modest hydrocarbon productions. A possible reason for this discrepancy could be the significantly higher roughness factors resulting from reduction of the thermally oxidized precursors as compared to the other methods of obtaining oxide-derived electrodes. A

very high roughness factor leads to higher activities at lower overpotentials, where the 2e$^-$ products from CO$_2$R, CO, and HCOO$^-$ are preferred. This could also lead to these catalysts being mass-transport limited in a region where they would otherwise produce significant amounts of >2e$^-$ hydrocarbons and/or oxygenates.

**6.2.2. Non-Oxide-Derived Copper.** While it is important to note that a thin native oxide surface layer is formed on Cu whenever exposed to ambient air, here we would like to briefly discuss "non-oxide-derived" copper catalysts. By this we mean to highlight several approaches other than those based on the intentional formation and reduction of a thick copper oxide layer on the surface that have been utilized for preparing 3-D copper electrodes, such as sputter deposition, electrodeposition, and dealloying.[130,330−335] Interestingly, similar trends as for the anodically treated and other Cu$_2$O-derived catalysts discussed previously were again observed in all of these studies. Increased C$_{2+}$ and lower C$_1$ product selectivities were reported compared to polycrystalline Cu, and specifically, ethylene and sometimes ethanol formation reached significant Faradaic efficiencies at lower overpotentials. It seems that many approaches can lead to significantly increased C$_{2+}$ over C$_1$ product selectivity from CO$_2$R compared to polycrystalline Cu. The independence of the resulting product distribution on the preparation method suggests that the reason for the improved selectivity is related to the broader impacts of nanostructuring (such as increased surface area), and not necessarily an oxide precursor.

This hypothesis was supported by two recent works where multiple different nanostructured Cu electrodes were prepared and tested for CO$_2$R. Lum et al. synthesized four different types of oxide-derived Cu electrodes, spanning the three different groups discussed above, and studied their C$_{2+}$ product selectivity from CO$_2$R between −0.7 and −1.0 V vs RHE.[97] The varying ECSA of the different catalysts enabled determination of an ideal roughness to optimize C$_{2+}$ product selectivity at the two extreme potentials, as shown in Figure 26. The authors attributed this optimum to a compromise between elevated local pH, which has been shown to enhance C$_{2+}$ product formation, and sufficient transport of CO$_2$ to the active sites. This hypothesis has been corroborated by mass transport modeling.[97,98] Ren et al. utilized a similar approach, where they prepared four different types of nanostructured electrodes by electrodeposition: three were oxide-derived and one was not.[289] The trends that they observed could all be related to the surface area of the electrode, regardless of whether the material was derived from an oxidized precursor or not. The authors concluded that in order to obtain selectivity toward certain products, the material should be designed to have a limiting current density in a potential region where Cu is selective for certain product(s).[289] If, for instance, 2e$^-$ products are desired, the electrodes should exhibit very high roughness so that significant current can be achieved at low overpotential. As discussed previously, such electrodes reach mass transport limitations early, and therefore produce small amounts of >2e$^-$ products. Thus, if the aim is to produce oxygenates and/or hydrocarbons, intermediate to low roughness is desirable, as was also illustrated by Lum et al. in Figure 26.[97]

As previously mentioned, many nanostructured electrodes are ill-defined, making it difficult to deconvolute the influence of different possible reasons for changes in behavior. Effects that can play a role include changes in mass transport and
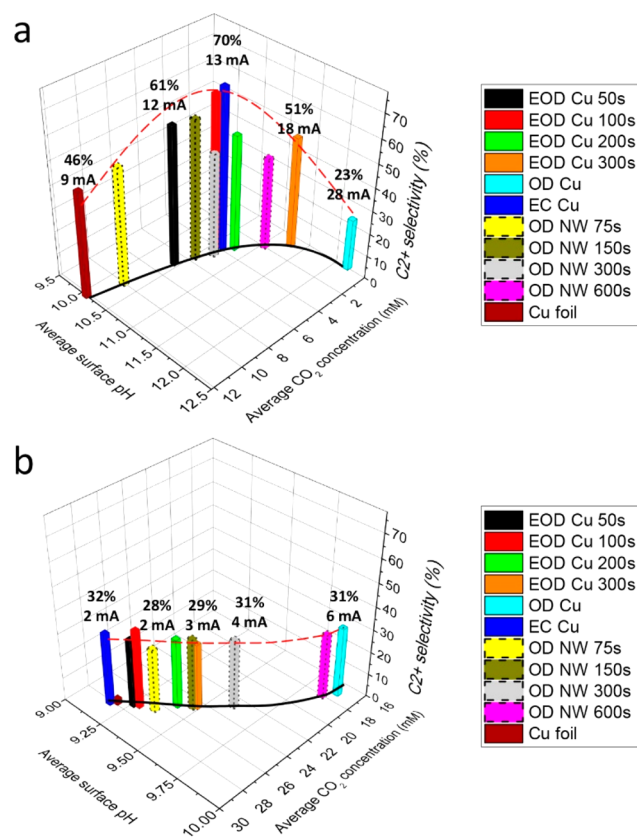


**Figure 26.** C$_{2+}$ product selectivity from CO$_2$ reduction on various oxide-derived Cu electrodes in 0.1 M KOH at (a) −1.0 V and (b) −0.7 V. Reprinted from Lum et al.[97] Copyright 2017, American Chemical Society.

increase in local pH, readsorption and further reduction of products, and higher occurrence of undercoordinated sites. One approach to try to deconvolute surface area effects from other effects is to prepare electrodes with ordered pore structure. Yang et al. prepared electrodes of more well-defined porosity by sputtering Cu onto a structured template.[331] This resulted in a Cu film with cylindrical pores of varying width and depth, as displayed in Figure 27. They found that pores of 30 nm diameter and 40 nm depth (Figure 27a) yield mainly C$_2$H$_4$ at −1.3 V vs RHE, where CH$_4$ is the main CO$_2$R product on polycrystalline electrodes. Deeper pores (Figure 27b) led to enhanced C$_2$H$_6$ selectivity, while wider pores (Figure 27c) gave product distributions more similar to polycrystalline Cu. The authors attributed the increase in C$_2$ production for the electrodes with narrow pores to an increased local pH. The change from ethylene to ethane with deeper pores could be caused by readsorption and further reduction of the products due to the longer retention time in the catalyst layer. Another similar study was performed by Song et al. on ordered, mesostructured Cu inverse-opal electrodes.[336] As expected from the above arguments, they observed improved C$_{2+}$ selectivity with increasing thickness of the porous Cu layer. These types of systematic studies are important in order to help identify the factors that lead to improved performance of 3-D electrodes. We therefore suggest this as an area of increased attention in the future.

**6.2.3. Role of Oxygen in CO$_2$R Electrocatalysis.** The role of oxygen in CO$_2$ electroreduction has emerged as a topic of acute discussion within the field in the past few years. The
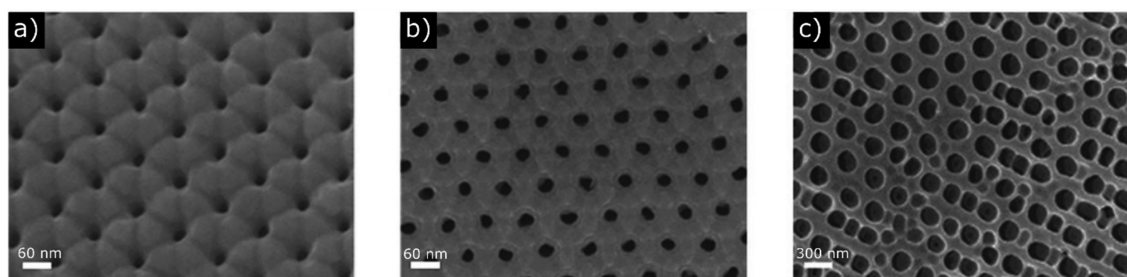
**Figure 27.** SEM images of mesoporous Cu films with holes of different dimensions: (a) 30 nm width and 40 nm depth, (b) 30 nm width and 70 nm depth, and (c) 300 nm width and 40 nm depth. Reprinted with permission from Yang et al.[331] Copyright 2016, John Wiley and Sons.

topic has, however, been debated for decades already, starting with the previously mentioned report by Frese in the early 1990s.[319] As described earlier, oxide-derived nanostructured materials have been shown to yield interesting selectivity effects for $CO_2R$ and COR. An important question is whether this is a result of the nanostructure, or oxygen from the oxidized precursor remaining close to the surface under reaction conditions. Intuitively, one would expect any oxides to be reduced under the $CO_2R$ conditions, due to the strong thermodynamic driving force from the negative potentials applied (see Table 5). Recent DFT calculations indeed

**Table 5. Equilibrium Potentials for the Reduction of Various Copper Oxide Species**[a]

| Reaction | $E^0$/V vs RHE |
|---|---|
| $CuO + 2(H^+ + e^-) \rightleftarrows Cu + H_2O$ | 0.56 |
| $2CuO + 2(H^+ + e^-) \rightleftarrows Cu_2O + H_2O$ | 0.66 |
| $Cu_2O + 2(H^+ + e^-) \rightleftarrows 2Cu + H_2O$ | 0.46 |
| $Cu(OH)_2 + 2(H^+ + e^-) \rightleftarrows Cu + 2H_2O$ | 0.53 |
| $Cu_2CO_3(OH)_2 + 4(H^+ + e^-) \rightleftarrows 2Cu + 3H_2O + CO_2$ | 0.55 |

[a]Calculated with Thermochemistry data from NIST as described in section 1 of the SI.

suggested that reduction of Cu oxides is more favorable than $CO_2R$ at the relevant potentials.[135] However, a number of reports explain that some amount of the initial oxide can be stabilized and affects catalysis. In the following, we will discuss the relevant studies that argue the two points of view.

DFT calculations have been applied to study both whether or not oxygen can be stable under reaction conditions and how it could potentially affect catalysis. Favaro et al. studied the effect of subsurface oxygen on the physisorption of $CO_2$ onto a Cu surface in a gaseous environment. Using DFT and ambient pressure X-ray photoelectron spectroscopy (APXPS), they showed that subsurface oxygen was critical to achieve stable adsorption of $CO_2$ onto the surface.[337] Similarly, Kim et al. used XPS depth profiling before and after $CO_2R$ as evidence that a copper oxide phase catalyzes the $CO_2R$.[329] There remains a gap to be addressed, however, between these *ex situ* results and true $CO_2R$ conditions, since adding electrolyte to the system and applying negative polarization of the cathode are likely to have a significant influence. Liu et al. suggested that subsurface oxygen close to the surface can actually be stabilized by the disordered near-surface structure and roughness of oxide-derived copper.[338] Furthermore, they argued that near-surface oxygen can enhance the CO binding strength by withdrawing electron density from surface atoms and reduce the σ repulsion between CO and surface Cu atoms. Other calculations showed that only oxygen in the topmost

two subsurface layers can have a non-negligible influence on the reactivity of surface atoms, but the barriers for diffusion of these oxygen atoms are too low for them to be stable under reaction conditions.[339,340]

A number of further *ex situ* studies have been carried out showing that oxygen is present after $CO_2R$.[319,329,341−344] These groups applied techniques such as X-ray photoelectron spectroscopy, Auger electron spectroscopy and TEM, showing copper oxides present throughout the catalyst. However, *ex situ* studies after transfer through air are problematic when studying copper, because of the rapid reoxidation upon exposure to $O_2$.[345,346] As discussed previously, reduction of Cu oxide films before or during $CO_2R$ leads to formation of nanostructured surfaces. The high abundance of defects on such surfaces ensures even faster oxidation in ambient air after $CO_2R$,[346] making it even harder to draw conclusions about their oxidation state under reaction conditions. Recently, Cavalco et al. kept their electrodes under an inert gas atmosphere when transferring them to characterization by TEM, and still saw significant amounts of oxygen.[343] It is, however, difficult to ensure that absolutely no oxygen reaches the sample at any point in the process. One way to get around oxygen contamination when applying *ex situ* techniques is using isotopically labeled oxygen. Lum et al. carried out depth profiling of oxide-derived Cu that had been oxidized anodically in $H_2^{18}O$.[346] They saw that after only 10 min, less than 1% of the original content of $^{18}O$ was remaining, similarly to $^{16}O$ control samples, as shown in Figure 28. This suggests that at least a large fraction of the initial oxide is reduced under reaction conditions. Some recent studies have prepared Cu materials with other dopants than oxygen, such as sulfur[143,347] and boron.[348] This way, materials can be prepared that are more resistant against reduction than those prepared with oxygen, while still retaining some of the effects that are thought to occur when O is present close to the surface. However, more work is needed to evaluate if this is actually a viable approach for future materials design.

Because of the rapid reoxidation of Cu in air, *operando* techniques are useful to study the oxidation state of these electrodes during $CO_2R$. A number of studies showed reduction of the oxidized precursor under reaction conditions using *operando* measurements such as X-ray absorption spectroscopy (XAS),[124] Raman spectroscopy,[95,128,129,135] and grazing incidence X-ray diffraction (GIXRD).[176] Other *operando* studies suggest that oxygen is present under reaction conditions.[125,249,349] However, there is uncertainty regarding these techniques as well. Catalysis happens at the surface, and only the reactivity of the topmost layers of atoms matter. As discussed earlier, the presence of different species, such as oxygen, close to the surface can alter this reactivity and affect
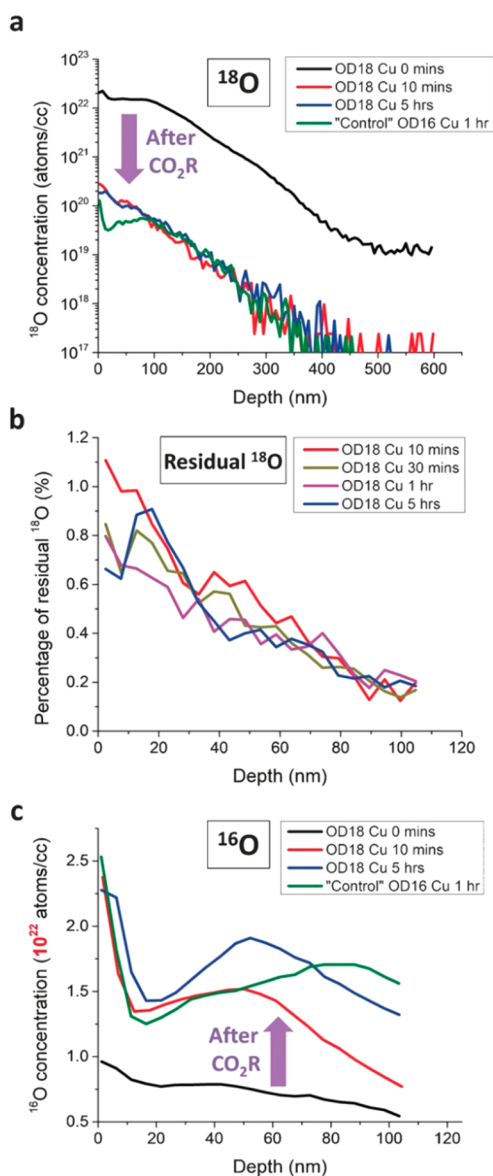
**Figure 28.** (a) $^{18}O$ and (c) $^{16}O$ content of OD Cu catalysts with different $CO_2R$ durations measured by SIMS. (b) The percentage of $^{18}O$ that remains in OD18 Cu after $CO_2R$. Reprinted with permission from Lum and Ager.[346] Copyright 2018, John Wiley and Sons.

catalysis, but they need to be within a few atomic layers underneath the surface.[338,340] Most of the operando techniques employed thus far cannot clearly distinguish whether the oxygen is at or close to the surface, or deeper in the bulk where it will not affect catalysis. On the other hand, even small amounts of oxygen at or close to the surface might affect reactivity, and most of the techniques would not be able to resolve such minute amounts of oxygen present at the surface.

As a general note, it is very challenging to design an experiment that conclusively determines the active site of a catalyst under reaction conditions. However, until evidence that oxygen species are stable close to the surface where they can influence catalysis is presented, it is the opinion of the authors that this phenomenon is unlikely given the strong thermodynamic driving force for reduction. As discussed above, the fact that $CO_2R$ on oxide-derived Cu materials lead to a similar product distribution as non-oxide-derived Cu further indicates that it is the nanostructure, and not the

oxidation state of the precursor material, that gives the altered $CO_2R$ performance.

**6.2.4. Activity Comparisons.** Throughout section 6.2, we have grouped the different 3-D materials into two main categories: oxide-derived and non-oxide-derived catalysts. Although a number of different approaches to nanostructuring have been applied in the literature, which have yielded electrodes with highly diverse structures, there are many similarities in their performance for $CO_2R$. Studies on 3-D electrodes carried out at low overpotentials reported improved selectivity toward carbon monoxide and/or formate compared to planar copper foils. At more negative potentials, some or full suppression of methane formation and enhanced selectivity toward ethylene and/or other $C_{2+}$ products has been reported.

Nanostructuring gives electrodes with increased roughness factors, varying from 2 to 850 in the studies discussed herein. This results in increased current density when normalized by geometric surface area. In Figure 29a, geometric $CO_2R$ current densities for many of the studies discussed throughout this section are shown, compared to data obtained on planar, polycrystalline Cu by Kuhl et al.[65] and Hori et al.[84] In this plot, all of the nanostructured materials exhibit higher geometric activity at a given potential compared to planar, polycrystalline copper, when not under mass transport limited contitions.
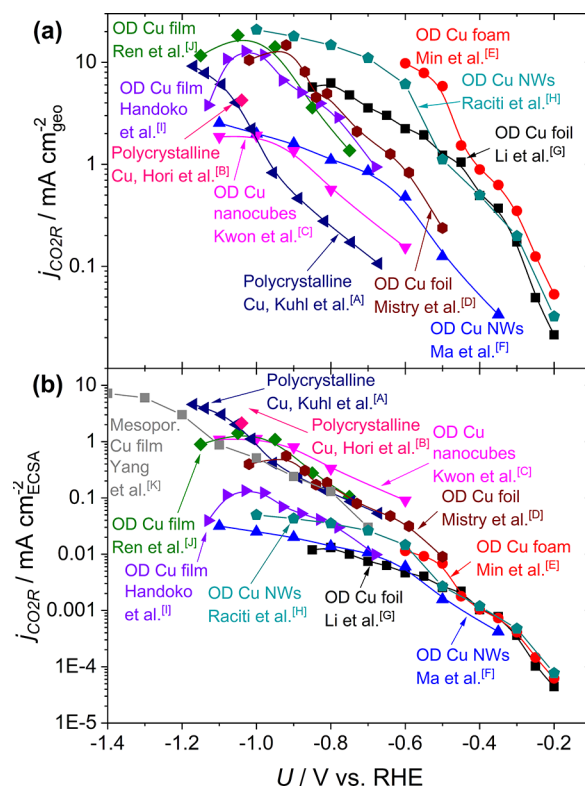


**Figure 29.** Comparison of $CO_2R$ activity for various nanostructured Cu electrocatalysts with polycrystalline Cu. (a) $CO_2R$ partial current density normalized to geometric surface area. (b) $CO_2R$ partial current density normalized to electrochemical surface area (ECSA). The data were obtained from the following studies: [A] Kuhl et al.;[65] [B] Hori et al.;[84] [C] Kwon et al.;[95] [D] Mistry et al.;[125] [E] Min et al.;[93] [F] Ma et al.;[92,320] [G] Li et al.;[89] [H] Raciti et al.;[91] [I] Handoko et al.;[215] [J] Ren et al.;[327] [K] Yang et al.[331] Studies [A,B] are polycrystalline Cu, [C–J] are oxide-derived, nanostructured Cu and [K] is non-oxide-derived nanostructured Cu. See Table S5 in the SI for the data contained in this plot.

This does not, however, reflect the intrinsic activity of the material, as discussed in section 2.1. Therefore, it is instructive to also compare the specific activity of the electrode, as shown in Figure 29b, where the activities are normalized to ECSA. Here we see that there is little or no difference in the total intrinsic $CO_2R$ activity among the different types of nanostructured electrodes. Furthermore, the intrinsic activity of these various Cu nanostructures is similar to that of planar, polycrystalline Cu. The similar intrinsic activity of all Cu electrodes is underlined by the Tafel-like behavior observed in Figure 29b, prior to diffusion limited conditions. This explains why high roughness factor materials tend to exhibit earlier onset; higher roughness electrodes yield higher overall current densities, which allows for the detection of products at lower overpotential, even at low turnover frequencies per surface site. The magnitude of the diffusion limited current density also scales with surface roughness, with high surface area materials reaching mass transport limitations at lower overpotential. These findings strongly suggest that nanostructuring does not alter the intrinsic activity of copper in any significant manner, perhaps within a factor of 2−4, for any synthesis method used. Furthermore, it does not seem that intrinsic $CO_2R$ activity is higher for oxide-derived materials (studies [C−J] in Figure 29), as compared to non-oxide-derived electrodes such as polycrystalline Cu (studies [A, B]) and mesostructured Cu (study [K]). This further corroborates the notion that the precursor material oxidation state is not a crucial factor for $CO_2R$ performance,[97,289] and that any subsurface oxygen that may or may not be present based on different preparations of Cu has little or no influence on intrinsic $CO_2R$ activity.

Although the ECSA-normalized activity is similar for the various types of nanostructured electrodes, there are differences in the product distribution. First, as mentioned previously, mass transport conditions generally have a large influence on the product distribution obtained from a catalyst material. When approaching mass transport limited conditions, the local pH close to the electrode surface increases. Since electrodes with high surface area reach mass transport limitations at relatively low overpotentials, improved $C_{2+}$ product selectivity can be observed under these conditions. However, as significant mass transport limitations are reached, too little $CO_2$ reaches the electrode surface, and $H_2$ evolution takes over. This is a likely reason for calcined oxide-derived Cu foils exhibiting a significant drop in $CO_2R$ selectivity at potentials more negative than −0.6 V vs RHE, and low hydrocarbon formation in general. The very high roughness factors cause the bulk of the non-mass-transport-limited activity to be in a low overpotential region where $CO_2R$ to CO and $HCOO^-$ is favored; meanwhile, these systems favored $C_{2+}$ oxygenates at low overpotentials when doing COR, which can be understood by the potential-dependent selectivity trends shown in Figure 24. Thus, a key finding here is that the roughness factor of the electrode in effect shifts the potential window where kinetically limited $CO_2R$ can take place, which has a very large impact on the product selectivity.

Electrode roughness is not the only important parameter though; morphological features such as pore size and shape can also strongly influence product distribution, as well as the retention time of products and intermediates in the catalyst structure. A good illustration of this is that studies investigating catalyst layer thickness or pore depth generally find that thicker nanostructures lead to more ethane on behalf of ethylene. Ethane is generally not observed on planar electrodes, and can

likely be attributed to readsorption and further reduction of ethylene. Although some clear trends are outlined above, more work is still needed to improve our understanding of which effects drive selectivity to different products, and eventually give us the possibility to steer $CO_2R$ toward desirable chemicals. Furthermore, since current densities of 100 mA/$cm^2$ or higher seems to be a minimum for commercialization to be realistic,[59] more work needs to be done to enhance mass transport of $CO_2$ to achieve higher reaction rates. A key strategy toward that end will be discussed subsequently.

## 6.3. Vapor-Fed Systems

All of the catalysts described thus far have been tested using conventional aqueous-phase $CO_2R$ reactors. While these have clearly been useful for gaining fundamental insights, the poor solubility of $CO_2$ in aqueous electrolytes (∼34 mM), along with the acid/base buffer equilibria ($CO_2/HCO_3^-/CO_3^{2-}$) described earlier lead to significant challenges in achieving high $CO_2R$ reaction rates. Vapor-fed systems can overcome these practical limitations by delivering gas phase $CO_2$ directly to the catalyst surface. Indeed, some of the best performing Cu catalyst systems reported today in terms of Faradaic efficiency, energy conversion efficiency, and stability use vapor-fed reactors.[126,131,292,330,347,350−353] We therefore wanted to take this opportunity to briefly discuss these reactor configurations and highlight promising developments in this area. For more information, we direct the readers to a recent perspective article that details the progress, challenges, and opportunities toward the development of practical $CO_2$ electrolyzers,[354] as well as a recent review on the same topic.[355]

In commercial electrocatalytic systems, such as fuel cells and water electrolyzers, a gas diffusion layer is typically employed as a support material in order to maximize transport of reactants to the catalyst surface. These layers comprise open, three-dimensional structures of relatively inert materials, such as carbon. Together with the porous catalyst, this forms what is known as a gas diffusion electrode (GDE). A GDE can be used with either a liquid electrolyte or a solid-state polymer electrolyte membrane. A membrane electrode assembly (MEA) refers to the latter case, whereby an assembled stack is composed of a polymer electrolyte membrane sandwiched between two GDEs. Here, ionomers are used to extend the electrolyte membrane material into the GDEs to provide intimate contact with the catalyst and ensure efficient transport of ions to/from the surface. This is important because the relevant reactions can only take place at triple-phase boundaries, which are points where the gaseous reactant, electron-conducting catalyst, and ion-conducting polymer or liquid electrolyte meet. Vapor-fed systems are thus inherently more complex than aqueous-phase systems due to the multitude of heterogeneous interfaces across a range of length scales (Figure 30) and will present many challenges in optimizing $CO_2R$ activity and selectivity.

While still in its infancy, research in these areas has already demonstrated promising activity and selectivity improvements compared to conventional aqueous-phase reactors.[126,131,292,330,347,350−352] For example, various vapor-fed reactors using Cu-based GDEs have achieved high $CO_2R$ geometric partial current densities to ethylene of around 150−473 mA/$cm^2$,[126,131,292,330,351,352] and to ethanol of around 40−108 mA/$cm^2$.[131,292,347,351,352] As discussed in subsection 3.3.1, alkaline electrolytes can improve selectivities and energy efficiencies to $C_{2+}$ products. This was illustrated in a recent
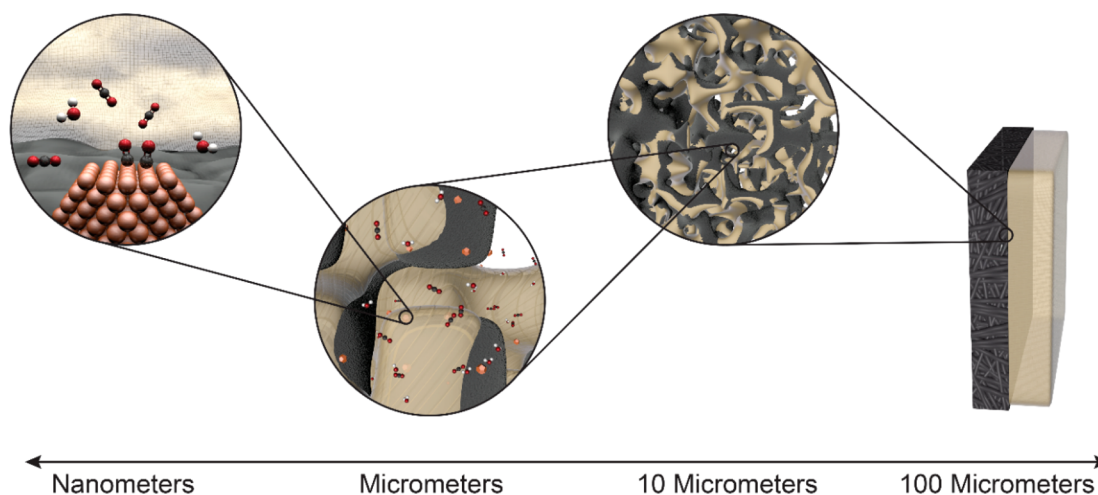
**Figure 30.** Schematic of a three-dimensional GDE depicting the multiple length scales where phenomena are occurring during electrochemical $CO_2R$. Reprinted from Higgins et al.[354] Copyright 2018, American Chemical Society,.

report where researchers tested KOH, $KHCO_3$, KCl, and $K_2SO_4$ electrolytes in their microfluidic $CO_2$ flow cell electrolyzer and found that an optimal production of $C_{2+}$ products (411 mA/cm$^2$ at −0.67 V vs RHE, corresponding to 62% Faradaic efficiency) could be achieved in KOH.[352] Another study employed a range of strongly basic conditions (1−10 M KOH) and could achieve a partial current density for $C_{2+}$ products as high as 608 mA/cm$^2$ at −0.67 V vs RHE (corresponding to 81% Faradaic efficiency).[351] These carbon-based GDEs were unfortunately found to degrade at such high reaction rates, but the stability was improved by incorporating a polymer layer to help prevent flooding. In this way, Sargent and co-workers were able to achieve ~70% Faradaic efficiency for $CO_2R$ to $C_2H_4$ at −0.55 V vs RHE for 150 h in 7 M KOH (although the current slowly declined from 100 to 75 mA/cm$^2$).[351] It is worth noting that for sustained $CO_2R$ under alkaline conditions, reactor systems will have to be carefully engineered to avoid neutralization of the electrolyte via $CO_2$ conversion to bicarbonate; otherwise, regeneration of the KOH will add to the costs and detract from the overall energy balance of the system. This could also be one advantage of performing COR instead of $CO_2R$ in such a device.

The studies discussed above demonstrate the promise of using vapor-phase $CO_2$ to overcome intrinsic limitations of aqueous-based systems, but there is still much work ahead in further developing and optimizing these practical device architectures for commercial application. The choice of electrolyte, catalyst, and GDE fabrication process will all have a significant impact on device performance and must ideally be designed to optimize transport of $CO_2$, products, electrons, and ions simultaneously. There is thus a large phase space to explore in tuning relevant properties of the gas diffusion layer(s), such as porosity, hydrophobicity, and thickness. Well-controlled studies that aim to understand the effects of nanoparticle size, shape, and loading, as well as catalyst−support and catalyst−ionomer interactions will also be essential. Translating this and other fundamental knowledge gained from probing catalyst morphology and electrolyte effects in aqueous-phase reactors to these complex vapor-fed systems will aid in their advancement. Furthermore, since $CO_2R$ in these 3-D architectures involves many processes over a range of length and time scales, it will become increasingly important to couple experimental and theoretical investiga-

tions. Continued development of microkinetic and 3-D transport modeling methods are promising candidates in that regard.

## 6.4. Summary

Nanostructuring gives electrodes with increased roughness factors, varying from 2 to 850 in the studies discussed in this section, which results in increased current density when normalized by geometric area of the electrode. However, when normalized by the ECSA of the electrode, it is found that the *intrinsic* activity of Cu catalysts is similar among all the different forms of electrodes reported to date, whether nanostructured or planar, and irrespective of the particular nanostructure or synthesis route. This highlights the importance of data normalization for determining whether higher catalytic activity results from a higher average turnover frequency or simply from an increased number of active sites.

While nanostructuring does not appear to change the intrinsic activity of Cu, interesting changes in product distribution have been observed. For example, many 3-D catalyst materials exhibit some or full $CH_4$ suppression and increased $C_{2+}$ product selectivity. This has largely been explained by mass transport modeling studies, which have shown that an ideal compromise between pH increase and $CO_2$ supply at the electrode surface gives an optimal $C_{2+}$ selectivity on rough electrodes.[97,98] More generally, since the number of active sites impacts the potential windows where the reaction is kinetically limited vs mass transport limited, the catalyst surface area has emerged as a key determinant of product selectivity. Other morphological factors such as preferential faceting, grain boundaries, and pore shape and size may also lead to changes in $CO_2R$ selectivity due to surface structure effects and/or readsorption and further reduction of products.

Nanostructured electrodes are particularly relevant because of their potential compatibility with vapor-fed reactors, a promising technology platform capable of achieving industrially relevant current densities. However, substantial efforts will be needed in order to understand how $CO_2R$ catalysts behave in such a different environment than the conventional aqueous-phase, lab-scale reactors that are typically employed today. We feel that research in these directions should be prioritized in order to begin accelerating the development of
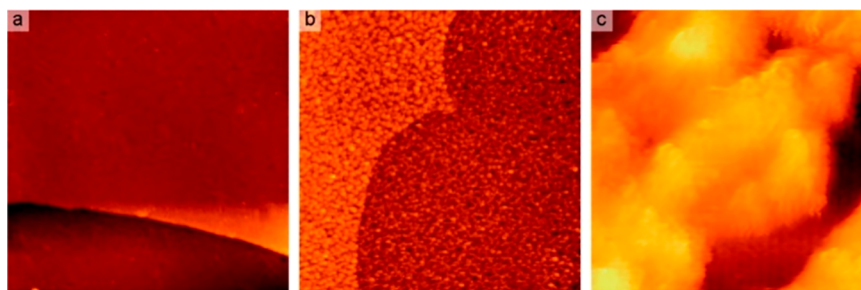
**Figure 31.** (a) Atomically flat morphology of the Cu overlayer in a CO-free electrolyte $(499 \text{ nm})^2$, $U = 0.02$ V, $U_B = 292$ mV, $I_T = 1$ nA. (b) Granular morphology of the Cu overlayer after exposure to a CO-saturated electrolyte $(499 \text{ nm})^2$, $U = 0.01$ V, $U_B = 356$ mV, $I_T = 10$ nA. (c) Disordered Cu overlayer with $(2 \times 2)$-CO structure inside the vacancies $(13.6 \text{ nm})^2$, $U = 0.01$ V, $U_B = 356$ mV, $I_T = 10$ nA. Reprinted from Varela et al.[381] Copyright 2013, American Chemical Society.

practical devices that convert $CO_2$ to high value fuels and chemicals.

# 7. COPPER BIMETALLICS

Changing structural properties of the catalyst material (e.g., via hierarchical nanostructuring, particle size/support effects, etc.) is one key tactic to alter the catalytic performance, as discussed in the previous section. Another approach being employed to improve the activity, selectivity, and stability of Cu for $CO_2$R is the preparation of bimetallic systems. Bimetallics can enhance performance compared to monometallic catalysts by a variety of mechanisms including electronic ligand and strain effects[356−361] and geometric ensemble effects.[356−358,362,363] The electronic effects refer to a change in the electronic structure of the host material after addition of another element, which alters the binding strength of intermediate adsorbates on the surface according to the d-band model.[359,364] Geometric ensemble effects refer to a change in the atomic arrangement of actives sites, which alters the way adsorbates interact with the surface and each other. In addition to simply changing the number or configuration of particular atoms in an ensemble, bifunctional active sites can also be created, where neighboring metals serve different catalytic roles. For example, it has been thought that bifunctional active sites for $CO_2$R could be created using a metal with higher oxygen affinity, allowing *COOH or *CHO to be stabilized by interacting with the surface through both the carbon and oxygen atoms compared to *CO, which tends to bind surfaces through the carbon atom in an upright geometry.[202,365] Additionally, isolated active sites can be formed that change the proximity of other adsorbates, which can impact the selectivity.[366]

There are a multitude of bulk systems that can be formed when two elements are mixed, including solid solutions, intermetallic compounds, and phase-separated systems. Details governing the formation of these bimetallics and their different properties are outside the scope of this Review. Instead, we will focus on the resulting model systems that allow for the study of the aforementioned electronic and geometric effects. These include bulk alloys, surface alloys (alloy layer supported on a monometallic core), near surface alloys (alloy beneath one or a few monometallic layers), or guest metal modified surfaces (e.g., islands or particles on a monometallic host). In addition, there are bimetallic overlayers, either planar or nanoparticulate (core−shell) structures, which refer to a monometallic surface supported on either a different metal, a bulk alloy, or a (near) surface alloy. Due to the large number of possible bimetallic combinations, with regard to both the composition and

structural arrangements, computational screening approaches have been used to aid in the search for improved $CO_2$R catalysts.[202,365−370] There have been a number of non-Cu-based bimetallics that have demonstrated synergistic activity or selectivity, primarily to $2e^-$ products.[371−376] This section will only focus on the experimental results obtained for Cu-based bimetallic systems in aqueous solutions under ambient conditions.

As described in subsection 1.2.2, early experimental work led by Hori and co-workers showed that on Fe, Ni, Pt, and Pd, the competing HER is primarily observed; on Ag, Au, and Zn the major product is CO; and on Cd, Pb, Hg, Tl, Sn, and In the major product is $HCOO^-$.[1,84] The Cu-based bimetallic combinations discussed in the following sections are thus organized according to these groupings by the dominant $CO_2$R selectivity of the guest metals. First, we will describe the structural properties of the studied model catalysts and summarize the main experimental findings with respect to their catalytic activity and selectivity for $CO_2$R compared to pure Cu. Then, we will provide some overall perspectives on the benefits of using bimetallics, pitfalls to avoid when investigating these systems, and suggestions for future studies.

## 7.1. Copper and $H_2$ Producing Guest Metals (Fe, Ni, Pt, Pd)

Mainly $H_2$ is formed during $CO_2$R on monometallic electrodes of group 8−10 transition metals.[1,84] Thus, Cu-M bimetallic electrodes (where M = Fe, Ni, Pt) typically result in increased HER activity and selectivity compared to pure Cu. This has been shown for a variety of model systems: Cu electrodes modified with Fe, Ni, or Pt deposits,[377,378] CuPt alloy nanocubes and nanocrystals,[379,380] and Cu overlayers on Pt electrodes.[381,382] Additional trends have been observed whereby increased guest metal coverage on Cu, increased Pt content in the nanoalloys, and decreased Cu overlayer thickness led to increased HER activity and/or selectivity. In the case of the Cu overlayers, only after the Cu layer was sufficiently thick (>5 nm) did the $H_2$ formation return to bulk Cu-like values.[382] In a separate study, it was demonstrated using electrochemical scanning tunneling microscopy (ECSTM) that the presence of CO formed during $CO_2$R destabilizes thinner Cu overlayers due to the very high binding affinity of CO on Pt.[381] This causes restructuring from a flat overlayer morphology into more complex three-dimensional particles, while simultaneously exposing the underlying Pt substrate, as shown in Figure 31.[381] Thus, the increased affinity for HER in the bimetallic systems likely results from increased exposure of these guest metals on the catalyst surface.

As one might expect, these systems also exhibit a concurrent decrease in overall $CO_2R$ activity and selectivity, and in general, only mixtures of $H_2$, CO, $CH_4$, and $C_2H_4$ were detected. Interestingly, with increasing Ni or Fe coverage on Cu, Hori found a linear correlation between the HER selectivity and $CH_4/C_2H_4$ ($C_1/C_2$) selectivity ratio.[377] It is worth noting, however, that the increase in $C_1/C_2$ ratio was due to significant $C_2H_4$ suppression rather than a boost in $CH_4$ production. This trend extends across many of these other systems, where $C_2H_4$ was only detected in trace quantities[378,381] or not at all.[379,380] Based on the mechanistic studies discussed earlier, this decreased $C_2H_4$ production may be attributed to increased H coverage on the surface, which can hinder C−C coupling. In the nanoalloys and guest metal modified Cu systems, this can also be due to a lack of adjacent Cu surface sites required for CO dimerization. However, for the thin Cu overlayer system, it was determined via ECSTM that even after sintering, the Cu ensembles would still be large enough to allow for C−C bond formation, but the $C_2H_4$ Faradaic efficiency did not exceed 0.6%.[381] Meanwhile, for thicker Cu overlayers (>5 nm), it was found that the ratio between $CH_4$ and $C_2H_4$ could be tuned as a function of overlayer thickness and potential.[382] Both of these studies point to tensile strain on Cu from lattice mismatch with the Pt substrate playing a role in the $CO_2R$ selectivity by altering the adsorption energy of reactive intermediates, as previously discussed. While these $C_1/C_2$ selectivity trends are interesting and merit further study to better understand, unfortunately it is clear that none of these bimetallics with highly HER active metals resulted in a more active $CO_2R$ catalyst for >2e⁻ products (Figure 36 in section 7.4).

Interestingly, earlier reports from Watanabe et al.[383,384] indicated that Cu−Ni alloys could have synergistic methanol production because they found that neither of the pure metals produced methanol, but their Cu−Ni alloys were shown to produce around 5−10% Faradaic efficiency. The different structural properties of the bimetallic electrodes (incorporating Ni as an overlayer/surface additive vs mixing as an alloy) might be the cause for the different products observed between this and the other reports discussed above. With improved product detection, however, methanol production has since been confirmed for both monometallic Cu and Ni electrodes by Kuhl et al.[203] Thus, it is unclear what, if any, synergistic effects were at play, and more thorough investigations are needed.

Palladium is somewhat unique in this grouping in that, according to Hori's data, Pd has very similar $H_2$ and CO Faradaic efficiencies (~27%), although there is ~40% of the current unaccounted for, which is likely from hydrogen absorption.[1] The ease with which hydrogen can be absorbed into Pd metal has attracted interest in this material for $CO_2R$, and early studies showed that Pd selectivity was heavily dependent on whether it was employed as a hydrogen-depleted or hydrogen-enriched surface, with the latter leading to greatly enhanced formate production.[385] Similarly, it was found that Pd and electrolytically charged Pd+H electrodes both modified with Cu displayed different selectivities, where Cu/Pd+H electrodes led to higher Faradaic efficiencies for the production of methane and especially of formate compared to Cu/Pd electrodes.[386,387] This effect was enhanced when the amount of absorbed hydrogen in the Pd electrodes was larger (Cu/Pd+H charged to 20 vs 100 Coulombs), and when the coverage of Cu was lower, likely because higher Cu coverages prevented hydrogen from discharging through the cracks in the Cu

film.[386,387] Production of CO and $C_{2+}$ products were not enhanced by the absorption of hydrogen.[387] Another study found a complete shift in selectivity from $C_2H_4$ (32.1% → 3.4%) to $C_2H_6$ (<1% → 30.1%) at −1.0 V vs RHE on a $Cu_2O$-derived catalyst after Pd(II)-chloride was added to the electrolyte, while the production of other carbonaceous species remained almost unchanged.[388] Mechanistic studies on this system lead the authors to suggest that $CO_2R$ on the Cu sites first produces $C_2H_4$, which is then hydrogenated to $C_2H_6$ with the assistance of adsorbed $PdCl_x$. Ultimately, the practicality of this system may be limited since $PdCl_2$ served as a sacrificial dopant, resulting in less than 100% total Faradaic efficiency due to reduction of the $PdCl_2$ and decreasing $C_2H_6$ selectivity over time as this species was depleted. Regardless, both of these studies point to Pd serving as an active hydrogen source, shifting $CO_2R$ selectivity toward hydrogenated products.

While these bimetallics utilized Pd or Cu as substrates for deposition of the other component, Cu−Pd alloys have also been reported and displayed a very different trend. Composition-dependent studies of Cu−Pd alloy nanoparticles[389] and electrodeposited mesoporous films[390] resulted in enhanced activity and selectivity to CO, with optimum ratios of Cu:Pd producing around 80% CO at −0.8 V vs RHE. Both studies attribute the enhanced CO production to a ligand effect, where Cu weakens the CO adsorption energy on adjacent Pd sites. Another reason for CO being the dominant $CO_2R$ product reported in these studies could be due to a lower *H coverage resulting from Pd−H bond weakening in Cu−Pd alloys, preventing CO hydrogenation.[390,391] While electronic effects may certainly have an impact, other studies suggest that geometric effects play the primary role in governing selectivity of Cu−Pd bimetallics. GDEs with a 1:1 ratio of CuPd were systematically studied in ordered, disordered, and phase separated atomic arrangements (Figure 32).[392] Both intermetallic mixing patterns primarily made CO
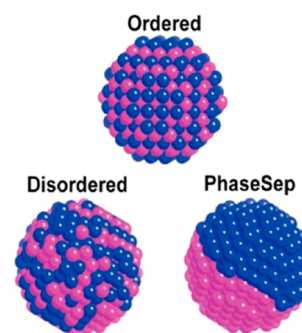


**Figure 32.** Schematics of ordered, disordered, and phase separated particles with 1:1 composition of CuPd. Reprinted from Ma et al.[392] Copyright 2017, American Chemical Society.

over a range of potentials, similar to the other two Cu−Pd alloy systems, while the phase separated CuPd electrode showed a very clear difference in selectivity and made >60% $C_{2+}$ products. Furthermore, a compositional study of disordered Cu−Pd electrodes also resulted in higher selectivity for $C_{2+}$ products as the concentration of Cu increased from Pd < $CuPd_3$ < CuPd < $Cu_3Pd$ < Cu.[392] Likely, the hydrogen absorption ability of Pd and the C−C coupling ability of Cu are both diminished upon increased mixing. Thus, bimetallic systems where Cu and Pd are sufficiently separated likely lead to more hydrogenated and/or $C_{2+}$ products, whereas bimetallic

systems with increased mixing between these two elements may lead to more CO. While this provides compelling evidence for geometric effects driving the selectivity, increasing the degree of mixing should enhance any ligand effects as well. This is why, in general, it is extremely challenging to deconvolute ligand/strain effects from geometric effects.

## 7.2. Copper and CO Producing Guest Metals (Ag, Au, Zn)

Silver, gold, and zinc are all highly selective for CO production from $CO_2R$ in aqueous solutions under ambient conditions.[1,84] As a result, many Cu-M bimetallic electrodes (where M = Ag, Au, Zn) have shown increased selectivity, and in some cases higher intrinsic activity, for making CO.[154,393−397] Alternatively, some Cu-M bimetallic electrodes (where M = Ag, Au, Zn) have demonstrated synergistic effects leading to improved activity or selectivity for C−C coupled products.[72,122,127,129,131,398−402] The different factors leading to these two broader outcomes will be discussed subsequently.

### 7.2.1. Synergistic Effects for CO Production.
Several composition-dependent studies have shown increasing CO selectivity with increasing guest metal content, and this was demonstrated for a variety of bimetallic structures including: Cu−Ag dendritic electrodeposits,[393] small coverages of Au on Cu,[394] $Au_xCu_{1−x}$ alloys formed via pulsed laser deposition with and without $O_2$ present,[395] $Au_xCu_{100-x}$ bulk alloys,[154] and ~10−11 nm Cu−Au alloy nanoparticles.[396] This can be expected due to the weaker binding of CO on Ag and Au, favoring CO desorption in these systems.[276] There does exist some synergistic effect though, since several Cu−Au bimetallics showed higher activities for CO production compared to pure Au electrodes tested in each study.[154,396,397] Several explanations for this include the following: CO adsorbed on Cu sites can further promote CO desorption on Au sites due to dipole repulsion,[154] or neighboring Cu atoms can instead form a bond with the oxygen end of *COOH via a bifunctional mechanism, stabilizing this intermediate for CO production on Au sites.[396] It is unclear to what extent these may be true, but both suggest that an optimal surface Cu:Au composition is required for enhanced CO activity in these alloys. It is worth noting that the optimal bulk composition was different in these two studies, but this could be due to a morphology effect for the planar vs nanoparticle alloy configurations and/or the true *in situ* surface compositions differed from the measured bulk compositions.

Alternatively, a third study on CuAu (1:1) alloy nanoparticles actually ascribed their enhanced CO activity to a compressively strained Au surface layer that formed as a result of a disorder-to-order transformation.[397] The disordered CuAu nanoparticles were largely selective for $H_2$, in agreement with the group's previous composition-dependent study,[396] but the ordered CuAu nanoparticles were found to have higher specific and mass activities for CO production compared to pure Au nanoparticles. Since surface characterization revealed that a three-atoms-thick Au shell formed on top of the ordered CuAu alloy core, bifunctional effects were ruled out in this specific system; instead, it was suggested on the basis of a complementary DFT study that 6% compressive strain and vertical ligand effects contributed to the catalytic activity.[397] While enhanced CO activity has been demonstrated in these Cu−Au alloy and core−shell systems, it is worth noting that none have shown a higher average turnover frequency than the state-of-the-art Au catalysts (Figure 37 in section 7.4). Cu−Au

bimetallics may offer an interesting opportunity though to rationally design electrocatalysts yielding optimal and tunable syngas ($H_2$ and CO) compositions, as demonstrated in a systematic study of Cu monolayer coverage on Au nano-needles.[132]

Another report sought to take advantage of strain and vertical ligand effects by synthesizing Au core Cu shell nanoparticles (Au@Cu) with different Cu shell thicknesses (7−10, 14−18, 30−40 layers).[403] The cubic Au nanoparticle core resulted in epitaxial growth of Cu(100) for low and intermediate quantities of Cu layers, but this broke down for the largest number of Cu layers, which looked to be more (111) in character. Therefore, this system has several competing effects including strain, surface structure, roughness, and particle size differences that make it tough to ascribe the activity and selectivity to any one of these in particular. In addition, all three samples showed time-dependent selectivity over the course of an hour.[403] While they do not confirm with structural characterization after electrochemistry, this could be due, at least in part, to Cu overlayer instability. Previous work investigating Cu overlayers on Au(100)[404] and Au(111)[404,405] observed alloy formation for Cu monolayers[404,405] and multilayers[405] under strongly cathodic potentials, while submonolayers[404] relieved the interface tension by structural collapse. Thus, the significant (12.5%) tensile strain between Cu and Au may simply be too unstable to yield a certain benefit, especially given the already high mobility of Au and Cu at room temperature. The Au overlayer on intermetallic CuAu nanoparticles generated by the disorder-to-order transformation resulted in an intermediate compressive strain (6%) for Au.[397] The reduced interfacial tension, plus the fact that the Au shell is already supported on an alloy phase, may decrease the driving force for overlayer instability. While extended tests over 12 h do show some loss of activity (15%) and gold content,[397] near surface alloys could still be a promising paradigm to investigate moving forward for achieving stable strain effects.

### 7.2.2. Synergistic Effects for >2e⁻ Products.
There are two key effects in some Cu-M bimetallic electrodes (where M = Ag, Au, Zn) that have led to improved activity or selectivity for C−C coupled and oxygenated products: CO spillover and electronic effects. In the first case, by co-locating domains of Cu with those of a CO-generating metal, such as Ag, Au, and Zn, additional CO can be supplied to Cu via eased surface diffusion over short length scales and/or by simply increasing the local CO concentration within the diffusion boundary layer, which in turn can lead to a higher coverage of *CO. One potential demonstration of this concept was shown in a study on Cu−Ag bimetallic electrodes using a pulsed $CO_2$ electro-reduction technique, which yielded higher Faradaic efficiencies for the production of $C_{2+}$ compounds such as $CH_3CHO$, $C_2H_5OH$, and $C_2H_4$ compared to pure Cu and Ag metal electrodes.[122] By alternating cathodic and anodic biases, it was expected that desorption of CO occurred on Ag but not from Cu, allowing for facile C−C coupling on Cu due to a higher partial pressure of CO near the surface of the electrode. Another group electrodeposited Cu−Au alloys onto a nanoporous Cu film (NCF) and found these led to higher alcohol selectivities compared to the NCF alone.[398] They also compared the best Cu−Au alloy composition electrodeposited on the NCF to that deposited on a flat copper plate and found that the alcohol selectivity was much lower using the copper plate substrate, suggesting that the nanostructured morphology and/or surface area has a strong impact on this effect. Linear

sweep voltammetry in CO yielded a higher current than in Ar, so while CO spillover is not mentioned explicitly, the authors use this result to suggest that catalyzing conversion of intermediary CO could be the cause for the improved alcohol selectivity.[398] Unfortunately, the results are only presented in terms of selectivity (Faradaic efficiency), no current density information for the bulk electrolysis was provided, so we were unable to determine if the intrinsic activity toward alcohols was improved.

There have been a few recent reports that have more directly linked observed improvements in C$_{2+}$ activity and/or selectivity to a CO spillover effect.[127,129,131,399,400] One system that clearly exhibited synergistic activity and selectivity for C$_{2+}$ alcohols superior to that of Cu, Au, or CuAu alloys was a polycrystalline Cu foil decorated with Au nanoparticles (Au/Cu).[399] In fact, the Au/Cu catalyst reduced the overpotential by >260 mV for the production of alcohols and had a >100× higher rate of CO$_2$ reduction to >2e$^-$ products in this low overpotential region, as shown in Figure 33. These improve-
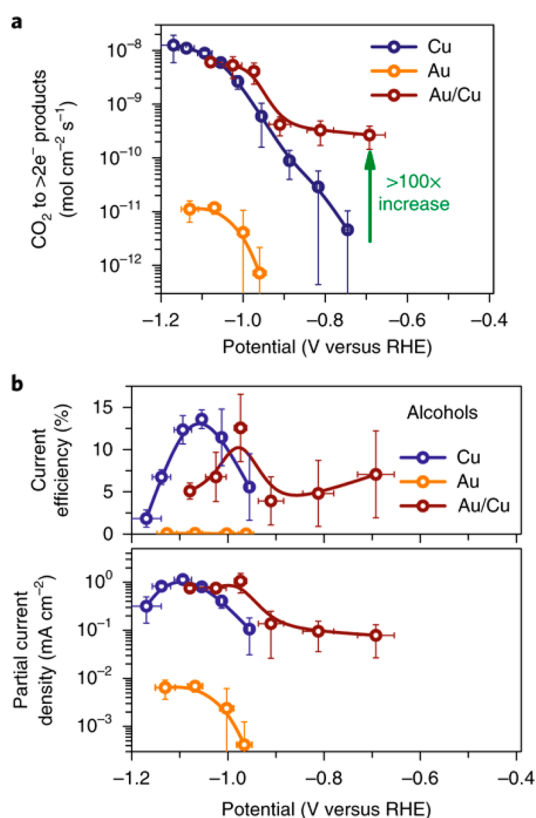


**Figure 33.** (a) CO$_2$R rate to >2e$^-$ products; (b) Current efficiencies and partial current densities to alcohols. Reprinted with permission from Morales-Guio et al.[399] Copyright 2018, Springer Nature.

ments are attributed to a tandem catalysis mechanism, where these two separate metals operate in close proximity with complementary surface chemistry. This hypothesis was supported by a control experiment performed on a surface alloy (Au$_{0.01}$Cu$_{0.99}$), which did not reproduce the trend of enhanced alcohol production at low overpotentials. The CO spillover effect was further corroborated by transport modeling, which indicated that the Au nanoparticles provide a higher concentration of CO near the Au/Cu surface than what Cu could produce alone or than what could be sustained through transport of CO from the bulk.[399] Having this local CO source

within the electrode double layer sidesteps the issue of low CO solubility in aqueous electrolytes, leading to the increased activity for C$_{2+}$ products at low overpotentials. A similar Au on Cu system mentioned earlier[394] only reported on electrolysis data at −1.85 V vs SCE, in the high overpotential region where this enhancement in minimized. In addition, Morales-Guio et al. found that there was an optimal range for Au nanoparticle loading required to observe the synergistic effect to >2e$^-$ products.[399] These reasons, as well as differences in product detection capabilities, could possibly explain why this effect was not observed previously.

Investigations of oxide-derived Cu$_x$Zn phase separated electrodes[129] and Ag−Cu$_2$O phase blended and phase separated electrodes[127] showed enhancements in C$_{2+}$ selectivity, particularly for ethanol, and a CO spillover mechanism was again proposed. These bimetallic electrodes yielded some of the highest ethanol Faradaic efficiencies reported (Ag−Cu$_2$O phase blended: 34% at −1.2 V vs RHE;[127] Cu$_4$Zn: 29% at −1.05 V vs RHE[129]). It is noteworthy, however, that the enhancements in ethanol selectivity compared to their monometallic Cu control samples only occur at high overpotentials ($E \leq -0.9$ V vs RHE). This is in stark contrast to the Au/Cu system, which achieved higher selectivities at lower overpotentials (−1.0 V vs RHE $\leq E \leq$ −0.7 V vs RHE) and reached a maximum in alcohol partial current density 90 mV earlier than on Cu.[399] This can likely be rationalized by the higher overpotentials required for CO production on Ag and Zn compared to Au (see Table 3),[1] which may shift the potential region where CO spillover can be a benefit. As for why ethanol is preferred over ethylene in these systems, it is likely that the lower rates of hydrogen production on the Cu$_x$Zn and Ag−Cu$_2$O electrodes and operation in the low overpotential region on Au/Cu could shift the selectivity toward oxygenated C−C coupled products (i.e., ethanol) rather than hydrogenated C−C coupled products (i.e., ethylene). As discussed previously, while the selectivity is an important metric to consider, this alone does not tell you about the activity of the catalyst for CO$_2$ reduction; for this, we must examine the (partial) current densities. Since the authors primarily discuss activity based on the geometric current density despite the different roughness factors (RF) of these catalysts[129] or do not report the catalysts' RF,[127] we will address their activity in section 7.4.

Finally, it is worth discussing another report that has studied this tandem/sequential catalysis mechanism in detail using a series of microfabricated electrodes (Figure 34).[400] In the first design, separate, interdigitated Au and Cu electrodes on an insulating SiO$_2$ substrate allowed for each electrode to be actuated individually or simultaneously. When the electrodes were actuated simultaneously, there was a significant drop in the CO partial current density compared to when only Au was actuated, which suggests that some of the CO formed on Au lines was consumed by the Cu lines, validating the sequential catalysis concept.[400] Interestingly, there was also a subtle shift in C$_{2+}$ product distribution to favor oxygenates over ethylene production with decreasing Cu coverage, while all variations of the device maintained a lower oxygenates to ethylene ratio when only Cu was actuated.

The researchers then probed this effect further by systematically fabricating a series of electrodes where Cu was patterned directly onto Au or Ag substrates, which allowed for fine control over the spacing and coverage of Cu. As the coverage of Cu was decreased from 77.2% to 2.4%, the ratio of
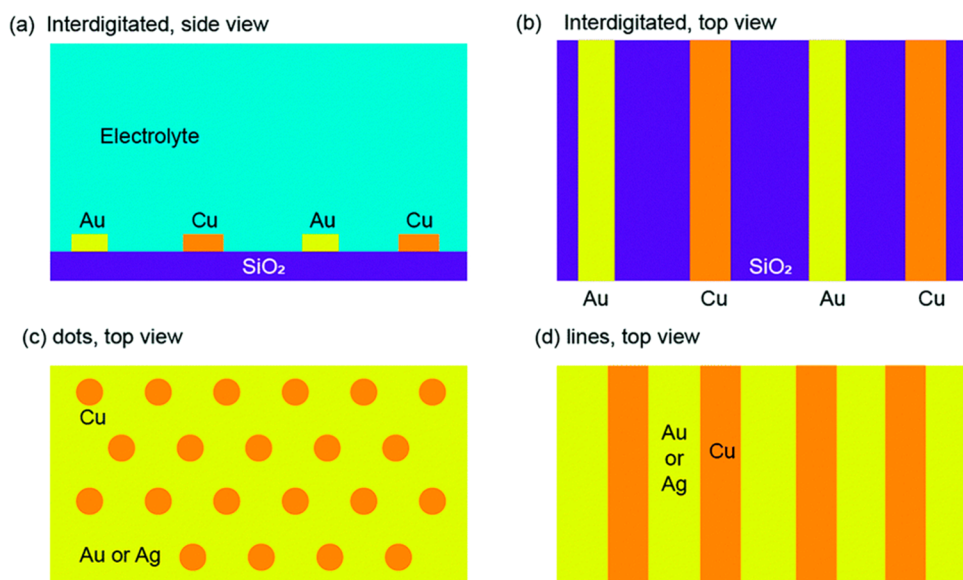
**Figure 34.** Schematics of interdigitated bimetallic electrodes, (a) and (b), and micropatterned electrodes, (c) and (d). Separation of the two metals in the interdigitated design allow for their independent operation. In all three designs, the areal ratio of the CO-producing metal, Au or Ag, to Cu can be varied. Reproduced from Lum et al.[400] with permission from the Royal Society of Chemistry.

oxygenates to ethylene Faradaic efficiency increased from 0.72 to 2.39, which mainly resulted from a decrease in ethylene and increases in acetaldehyde, acetate, and propionaldehyde selectivities.[400] Meanwhile, the total $C_{2+}$ Faradaic efficiency was maintained in the 50−65% range regardless of Cu coverage in these tandem/sequential catalyst devices, although, as one may expect, the partial current densities dropped with decreasing Cu coverage. Through a combination of control experiments and modeling, the reason behind the improved selectivity toward oxygenates in these devices was proposed to be due to CO transfer from the Au or Ag substrate inducing a higher coverage of *CO on the Cu surface.[400] This increased *CO would likely come at the expense of *H coverage, which could result in slower surface hydrogenation rates and, in turn, favor the formation of oxygenates instead of hydrocarbons. All in all, the studies discussed thus far in this subsection showcase a new design principle for tandem or sequential catalysis; by employing a cocatalyst that generates an *in situ* source of mobile CO, $CO_2R$ to >2e$^-$ products, particularly $C_{2+}$ oxygenates, can be enhanced. Future work can advance tandem catalysis system designs by tuning the materials' surface structures, morphologies, and compositions.

Bimetallic Cu−Ag thin films have also been reported to exhibit HER suppression and higher selectivity for $C_{2+}$ oxygenates through other means.[72,401] While CO spillover could still be a contributor in these systems, the dominant cause thought to be leading to these selectivity enhancements was tuning of adsorbate and reaction intermediate binding energies by incorporation of Ag into Cu. In the first case, CuAg metal foils consisting of segregated Cu and Ag phases were prepared by arc melting, quenching, and cold rolling, and it was suggested that formation of CuAg surface alloys under electrochemical reaction conditions leads to compressive strain on Cu surface atoms.[72] This compressive strain, as evidenced by an observable shift of the valence band structure of Cu to deeper levels, weakens the adsorption energy of *H, resulting in a 60−75% reduction in the HER activity. Interestingly, this was also correlated to a 10−15% increase in the total selectivity for $C_{2+}$ products and a product distribution shift from

hydrocarbons to oxygenates. Moreover, acetate and acetaldehyde accounted for a substantial portion of the $C_{2+}$ oxygenate selectivity, reaching up to a combined 15% Faradaic efficiency, which is noteworthy given that these are typically minor (<1%) products on pure Cu. This selectivity modification is attributed to reduced rates of C−O bond scission resulting from the HER suppression and the reduced oxophilicity of the compressively strained Cu, which presumably inhibits the ability of Cu to reduce these carbonyl-containing products further.[72] It is worth noting though that this did not impact the ability of Cu to make products derived from CO (i.e., the activity to >2e$^-$ products remained unchanged when normalized to the nominal Cu composition).[72]

In the second case, CuAg thin films across a range of nominal CuAg compositions were formed via physical vapor deposition, and many of the same trends were observed including HER suppression, decreased hydrocarbon selectivity, and increased oxygenate selectivity, particularly for the carbonyl products.[401] In this case, however, the overall intrinsic $CO_2R$ activity toward further reduced products was decreased for CuAg versus Cu. This is attributed to the significant nonequilibrium bulk-phase miscibility between Ag and Cu achieved in these films,[401] compared to the previous work which had minimal miscibility of Ag in Cu (<3 at. %).[72] This significant Ag miscibility in Cu is also thought to be responsible for the observed selectivity enhancements by tuning the electronic structure of Cu, decreasing the binding energy of *H and oxygenated reaction intermediates. Additional trends in product distribution were also discussed, including the significant suppression of $CH_4$ leading to an overall higher selectivity for C−C coupled products in these CuAg films compared to pure Cu.[401] With careful catalyst characterization, these studies demonstrate how formation of alloys using two metals that are thermodynamically immiscible under ambient conditions can be an effective strategy to alter activity (reduced HER) and selectivity (increased $C_{2+}$ oxygenates) in bimetallic systems.

Another Cu−Ag system has also demonstrated a higher selectivity for acetate formation (∼21% at −1.33 V vs RHE at

0 °C).[402] In this case, however, they were separate ~6 nm Cu and Ag nanoparticles immobilized on a polymer/glassy carbon electrode, and acetate was only observed over the bimetallic when benzotriazole (BTA) was in the electrolyte (over the Cu control sample it was observed in minor quantities, <1% Faradaic efficiency, both with and without BTA). While the selectivity changed with the ratio of Ag present, indicating the Ag clusters may play an important role through the CO spillover mechanism discussed earlier, clearly the electrolyte additive has a dominant impact on the product formation since without BTA, the main $CO_2R$ product over the bimetallic electrode was CO.[402]

### 7.3. Copper and HCOO⁻ Producing Guest Metals (In, Sn)

The p-block metals are generally characterized by their high selectivity for formate production at high overpotentials.[1,84] They also require a relatively high overpotential for the HER, which has drawn significant interest in employing them in bimetallic Cu systems as a strategy to reduce the selectivity for this competing side reaction. In addition, In and Sn electrodes have previously been demonstrated to exhibit a kinetically metastable oxide at the electrode/electrolyte interface at potentials where $CO_2R$ is observed, which can strongly influence the electrocatalytic properties of these systems.[141,406] This also widens the range of surface chemistries that can be created by these bimetallic systems, so careful characterization of the electrode surface is crucial. Unfortunately, *ex situ* characterization methods are often complicated by the oxophilicity of these elements and are particularly difficult given the nanostructured nature of the bimetallic catalysts in this section. Thus, comparisons and conclusions based on composition and/or oxidation state need to be taken with caution. In addition, it is impossible to identify which catalysts have a higher average turnover frequency because almost all of these studies reported current densities using the geometric electrode area. Thus, we will focus much of the remaining discussion of these Cu-M bimetallics (where M = In, Sn) on selectivity trends.

The key trends observed in Cu-M (where M = In, Sn) systems include synergistic CO production, HER suppression, and suppression of further reduced (>2e⁻) products.[407−418] In addition, several bimetallics maintained a higher selectivity to HCOO⁻.[407,408,419,420] In two of these cases, thick Sn deposits were employed on top of Cu substrates and resulted in overall Sn-like behavior with high selectivity (>80−90%) to HCOO⁻ formation.[419,420] Thus, the Cu here mainly seems to serve as a support to provide a route for making high surface area Sn electrodes to increase the production of HCOO⁻, rather than engendering any bimetallic effects. On the other hand, Cu core $SnO_2$ shell nanoparticles (Cu@$SnO_2$) were investigated for $CO_2R$, and while the thicker (1.8 nm) shell was again more selective for HCOO⁻ (<1% CO), the thinner shell (0.8 nm) instead resulted in very high selectivity for CO (>90% from −0.6 to −0.9 V vs RHE).[407] DFT calculations suggested that the combination of compression (~10%) due to the lattice mismatch between the core and shell and self-doping of Cu atoms diffusing out from the core to the shell resulted in the selectivity toward CO over HCOO⁻. An analogous study on Cu core $In_2O_3$ shell nanoparticles reported similar results and reasoning; lattice compression and Cu doping of the $In_2O_3$ shell led to enhanced CO generation, particularly for the thinnest shell (68% at −0.7 V vs RHE), while the thickest shell had a higher selectivity for HCOO⁻.[417] These core−shell

catalysts both show that the existence of Cu at the surface is an important factor governing the CO selectivity; there is further support for this design criteria in the reports discussed subsequently.

Two studies of Sn deposited on Cu oxide nanowires[411] and oxide-derived Cu substrates[412] both demonstrated very high CO selectivity for optimized samples (90% CO at −0.8 V vs RHE;[411] >90% CO between −0.5 and −0.8 V vs RHE[412]), which drastically falls after there is enough Sn on the surface to surpass a full monolayer of coverage on Cu. Similarly, a Cu foam sparsely decorated with Sn (2−3 at. %) was found to achieve >90% CO selectivity from −0.6 to −1.0 V vs RHE.[418] Two studies of Cu−In alloys synthesized from reduction of an oxide-derived Cu substrate in In solution[413] and reduction of $CuInO_2$[414] also demonstrated high CO selectivity (>75% CO between −0.4 and −0.7 V vs RHE;[413] 70% at −0.8 V vs RHE[414]). While the resulting bimetallic structures range from no evidence of alloy formation,[411,418] to near surface alloy formation,[412,413] to bulk alloy formation,[414] similar reasoning for the enhanced CO selectivity is proposed; namely, it is thought that incorporation of In/Sn disrupts favorable multi-Cu binding sites for protons while leaving CO binding sites unaffected, leading to HER suppression and enhanced CO selectivity at moderate overpotentials.[411−414,418] This is supported by complementary DFT studies by the Takanabe group.[412−414]

Alternatively, it has also been proposed that a metastable $In(OH)_3$ phase generated *in situ* is responsible for enhanced CO selectivity in oxide-derived Cu−In bimetallics.[415] In this report, several CuIn catalysts were synthesized from different oxide precursors, and while they initially showed different performance and morphologies, these catalysts evolved over repeated catalytic cycles to achieve similar CO selectivity (~50%) in parallel with appearance of an $In(OH)_3$ shell. Furthermore, when $In(OH)_3$ was etched off, the CO selectivity decreased until the hydroxide reappeared.[415] Thus, it was hypothesized that the synergistic effect observed in these systems was due to the existence of bifunctional active sites at metal−oxide interfaces. Therefore, following this study, the same researchers conducted systematic experiments on a series of microfabricated electrodes seeking to establish a relationship between the CO activity and the length of these metal-oxide interfaces.[409] By varying the amount of In/$In_2O_3$ dots patterned onto Cu/$Cu_2O$ substrates, the interfacial density ($\rho_{int}$) could be varied across 2 orders of magnitude; meanwhile, the total geometric surface area of each single-phase component was kept constant so as to avoid contributions from differences in coverage. In this way, the researchers did observe a positive correlation between the CO activity and $\rho_{int}$ for 2/3 of the variations studied ($In_2O_3$/$Cu_2O$ and In/$Cu_2O$, not $In_2O_3$/Cu), but not for the reason they initially expected.

Ultimately, it was found that oxidic indium was not important, but the presence of $Cu_2O$, which was reduced to metallic Cu under reaction conditions, was necessary for this synergistic effect to occur. By contrast, all electrodes using a Cu substrate showed similar, low activity for CO regardless of $\rho_{int}$ (Figure 35a).[409] Also, as shown in Figure 35b, only the two electrode versions using $Cu_2O$ substrates displayed significant diffusion of In from the dots into the surroundings. Taken together, these results indicate that these In-modified Cu "halos" around the dots were responsible for the high activity for CO evolution rather than metal−oxide interfaces (both Cu and In were found to be metallic under reaction conditions
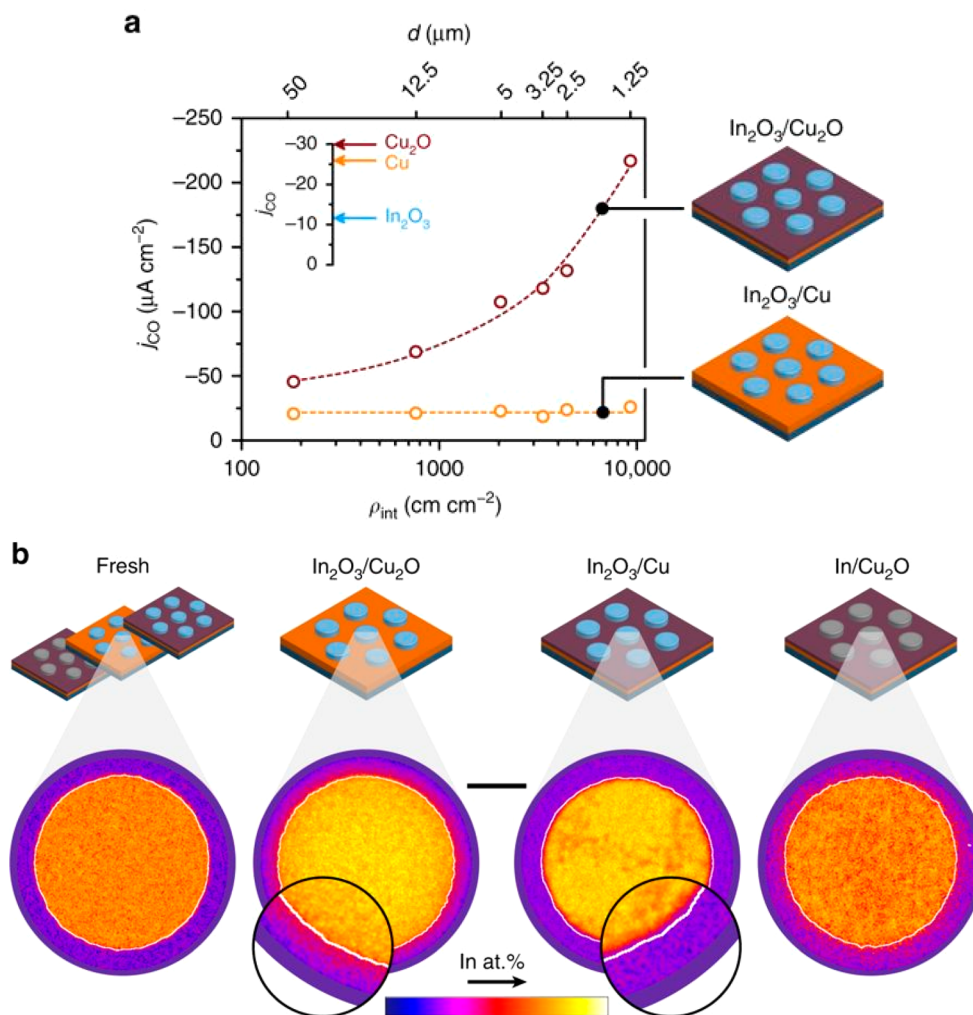
**Figure 35.** (a) Partial current density for CO evolution ($j_{CO}$) over microfabricated $In_2O_3/Cu_2O$ and $In_2O_3/Cu$ electrodes as a function of the interfacial density ($\rho_{int}$) at −0.6 V vs RHE. Note: the corresponding island diameter ($d$) is indicated on the top *x*-axis, the trendlines were added as a visual aid, and the inset shows the corresponding partial current densities measured over the single-phase control samples. (b) Elemental distribution of indium over individual islands for the 3 electrode variations ($In_2O_3/Cu_2O$, $In_2O_3/Cu$, $In/Cu_2O$), with a representative island prior to the reaction shown as reference (Fresh). Note: the white contours indicating the border of the corresponding fresh islands were added as a visual aid, and the scale bar is 5 $\mu$m. Reprinted from Larrazábal et al.[409] This work is licensed under a Creative Commons Attribution 4.0 International License (https://creativecommons.org/licenses/by/4.0/).

anyway).[409] Thus, with regard to their previous work, the authors now suggested that the succession of reduction/oxidation cycles could aid in the formation of highly active, indium-poor metallic Cu compositions, similar to those found in this study, by accumulating In into an $In(OH)_3$ sink, although the possibility of active sites existing at metal-oxide interfaces cannot be completely ruled out at this time.[409]

In light of this follow-up study by Larrazábal et al., it is clear that the interfaces between In/Sn and Cu on the surface is emerging as a key factor governing the high CO selectivity observed in these bimetallic electrodes. This is further supported by a combined theory-experiment study on In-modified ($Cu(OH)_2$-derived) Cu nanowires.[410] The composition where the highest number of Cu−In interfacial sites were formed was found to be the optimal sample, achieving ~93% Faradaic efficiency for CO at −0.6 to −0.8 V vs RHE. DFT calculations also confirmed the crucial role of metallic Cu−In interfaces in tuning the stability of key reaction intermediates; these interfacial sites were found to significantly decrease the barrier for *COOH formation while still allowing

for facile release of *CO, and weakly adsorbed *H and strongly adsorbed *OCHO on these sites could be the cause for suppression of $H_2$ and >2e⁻ products.[410]

Finally, it is worth briefly revisiting the role of the oxide(s) in these bimetallic electrodes. Many of these studies suggested that the structure of the oxide precursor(s) governs the alloy formation and resulting CO activity for several reasons including compositional[416] and morphological effects.[408,413,414] Interestingly, in the work by Larrazábal et al., a control experiment where indium was deposited on an already oxide-derived Cu substrate did not exhibit the same synergistic effect, which indicates that the *in situ* reduction of the $Cu_2O$-based electrodes is required for diffusion of In to create the CO-selective, In-modified Cu "halos".[409] This could perhaps explain the formation of highly active Cu−In and Cu−Sn surfaces that started with an oxide precursor mentioned earlier in this section. Although the oxidation state of Cu, In, and Sn during $CO_2R$ is still an open area of debate, at least partial (if not full) reduction of these oxide species under reaction conditions seems beneficial to encourage diffusion of these

components and create optimal interfacial sites. Unfortunately, untangling the complex trade-off between the various possible effects in these nanostructured, bimetallic catalysts is incredibly difficult, so again, caution must be taken when trying to draw comparisons between systems or identify concrete structure–activity relationships. While there is clearly more work that needs to be done to better understand the factors governing the activity and selectivity of Cu−In and Cu−Sn, these high surface area Cu bimetallics with p-block metals have certainly shown promising CO selectivities and geometric activities (Figure 37 in section 7.4).

## 7.4. Activity Comparisons

In this section, we presented the main findings for different classes of Cu-based bimetallic systems. Before reiterating the key selectivity trends and presenting activity comparisons, we wish to start by providing some overall perspectives on the challenges faced in studying and comparing the activity of bimetallic catalysts. First, as discussed in section 2.4, benchmarking and reporting how the pure metal components perform in a given experimental setup is highly recommended to help validate trends observed for a given bimetallic catalyst. Second, identifying active sites on the surface of bimetallics under *operando* conditions can represent a major challenge. In particular, the composition at the surface of a bimetallic can be very different than in the bulk due to segregation of one component. This can be induced by fundamental differences in the materials' properties (oxophilicity, CO binding strength, miscibility, etc.) upon exposure to different environments (air *ex situ*, electrolyte and/or applied potentials *in situ*), as well as result from different catalyst synthesis methods and pretreatment procedures. Indeed, many studies discussed herein observed surface enrichment of one component either as a result of the synthesis method[132,389,390,393,397,417] and/or electrochemical testing.[72,381,390,395,404,405,413,415] Unfortunately, this makes comparisons between bimetallic catalysts more difficult; for example, two different bulk compositions may ultimately have similar surface compositions during electrolysis, and *vice versa*. This, in turn, can limit the scope of theoretical predictions and/or hinder our ability to match them with experimental results.

Third, while nanostructured bimetallics are interesting to explore in their own right, one must be careful when trying to draw structure−composition−activity relationships from these systems. Some reports on high surface area bimetallic electrodes noted different morphological features as a function of composition, which increases the difficulty of making systematic assessments.[129,390,393,403,408] In addition, some studies tried testing a flat bimetallic catalyst to serve as a standard for comparison to their nanostructured catalyst,[412,413] but this still has its pitfalls because the same surface ratio and dispersion of individual metal components may not be readily replicated between low and high surface area morphologies. In general, trying to decouple the impacts resulting from nanostructuring (increased surface area, faceting, grain boundaries, nanoparticle size and support effects, mass transport limitations) and those resulting from the bimetallic ensemble (composition/phase, atomic arrangement of each component, strain) is extremely difficult. Thus, when trying to draw conclusions about the intrinsic activity or selectivity of bimetallics, planar catalysts that minimize the effects of nanostructuring are ideal.

Finally, it is crucial to measure the ECSA of tested electrodes in order to determine whether a higher surface area catalyst truly has a greater average turnover frequency rather than greater activity simply resulting from an increased number of active sites. In light of the challenges in comparing bimetallic electrodes that were just discussed, getting an accurate measure of the ECSA of bimetallics can be especially difficult. As mentioned previously in section 2.1, there exists a variety of methods for determining the ECSA, and researchers should keep in mind the limitations of each in order to choose the technique most suitable for the materials being studied. The most common method for estimating the ECSA of $CO_2R$ electrocatalysts has been to use double-layer capacitance ($C_{dl}$) measurements. Ideally, a rough Cu-M catalyst would be compared to a planar Cu-M catalyst of the same surface composition; although as discussed earlier, this can be difficult to replicate and validate since changes in surface composition and morphology may also occur under reaction conditions. These discrepancies in composition may only have a small impact if the capacitance of the two materials are similar, but this introduces more uncertainty when the capacitance of the two materials are quite different. In the case of Cu-M materials, since other M do not convert $CO_2$ to >2e$^-$ products to any appreciable degree, ECSA estimates for Cu-M catalysts can compare the $C_{dl}$ of Cu-M to the $C_{dl}$ of planar Cu when looking to see if the intrinsic activity has been improved beyond that of pure Cu. In any case, it should be noted that the ECSA of bimetallic systems as determined by $C_{dl}$ ratios is typically a conservative estimate for the total number of active sites, since it is unlikely that the entire surface will be active in a bimetallic electrode. Still, any promotion in activity observed using this conservative estimate indicates that at least part of the enhancement is due to improved intrinsic reaction rates and not purely resulting from an increased number of active sites. Therefore, despite the difficulties and limitations, we urge researchers to make their best attempts to measure and report the ECSA of tested electrodes.

Unfortunately, only a limited number of Cu-M bimetallics have been reported with the requisite information to compare catalytic activity on an average turnover frequency basis. Figures 36 and 37 provide the total $CO_2R$ current density to >2e$^-$ products and CO, respectively, normalized by both the exposed geometric area and ECSA when available for catalysts tested in aqueous-phase reactors. The few bimetallic $CO_2R$ catalysts that have been tested in vapor-fed reactors were not included for this direct comparison due to the vastly different reactant mass transport conditions. Also, in cases where multiple variations of Cu-M bimetallics were examined in a single study, only the optimal material was generally included for clarity, in addition to the monometallic control sample if tested.

In Figure 36, both planar[65] and high surface area[89] Cu control samples are included for reference. While a number of studies have reported bimetallics with increased selectivity to >2e$^-$ products, Figure 36a shows that this improvement is generally accompanied by a similar or lower geometric activity as compared to the corresponding Cu standard. It is worth noting that despite the decreased partial current densities, in some cases the $CO_2R$ energy efficiencies may be higher on the bimetallics compared to the Cu control samples. This was demonstrated by Lum et al.; the 4.3% Cu dots on Ag sample shown in Figure 36a had the highest energy efficiency (21.4%)

for generation of $C_{2+}$ products, while the 2.3% Cu dots sample had the highest total $CO_2R$ energy efficiency (32.8%).[400]
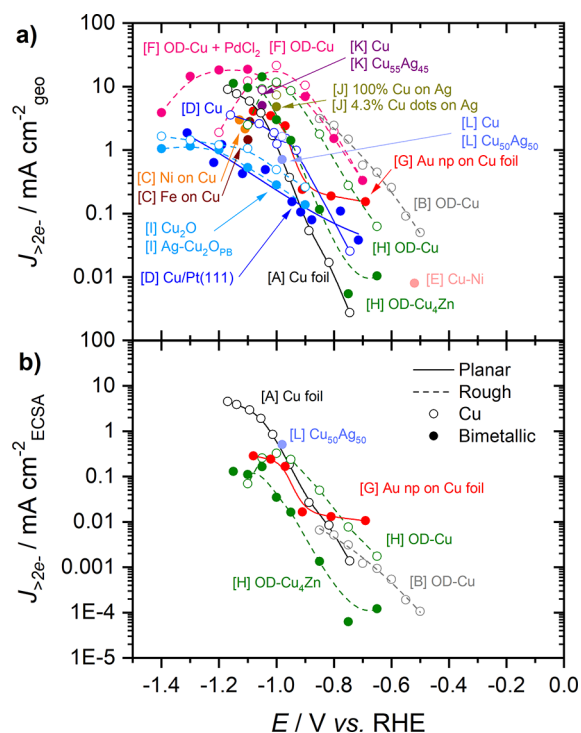


**Figure 36.** Cu-based bimetallic catalysts' total current density to further reduced (>2e⁻) products normalized by (a) the geometric area and (b) the ECSA. The data were obtained from the following studies: [A] Cu foil by Kuhl et al.;[65] [B] OD-Cu by Li et al.;[89] [C] Ni and Fe deposits on Cu (two points shown for the beginning and end compositions formed by the *in situ* electrodeposition) by Hori et al.;[377] [D] Cu overlayer on Pt(111) and Cu control sample by Varela et al.;[381] [E] $Cu_{90.5}Ni_{9.5}$ alloy by Watanabe et al.;[384] [F] OD-Cu with $PdCl_2$ in the electrolyte forming deposits on the surface, as well as an OD-Cu control sample, by Chen et al.;[388] [G] Au nanoparticles on Cu foil by Morales-Guio et al.;[399] [H] OD-$Cu_4Zn$ and OC-Cu control sample by Ren et al.;[129] [I] Ag−$Cu_2O_{PB}$ (PB = phase blended) and $Cu_2O$ standard both deposited on Toray paper by Lee et al.;[127] [J] 4.3% Cu dots patterned on an Ag substrate and a 100% Cu (fully coated on Ag substrate) control sample by Lum et al.;[400] [K] $Cu_{55}Ag_{45}$ bimetallic foil and Cu foil standard by Clark et al.;[72] [L] $Cu_{50}Ag_{50}$ thin film bimetallic and Cu control sample by Higgins et al.[401] See Table S6 in the SI for the data contained in this plot.

From Figure 36b, it quickly becomes clear that the only aqueous-phase bimetallic catalyst system with a higher activity than pure Cu is the Au nanoparticles on Cu foil catalyst.[399] The OD-$Cu_4Zn$ catalyst[129] has a larger RF than the OD-Cu standard, so while it achieves an equivalent $CO_2R$ rate to >2e⁻ products when normalized by the geometric electrode area, this results in a lower average turnover frequency when normalized by the ECSA. Another bimetallic catalyst system that demonstrated higher activity than pure Cu was the CuAg wire reported by Hoang et al.[131] While the Cu wire catalyst initially shows higher current densities to $C_{2+}$ products at lower overpotentials then levels off (likely due to the lack of *CO resulting from the high turnover rate in this region), the $C_{2+}$ activity of the CuAg wire catalyst continues to increase and surpasses that of the Cu wire at −0.7 V vs RHE. These results were not included in Figure 36 since they were obtained in a vapor-fed device, but it is worth noting the impressive $C_{2+}$
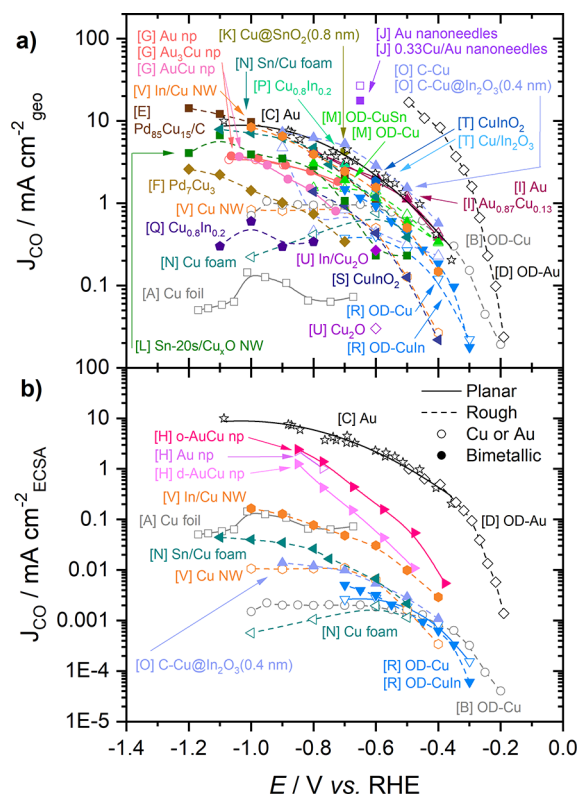
**Figure 37.** Cu-based bimetallic catalysts' total current density to CO production normalized by (a) the geometric area and (b) the ECSA. The data were obtained from the following studies: [A] Cu foil by Kuhl et al.;[65] [B] OD-Cu by Li et al.;[89] [C] Au by Hori et al.;[421] [D] OD-Au by Chen et al.;[422] [E] $Pd_{85}Cu_{15}/C$ alloy nanoparticles supported on carbon black by Yin et al.;[389] [F] $Pd_7Cu_3$ electro-deposited mesoporous films by Li et al.;[390] [G] AuCu, $Au_3Cu$, and Au nanoparticles by Kim et al.;[396] [H] ordered (o-) and disordered (d-) AuCu nanoparticles and Au nanoparticle control sample by Kim et al.;[397] [I] Au and $Au_{0.87}Cu_{0.13}$ prepared by pulsed laser deposition in 220 mTorr $O_2$ by Roy et al.;[395] [J] 33% Cu coverage on Au nanoneedles and Au nanoneedles by Ross et al.;[132] [K] Cu@$SnO_2$ (0.8 nm) core−shell nanoparticles by Li et al.;[407] [L] Sn deposited for 20 s on $Cu_2O$ nanowires by Zhao et al.;[411] [M] OD-CuSn and OD-Cu control sample by Sarfraz et al.;[412] [N] 2−3 at. % Sn on Cu10 foam (Sn/Cu foam) and Cu10 foam standard (Cu10 = 10 min electrodeposition) by Zeng et al.;[418] [O] Carbon-supported Cu@$In_2O_3$ (0.4 nm) core−shell nanoparticles and carbon-supported Cu nanoparticle control sample by Xie et al.;[417] [P] $Cu_{0.8}In_{0.2}$ by He et al.;[416] [Q] $Cu_{0.8}In_{0.2}$ by Hoffman et al.;[408] [R] OD-CuIn and OD-Cu control sample by Rasul et al.;[413] [S] $CuInO_2$-derived by Jedidi et al.;[414] [T] $Cu/In_2O_3$-derived and $CuInO_2$-derived by Larrazábal et al.;[415] [U] In dots microfabricated on $Cu_2O$ substrate (In/$Cu_2O$) and $Cu_2O$ control sample by Larrazábal et al.;[409] [V] In deposited on Cu nanowires (Cu(OH)$_2$ derived) using 20 mM $InCl_3$ solution and Cu nanowire control sample by Luo et al.[410] See Table S7 in the SI for the data contained in this plot.

activity and selectivity metrics achieved by the CuAg wire catalyst at this potential: 60% $C_2H_4$ and 25% $C_2H_5OH$ at a total current density of ∼ −300 mA/cm².[131] This cannot be explained by surface area differences alone because the bimetallic has a 10% higher ECSA but 60% higher current density than the Cu wire at this potential. Experiments where CO is mixed into the vapor feed during $CO_2R$ show that the $C_{2+}$ saturation region displayed by the Cu wire catalyst disappears, and instead the current continues to increase with increasing overpotential, like that observed for the CuAg

wire.[131] Therefore, CO spillover from Ag is likely a key mechanism by which the bimetallic wire achieves the improved performance at higher overpotentials. This once again highlights the potential of tandem catalyst systems that can effectively decouple multiple $CO_2R$ steps, bypassing design limitations intrinsic to monometallic electrodes.

In Figure 37, both planar[65,421] and high surface area[89,422] Cu and Au control samples are included for reference. In Figure 37a we can see that many rough Cu-based bimetallics have had activity comparable to pure Au on a geometric area-normalized basis. While this is encouraging for increasing cost-effectiveness for $CO_2R$ to CO catalysis by reducing noble metal usage, we can see in Figure 37b that pure Au is still orders of magnitude more active on an average turnover frequency basis. Also, it is interesting to note that the ECSA-normalized CO partial current densities for Cu-M bimetallics with In or Sn essentially fall in between the planar and high surface area Cu standards; only those with Au have activity higher than Cu, closer to that of Au. Thus, while many of these high surface area Cu-M catalysts with p-block metals have demonstrated impressive CO selectivity (>90%), the *intrinsic* activity for $CO_2R$ to CO on copper does not seem to have been enhanced in these systems. Again, the sample pool is very limited here though due to a lack of reporting the ECSA of these materials. Future studies on Cu-M bimetallics should strive to include the roughness factors of these materials so that the intrinsic activity can be more readily compared.

### 7.5. Summary

Here we examined Cu-M bimetallic combinations across three groups, where the guest metal M is either highly selective to $H_2$, CO, or $HCOO^-$. In all cases, the synergistic effects are generally diminished when the surface is dominated by the guest metal, causing the activity and selectivity to mimic that of the pure M component. For $H_2$-selective metals, increased HER activity and decreased $CO_2R$ activity have typically been observed. Interestingly, the $C_{2+}$ pathway(s) in particular get disrupted, as the main further reduced product formed in these systems was $CH_4$, with $C_2H_4$ formation significantly suppressed. For CO-selective metals, high activity and selectivity for CO have been noted, as well as some synergistic activity and selectivity to $C_{2+}$ products (especially oxygenates) resulting from CO spillover and electronic effects, respectively. Finally, for $HCOO^-$-selective metals, HER suppression and high selectivity for CO, along with inhibition of all further reduced products, have typically been observed.

At this time, it appears that the intrinsic activity of Cu (for >2e$^-$ products) and Au (for CO) have not been outmatched by bimetallic systems, except in the two demonstrations of tandem catalysis via CO spillover from Au nanoparticles on Cu foil[399] and from Ag in a CuAg wire gas diffusion electrode.[131] In these cases, the two monometallic catalysts operate in synergy whereby Au/Ag provides a higher concentration of CO near the electrode surface than what Cu could produce alone or than what could be sustained through transport of CO from the bulk electrolyte, allowing for increased rates of $C_{2+}$ product formation compared to pure Cu. While there have been notable electronic and geometric effects demonstrated in Cu bimetallic systems, it appears that these have predominantly contributed to product distribution trends such as HER suppression, >2e$^-$ products suppression, increased CO selectivity, and/or increased selectivity to $C_{2+}$ oxygenates including ethanol or the carbonyl products. In these cases,

weakening or disrupting sites for *H binding seems to be a key factor leading to enhanced $CO_2R$ selectivities. It is possible that poisoning of oxophillic sites by formate may prevent the predicted ability of bifunctional active sites to break scaling relations for $CO_2R$ to >2e$^-$ products.[202,365] Therefore, electrochemical CO reduction (COR) on Cu-based bimetallics may be of interest for future work, since starting from CO as the reactant both eliminates the $HCOO^-$ pathway and allows for a broader range of pH conditions to be tested. Characterization and stability of these bimetallic system has also presented major challenges, as segregation and/or oxidation state changes of the individual metals can occur under reaction conditions and/or upon exposure to air for *ex situ* characterization. Therefore, another area for future work includes further development of *operando* spectroscopic techniques to help elucidate the true chemical state and structure of active sites in Cu bimetallics during electrochemical $CO_2R$.

## 8. CONCLUSIONS AND FUTURE OUTLOOK

Coupling electrochemical $CO_2$ reduction ($CO_2R$) with a renewable energy source to create high value fuels and chemicals is a promising strategy to help achieve a sustainable global energy economy. Not only could this serve as a renewable source of traditionally fossil-derived resources, but it could also enable storage of energy from intrinsically variable electricity generators such as wind and solar. In this Review, we took a detailed look at the state of electrochemical $CO_2$ reduction on Cu and the key levers that have been used to tune its activity and selectivity, including surface faceting, electrolyte effects, electrochemical conditions, nanostructuring, and preparation of bimetallics. First, we would like to emphasize the following key points:

(1) Nanostructuring does not alter the *intrinsic activity* of copper in any significant manner, independent of the method used. While other morphological features may also play a role, we believe that increased surface area is the dominant factor altering the product selectivity of nanostructured Cu materials, since this impacts the potential window where $CO_2R$/COR current densities are optimized.

(2) (a) Significant methods to increase the intrinsic activity of copper through bimetallic electronic or geometric effects have not yet been found. Notably, a tandem/sequential catalysis scheme has emerged as a promising paradigm for achieving higher activity and selectivity to $C_{2+}$ products, particularly oxygenates. By co-locating domains of Cu with those of a CO-generating metal (e.g., Ag, Au, and Zn), additional CO can be supplied to the Cu surface. (b) Bimetallic electronic and geometric effects have, however, resulted in product distribution changes such as HER suppression, >2e$^-$ product suppression, and/or increased CO selectivity compared to pure Cu. It is also worth noting that higher selectivities to oxygenates such as acetate and acetaldehyde have been achieved in several Cu–Ag systems.

(3) It is important to consider the chemical potential of the reactants and electrolytes since this could easily change the catalyst surface structure and composition. The inherent mobility of copper and the ease with which it is oxidized present challenges in maintaining stable

surfaces. This can explain the large observed dependency of $CO_2R$ performance on the catalyst preparation and testing methods.

(4) Theoretical studies have indicated that step sites may very well dominate $CO_2R$ activity, although experimental validation of this remains a challenge. Copper surfaces have been shown to reconstruct under reaction conditions. Thus, the formation of undercoordinated defects or step sites during preparation or testing of single crystal electrodes could explain why they have demonstrated similar overall activity.

(5) It is crucial to report the electrochemically active surface area (ECSA) of tested electrodes whenever possible in order to determine if greater catalytic activity can be attributed to improved intrinsic activity (higher average turnover frequency) rather than an increased number of active sites (larger surface area). It is also important to keep in mind the ambiguities of measuring ECSA and choose the method most appropriate for the system at hand.

(6) Catalysts with different roughness factors and/or catalysts tested under different electrolyte and electrochemical conditions will reach mass transport limitations at different rates. Thus, it is not always straightforward to compare electrodes tested at the same applied potential, since these different conditions may lead to different kinetic overpotentials. When investigating the *intrinsic* behavior of novel electrocatalyst materials, we underline the importance of comparing data in potential windows governed by the intrinsic reaction kinetics, so as not to convolute the impacts of catalyst properties and mass transport effects.

Electrochemical $CO_2$ reduction on copper catalysts holds significant promise, but there is still much work to be done before low-cost, scalable deployment of $CO_2R$ technologies can be realized. Toward this end, we need not only greater fundamental understanding of $CO_2R$ mechanisms, but increased practical performance metrics as well. We will briefly discuss our outlook on key areas for future studies in these spaces.

To date, most of the catalyst characterization techniques have been conducted *ex situ* before and/or after $CO_2R$ due to the complexity of the electrified electrode/electrolyte interface. There has been an increasing trend, however, in the development and implementation of *in situ/operando* characterization techniques, with recent studies providing new insights highlighted in each section of this Review. We urge the further advancement of these techniques, as they can provide crucial insights regarding the catalyst surface structure, composition, oxidation state, and adsorbed intermediates under reaction conditions. These will be invaluable tools for providing better understanding of active sites, elucidation of reaction mechanisms, and validation of predictions from theoretical studies. For more details on the state of surface characterization techniques for $CO_2R$ and the progress in this area of research, we direct the reader to a reference module by Soriaga et al.[423] and a recent review article by Handoko et al.[10]

The developments in theoretical modeling of the electrochemical interface have yielded significant progress in identifying key active site motifs, reaction intermediates and descriptors, solvation and ion promotion effects, and $CO_2R$ pathways. While much of the focus has been on analyzing the reaction energetics and thermodynamics, further developments

in kinetic modeling will be required to better understand the interplay between coverage, potential dependence of activation energies, adsorbate−adsorbate interactions, and pH effects. The development of machine-learning algorithms also presents an opportunity to develop predictive capabilities and screening methods, which can aid materials discovery efforts and promote the rational design of $CO_2R$ catalysts.[424−426] Challenges remain in the reconciliation of conclusions between existing theoretical approaches, the advancement of functionals for describing charge at the electrochemical interface, and the evaluation of kinetics and reaction barriers of elementary steps under reaction conditions. Multiscale modeling of transport effects will also be critical to gain a better understanding of interfacial processes, especially for more practical high surface area catalysts and vapor-fed reactors. These developments will lead to increased and improved coupling between experimental and theoretical $CO_2R$ studies.

Next, we feel that the field must begin developing the necessary catalysts and reactor systems to enable scalable (low cost), selective, and energy efficient conversion of $CO_2$ to useful fuels and chemicals. It is often cited how Cu typically requires ∼1 V overpotential to form valuable hydrocarbons and alcohols,[1] but this mainly applies to planar systems. Nanostructuring, along with the use of alkaline electrolytes and larger-sized alkali cations, has provided a route to decreasing the required overpotential and altering the selectivity to certain products. Most notably, immense progress has been made in recent years in development of gas diffusion electrode (GDE) and continuous flow devices.[13,126,131,292,330,347,350−354,427] For example, a recent report achieved ∼70% $C_2H_4$ selectivity over 150 h of operation between 75 and 100 mA/cm$^2$, and a full-cell energy efficiency for $CO_2$ conversion to $C_2H_4$ of 34%.[351] While this value is lower than the 60−80% energy efficiency typically achieved for water splitting, it is quite reasonable given the relative maturity of that field compared to $CO_2R$, as well as the significant difference in potential product values. Thus, while there is always a need for fundamental research, the field is at a stage where we can start accelerating the development of practical devices. This includes optimization of device components (catalysts, supports, membrane, electrolyte) and conditions (flow rate, temperature, pressure, etc.), as well as testing the tolerance to more realistic conditions. For example, many potential $CO_2$ sources for initial commercial applications (such as industrial plant flue gas, biogas, etc.) will have diluted $CO_2$ streams with different potential contaminants.[428] Renewably-powered $CO_2R$ may also have interrupted/variable power input depending on the source (such as intermittent wind and solar), so tolerance to factors like these must be taken into account for large scale deployment of $CO_2R$ technologies. In addition, complicated product separations may result in significant additional energy requirements, which should ideally be minimized.[428]

Finally, we will briefly discuss three other focus areas for improving $CO_2R$ activity and selectivity. First, the competing HER remains a significant issue for $CO_2R$ in aqueous systems. While progress has been made in improving $CO_2R$ selectivity by employing basic electrolytes, we additionally suggest the investigation of $CO_2R$ in nonaqueous and solid polymer electrolytes. Second, while this Review focused on Cu catalysts, there are also several emerging classes of catalysts that hold the potential to break scaling relations between reaction intermediates, including stable alloys, single atom catalysts, (doped) carbon materials, metal organic frameworks (MOFs),

covalent organic frameworks (COFs), materials with three-dimensional active sites that can induce confinement effects, and functionalized surfaces (tethering promoters/ligands to the electrode surface).[57,202,373,429] Materials discovery efforts should continue in these directions to identify novel catalyst materials with enhanced properties. Finally, CO reduction has been increasingly studied in recent years, both as a proxy to better understand $CO_2$ reduction mechanisms, as well as for fundamental understanding of this important reaction in its own right. If viable COR catalysts are developed, this could enable tandem or cascaded reaction systems in which $CO_2R$ is split into two separate steps: (1) $CO_2$ reduction to CO, then (2) CO reduction to the desired product(s). Unique synergies could also be achieved by coupling $CO_2$ electroreduction with alternate types of catalytic processes (biological, thermal, etc.).

In summary, while many challenges and opportunities remain in developing catalysts and reactor systems with high activity, selectivity, stability, and scalability, much progress has also been attained in recent years, priming this technology for commercial application. With continued research and development, electrochemical $CO_2$ reduction could have a substantial impact on the sustainability of our global energy economy.

## ASSOCIATED CONTENT

### Ⓢ Supporting Information

The Supporting Information is available free of charge on the ACS Publications website at DOI: 10.1021/acs.chemrev.8b00705.

> Thermochemistry: Raw Data and Calculations; Economics: Raw Data and Calculations; Computational Studies: Energetics and Kinetics of Elementary Steps; Tabulated Data for Activity Comparison Plots.(PDF)

## AUTHOR INFORMATION

### Corresponding Authors

*E-mail: ibchork@fysik.dtu.dk.
*E-mail: jaramillo@stanford.edu.
*E-mail: jkno@dtu.dk.

### ORCID ⓘ

Erlend Bertheussen: 0000-0002-6482-8937
Ifan E. L. Stephens: 0000-0003-2157-492X
Karen Chan: 0000-0002-6897-1108
Christopher Hahn: 0000-0002-2772-6341
Thomas F. Jaramillo: 0000-0001-9900-0622
Ib Chorkendorff: 0000-0003-2738-0325

### Author Contributions

#Stephanie Nitopi and Erlend Bertheussen contributed equally to this work.

### Notes

The authors declare no competing financial interest.

### Biographies

Stephanie Nitopi is currently a Ph.D. candidate in the Chemical Engineering department at Stanford University, and a member of Professor Tom Jaramillo's group and the SUNCAT Center for Interface Science and Catalysis. She was a recipient of a Stanford Graduate Fellowship in Science & Engineering, and her research has focused on the electrochemical conversion of carbon dioxide to fuels and chemicals on copper catalysts. Prior to Stanford, Stephanie was in

the Schreyer Honors College at The Pennsylvania State University where she received her B.S. in Chemical Engineering in 2014.

Erlend Bertheussen received his Bachelor's degree in Nanotechnology from the University of Bergen in 2012. He then moved to Denmark to do a Master's in Physics and Nanotechnology at the Technical University of Denmark (DTU), where his interest for electrochemical energy conversion started. He subsequently started a Ph.D. degree in Physics at DTU, where he performed work within the field of CO reduction on copper electrodes. After graduating in the spring of 2018, he took a position as an R&D Engineer in the start-up company RenCat ApS.

Soren B. Scott received a Bachelor's in Chemistry from the University of Copenhagen in 2013 before being introduced to the idea of $CO_2$ electroreduction while working as a research assistant at the Joint Center for Artificial Photosynthesis at Lawrence Berkeley National Lab. He returned to Denmark for a Master's in Chemical Engineering at the Technical University of Denmark (DTU, 2016) and has since then been a Ph.D. student at DTU's Department of Physics. In 2018, Soren was awarded an EliteForsk travel grant from the Danish Ministry of Higher Education and Science. His current research uses in situ mass spectrometry to probe electrocatalytic interfaces.

Xinyan Liu received her B.S. in chemical engineering from Tsinghua University (Beijing, China) in 2013. She then obtained her Ph.D. in chemical engineering from Stanford University in 2018 under the supervision of Prof. Jens K. Nørskov, during which she has worked on density functional theory based microkinetic modeling of Fischer–Tropsch synthesis, electrochemical hydrogen evolution reaction, and electrochemical carbon monoxide/dioxide reduction reactions. Her expertise is in microkinetic modeling and data mining.

Albert K. Engstfeld (1983, Germany) graduated from the Ulm University in 2009 in chemistry with specialization in physical chemistry and surface science. He received his Ph.D. in 2015 from Ulm University on "Design and electrochemical/−catalytic properties of well-defined bimetallic model catalyst electrodes," research conducted under the supervision of Prof. R.J. Behm. After a postdoc position at the Institute for Surface Physics & Catalysis (Technical University of Denmark), he returned in 2017 to Ulm University. He is currently working as a group leader (Nanostructured Metal Surfaces) at the Institute of Surface Chemistry and Catalysis. By combining an ultrahigh vacuum system with electrochemical methods, he is focused on a fundamental understanding of restructuring/corrosion processes and electrocatalytic properties of nanostructured (bi)metallic single crystal model electrodes on an atomic scale level.

Sebastian Horch received his Ph.D. degree in Physics (1994) from Bonn University, Germany. He was Feodor Lynen Research Fellow at Arizona State University in 1995. Until 1999, he was Assistant Research Professor in the Center for Atomic-scale Materials Physics (CAMP) at Aarhus University, Denmark. Since 1999, he is Associate Professor at the Department of Physics, Denmarks Technical University (DTU). His main area of research is Surface Science using high resolution scanning probe microscopy.

Brian Seger completed his Ph.D. in chemical engineering from Notre Dame under Prof. Prashant Kamat in 2009. After completing postdocs at the University of Queensland under Lian Zhou Wang and at DTU under Prof. Ib Chorkendorff, he became an assistant professor in the Surface Science and Catalysis section of DTU Physics in 2014 and then promoted to associated professor in 2017. He has published 45 peer reviewed papers that have been cited over 5,000 times. His research focuses on electrochemical $CO_2$ reduction, photoelectrochemistry, semiconductor-electrolyte interfaces, and electro-synthesis reactions.

Ifan E. L. Stephens was appointed as Senior Lecturer at the Department of Materials at Imperial College London in July 2017. Prior to Imperial, he was at the Department of Physics at the Technical University of Denmark (DTU); he was first employed as a postdoctoral researcher, then as assistant professor and finally as associate professor and leader of the Electrocatalysis Group there. In 2015, the Department of Mechanical Engineering at Massachusetts Institute of Technology (MIT) awarded Ifan the Peabody Visiting Associate Professorship. His team conducts model electrocatalysis experiments to enable the large-scale conversion of renewable energy to fuels and chemicals and vice versa. Ifan has authored or coauthored more than 60 papers in peer reviewed journals. He is coinventor on one patent and five patent applications. He is cofounder of the spinoff company, HPNow.

Karen Chan is an Associate Professor at the Department of Physics, Technical University of Denmark. Prior to this she was Associate Staff Scientist at SLAC National Accelerator Laboratory as part of the Joint Center for Artificial Photosynthesis. Her expertise is in the atomistic and continuum level modeling of electrochemical interfaces with applications in sustainable energy conversion. She obtained her Ph.D. in 2013, advised by Michael Eikerling and held a postdoc fellowship from 2013–2016 at Stanford University, advised by Jens K. Nørskov.

Christopher Hahn completed his doctorate at the University of California Berkeley in 2012, where he studied bandgap engineering of 1-dimensional nitride and oxynitride materials for solar water splitting. After receiving his Ph.D., he conducted his postdoctoral research on catalyst discovery for electrochemical $CO_2$ reduction at Stanford University within the SUNCAT Center for Interface Science and Catalysis. He began his current position at SLAC National Accelerator Laboratory in 2015, where he is conducting research with the Joint Center for Artificial Photosynthesis on catalyst discovery and understanding reaction mechanisms for electrochemical $CO_2$ reduction.

Jens K. Nørskov is the Villum Kann Rasumussen professor at the Technical University of Denmark. His research aims at developing theoretical methods and concepts to understand and predict properties of materials. He is particularly interested in surface chemical properties, heterogeneous catalysis, electro-catalysis, and applications in energy conversion.

Thomas Francisco Jaramillo is an Associate Professor of Chemical Engineering at Stanford University and of Photon Sciences at SLAC National Accelerator Laboratory, where he is the Director of the SUNCAT Center for Interface Science and Catalysis. A native of Puerto Rico, Prof. Jaramillo earned his B.S. in Chemical Engineering at Stanford University, followed by M.S. and Ph.D. in Chemical Engineering at the University of California at Santa Barbara (UCSB). Prof. Jaramillo conducted postdoctoral research in the Department of Physics at the Technical University of Denmark (DTU) as a Hans Christian Ørsted Postdoctoral Fellow. Prof. Jaramillo's research efforts are aimed at developing catalysts and processes that can accelerate important chemical transformations related to energy conversion with improved sustainability, efficiency, and durability. Prof. Jaramillo has earned a number of honors and awards for his efforts, including the Resonate Award from the Resnick Institute (2014), the Presidential Early Career Award for Scientists & Engineers (PECASE, 2011), the U.S. Dept. of Energy Hydrogen and Fuel Cell Program Research & Development Award (2011), the National Science Foundation (NSF) CAREER Award (2011), and the Mohr-Davidow Ventures (MDV) Innovator Award (2009).

Ib Chorkendorff is Professor in Heterogeneous Catalysis at DTU Physics. He earned his Ph.D. in 1985 at Odense University Denmark,

and after a postdoc at University of Pittsburgh, USA, he was employed in 1987 at DTU as Associate Professor for starting up the field of experimental surface science and catalysis. From 2005 to 2016 he was director of the Danish National Research Foundation Center for Individual Nanoparticle Functionality (CINF) and from 2016 he has been director of The Villum Center for the Science of Sustainable Fuels and Chemicals (V-SUSTAIN). Ib Chorkendorff's research activities focus on finding new catalysts for improving energy production/conversion and for environmental protection. He has author or coauthored more than 330 scientific papers,18 patents, and one textbook "Concepts of Modern Catalysis and Kinetics". He is cofounder of three start-up companies RENCAT APS, HPNOW APS and Spectroinlets APS. Ib Chorkendorff has received numerous prices and honors among others the Ulrik and Marie Brinch award and the Ingeborg and Leo Dannin's Prize for Natural Science Research. He is elected Fellow of The Academy for Technical Sciences (ATV) and Elected member of the Royal Danish Academy of Sciences and Letters.

## REFERENCES

(1) Hori, Y. Electrochemical $CO_2$ Reduction on Metal Electrodes. In *Modern Aspects of Electrochemistry*, Vayenas, C. G.; White, R. E.; Gamboa-Aldeco, M. E., Eds.; Springer, 2008; Vol. 42, pp 89−189.

(2) Gattrell, M.; Gupta, N.; Co, A. A Review of the Aqueous Electrochemical Reduction of CO2 to Hydrocarbons at Copper. *J. Electroanal. Chem.* **2006**, *594*, 1−19.

(3) Vasileff, A.; Xu, C.; Jiao, Y.; Zheng, Y.; Qiao, S.-Z. Surface and Interface Engineering in Copper-Based Bimetallic Materials for Selective CO2 Electroreduction. *Chem.* **2018**, *4*, 1809−1831.

(4) Gamler, J. T. L.; Ashberry, H. M.; Skrabalak, S. E.; Koczkur, K. M. Random Alloyed versus Intermetallic Nanoparticles: A Comparison of Electrocatalytic Performance. *Adv. Mater.* **2018**, *30*, 1801563.

(5) Birhanu, M. K.; Tsai, M.-C.; Kahsay, A. W.; Chen, C.-T.; Zeleke, T. S.; Ibrahim, K. B.; Huang, C.-J.; Su, W.-N.; Hwang, B.-J. Copper and Copper-Based Bimetallic Catalysts for Carbon Dioxide Electroreduction. *Adv. Mater. Interfaces* **2018**, *5*, 1800919.

(6) Xie, H.; Wang, T.; Liang, J.; Li, Q.; Sun, S. Cu-Based Nanocatalysts for Electrochemical Reduction of CO2. *Nano Today* **2018**, *21*, 41−54.

(7) Gu, Z.; Shen, H.; Shang, L.; Lv, X.; Qian, L.; Zheng, G. Nanostructured Copper-Based Electrocatalysts for CO2 Reduction. *Small Methods* **2018**, *2*, 1800121.

(8) Rendón-Calle, A.; Builes, S.; Calle-Vallejo, F. A Brief Review of the Computational Modeling of CO2 Electroreduction on Cu Electrodes. *Curr. Opin. Electrochem.* **2018**, *9*, 158−165.

(9) Raciti, D.; Wang, C. Recent Advances in CO2 Reduction Electrocatalysis on Copper. *ACS Energy Lett.* **2018**, *3*, 1545−1556.

(10) Handoko, A. D.; Wei, F.; Jenndy; Yeo, B. S.; Seh, Z. W. Understanding Heterogeneous Electrocatalytic Carbon Dioxide Reduction through Operando Techniques. *Nat. Catal.* **2018**, *1*, 922−934.

(11) Lee, C. W.; Yang, K. D.; Nam, D.-H.; Jang, J. H.; Cho, N. H.; Im, S. W.; Nam, K. T. Defining a Materials Database for the Design of Copper Binary Alloy Catalysts for Electrochemical CO2 Conversion. *Adv. Mater.* **2018**, *30*, 1704717.

(12) Arán-Ais, R. M.; Gao, D.; Roldan Cuenya, B. Structure- and Electrolyte-Sensitivity in CO2 Electroreduction. *Acc. Chem. Res.* **2018**, *51*, 2906−2917.

(13) Jhong, H. R. M.; Ma, S.; Kenis, P. J. A. Electrochemical Conversion of CO2 to Useful Chemicals: Current Status, Remaining Challenges, and Future Opportunities. *Curr. Opin. Chem. Eng.* **2013**, *2*, 191−199.

(14) Xu, S.; Carter, E. A. Theoretical Insights into Heterogeneous (Photo)Electrochemical CO 2 Reduction. *Chem. Rev.* **2018**, DOI: 10.1021/acs.chemrev.8b00481.

(15) Qiao, J.; Liu, Y.; Hong, F.; Zhang, J. A Review of Catalysts for the Electroreduction of Carbon Dioxide to Produce Low-Carbon Fuels. *Chem. Soc. Rev.* **2014**, *43*, 631−675.

(16) Kortlever, R.; Shen, J.; Schouten, K. J. P.; Calle-Vallejo, F.; Koper, M. T. M. Catalysts and Reaction Pathways for the Electrochemical Reduction of Carbon Dioxide. *J. Phys. Chem. Lett.* **2015**, *6*, 4073−4082.

(17) Zhu, D. D.; Liu, J. L.; Qiao, S. Z. Recent Advances in Inorganic Heterogeneous Electrocatalysts for Reduction of Carbon Dioxide. *Adv. Mater.* **2016**, *28*, 3423−3452.

(18) Zhang, B.; Zhang, J. Rational Design of Cu-Based Electrocatalysts for Electrochemical Reduction of Carbon Dioxide. *J. Energy Chem.* **2017**, *26*, 1050−1066.

(19) Vickers, J. W.; Alfonso, D.; Kauffman, D. R. Electrochemical Carbon Dioxide Reduction at Nanostructured Gold, Copper, and Alloy Materials. *Energy Technol.* **2017**, *5*, 775−795.

(20) Pander, J. E.; Ren, D.; Huang, Y.; Loo, N. W. X.; Hong, S. H. L.; Yeo, B. S. Understanding the Heterogeneous Electrocatalytic Reduction of Carbon Dioxide on Oxide-Derived Catalysts. *ChemElectroChem* **2018**, *5*, 219−237.

(21) He, J.; Johnson, N. J. J.; Huang, A.; Berlinguette, C. P. Electrocatalytic Alloys for CO 2 Reduction. *ChemSusChem* **2018**, *11*, 48−57.

(22) Intergovernmental Panel on Climate Change. *Climate Change 2014: Synthesis Report*; 2014.

(23) Conference of the Parties to the United Nations Framework Convention on Climate Change. *Adoption of the Paris Agreement*; 2015; pp 1−32.

(24) Intergovernmental Panel on Climate Change. *IPCC Special Report on the Impacts of Global Warming of 1.5 °C - Summary for Policy Makers*; Incheon, 2018.

(25) International Energy Agency. *IEA2017.Pdf*; IEA Newsroom; 2017.

(26) Obama, B. The Irreversible Momentum of Clean Energy. *Science* **2017**, *355*, 126−129.

(27) World Bank Group: IEA Statistics. GDP per unit of energy use https://data.worldbank.org/indicator/EG.GDP.PUSE.KO.PP?contextual=default&locations=US-CN-EU-1W.

(28) Chu, S.; Cui, Y.; Liu, N. The Path towards Sustainable Energy. *Nat. Mater.* **2017**, *16*, 16−22.

(29) Randall, T. *Wind and Solar Are Crushing Fossil Fuels*; Bloomberg. 2016.

(30) Davis, S. J.; Lewis, N. S.; Shaner, M.; Aggarwal, S.; Arent, D.; Azevedo, I. L.; Benson, S. M.; Bradley, T.; Brouwer, J.; Chiang, Y.-M.; et al. Net-Zero Emissions Energy Systems. *Science* **2018**, *360*, No. eaas9793.

(31) Yang, Z.; Zhang, J.; Kintner-Meyer, M. C. W.; Lu, X.; Choi, D.; Lemmon, J. P.; Liu, J. Electrochemical Energy Storage for Green Grid. *Chem. Rev.* **2011**, *111*, 3577−3613.

(32) Gyuk, I.; Johnson, M.; Vetrano, J.; Lynn, K.; Parks, W.; Handa, R.; Kannberg, L. D.; Hearne, S.; Waldrip, K.; Braccio, R. *Grid Energy Storage*; 2013.

(33) van Oss, H. G. *Cement in January* 2018.

(34) World Steel Association. *Worl Steel Figures 2018*; Brussels and Beijing, 2018.

(35) Geyer, R.; Jambeck, J. R.; Law, K. L. Production, Use, and Fate of All Plastics Ever Made. *Sci. Adv.* **2017**, *3*, 19−24.

(36) Apodaca, L. E. *Mineral Commodity Summaries - Ammonia*; 2016; Vol. 32.

(37) Bray, E. L. *Mineral Commodity Summaries - Aluminum*; 2017; Vol. 1.

(38) Houghton, R. A. Balancing the Global Carbon Budget. *Annu. Rev. Earth Planet. Sci.* **2007**, *35*, 313−347.

(39) Le Quéré, C.; Moriarty, R.; Andrew, R. M.; Canadell, J. G.; Sitch, S.; Korsbakken, J. I.; Friedlingstein, P.; Peters, G. P.; Andres, R. J.; Boden, T. A.; et al. Global Carbon Budget 2015. *Earth Syst. Sci. Data* **2015**, *7*, 349−396.

(40) Majumdar, A.; Deutch, J.; Bras, R.; Benson, S.; Carter, E.; Ort, D.; Ramage, M.; Socolow, R.; Toone, E.; Whitesides, G.; et al. *Task Force on the RD&D Strategy for CO 2 Utilization and/or Negative Emissions at the Gigatonne Scale*; 2016.

(41) Global CCS Institute. *The Global Status of CCS*; 2013.

(42) North American Carbon Atlas Partnership. *The North American Carbon Storage Atlas*; 2012.

(43) Rubin, E. S.; Davison, J. E.; Herzog, H. J. The Cost of CO2 Capture and Storage. *Int. J. Greenhouse Gas Control* **2015**, *40*, 378−400.

(44) Appel, A. M.; Bercaw, J. E.; Bocarsly, A. B.; Dobbek, H.; DuBois, D. L.; Dupuis, M.; Ferry, J. G.; Fujita, E.; Hille, R.; Kenis, P. J. A.; et al. Frontiers, Opportunities, and Challenges in Biochemical and Chemical Catalysis of CO2 Fixation. *Chem. Rev.* **2013**, *113*, 6621−6658.

(45) Searchinger, T.; Heimlich, R.; Houghton, R. A.; Dong, F.; Elobeid, A.; Fabiosa, J.; Tokgoz, S.; Hayes, D.; Yu, T.-H. Use of U.S. Croplands for Biofuels Increases Greenhouse Gases Through Emissions from Land-Use Change. *Science* **2008**, *319*, 1238−1240.

(46) Al-Riffai, P.; Dimaranan, B.; Laborde, D. *Global Trade and Environmental Impact Study of the EU Biofuels Mandate*; 2010.

(47) Baik, E.; Sanchez, D. L.; Turner, P. A.; Mach, K. J.; Field, C. B.; Benson, S. M. Geospatial Analysis of Near-Term Potential for Carbon-Negative Bioenergy in the United States. *Proc. Natl. Acad. Sci. U. S. A.* **2018**, *115*, 3290−3295.

(48) Turner, P. A.; Mach, K. J.; Lobell, D. B.; Benson, S. M.; Baik, E.; Sanchez, D. L.; Field, C. B. The Global Overlap of Bioenergy and Carbon Sequestration Potential. *Clim. Change* **2018**, *148*, 1−10.

(49) Kaul, M.; Mohren, G. M. J.; Dadhwal, V. K. Carbon Storage and Sequestration Potential of Selected Tree Species in India. *Mitig. Adapt. Strateg. Glob. Chang.* **2010**, *15*, 489−510.

(50) Eckert, M.; Fleischmann, G.; Jira, R.; Bolt, H. M.; Golka, K. *Ullmann's Encyclopedia of Industrial Chemistry*; Wiley-VCH Verlag GmbH & Co. KGaA: Weinheim, Germany, 2000.

(51) Chorkendorff, I.; Niemantsverdriet, J. W. *Concepts of Modern Catalysis and Kinetics*; Wiley-VCH Verlag GmbH & Co. KGaA: Weinheim, FRG, 2003.

(52) Rönsch, S.; Schneider, J.; Matthischke, S.; Schlüter, M.; Götz, M.; Lefebvre, J.; Prabhakaran, P.; Bajohr, S. Review on Methanation - From Fundamentals to Current Projects. *Fuel* **2016**, *166*, 276−296.

(53) Yang, J.; Ma, W.; Chen, D.; Holmen, A.; Davis, B. H. Fischer−Tropsch Synthesis: A Review of the Effect of CO Conversion on Methane Selectivity. *Appl. Catal., A* **2014**, *470*, 250−260.

(54) Jadhav, S. G.; Vaidya, P. D.; Bhanage, B. M.; Joshi, J. B. Catalytic Carbon Dioxide Hydrogenation to Methanol: A Review of Recent Studies. *Chem. Eng. Res. Des.* **2014**, *92*, 2557−2567.

(55) Olah, G. A.; Goeppert, A.; Prakash, G. K. S. *Beyond Oil and Gas: The Methanol Economy*, 2nd ed.; 2009.

(56) Studt, F.; Behrens, M.; Kunkes, E. L.; Thomas, N.; Zander, S.; Tarasov, A.; Schumann, J.; Frei, E.; Varley, J. B.; Abild-Pedersen, F.; et al. The Mechanism of CO and CO2 Hydrogenation to Methanol over Cu-Based Catalysts. *ChemCatChem* **2015**, *7*, 1105−1111.

(57) Seh, Z. W.; Kibsgaard, J.; Dickens, C. F.; Chorkendorff, I.; Nørskov, J. K.; Jaramillo, T. F. Combining Theory and Experiment in Electrocatalysis: Insights into Materials Design. *Science* **2017**, *355*, No. eaad4998.

(58) Carmo, M.; Fritz, D. L.; Mergel, J.; Stolten, D. A Comprehensive Review on PEM Water Electrolysis. *Int. J. Hydrogen Energy* **2013**, *38*, 4901−4934.

(59) Whipple, D. T.; Kenis, P. J. A. Prospects of CO2 Utilization via Direct Heterogeneous Electrochemical Reduction. *J. Phys. Chem. Lett.* **2010**, *1*, 3451−3458.

(60) Graves, C.; Ebbesen, S. D.; Mogensen, M.; Lackner, K. S. Sustainable Hydrocarbon Fuels by Recycling CO2 and H2O with Renewable or Nuclear Energy. *Renewable Sustainable Energy Rev.* **2011**, *15*, 1−23.

(61) Kondratenko, E. V.; Mul, G.; Baltrusaitis, J.; Larrazábal, G. O.; Pérez-Ramírez, J. Status and Perspectives of CO2 Conversion into Fuels and Chemicals by Catalytic, Photocatalytic and Electrocatalytic Processes. *Energy Environ. Sci.* **2013**, *6*, 3112−3135.

(62) Götz, M.; Lefebvre, J.; Mörs, F.; McDaniel Koch, A.; Graf, F.; Bajohr, S.; Reimert, R.; Kolb, T. Renewable Power-to-Gas: A Technological and Economic Review. *Renewable Energy* **2016**, *85*, 1371−1390.

(63) Dau, H.; Limberg, C.; Reier, T.; Risch, M.; Roggan, S.; Strasser, P. The Mechanism of Water Oxidation: From Electrolysis via Homogeneous to Biological Catalysis. *ChemCatChem* **2010**, *2*, 724−761.

(64) *NIST Chemistry WebBook, NIST Standard Reference Database Number 69*, Mallard, P. J.; Linstrom, W. G., Eds.; National Institute of Standards and Technology: Gaithersburg MD, 20899.

(65) Kuhl, K. P.; Cave, E. R.; Abram, D. N.; Jaramillo, T. F. New Insights into the Electrochemical Reduction of Carbon Dioxide on Metallic Copper Surfaces. *Energy Environ. Sci.* **2012**, *5*, 7050−7059.

(66) Verma, S.; Kim, B.; Jhong, H. R. M.; Ma, S.; Kenis, P. J. A. A Gross-Margin Model for Defining Technoeconomic Benchmarks in the Electroreduction of CO2. *ChemSusChem* **2016**, *9*, 1972−1979.

(67) Oloman, C.; Li, H. Electrochemical Processing of Carbon Dioxide. *ChemSusChem* **2008**, *1*, 385−391.

(68) Spurgeon, J. M.; Kumar, B. A Comparative Technoeconomic Analysis of Pathways for Commercial Electrochemical CO2 Reduction to Liquid Products. *Energy Environ. Sci.* **2018**, *11*, 1536−1551.

(69) Jouny, M.; Luc, W.; Jiao, F. General Techno-Economic Analysis of CO2 Electrolysis Systems. *Ind. Eng. Chem. Res.* **2018**, *57*, 2165−2177.

(70) Li, C. W.; Ciston, J.; Kanan, M. W. Electroreduction of Carbon Monoxide to Liquid Fuel on Oxide-Derived Nanocrystalline Copper. *Nature* **2014**, *508*, 504−507.

(71) Bushuyev, O. S.; De Luna, P.; Dinh, C. T.; Tao, L.; Saur, G.; van de Lagemaat, J.; Kelley, S. O.; Sargent, E. H. What Should We Make with CO2 and How Can We Make It? *Joule* **2018**, *2*, 825−832.

(72) Clark, E. L.; Hahn, C.; Jaramillo, T. F.; Bell, A. T. Electrochemical CO2 Reduction over Compressively Strained CuAg Surface Alloys with Enhanced Multi-Carbon Oxygenate Selectivity. *J. Am. Chem. Soc.* **2017**, *139*, 15848−15857.

(73) Lewis, N. S.; Nocera, D. G. Powering the Planet: Chemical Challenges in Solar Energy Utilization. *Proc. Natl. Acad. Sci. U. S. A.* **2006**, *103*, 15729−15735.

(74) Afshar, A. A. N. *Chemical Profile: Formic Acid*; 2014.

(75) British Petroleum (BP). *Natural Gas*, 67th ed.; 2018.

(76) True, W. R. Global Ethylene Capacity Poised for Major Expansion. *Oil Gas J.* **2008**, *110*, 90−95.

(77) Eckert, M.; Fleischmann, G.; Jira, R.; Bolt, H. M.; Golka, K. *Ullmann's Encyclopedia of Industrial Chemistry*; WILEY-VCH Verlag, 2007.

(78) Kniel, L.; Stork, K.; Winter, O. *Ethylene - A Keystone to the Petrochemical Industry*; M. Dekker, New York, 1980.

(79) Mussatto, S. I.; Dragone, G.; Guimarães, P. M. R.; Silva, J. P. A.; Carneiro, L. M.; Roberto, I. C.; Vicente, A.; Domingues, L.; Teixeira, J. A. Technological Trends, Global Market, and Challenges of Bio-Ethanol Production. *Biotechnol. Adv.* **2010**, *28*, 817−830.

(80) Teeter, T. E.; Van Rysselberghe, P. Reduction of Carbon Dioxide on Mercury Cathodes. *J. Chem. Phys.* **1954**, *22*, 759−760.

(81) Hori, Y.; Kikuchi, K.; Suzuki, S. Production of CO and CH4 in Electrochemical Reduction of CO2 at Metal Electrodes in Aqueous Hydrogencarbonate Solutions. *Chem. Lett.* **1985**, *14*, 1695−1698.

(82) Hori, Y.; Kikuchi, K.; Murata, A.; Suzuki, S. Production of Methane and Ethylene in Electrochemical Reduction of Carbon Dioxide At Copper Electrode in Aqueous Hydrogencarbonate Solution. *Chem. Lett.* **1986**, *15*, 897−898.

(83) Hori, Y.; Murata, A.; Takahashi, R.; Suzuki, S. Enhanced Formation of Ethylene and Alcohols at Ambient Temperature and Pressure in Electrochemical Reduction of Carbon Dioxide at a Copper Electrode. *J. Chem. Soc., Chem. Commun.* **1988**, *0*, 17.

(84) Hori, Y.; Wakebe, H.; Tsukamoto, T.; Koga, O. Electrocatalytic Process of CO Selectivity in Electrochemical Reduction of CO2 at Metal Electrodes in Aqueous Media. *Electrochim. Acta* **1994**, *39*, 1833−1839.

(85) Hori, Y.; Murata, A.; Takahashi, R. Formation of Hydrocarbons in the Electrochemical Reduction of Carbon Dioxide at a Copper Electrode in Aqueous Solution. *J. Chem. Soc., Faraday Trans. 1* **1989**, *85*, 2309−2326.

(86) Bagger, A.; Ju, W.; Varela, A. S.; Strasser, P.; Rossmeisl, J. Electrochemical CO2 Reduction: A Classification Problem. *ChemPhysChem* **2017**, *18*, 3266−3273.

(87) Clark, E. L.; Resasco, J.; Landers, A.; Lin, J.; Chung, L.-T.; Walton, A.; Hahn, C.; Jaramillo, T. F.; Bell, A. T. Standards and Protocols for Data Acquisition and Reporting for Studies of the Electrochemical Reduction of Carbon Dioxide. *ACS Catal.* **2018**, *8*, 6560−6570.

(88) Pander, J. E.; Ren, D.; Yeo, B. S. Practices for the Collection and Reporting of Electrocatalytic Performance and Mechanistic Information for the CO2 Reduction Reaction. *Catal. Sci. Technol.* **2017**, *7*, 5820−5832.

(89) Li, C. W.; Kanan, M. W. CO2 Reduction at Low Overpotential on Cu Electrodes Resulting from the Reduction of Thick Cu2O Films. *J. Am. Chem. Soc.* **2012**, *134*, 7231−7234.

(90) Bertheussen, E.; Verdaguer-Casadevall, A.; Ravasio, D.; Montoya, J. H.; Trimarco, D. B.; Roy, C.; Meier, S.; Wendland, J.; Nørskov, J. K.; Stephens, I. E. L.; et al. Acetaldehyde as an Intermediate in the Electroreduction of Carbon Monoxide to Ethanol on Oxide-Derived Copper. *Angew. Chem., Int. Ed.* **2016**, *55*, 1450−1454.

(91) Raciti, D.; Livi, K. J.; Wang, C. Highly Dense Cu Nanowires for Low-Overpotential CO2 Reduction. *Nano Lett.* **2015**, *15*, 6829−6835.

(92) Ma, M.; Djanashvili, K.; Smith, W. A. Selective Electrochemical Reduction of CO2 to CO on CuO-Derived Cu Nanowires. *Phys. Chem. Chem. Phys.* **2015**, *17*, 20861−20867.

(93) Min, S.; Yang, X.; Lu, A. Y.; Tseng, C. C.; Hedhili, M. N.; Li, L. J.; Huang, K. W. Low Overpotential and High Current CO2 Reduction with Surface Reconstructed Cu Foam Electrodes. *Nano Energy* **2016**, *27*, 121−129.

(94) Roberts, F. S.; Kuhl, K. P.; Nilsson, A. High Selectivity for Ethylene from Carbon Dioxide Reduction over Copper Nanocube Electrocatalysts. *Angew. Chem., Int. Ed.* **2015**, *54*, 5179−5182.

(95) Kwon, Y.; Lum, Y.; Clark, E. L.; Ager, J. W.; Bell, A. T. CO2 Electroreduction with Enhanced Ethylene and Ethanol Selectivity by Nanostructuring Polycrystalline Copper. *ChemElectroChem* **2016**, *3*, 1012−1019.

(96) Singh, M. R.; Clark, E. L.; Bell, A. T. Effects of Electrolyte, Catalyst, and Membrane Composition and Operating Conditions on the Performance of Solar-Driven Electrochemical Reduction of Carbon Dioxide. *Phys. Chem. Chem. Phys.* **2015**, *17*, 18924−18936.

(97) Lum, Y.; Yue, B.; Lobaccaro, P.; Bell, A. T.; Ager, J. W. Optimizing C-C Coupling on Oxide-Derived Copper Catalysts for Electrochemical CO2 Reduction. *J. Phys. Chem. C* **2017**, *121*, 14191−14203.

(98) Raciti, D.; Mao, M.; Wang, C. Mass Transport Modelling for the Electroreduction of CO2 on Cu Nanowires. *Nanotechnology* **2018**, *29*, 044001.

(99) Gupta, N.; Gattrell, M.; MacDougall, B. Calculation for the Cathode Surface Concentrations in the Electrochemical Reduction of CO2 in KHCO3 Solutions. *J. Appl. Electrochem.* **2006**, *36*, 161−172.

(100) Clark, E. L.; Bell, A. T. Direct Observation of the Local Reaction Environment during the Electrochemical Reduction of CO2. *J. Am. Chem. Soc.* **2018**, *140*, 7012−7020.

(101) Hashiba, H.; Yotsuhashi, S.; Deguchi, M.; Yamada, Y. Systematic Analysis of Electrochemical CO2 Reduction with Various Reaction Parameters Using Combinatorial Reactors. *ACS Comb. Sci.* **2016**, *18*, 203−208.

(102) Hara, K.; Tsuneto, A.; Kudo, A.; Sakata, T. Electrochemical Reduction of CO2 on a Cu Electrode under High Pressure: Factors That Determine the Product Selectivity. *J. Electrochem. Soc.* **1994**, *141*, 2097−2103.

(103) Dewulf, D. W.; Jin, T.; Bard, A. J. Electrochemical and Surface Studies of Carbon Dioxide Reduction to Methane and Ethylene at Copper Electrodes in Aqueous Solutions. *J. Electrochem. Soc.* **1989**, *136*, 1686−1691.

(104) Wasmus, S.; Cattaneo, E.; Vielstich, W. Reduction of Carbon Dioxide to Methane and Ethene - An On-Line MS Study with Rotating Electrodes. *Electrochim. Acta* **1990**, *35*, 771−775.

(105) Yano, H.; Shirai, F.; Nakayama, M.; Ogura, K. Efficient Electrochemical Conversion of CO2 to CO, C2H4 and CH4 at a Three-Phase Interface on a Cu Net Electrode in Acidic Solution. *J. Electroanal. Chem.* **2002**, *519*, 93−100.

(106) Xie, J. F.; Huang, Y. X.; Li, W. W.; Song, X. N.; Xiong, L.; Yu, H. Q. Efficient Electrochemical CO2 Reduction on a Unique Chrysanthemum-like Cu Nanoflower Electrode and Direct Observation of Carbon Deposite. *Electrochim. Acta* **2014**, *139*, 137−144.

(107) Kyriacou, G.; Anagnostopoulos, A. Electroreduction of CO2 on Differently Prepared Copper Electrodes: The Influence of Electrode Treatment on the Current Efficiencies. *J. Electroanal. Chem.* **1992**, *322*, 233−246.

(108) Jermann, B.; Augustynski, J. Long-Term Activation of the Copper Cathode in the Course of CO2 Reduction. *Electrochim. Acta* **1994**, *39*, 1891−1896.

(109) Kas, R.; Kortlever, R.; Yılmaz, H.; Koper, M. T. M.; Mul, G. Manipulating the Hydrocarbon Selectivity of Copper Nanoparticles in CO2 Electroreduction by Process Conditions. *ChemElectroChem* **2015**, *2*, 354−358.

(110) Shiratsuchi, R.; Aikoh, Y.; Nogami, G. Pulsed Electroreduction of CO2 on Copper Electrodes. *J. Electrochem. Soc.* **1993**, *140*, 3479−3482.

(111) Hori, Y.; Konishi, H.; Futamura, T.; Murata, A.; Koga, O.; Sakurai, H.; Oguma, K. Deactivation of Copper Electrode" in Electrochemical Reduction of CO2. *Electrochim. Acta* **2005**, *50*, 5354−5369.

(112) Schouten, K. J. P.; Kwon, Y.; van der Ham, C. J. M.; Qin, Z.; Koper, M. T. M. A New Mechanism for the Selectivity to C1 and C2 Species in the Electrochemical Reduction of Carbon Dioxide on Copper Electrodes. *Chem. Sci.* **2011**, *2*, 1902−1909.

(113) Wuttig, A.; Surendranath, Y. Impurity Ion Complexation Enhances Carbon Dioxide Reduction Catalysis. *ACS Catal.* **2015**, *5*, 4479−4484.

(114) Bertheussen, E.; Hogg, T. V.; Abghoui, Y.; Engstfeld, A. K.; Chorkendorff, I.; Stephens, I. E. L. Electroreduction of CO on Polycrystalline Copper at Low Overpotentials. *ACS Energy Lett.* **2018**, *3*, 634−640.

(115) Kas, R.; Kortlever, R.; Milbrat, A.; Koper, M. T. M.; Mul, G.; Baltrusaitis, J. Electrochemical CO2 Reduction on Cu2O-Derived Copper Nanoparticles: Controlling the Catalytic Selectivity of Hydrocarbons. *Phys. Chem. Chem. Phys.* **2014**, *16*, 12194−12201.

(116) Chen, C. S.; Handoko, A. D.; Wan, J. H.; Ma, L.; Ren, D.; Yeo, B. S. Stable and Selective Electrochemical Reduction of Carbon Dioxide to Ethylene on Copper Mesocrystals. *Catal. Sci. Technol.* **2015**, *5*, 161−168.

(117) Lee, J.; Tak, Y. Electrocatalytic Activity of Cu Electrode in Electroreduction of CO2. *Electrochim. Acta* **2001**, *46*, 3015−3022.

(118) Dunwell, M.; Lu, Q.; Heyes, J. M.; Rosen, J.; Chen, J. G.; Yan, Y.; Jiao, F.; Xu, B. The Central Role of Bicarbonate in the Electrochemical Reduction of Carbon Dioxide on Gold. *J. Am. Chem. Soc.* **2017**, *139*, 3774−3783.

(119) Yano, J.; Yamasaki, S. Pulse-Mode Electrochemical Reduction of Carbon Dioxide Using Copper and Copper Oxide Electrodes for Selective Ethylene Formation. *J. Appl. Electrochem.* **2008**, *38*, 1721−1726.

(120) Kumar, B.; Brian, J. P.; Atla, V.; Kumari, S.; Bertram, K. A.; White, R. T.; Spurgeon, J. M. Controlling the Product Syngas H2:CO Ratio through Pulsed-Bias Electrochemical Reduction of CO2 on Copper. *ACS Catal.* **2016**, *6*, 4739−4745.

(121) Le Duff, C. S.; Lawrence, M. J.; Rodriguez, P. Role of the Adsorbed Oxygen Species in the Selective Electrochemical Reduction of CO2 to Alcohols and Carbonyls on Copper Electrodes. *Angew. Chem., Int. Ed.* **2017**, *56*, 12919−12924.

(122) Ishimaru, S.; Shiratsuchi, R.; Nogami, G. Pulsed Electro-reduction of CO2 on Cu-Ag Alloy Electrodes. *J. Electrochem. Soc.* **2000**, *147*, 1864−1867.

(123) Kimura, K. W.; Fritz, K. E.; Kim, J.; Suntivich, J.; Abruña, H. D.; Hanrath, T. Controlled Selectivity of CO2 Reduction on Copper by Pulsing the Electrochemical Potential. *ChemSusChem* **2018**, *11*, 1781−1786.

(124) Eilert, A.; Roberts, F. S.; Friebel, D.; Nilsson, A. Formation of Copper Catalysts for CO2 Reduction with High Ethylene/Methane Product Ratio Investigated with In Situ X-Ray Absorption Spectroscopy. *J. Phys. Chem. Lett.* **2016**, *7*, 1466−1470.

(125) Mistry, H.; Varela, A. S.; Bonifacio, C. S.; Zegkinoglou, I.; Sinev, I.; Choi, Y.; Kisslinger, K.; Stach, E. A.; Yang, J. C.; Strasser, P.; et al. Highly Selective Plasma-Activated Copper Catalysts for Carbon Dioxide Reduction to Ethylene. *Nat. Commun.* **2016**, *7*, 1−8.

(126) De Luna, P.; Quintero-Bermudez, R.; Dinh, C.-T.; Ross, M. B.; Bushuyev, O. S.; Todorovic, P.; Regier, T.; Kelley, S. O.; Yang, P.; Sargent, E. H. Catalyst Electro-Redeposition Controls Morphology and Oxidation State for Selective Carbon Dioxide Reduction. *Nat. Catal.* **2018**, *1*, 103−110.

(127) Lee, S.; Park, G.; Lee, J. Importance of Ag-Cu Biphasic Boundaries for Selective Electrochemical Reduction of CO2 to Ethanol. *ACS Catal.* **2017**, *7*, 8594−8604.

(128) Ren, D.; Deng, Y.; Handoko, A. D.; Chen, C. S.; Malkhandi, S.; Yeo, B. S. Selective Electrochemical Reduction of Carbon Dioxide to Ethylene and Ethanol on Copper(I) Oxide Catalysts. *ACS Catal.* **2015**, *5*, 2814−2821.

(129) Ren, D.; Ang, B. S.-H.; Yeo, B. S. Tuning the Selectivity of Carbon Dioxide Electroreduction toward Ethanol on Oxide-Derived CuxZn Catalysts. *ACS Catal.* **2016**, *6*, 8239−8247.

(130) Hoang, T. T. H.; Ma, S.; Gold, J. I.; Kenis, P. J. A.; Gewirth, A. A. Nanoporous Copper Films by Additive-Controlled Electro-deposition: CO2 Reduction Catalysis. *ACS Catal.* **2017**, *7*, 3313−3321.

(131) Hoang, T. T. H.; Verma, S.; Ma, S.; Fister, T. T.; Timoshenko, J.; Frenkel, A. I.; Kenis, P. J. A.; Gewirth, A. A. Nanoporous Copper−Silver Alloys by Additive-Controlled Electrodeposition for the Selective Electroreduction of CO 2 to Ethylene and Ethanol. *J. Am. Chem. Soc.* **2018**, *140*, 5791−5797.

(132) Ross, M. B.; Dinh, C. T.; Li, Y.; Kim, D.; De Luna, P.; Sargent, E. H.; Yang, P. Tunable Cu Enrichment Enables Designer Syngas Electrosynthesis from CO2. *J. Am. Chem. Soc.* **2017**, *139*, 9359−9363.

(133) Gunathunge, C. M.; Li, X.; Li, J.; Hicks, R. P.; Ovalle, V. J.; Waegele, M. M. Spectroscopic Observation of Reversible Surface Reconstruction of Copper Electrodes under CO2 Reduction. *J. Phys. Chem. C* **2017**, *121*, 12337−12344.

(134) Chernyshova, I. V.; Somasundaran, P.; Ponnurangam, S. On the Origin of the Elusive First Intermediate of CO2 Electroreduction. *Proc. Natl. Acad. Sci. U. S. A.* **2018**, *115*, E9261−E9270.

(135) Mandal, L.; Yang, K. R.; Motapothula, M. R.; Ren, D.; Lobaccaro, P.; Patra, A.; Sherburne, M.; Batista, V. S.; Yeo, B. S.; Ager, J. W.; et al. Investigating the Role of Copper Oxide in

Electrochemical CO2 Reduction in Real Time. *ACS Appl. Mater. Interfaces* **2018**, *10*, 8574−8584.

(136) Figueiredo, M. C.; Ledezma-Yanez, I.; Koper, M. T. M. In Situ Spectroscopic Study of CO2 Electroreduction at Copper Electrodes in Acetonitrile. *ACS Catal.* **2016**, *6*, 2382−2392.

(137) Gunathunge, C. M.; Ovalle, V. J.; Waegele, M. M. Probing Promoting Effects of Alkali Cations on the Reduction of CO at the Aqueous Electrolyte/Copper Interface. *Phys. Chem. Chem. Phys.* **2017**, *19*, 30166−30172.

(138) Wuttig, A.; Yaguchi, M.; Motobayashi, K.; Osawa, M.; Surendranath, Y. Inhibited Proton Transfer Enhances Au-Catalyzed CO2-to-Fuels Selectivity. *Proc. Natl. Acad. Sci. U. S. A.* **2016**, *113*, E4585−E4593.

(139) Zhu, S.; Jiang, B.; Cai, W.-B.; Shao, M. Direct Observation on Reaction Intermediates and the Role of Bicarbonate Anions in CO2 Electrochemical Reduction Reaction on Cu Surfaces. *J. Am. Chem. Soc.* **2017**, *139*, 15664−15667.

(140) Pérez-Gallent, E.; Figueiredo, M. C.; Calle-Vallejo, F.; Koper, M. T. M. Spectroscopic Observation of a Hydrogenated CO Dimer Intermediate During CO Reduction on Cu(100) Electrodes. *Angew. Chem., Int. Ed.* **2017**, *56*, 3621−3624.

(141) Baruch, M. F.; Pander, J. E.; White, J. L.; Bocarsly, A. B. Mechanistic Insights into the Reduction of CO2 on Tin Electrodes Using in Situ ATR-IR Spectroscopy. *ACS Catal.* **2015**, *5*, 3148−3156.

(142) Pander, J. E.; Baruch, M. F.; Bocarsly, A. B. Probing the Mechanism of Aqueous CO2 Reduction on Post-Transition-Metal Electrodes Using ATR-IR Spectroelectrochemistry. *ACS Catal.* **2016**, *6*, 7824−7833.

(143) Phillips, K. R.; Katayama, Y.; Hwang, J.; Shao-Horn, Y. Sulfide-Derived Copper for Electrochemical Conversion of CO2 to Formic Acid. *J. Phys. Chem. Lett.* **2018**, *9*, 4407−4412.

(144) Hori, Y.; Murata, A.; Tsukamoto, T.; Wakebe, H.; Koga, O.; Yamazaki, H. Adsorption of Carbon Monoxide at a Copper Electrode Accompanied by Electron Transfer Observed by Voltammetry and IR Spectroscopy. *Electrochim. Acta* **1994**, *39*, 2495−2500.

(145) Hori, Y.; Koga, O.; Yamazaki, H.; Matsuo, T. Infrared Spectroscopy of Adsorbed CO and Intermediate Species in Electrochemical Reduction of CO2 to Hydrocarbons on a Cu Electrode. *Electrochim. Acta* **1995**, *40*, 2617−2622.

(146) Wuttig, A.; Liu, C.; Peng, Q.; Yaguchi, M.; Hendon, C. H.; Motobayashi, K.; Ye, S.; Osawa, M.; Surendranath, Y. Tracking a Common Surface-Bound Intermediate during CO2-to-Fuels Catalysis. *ACS Cent. Sci.* **2016**, *2*, 522−528.

(147) Gunathunge, C. M.; Ovalle, V. J.; Li, Y.; Janik, M. J.; Waegele, M. M. Existence of an Electrochemically Inert CO Population on Cu Electrodes in Alkaline PH. *ACS Catal.* **2018**, *8*, 7507−7516.

(148) Ayemoba, O.; Cuesta, A. Spectroscopic Evidence of Size-Dependent Buffering of Interfacial PH by Cation Hydrolysis during CO2 Electroreduction. *ACS Appl. Mater. Interfaces* **2017**, *9*, 27377−27382.

(149) Dunwell, M.; Yang, X.; Setzler, B. P.; Anibal, J.; Yan, Y.; Xu, B. Examination of Near-Electrode Concentration Gradients and Kinetic Impacts on the Electrochemical Reduction of CO2 Using Surface-Enhanced Infrared Spectroscopy. *ACS Catal.* **2018**, *8*, 3999−4008.

(150) Hori, Y.; Wakebe, H.; Tsukamoto, T.; Koga, O. Adsorption of CO Accompanied with Simultaneous Charge Transfer on Copper Single Crystal Electrodes Related with Electrochemical Reduction of CO2 to Hydrocarbons. *Surf. Sci.* **1995**, *335*, 258−263.

(151) Hori, Y.; Takahashi, I.; Koga, O.; Hoshi, N. Selective Formation of C2 Compounds from Electrochemical Reduction of CO2 at a Series of Copper Single Crystal Electrodes. *J. Phys. Chem. B* **2002**, *106*, 15−17.

(152) Takahashi, I.; Koga, O.; Hoshi, N.; Hori, Y. Electrochemical Reduction of CO2 at Copper Single Crystal Cu(S)-[n(111)×(111)] and Cu(S)-[n(110)×(100)] Electrodes. *J. Electroanal. Chem.* **2002**, *533*, 135−143.

(153) Hori, Y.; Takahashi, I.; Koga, O.; Hoshi, N. Electrochemical Reduction of Carbon Dioxide at Various Series of Copper Single Crystal Electrodes. *J. Mol. Catal. A: Chem.* **2003**, *199*, 39−47.

(154) Christophe, J.; Doneux, T.; Buess-Herman, C. Electroreduction of Carbon Dioxide on Copper-Based Electrodes: Activity of Copper Single Crystals and Copper-Gold Alloys. *Electrocatalysis* **2012**, *3*, 139−146.

(155) Huang, Y.; Handoko, A. D.; Hirunsit, P.; Yeo, B. S. Electrochemical Reduction of CO2 Using Copper Single-Crystal Surfaces: Effects of CO* Coverage on the Selective Formation of Ethylene. *ACS Catal.* **2017**, *7*, 1749−1756.

(156) Yoshihara, N.; Arita, M.; Noda, M. Electrochemical Reduction of Carbon Dioxide on Single-Crystal Copper Membrane. *ECS Trans.* **2015**, *66*, 83−89.

(157) Hahn, C.; Hatsukade, T.; Kim, Y. G.; Vailionis, A.; Baricuatro, J. H.; Higgins, D. C.; Nitopi, S. A.; Soriaga, M. P.; Jaramillo, T. F. Engineering Cu Surfaces for the Electrocatalytic Conversion of CO2: Controlling Selectivity toward Oxygenates and Hydrocarbons. *Proc. Natl. Acad. Sci. U. S. A.* **2017**, *114*, 5918−5923.

(158) Frese, K. W. *Electrochemical Reduction of CO₂ at Solid Electrodes*; Elsevier: Amsterdam, 1993.

(159) Hori, Y.; Takahashi, R.; Yoshinami, Y.; Murata, A. Electrochemical Reduction of CO at a Copper Electrode. *J. Phys. Chem. B* **1997**, *101*, 7075−7081.

(160) Hori, Y.; Murata, A.; Takahashi, R.; Suzuki, S. Electro-reduction of CO To CH4 and C2H4 At a Copper Electrode in Aqueous-Solutions At Ambient-Temperature and Pressure. *J. Am. Chem. Soc.* **1987**, *109*, 5022−5023.

(161) Kim, J. J.; Summers, D. P.; Frese, K. W., Jr. Reduction of Carbon Dioxide and Carbon Monoxide to Methane on Copper Foil Electrodes. *J. Electroanal. Chem. Interfacial Electrochem.* **1988**, *245*, 223−244.

(162) Hori, Y.; Koga, O.; Watanabe, Y.; Matsuo, T. FTIR Measurements of Charge Displacement Adsorption of CO on Poly- and Single Crystal (100) of Cu Electrodes. *Electrochim. Acta* **1998**, *44*, 1389−1395.

(163) Schouten, K. J. P.; Qin, Z.; Pérez Gallent, E.; Koper, M. T. M. Two Pathways for the Formation of Ethylene in CO Reduction on Single-Crystal Copper Electrodes. *J. Am. Chem. Soc.* **2012**, *134*, 9864−9867.

(164) Schouten, K. J. P.; Gallent, E. P.; Koper, M. T. M. The Electrochemical Characterization of Copper Single-Crystal Electrodes in Alkaline Media. *J. Electroanal. Chem.* **2013**, *699*, 6−9.

(165) Schouten, K. J. P.; Pérez Gallent, E.; Koper, M. T. M. The Influence of PH on the Reduction of CO and CO2 to Hydrocarbons on Copper Electrodes. *J. Electroanal. Chem.* **2014**, *716*, 53−57.

(166) Schouten, K. J. P.; Pérez Gallent, E.; Koper, M. T. M. Structure Sensitivity of the Electrochemical Reduction of Carbon Monoxide on Copper Single Crystals. *ACS Catal.* **2013**, *3*, 1292−1295.

(167) Dahl, S.; Logadottir, A.; Egeberg, R. C.; Larsen, J. H.; Chorkendorff, I.; Törnqvist, E.; Nørskov, J. K. Role of Steps in N2 Activation on Ru(0001). *Phys. Rev. Lett.* **1999**, *83*, 1814−1817.

(168) Liu, X.; Xiao, J.; Peng, H.; Hong, X.; Chan, K.; Nørskov, J. K. Understanding Trends in Electrochemical Carbon Dioxide Reduction Rates. *Nat. Commun.* **2017**, *8*, 15438.

(169) Climent, V.; Feliu, J. M. Thirty Years of Platinum Single Crystal Electrochemistry. *J. Solid State Electrochem.* **2011**, *15*, 1297−1315.

(170) Gómez-Marín, A. M.; Feliu, J. M. Pt(111) Surface Disorder Kinetics in Perchloric Acid Solutions and the Influence of Specific Anion Adsorption. *Electrochim. Acta* **2012**, *82*, 558−569.

(171) Engstfeld, A. K.; Maagaard, T.; Horch, S.; Chorkendorff, I.; Stephens, I. E. L. Polycrystalline and Single-Crystal Cu Electrodes: Influence of Experimental Conditions on the Electrochemical Properties in Alkaline Media. *Chem. - Eur. J.* **2018**, *24*, 17743−17755.

(172) Schlaup, C.; Horch, S. In-Situ STM Study of Phosphate Adsorption on Cu(111), Au(111) and Cu/Au(111) Electrodes. *Surf. Sci.* **2013**, *608*, 44−54.

(173) Kim, Y.-G.; Javier, A.; Baricuatro, J. H.; Soriaga, M. P. Regulating the Product Distribution of CO Reduction by the Atomic-

Level Structural Modification of the Cu Electrode Surface. *Electrocatalysis* **2016**, 7, 391−399.

(174) Eren, B.; Zherebetskyy, D.; Patera, L. L.; Wu, C. H.; Somorjai, G. A.; Salmeron, M. Activation of Cu(111) Surface by Decomposition into Nanoclusters Driven by CO Adsorption. *Science* **2016**, 351, 475−478.

(175) Tang, M. T.; Ulissi, Z. W.; Chan, K. Theoretical Investigations of Transition Metal Surface Energies under Lattice Strain and CO Environment. *J. Phys. Chem. C* **2018**, 122, 14481−14487.

(176) Scott, S. B.; Hogg, T. V.; Landers, A. T.; Maagaard, T.; Bertheussen, E.; Lin, J. C.; Davis, R. C.; Beeman, J. W.; Higgins, D.; Drisdell, W. S.; et al. Absence of Oxidized Phases in Cu under CO Reduction Conditions. *ACS Energy Lett.* **2019**, 4, 803−804.

(177) Hori, Y.; Murata, A.; Yoshinami, Y. Adsorption of CO, Intermediately Formed in Electrochemical Reduction of CO2, at a Copper Electrode. *J. Chem. Soc., Faraday Trans.* **1991**, 87, 125−128.

(178) Kim, Y. G.; Baricuatro, J. H.; Javier, A.; Gregoire, J. M.; Soriaga, M. P. The Evolution of the Polycrystalline Copper Surface, First to Cu(111) and Then to Cu(100), at a Fixed CO2RR Potential: A Study by Operando EC-STM. *Langmuir* **2014**, 30, 15053−15056.

(179) Kim, Y. G.; Soriaga, M. P. Cathodic Regeneration of a Clean and Ordered Cu(100)-(1 × 1) Surface from an Air-Oxidized and Disordered Electrode: An Operando STM Study. *J. Electroanal. Chem.* **2014**, 734, 7−9.

(180) Kim, Y. G.; Javier, A.; Baricuatro, J. H.; Torelli, D.; Cummins, K. D.; Tsang, C. F.; Hemminger, J. C.; Soriaga, M. P. Surface Reconstruction of Pure-Cu Single-Crystal Electrodes under CO-Reduction Potentials in Alkaline Solutions: A Study by Seriatim ECSTM-DEMS. *J. Electroanal. Chem.* **2016**, 780, 290−295.

(181) Kim, Y.; Baricuatro, J. H.; Soriaga, M. P. Surface Reconstruction of Polycrystalline Cu Electrodes in Aqueous KHCO3 Electrolyte at Potentials in the Early Stages of CO2 Reduction. *Electrocatalysis* **2018**, 9, 526−530.

(182) Gasteiger, H. A.; Kocha, S. S.; Sompalli, B.; Wagner, F. T. Activity Benchmarks and Requirements for Pt, Pt-Alloy, and Non-Pt Oxygen Reduction Catalysts for PEMFCs. *Appl. Catal., B* **2005**, 56, 9−35.

(183) Droog, J. M. M.; Schlenter, B. Oxygen Electrosorption on Copper Single Crystal Electrodes in Sodium Hydroxide Solution. *J. Electroanal. Chem. Interfacial Electrochem.* **1980**, 112, 387−390.

(184) Jović, V. D.; Jović, B. M. Surface Reconstruction during the Adsorption/Desorption of OH - Species onto Cu(111) and Cu(100) in 0.1 M NaOH Solution. *J. Serb. Chem. Soc.* **2002**, 67, 531−546.

(185) Jovic, V. D.; Jovic, B. M. EIS and Differential Capacitance Measurements onto Single Crystal Faces in Different Solutions Part II : Cu (111) and Cu (100) in 0. 1 M NaOH. *J. Electroanal. Chem.* **2003**, 541, 13−21.

(186) Matsuoka, O.; Ono, S. S.; Nozoye, H.; Yamamoto, S. Structure and Dynamics of Oxy-Overlayer on Cu(1 1 1) Electrode Surfaces in Alkaline Aqueous Solution Revealed by Electrochemical STM and Quartz Crystal Microbalance Measurement. *Surf. Sci.* **2003**, 545, 8−18.

(187) Bockris, J. O.; Pentland, N. The Mechanism of Hydrogen Evolution at Copper Cathodes in Aqueous Solutions. *Trans. Faraday Soc.* **1952**, 48, 833−839.

(188) Pentland, N.; Bockris, J. O.; Sheldon, E. Hydrogen Evolution Reaction on Copper, Gold, Molybdenum, Palladium, Rhodium, and Iron. *J. Electrochem. Soc.* **1957**, 104, 182−194.

(189) Sharifi-Asl, S.; Macdonald, D. D. Investigation of the Kinetics and Mechanism of the Hydrogen Evolution Reaction on Copper. *J. Electrochem. Soc.* **2013**, 160, H382−H391.

(190) Łukomska, A.; Sobkowski, J. Potential of Zero Charge of Monocrystalline Copper Electrodes in Perchlorate Solutions. *J. Electroanal. Chem.* **2004**, 567, 95−102.

(191) Siegenthaler, H.; Jüttner, K. Voltammetric Investigation of Lead Adsorption on Cu(111) Single Crystal Substrates. *J. Electroanal. Chem. Interfacial Electrochem.* **1984**, 163, 327−343.

(192) Hernandez Creus, A.; Souto, R. M.; Gonz, S.; Laz, M. M.; Salvarezza, R. C.; Arvia, A. J. The Electrochemical Faceting of Copper

in 85% Aqueous O-Phosphoric Acid by Using a Potential Reversal Technique. *Appl. Surf. Sci.* **1994**, 81, 387−398.

(193) Burke, L. D.; Collins, J. A.; Horgan, M. A.; Hurley, L. M.; O'Mullane, A. P. Importance of the Active States of Surface Atoms with Regard to the Electrocatalytic Behaviour of Metal Electrodes in Aqueous Media. *Electrochim. Acta* **2000**, 45, 4127−4134.

(194) Hampson, N. A.; Latham, R. J.; Lee, J. B.; Macdonald, K. I. Oxidations at Copper Electrodes: Part I. The Differential Capacitance of Polycrystalline Copper in Alkali. *J. Electroanal. Chem. Interfacial Electrochem.* **1971**, 31, 57−62.

(195) Nakahara, S.; Okinaka, Y. The Hydrogen Effect in Copper. *Mater. Sci. Eng., A* **1988**, 101, 227−230.

(196) Rosca, V.; Duca, M.; de Groot, M. T.; Koper, M. T. M. Nitrogen Cycle Electrocatalysis. *Chem. Rev.* **2009**, 109, 2209−2244.

(197) Duca, M.; Koper, M. T. M. Powering Denitrification: The Perspectives of Electrocatalytic Nitrate Reduction. *Energy Environ. Sci.* **2012**, 5, 9726−9742.

(198) Vvedenskii, A.; Grushevskaya, S.; Ganzha, S.; Eliseev, D.; Abakumova, L. I. Copper Oxides: Kinetics of Formation and Semiconducting Properties. Part II. Copper Single Crystals. *J. Solid State Electrochem.* **2014**, 18, 3437−3451.

(199) Strehblow, H. H. Passivity of Metals Studied by Surface Analytical Methods, a Review. *Electrochim. Acta* **2016**, 212, 630−648.

(200) Wang, L.; Nitopi, S. A.; Bertheussen, E.; Orazov, M.; Morales-Guio, C. G.; Liu, X.; Higgins, D. C.; Chan, K.; Nørskov, J. K.; Hahn, C.; et al. Electrochemical Carbon Monoxide Reduction on Polycrystalline Copper: Effects of Potential, Pressure, and PH on Selectivity toward Multicarbon and Oxygenated Products. *ACS Catal.* **2018**, 8, 7445−7454.

(201) Peterson, A. A.; Abild-Pedersen, F.; Studt, F.; Rossmeisl, J.; Nørskov, J. K. How Copper Catalyzes the Electroreduction of Carbon Dioxide into Hydrocarbon Fuels. *Energy Environ. Sci.* **2010**, 3, 1311−1315.

(202) Peterson, A. A.; Nørskov, J. K. Activity Descriptors for CO2 Electroreduction to Methane on Transition-Metal Catalysts. *J. Phys. Chem. Lett.* **2012**, 3, 251−258.

(203) Kuhl, K. P.; Hatsukade, T.; Cave, E. R.; Abram, D. N.; Kibsgaard, J.; Jaramillo, T. F. Electrocatalytic Conversion of Carbon Dioxide to Methane and Methanol on Transition Metal Surfaces. *J. Am. Chem. Soc.* **2014**, 136, 14107−14113.

(204) Sabatier, P. Hydrogenations et Deshydrogenations Par Catalyse. *Ber. Dtsch. Chem. Ges.* **1911**, 44, 1984−2001.

(205) Ooka, H.; Figueiredo, M. C.; Koper, M. T. M. M. Competition between Hydrogen Evolution and Carbon Dioxide Reduction on Copper Electrodes in Mildly Acidic Media. *Langmuir* **2017**, 33, 9307−9313.

(206) Cook, R. L.; MacDuff, R. C.; Sammells, A. F. Evidence for Formaldehyde, Formic Acid, and Acetaldehyde as Possible Intermediates during Electrochemical Carbon Dioxide Reduction at Copper. *J. Electrochem. Soc.* **1989**, 136, 1982−1984.

(207) Garza, A.; Bell, A. T.; Head-Gordon, M. On the Mechanism of CO2 Reduction at Copper Surfaces: Pathways to C2 Products. *ACS Catal.* **2018**, 8, 1490−1499.

(208) Resasco, J.; Chen, L. D.; Clark, E.; Tsai, C.; Hahn, C.; Jaramillo, T. F.; Chan, K.; Bell, A. T. Promoter Effects of Alkali Metal Cations on the Electrochemical Reduction of Carbon Dioxide. *J. Am. Chem. Soc.* **2017**, 139, 11277−11287.

(209) Ledezma-Yanez, I.; Gallent, E. P.; Koper, M. T. M.; Calle-Vallejo, F. Structure-Sensitive Electroreduction of Acetaldehyde to Ethanol on Copper and Its Mechanistic Implications for CO and CO2 Reduction. *Catal. Today* **2016**, 262, 90−94.

(210) Lum, Y.; Cheng, T.; Goddard, W. A.; Ager, J. W. Electrochemical CO Reduction Builds Solvent Water into Oxygenate Products. *J. Am. Chem. Soc.* **2018**, 140, 9337−9340.

(211) Birdja, Y. Y.; Koper, M. T. M. The Importance of Cannizzaro-Type Reactions during Electrocatalytic Reduction of Carbon Dioxide. *J. Am. Chem. Soc.* **2017**, 139, 2030−2034.

(212) Liu, X.; Schlexer, P.; Xiao, J.; Ji, Y.; Wang, L.; Sandberg, R. B.; Tang, M.; Brown, K. S.; Peng, H.; Ringe, S.; et al. PH Effects on the

Electrochemical Reduction of CO(2) towards C2 Products on Stepped Copper. *Nat. Commun.* **2019**, *10*, 32.

(213) Pinsent, B. R. W.; Pearson, L.; Roughton, F. J. W. The Kinetics of Combination of Carbon Dioxide with Hydroxide Ions. *Trans. Faraday Soc.* **1956**, *52*, 1512−1520.

(214) Singh, M. R.; Kwon, Y.; Lum, Y.; Ager, J. W.; Bell, A. T. Hydrolysis of Electrolyte Cations Enhances the Electrochemical Reduction of CO2 over Ag and Cu. *J. Am. Chem. Soc.* **2016**, *138*, 13006−13012.

(215) Handoko, A. D.; Ong, C. W.; Huang, Y.; Lee, Z. G.; Lin, L.; Panetti, G. B.; Yeo, B. S. Mechanistic Insights into the Selective Electroreduction of Carbon Dioxide to Ethylene on Cu2O-Derived Copper Catalysts. *J. Phys. Chem. C* **2016**, *120*, 20058−20067.

(216) Lim, C. F. C.; Harrington, D. A.; Marshall, A. T. Effects of Mass Transfer on the Electrocatalytic CO2 Reduction on Cu. *Electrochim. Acta* **2017**, *238*, 56−63.

(217) Resasco, J.; Lum, Y.; Clark, E.; Zeledon, J. Z.; Bell, A. T. Effects of Anion Identity and Concentration on Electrochemical Reduction of CO2. *ChemElectroChem* **2018**, *5*, 1064−1072.

(218) Strmcnik, D.; Uchimura, M.; Wang, C.; Subbaraman, R.; Danilovic, N.; van der Vliet, D.; Paulikas, A. P.; Stamenkovic, V. R.; Markovic, N. M. Improving the Hydrogen Oxidation Reaction Rate by Promotion of Hydroxyl Adsorption. *Nat. Chem.* **2013**, *5*, 300−306.

(219) Strmcnik, D.; Lopes, P. P.; Genorio, B.; Stamenkovic, V. R.; Markovic, N. M. Design Principles for Hydrogen Evolution Reaction Catalyst Materials. *Nano Energy* **2016**, *29*, 29−36.

(220) Grozovski, V.; Vesztergom, S.; Láng, G. G.; Broekmann, P. Electrochemical Hydrogen Evolution: H+ or H2O Reduction? A Rotating Disk Electrode Study. *J. Electrochem. Soc.* **2017**, *164*, E3171−E3178.

(221) Hall, A. S.; Yoon, Y.; Wuttig, A.; Surendranath, Y. Mesostructure-Induced Selectivity in CO2 Reduction Catalysis. *J. Am. Chem. Soc.* **2015**, *137*, 14834−14837.

(222) Wuttig, A.; Yoon, Y.; Ryu, J.; Surendranath, Y. Bicarbonate Is Not a General Acid in Au-Catalyzed CO2 Electroreduction. *J. Am. Chem. Soc.* **2017**, *139*, 17109−17113.

(223) Yoon, Y.; Hall, A. S.; Surendranath, Y. Tuning of Silver Catalyst Mesostructure Promotes Selective Carbon Dioxide Conversion into Fuels. *Angew. Chem., Int. Ed.* **2016**, *55*, 15282−15286.

(224) Murata, A.; Hori, Y. Product Selectivity Affected by Cationic Species in Electrochemical Reduction of CO2 and CO at a Cu Electrode. *Bull. Chem. Soc. Jpn.* **1991**, *64*, 123−127.

(225) Kyriacou, G. Z.; Anagnostopoulos, A. K. Influence of CO$_2$ Partial Pressure and the Supporting Electrolyte Cation on the Product Distribution in CO$_2$ Electroreduction. *J. Appl. Electrochem.* **1993**, *23*, 483−486.

(226) Pérez-Gallent, E.; Marcandalli, G.; Figueiredo, M. C.; Calle-Vallejo, F.; Koper, M. T. M. Structure- and Potential-Dependent Cation Effects on CO Reduction at Copper Single-Crystal Electrodes. *J. Am. Chem. Soc.* **2017**, *139*, 16412−16419.

(227) Frumkin, A. N. Influence of Cation Adsorption on the Kinetics of Electrode Processes. *Trans. Faraday Soc.* **1959**, *55*, 156−167.

(228) Mills, J. N.; McCrum, I. T.; Janik, M. J. Alkali Cation Specific Adsorption onto Fcc(111) Transition Metal Electrodes. *Phys. Chem. Chem. Phys.* **2014**, *16*, 13699−13707.

(229) Strmcnik, D.; Kodama, K.; Van Der Vliet, D.; Greeley, J.; Stamenkovic, V. R.; Marković, N. M. The Role of Non-Covalent Interactions in Electrocatalytic Fuel-Cell Reactions on Platinum. *Nat. Chem.* **2009**, *1*, 466−472.

(230) Strmcnik, D.; van der Vliet, D. F.; Chang, K.-C.; Komanicky, V.; Kodama, K.; You, H.; Stamenkovic, V. R.; Marković, N. M. Effects of Li+, K+, and Ba2+ Cations on the ORR at Model and High Surface Area Pt and Au Surfaces in Alkaline Solutions. *J. Phys. Chem. Lett.* **2011**, *2*, 2733−2736.

(231) Akhade, S. A.; McCrum, I. T.; Janik, M. J. The Impact of Specifically Adsorbed Ions on the Copper-Catalyzed Electroreduction of CO2. *J. Electrochem. Soc.* **2016**, *163*, F477−F484.

(232) Chen, L. D.; Urushihara, M.; Chan, K.; Nørskov, J. K. Electric Field Effects in Electrochemical CO2 Reduction. *ACS Catal.* **2016**, *6*, 7133−7139.

(233) Montoya, J. H.; Shi, C.; Chan, K.; Nørskov, J. K. Theoretical Insights into a CO Dimerization Mechanism in CO2 Electro-reduction. *J. Phys. Chem. Lett.* **2015**, *6*, 2032−2037.

(234) Thorson, M. R.; Siil, K. I.; Kenis, P. J. A. Effect of Cations on the Electrochemical Conversion of CO2 to CO. *J. Electrochem. Soc.* **2013**, *160*, F69−F74.

(235) Schizodimou, A.; Kyriacou, G. Acceleration of the Reduction of Carbon Dioxide in the Presence of Multivalent Cations. *Electrochim. Acta* **2012**, *78*, 171−176.

(236) Rosen, B. A.; Salehi-Khojin, A.; Thorson, M. R.; Zhu, W.; Whipple, D. T.; Kenis, P. J.; Masel, R. I. Ionic Liquid-Mediated Selective Conversion of CO2 to CO at Low Overpotentials. *Science* **2011**, *334*, 643−644.

(237) Rosen, B. A.; Haan, J. L.; Mukherjee, P.; Braunschweig, B.; Zhu, W.; Salehi-Khojin, A.; Dlott, D. D.; Masel, R. I. In Situ Spectroscopic Examination of a Low Overpotential Pathway for Carbon Dioxide Conversion to Carbon Monoxide. *J. Phys. Chem. C* **2012**, *116*, 15307−15312.

(238) Asadi, M.; Kumar, B.; Behranginia, A.; Rosen, B. A.; Baskin, A.; Repnin, N.; Pisasale, D.; Phillips, P.; Zhu, W.; Haasch, R.; et al. Robust Carbon Dioxide Reduction on Molybdenum Disulphide Edges. *Nat. Commun.* **2014**, *5*, 4470.

(239) Feaster, J. T.; Jongerius, A. L.; Liu, X.; Urushihara, M.; Nitopi, S. A.; Hahn, C.; Chan, K.; Nørskov, J. K.; Jaramillo, T. F. Understanding the Influence of [EMIM]Cl on the Suppression of the Hydrogen Evolution Reaction on Transition Metal Electrodes. *Langmuir* **2017**, *33*, 9464−9471.

(240) Neubauer, S. S.; Schmid, B.; Reller, C.; Guldi, D. M.; Schmid, G. Alkalinity Initiated Decomposition of Mediating Imidazolium Ions in High Current Density CO2 Electrolysis. *ChemElectroChem* **2017**, *4*, 160−167.

(241) Varela, A. S.; Kroschel, M.; Reier, T.; Strasser, P. Controlling the Selectivity of CO2 Electroreduction on Copper: The Effect of the Electrolyte Concentration and the Importance of the Local PH. *Catal. Today* **2016**, *260*, 8−13.

(242) Ogura, K.; Oohara, R.; Kudo, Y. Reduction of CO2 to Ethylene at Three-Phase Interface Effects of Electrode Substrate and Catalytic Coating. *J. Electrochem. Soc.* **2005**, *152*, D213−D219.

(243) Yano, H.; Tanaka, T.; Nakayama, M.; Ogura, K. Selective Electrochemical Reduction of CO2 to Ethylene at a Three-Phase Interface on Copper(I) Halide-Confined Cu-Mesh Electrodes in Acidic Solutions of Potassium Halides. *J. Electroanal. Chem.* **2004**, *565*, 287−293.

(244) Ogura, K.; Ferrell, J. R.; Cugini, A. V.; Smotkin, E. S.; Salazar-Villalpando, M. D. CO2 Attraction by Specifically Adsorbed Anions and Subsequent Accelerated Electrochemical Reduction. *Electrochim. Acta* **2010**, *56*, 381−386.

(245) Ogura, K.; Salazar-Villalpando, M. D. CO2 Electrochemical Reduction via Adsorbed Halide Anions. *JOM* **2011**, *63*, 35−38.

(246) McCrum, I. T.; Akhade, S. A.; Janik, M. J. Electrochemical Specific Adsorption of Halides on Cu 111,100, and 211: A Density Functional Theory Study. *Electrochim. Acta* **2015**, *173*, 302−309.

(247) Varela, A. S.; Ju, W.; Reier, T.; Strasser, P. Tuning the Catalytic Activity and Selectivity of Cu for CO2 Electroreduction in the Presence of Halides. *ACS Catal.* **2016**, *6*, 2136−2144.

(248) Gao, D.; Scholten, F.; Roldan Cuenya, B. Improved CO2 Electroreduction Performance on Plasma-Activated Cu Catalysts via Electrolyte Design: Halide Effect. *ACS Catal.* **2017**, *7*, 5112−5120.

(249) Lee, S.; Kim, D.; Lee, J. Electrocatalytic Production of C3-C4 Compounds by Conversion of CO2 on a Chloride-Induced Bi-Phasic Cu2O-Cu Catalyst. *Angew. Chem., Int. Ed.* **2015**, *54*, 14701−14705.

(250) Lobaccaro, P.; Singh, M. R.; Clark, E. L.; Kwon, Y.; Bell, A. T.; Ager, J. W. Effects of Temperature and Gas−liquid Mass Transfer on the Operation of Small Electrochemical Cells for the Quantitative Evaluation of CO2 Reduction Electrocatalysts. *Phys. Chem. Chem. Phys.* **2016**, *18*, 26777−26785.

(251) Kaneco, S.; Hiei, N.; Xing, Y.; Katsumata, H.; Ohnishi, H.; Suzuki, T.; Ohta, K. Electrochemical Conversion of Carbon Dioxide to Methane in Aqueous NaHCO3 Solution at Less than 273 K. *Electrochim. Acta* **2002**, *48*, 51−55.

(252) Kaneco, S.; Hiei, N.; Xing, Y.; Katsumata, H.; Ohnishi, H.; Suzuki, T.; Ohta, K. High-Efficiency Electrochemical CO2-to-Methane Reduction Method Using Aqueous KHCO3Media at Less than 273 K. *J. Solid State Electrochem.* **2003**, *7*, 152−156.

(253) Azuma, M.; Hashimoto, K.; Watanabe, M. Electrochemical Reduction of Carbon Dioxide on Various Metal Electrodes in Low-Temperature Aqueous KHC03 Media. *J. Electrochem. Soc.* **1990**, *137*, 1772−1778.

(254) Ahn, S. T.; Abu-Baker, I.; Palmore, G. T. R. Electroreduction of CO2 on Polycrystalline Copper: Effect of Temperature on Product Selectivity. *Catal. Today* **2017**, *288*, 24−29.

(255) Hatsukade, T. *Investigating the Effects of Chemical Composition and Surface Structure of Catalysts on the Electrochemical Reduction of Carbon Dioxide*; Stanford University, 2016.

(256) Nørskov, J. K.; Rossmeisl, J.; Logadottir, A.; Lindqvist, L.; Kitchin, J. R.; Bligaard, T.; Jónsson, H. Origin of the Overpotential for Oxygen Reduction at a Fuel-Cell Cathode. *J. Phys. Chem. B* **2004**, *108*, 17886−17892.

(257) Karlberg, G. S.; Rossmeisl, J.; Nørskov, J. K. Estimations of Electric Field Effects on the Oxygen Reduction Reaction Based on the Density Functional Theory. *Phys. Chem. Chem. Phys.* **2007**, *9*, 5158−5161.

(258) Karlberg, G. S.; Jaramillo, T. F.; Skúlason, E.; Rossmeisl, J.; Bligaard, T.; Nørskov, J. K. Cyclic Voltammograms for H on Pt(111) and Pt(100) from First Principles. *Phys. Rev. Lett.* **2007**, *99*, 126101.

(259) Cheng, T.; Xiao, H.; Goddard, W. A. Full Atomistic Reaction Mechanism with Kinetics for CO Reduction on Cu(100) from Ab Initio Molecular Dynamics Free-Energy Calculations at 298 K. *Proc. Natl. Acad. Sci. U. S. A.* **2017**, *114*, 1795−1800.

(260) Goodpaster, J. D.; Bell, A. T.; Head-Gordon, M. Identification of Possible Pathways for C-C Bond Formation during Electrochemical Reduction of CO2: New Theoretical Insights from an Improved Electrochemical Model. *J. Phys. Chem. Lett.* **2016**, *7*, 1471−1477.

(261) Xiao, H.; Cheng, T.; Goddard, W. A.; Sundararaman, R. Mechanistic Explanation of the PH Dependence and Onset Potentials for Hydrocarbon Products from Electrochemical Reduction of CO on Cu (111). *J. Am. Chem. Soc.* **2016**, *138*, 483−486.

(262) Nie, X.; Luo, W.; Janik, M. J.; Asthagiri, A. Reaction Mechanisms of CO2 Electrochemical Reduction on Cu(111) Determined with Density Functional Theory. *J. Catal.* **2014**, *312*, 108−122.

(263) Nie, X.; Esopi, M. R.; Janik, M. J.; Asthagiri, A. Selectivity of CO2 Reduction on Copper Electrodes: The Role of the Kinetics of Elementary Steps. *Angew. Chem., Int. Ed.* **2013**, *52*, 2459−2462.

(264) Mathew, K.; Sundararaman, R.; Letchworth-Weaver, K.; Arias, T. A.; Hennig, R. G. Implicit Solvation Model for Density-Functional Study of Nanocrystal Surfaces and Reaction Pathways. *J. Chem. Phys.* **2014**, *140*, 084106.

(265) Schmickler, W.; Santos, E. *Interfacial Electrochemistry*; Springer Berlin Heidelberg, 2010.

(266) Mathew, K.; Hennig, R. *Implicit Self-Consistent Description of Electrolyte in Plane-Wave Density-Functional Theory*. 2016.

(267) Grün, F.; Jardat, M.; Turq, P.; Amatore, C. Relaxation of the Electrical Double Layer after an Electron Transfer Approached by Brownian Dynamics Simulation. *J. Chem. Phys.* **2004**, *120*, 9648−9655.

(268) Kling, M. F.; Vrakking, M. J. J. Attosecond Electron Dynamics. *Annu. Rev. Phys. Chem.* **2008**, *59*, 463−492.

(269) Chan, K.; Nørskov, J. K. Electrochemical Barriers Made Simple. *J. Phys. Chem. Lett.* **2015**, *6*, 2663−2668.

(270) Chan, K.; Nørskov, J. K. Potential Dependence of Electrochemical Barriers from Ab Initio Calculations. *J. Phys. Chem. Lett.* **2016**, *7*, 1686−1690.

(271) Björketun, M. E.; Zeng, Z.; Ahmed, R.; Tripkovic, V.; Thygesen, K. S.; Rossmeisl, J. Avoiding Pitfalls in the Modeling of Electrochemical Interfaces. *Chem. Phys. Lett.* **2013**, *555*, 145−148.

(272) Chen, L. D.; Bajdich, M.; Martirez, J. M. P.; Krauter, C. M.; Gauthier, J. A.; Carter, E. A.; Luntz, A. C.; Chan, K.; Nørskov, J. K. Understanding the Apparent Fractional Charge of Protons in the Aqueous Electrochemical Double Layer. *Nat. Commun.* **2018**, *9*, 1−8.

(273) Shi, C.; Chan, K.; Yoo, J. S.; Nørskov, J. K. Barriers of Electrochemical CO2 Reduction on Transition Metals. *Org. Process Res. Dev.* **2016**, *20*, 1424−1430.

(274) Cheng, T.; Xiao, H.; Goddard, W. A. Free-Energy Barriers and Reaction Mechanisms for the Electrochemical Reduction of CO on the Cu(100) Surface, Including Multiple Layers of Explicit Solvent at PH 0. *J. Phys. Chem. Lett.* **2015**, *6*, 4767−4773.

(275) Luo, W.; Nie, X.; Janik, M. J.; Asthagiri, A. Facet Dependence of CO2 Reduction Paths on Cu Electrodes. *ACS Catal.* **2016**, *6*, 219−229.

(276) Shi, C.; Hansen, H. A.; Lausche, A. C.; Nørskov, J. K. Trends in Electrochemical CO2 Reduction Activity for Open and Close-Packed Metal Surfaces. *Phys. Chem. Chem. Phys.* **2014**, *16*, 4720−4727.

(277) Nørskov, J. K.; Studt, F.; Abild-Pedersen, F.; Bligaard, T. *Fundamental Concepts in Heterogeneous Catalysis*; John Wiley & Sons, Inc: Hoboken, NJ, USA, 2014.

(278) Cheng, T.; Xiao, H.; Goddard, W. A. Reaction Mechanisms for the Electrochemical Reduction of CO2 to CO and Formate on the Cu(100) Surface at 298 K from Quantum Mechanics Free Energy Calculations with Explicit Water. *J. Am. Chem. Soc.* **2016**, *138*, 13802−13805.

(279) Nie, X.; Griffin, G. L.; Janik, M. J.; Asthagiri, A. Surface Phases of Cu2O(111) under CO2 Electrochemical Reduction Conditions. *Catal. Commun.* **2014**, *52*, 88−91.

(280) Montoya, J. H.; Peterson, A. A.; Nørskov, J. K. Insights into C-C Coupling in CO2 Electroreduction on Copper Electrodes. *ChemCatChem* **2013**, *5*, 737−742.

(281) Sandberg, R. B.; Montoya, J. H.; Chan, K.; Nørskov, J. K. CO-CO Coupling on Cu Facets: Coverage, Strain and Field Effects. *Surf. Sci.* **2016**, *654*, 56−62.

(282) Jiang, K.; Sandberg, R. B.; Akey, A. J.; Liu, X.; Bell, D. C.; Nørskov, J. K.; Chan, K.; Wang, H. Metal Ion Cycling of Cu Foil for Selective C−C Coupling in Electrochemical CO2 Reduction. *Nat. Catal.* **2018**, *1*, 111−119.

(283) Calle-Vallejo, F.; Koper, M. T. M. Theoretical Considerations on the Electroreduction of CO to C2 Species on Cu(100) Electrodes. *Angew. Chem., Int. Ed.* **2013**, *52*, 7282−7285.

(284) Lausche, A. C.; Medford, A. J.; Khan, T. S.; Xu, Y.; Bligaard, T.; Abild-Pedersen, F.; Nørskov, J. K.; Studt, F. On the Effect of Coverage-Dependent Adsorbate−adsorbate Interactions for CO Methanation on Transition Metal Surfaces. *J. Catal.* **2013**, *307*, 275−282.

(285) Roberts, F. S.; Kuhl, K. P.; Nilsson, A. Electroreduction of Carbon Monoxide over a Copper Nanocube Catalyst: Surface Structure and PH Dependence on Selectivity. *ChemCatChem* **2016**, *8*, 1119−1124.

(286) Singh, M. R.; Goodpaster, J. D.; Weber, A. Z.; Head-gordon, M.; Bell, A. T. Mechanistic Insights into Electrochemical Reduction of CO2 over Ag Using Density Functional Theory and Transport Models. *Proc. Natl. Acad. Sci. U. S. A.* **2017**, *114*, E8812−E8821.

(287) Feaster, J. T.; Shi, C.; Cave, E. R.; Hatsukade, T.; Abram, D. N.; Kuhl, K. P.; Hahn, C.; Nørskov, J. K.; Jaramillo, T. F. Understanding Selectivity for the Electrochemical Reduction of Carbon Dioxide to Formic Acid and Carbon Monoxide on Metal Electrodes. *ACS Catal.* **2017**, *7*, 4822−4827.

(288) Schmid, B.; Reller, C.; Neubauer, S. S.; Fleischer, M.; Dorta, R.; Schmid, G. Reactivity of Copper Electrodes towards Functional Groups and Small Molecules in the Context of CO2 Electro-Reductions. *Catalysts* **2017**, *7*, 161.

(289) Ren, D.; Fong, J.; Yeo, B. S. The Effects of Currents and Potentials on the Selectivities of Copper toward Carbon Dioxide Electroreduction. *Nat. Commun.* **2018**, *9*, 925.

(290) Scott, S. B. *Investigating the Electrochemical Reduction of Carbon Dioxide Using In Situ Mass Spectrometry*; Technical University of Denmark, 2016.

(291) Akhade, S. A.; Luo, W.; Nie, X.; Asthagiri, A.; Janik, M. J. Theoretical Insight on Reactivity Trends in CO2 Electroreduction across Transition Metals. *Catal. Sci. Technol.* **2016**, *6*, 1042–1053.

(292) Ma, S.; Sadakiyo, M.; Luo, R.; Heima, M.; Yamauchi, M.; Kenis, P. J. A. One-Step Electrosynthesis of Ethylene and Ethanol from CO2 in an Alkaline Electrolyzer. *J. Power Sources* **2016**, *301*, 219–228.

(293) Handoko, A. D.; Chan, K. W.; Yeo, B. S. −CH3Mediated Pathway for the Electroreduction of CO2 to Ethane and Ethanol on Thick Oxide-Derived Copper Catalysts at Low Overpotentials. *ACS Energy Lett.* **2017**, *2*, 2103–2109.

(294) Smith, B. D.; Irish, D. E.; Kedzierzawski, P.; Augustynski, J. A Surface Enhanced Roman Scattering Study of the Intermediate and Poisoning Species Formed during the Electrochemical Reduction of CO2 on Copper. *J. Electrochem. Soc.* **1997**, *144*, 4288–4296.

(295) Mistry, H.; Varela, A. S.; Kühl, S.; Strasser, P.; Cuenya, B. R. Nanostructured Electrocatalysts with Tunable Activity and Selectivity. *Nat. Rev. Mater.* **2016**, *1*, 16009.

(296) Lu, Q.; Rosen, J.; Jiao, F. Nanostructured Metallic Electrocatalysts for Carbon Dioxide Reduction. *ChemCatChem* **2015**, *7*, 38–47.

(297) Vesborg, P. C. K.; Jaramillo, T. F. Addressing the Terawatt Challenge: Scalability in the Supply of Chemical Elements for Renewable Energy. *RSC Adv.* **2012**, *2*, 7933–7947.

(298) Reske, R.; Mistry, H.; Behafarid, F.; Roldan Cuenya, B.; Strasser, P. Particle Size Effects in the Catalytic Electroreduction of CO2 on Cu Nanoparticles. *J. Am. Chem. Soc.* **2014**, *136*, 6978–6986.

(299) Manthiram, K.; Beberwyck, B. J.; Alivisatos, A. P. Enhanced Electrochemical Methanation of Carbon Dioxide with a Dispersible Nanoscale Copper Catalyst. *J. Am. Chem. Soc.* **2014**, *136*, 13319–13325.

(300) Loiudice, A.; Lobaccaro, P.; Kamali, E. A.; Thao, T.; Huang, B. H.; Ager, J. W.; Buonsanti, R. Tailoring Copper Nanocrystals towards C2 Products in Electrochemical CO2 Reduction. *Angew. Chem., Int. Ed.* **2016**, *55*, 5789–5792.

(301) Mistry, H.; Behafarid, F.; Reske, R.; Varela, A. S.; Strasser, P.; Roldan Cuenya, B. Tuning Catalytic Selectivity at the Mesoscale via Interparticle Interactions. *ACS Catal.* **2016**, *6*, 1075–1080.

(302) Kim, D.; Kley, C. S.; Li, Y.; Yang, P. Copper Nanoparticle Ensembles for Selective Electroreduction of CO2 to C2−C3 Products. *Proc. Natl. Acad. Sci. U. S. A.* **2017**, *114*, 10560–10565.

(303) Li, Y.; Cui, F.; Ross, M. B.; Kim, D.; Sun, Y.; Yang, P. Structure-Sensitive CO2 Electroreduction to Hydrocarbons on Ultrathin Five-Fold Twinned Copper Nanowires. *Nano Lett.* **2017**, *17*, 1312–1317.

(304) Wang, Z.; Yang, G.; Zhang, Z.; Jin, M.; Yin, Y. Selectivity on Etching: Creation of High-Energy Facets on Copper Nanocrystals for CO2 Electrochemical Reduction. *ACS Nano* **2016**, *10*, 4559–4564.

(305) Baturina, O. A.; Lu, Q.; Padilla, M. A.; Xin, L.; Li, W.; Serov, A.; Artyushkova, K.; Atanassov, P.; Xu, F.; Epshteyn, A.; et al. CO2 Electroreduction to Hydrocarbons on Carbon-Supported Cu Nano-particles. *ACS Catal.* **2014**, *4*, 3682–3695.

(306) Gupta, K.; Bersani, M.; Darr, J. A. Highly Efficient Electro-Reduction of CO2 to Formic Acid by Nano-Copper. *J. Mater. Chem. A* **2016**, *4*, 13786–13794.

(307) Stephens, I. E. L.; Bondarenko, A. S.; Grønbjerg, U.; Rossmeisl, J.; Chorkendorff, I. Understanding the Electrocatalysis of Oxygen Reduction on Platinum and Its Alloys. *Energy Environ. Sci.* **2012**, *5*, 6744–6762.

(308) Hammer, B.; Morikawa, Y.; Nørskov, J. K. CO Chemisorption at Metal Surfaces and Overlayers. *Phys. Rev. Lett.* **1996**, *76*, 2141–2144.

(309) Grosse, P.; Gao, D.; Scholten, F.; Sinev, I.; Mistry, H.; Roldan Cuenya, B. Dynamic Changes in the Structure, Chemical State and Catalytic Selectivity of Cu Nanocubes during CO2 Electroreduction: Size and Support Effects. *Angew. Chem., Int. Ed.* **2018**, *57*, 6192–6197.

(310) Waugh, K. C. Methanol Synthesis. *Catal. Today* **1992**, *15*, 51–75.

(311) Song, Y.; Peng, R.; Hensley, D. K.; Bonnesen, P. V.; Liang, L.; Wu, Z.; Meyer, H. M.; Chi, M.; Ma, C.; Sumpter, B. G.; et al. High-Selectivity Electrochemical Conversion of CO2 to Ethanol Using a Copper Nanoparticle/N-Doped Graphene Electrode. *ChemistrySelect* **2016**, *1*, 6054.

(312) Yuan, J.; Zhang, J.-J.; Yang, M.-P.; Meng, W.-J.; Wang, H.; Lu, J.-X. CuO Nanoparticles Supported on TiO2 with High Efficiency for CO2 Electrochemical Reduction to Ethanol. *Catalysts* **2018**, *8*, 171.

(313) Huo, Y.; Peng, X.; Liu, X.; Li, H.; Luo, J. High Selectivity Toward C2H4 Production over Cu Particles Supported by Butterfly-Wing-Derived Carbon Frameworks. *ACS Appl. Mater. Interfaces* **2018**, *10*, 12618–12625.

(314) Yang, H.-J.; Yang, H.; Hong, Y.-H.; Zhang, P.-Y.; Wang, T.; Chen, L.-N.; Zhang, F.-Y.; Wu, Q.-H.; Tian, N.; Zhou, Z.-Y.; et al. Promoting Ethylene Selectivity from CO2 Electroreduction on CuO Supported onto CO2 Capture Materials. *ChemSusChem* **2018**, *11*, 881–887.

(315) Feng, X.; Jiang, K.; Fan, S.; Kanan, M. W. A Direct Grain-Boundary-Activity Correlation for CO Electroreduction on Cu Nanoparticles. *ACS Cent. Sci.* **2016**, *2*, 169–174.

(316) Gao, D.; Zhang, Y.; Zhou, Z.; Cai, F.; Zhao, X.; Huang, W.; Li, Y.; Zhu, J.; Liu, P.; Yang, F.; et al. Enhancing CO2 Electroreduction with the Metal-Oxide Interface. *J. Am. Chem. Soc.* **2017**, *139*, 5652–5655.

(317) Rogers, C.; Perkins, W. S.; Veber, G.; Williams, T. E.; Cloke, R. R.; Fischer, F. R. Synergistic Enhancement of Electrocatalytic CO2 Reduction with Gold Nanoparticles Embedded in Functional Graphene Nanoribbon Composite Electrodes. *J. Am. Chem. Soc.* **2017**, *139*, 4052–4061.

(318) Velázquez, A.; Centellas, F.; Garrido, J. A.; Arias, C.; Rodríguez, R. M.; Brillas, E.; Cabot, P. L. Structure of Carbon-Supported Pt-Ru Nanoparticles and Their Electrocatalytic Behavior for Hydrogen Oxidation Reaction. *J. Power Sources* **2010**, *195*, 710–719.

(319) Frese, K. W. Electrochemical Reduction of CO2 at Intentionally Oxidized Copper Electrodes. *J. Electrochem. Soc.* **1991**, *138*, 3338–3340.

(320) Ma, M.; Djanashvili, K.; Smith, W. A. Controllable Hydrocarbon Formation from the Electrochemical Reduction of CO2 over Cu Nanowire Arrays. *Angew. Chem., Int. Ed.* **2016**, *55*, 6680–6684.

(321) Rahaman, M.; Dutta, A.; Zanetti, A.; Broekmann, P. Electrochemical Reduction of CO2 into Multicarbon Alcohols on Activated Cu Mesh Catalysts: An Identical Location (IL) Study. *ACS Catal.* **2017**, *7*, 7946–7956.

(322) Raciti, D.; Cao, L.; Livi, K. J. T.; Rottmann, P. F.; Tang, X.; Li, C.; Hicks, Z.; Bowen, K. H.; Hemker, K. J.; Mueller, T.; et al. Low-Overpotential Electroreduction of Carbon Monoxide Using Copper Nanowires. *ACS Catal.* **2017**, *7*, 4467–4472.

(323) Haynes, W. M. *Handbook of Chemistry and Physics*, 96th ed., Haynes, W. M.; Bruno, T. J.; Lide, D. R., Eds.; CRC Press: Boca Raton, FL, 2015.

(324) Verdaguer-Casadevall, A.; Li, C. W.; Johansson, T. P.; Scott, S. B.; McKeown, J. T.; Kumar, M.; Stephens, I. E. L.; Kanan, M. W.; Chorkendorff, I. Probing the Active Surface Sites for CO Reduction on Oxide-Derived Copper Electrocatalysts. *J. Am. Chem. Soc.* **2015**, *137*, 9808–9811.

(325) Wang, Y.; Raciti, D.; Wang, C. High-Flux CO Reduction Enabled by Three-Dimensional Nanostructured Copper Electrodes. *ACS Catal.* **2018**, *8*, 5657–5663.

(326) Tang, W.; Peterson, A. A.; Varela, A. S.; Jovanov, Z. P.; Bech, L.; Durand, W. J.; Dahl, S.; Nørskov, J. K.; Chorkendorff, I. The Importance of Surface Morphology in Controlling the Selectivity of

Polycrystalline Copper for CO2 Electroreduction. *Phys. Chem. Chem. Phys.* **2012**, *14*, 76−81.

(327) Ren, D.; Wong, N. T.; Handoko, A. D.; Huang, Y.; Yeo, B. S. Mechanistic Insights into the Enhanced Activity and Stability of Agglomerated Cu Nanocrystals for the Electrochemical Reduction of Carbon Dioxide to N-Propanol. *J. Phys. Chem. Lett.* **2016**, *7*, 20−24.

(328) Gao, D.; Zegkinoglou, I.; Divins, N. J.; Scholten, F.; Sinev, I.; Grosse, P.; Roldan Cuenya, B. Plasma-Activated Copper Nanocube Catalysts for Efficient Carbon Dioxide Electroreduction to Hydrocarbons and Alcohols. *ACS Nano* **2017**, *11*, 4825−4831.

(329) Kim, D.; Lee, S.; Ocon, J. D.; Jeong, B.; Lee, J. K.; Lee, J. Insights into Autonomously Formed Oxygen-Evacuated Cu2O Electrode for the Selective Production of C2H4 from CO2. *Phys. Chem. Chem. Phys.* **2015**, *17*, 824−830.

(330) Reller, C.; Krause, R.; Volkova, E.; Schmid, B.; Neubauer, S.; Rucki, A.; Schuster, M.; Schmid, G. Selective Electroreduction of CO2 toward Ethylene on Nano Dendritic Copper Catalysts at High Current Density. *Adv. Energy Mater.* **2017**, *7*, 1602114.

(331) Yang, K. D.; Ko, W. R.; Lee, J. H.; Kim, S. J.; Lee, H.; Lee, M. H.; Nam, K. T. Morphology-Directed Selective Production of Ethylene or Ethane from CO2 on a Cu Mesopore Electrode. *Angew. Chem., Int. Ed.* **2017**, *56*, 796−800.

(332) Dutta, A.; Rahaman, M.; Luedi, N. C.; Mohos, M.; Broekmann, P. Morphology Matters: Tuning the Product Distribution of CO2 Electroreduction on Oxide-Derived Cu Foam Catalysts. *ACS Catal.* **2016**, *6*, 3804−3814.

(333) Dutta, A.; Rahaman, M.; Mohos, M.; Zanetti, A.; Broekmann, P. Electrochemical CO2 Conversion Using Skeleton (Sponge) Type of Cu Catalysts. *ACS Catal.* **2017**, *7*, 5431−5437.

(334) Gonçalves, M. R.; Gomes, A.; Condeço, J.; Fernandes, T. R. C.; Pardal, T.; Sequeira, C. A. C.; Branco, J. B. Electrochemical Conversion of CO2 to C2 Hydrocarbons Using Different Ex Situ Copper Electrodeposits. *Electrochim. Acta* **2013**, *102*, 388−392.

(335) Peng, Y.; Wu, T.; Sun, L.; Nsanzimana, J. M. V.; Fisher, A. C.; Wang, X. Selective Electrochemical Reduction of CO2 to Ethylene on Nanopores Modified Copper Electrodes in Aqueous Solution. *ACS Appl. Mater. Interfaces* **2017**, *9*, 32782−32789.

(336) Song, H.; Im, M.; Song, J. T.; Lim, J. A.; Kim, B. S.; Kwon, Y.; Ryu, S.; Oh, J. Effect of Mass Transfer and Kinetics in Ordered Cu-Mesostructures for Electrochemical CO2 Reduction. *Appl. Catal., B* **2018**, *232*, 391−396.

(337) Favaro, M.; Xiao, H.; Cheng, T.; Goddard, W. A.; Yano, J.; Crumlin, E. J. Subsurface Oxide Plays a Critical Role in CO2 Activation by Cu(111) Surfaces to Form Chemisorbed CO2, the First Step in Reduction of CO2. *Proc. Natl. Acad. Sci. U. S. A.* **2017**, *114*, 6706−6711.

(338) Liu, C.; Lourenço, M. P.; Hedström, S.; Cavalca, F.; Diaz-Morales, O.; Duarte, H. A.; Nilsson, A.; Pettersson, L. G. M. Stability and Effects of Subsurface Oxygen in Oxide-Derived Cu Catalyst for CO2 Reduction. *J. Phys. Chem. C* **2017**, *121*, 25010−25017.

(339) Garza, A.; Bell, A. T.; Head-Gordon, M. Is Subsurface Oxygen Necessary for the Electrochemical Reduction of CO 2 on Copper? *J. Phys. Chem. Lett.* **2018**, *9*, 601−606.

(340) Fields, M.; Hong, X.; Nørskov, J. K.; Chan, K. Role of Subsurface Oxygen on Cu Surfaces for CO2 Electrochemical Reduction. *J. Phys. Chem. C* **2018**, *122*, 16209−16215.

(341) Terunuma, Y.; Saitoh, A.; Momose, Y. Relationship between Hydrocarbon Production in the Electrochemical Reduction of CO2 and the Characteristics of the Cu Electrode. *J. Electroanal. Chem.* **1997**, *434*, 69−75.

(342) Le, M.; Ren, M.; Zhang, Z.; Sprunger, P. T.; Kurtz, R. L.; Flake, J. C. Electrochemical Reduction of CO2 to CH3OH at Copper Oxide Surfaces. *J. Electrochem. Soc.* **2011**, *158*, E45−E49.

(343) Cavalca, F.; Ferragut, R.; Aghion, S.; Eilert, A.; Diaz-Morales, O.; Liu, C.; Koh, A. L.; Hansen, T. W.; Pettersson, L. G. M.; Nilsson, A. Nature and Distribution of Stable Subsurface Oxygen in Copper Electrodes During Electrochemical CO2 Reduction. *J. Phys. Chem. C* **2017**, *121*, 25003−25009.

(344) Lee, S. Y.; Jung, H.; Kim, N.-K.; Oh, H.-S.; Min, B. K.; Hwang, Y. J. Mixed Copper States in Anodized Cu Electrocatalyst for Stable and Selective Ethylene Production from CO2 Reduction. *J. Am. Chem. Soc.* **2018**, *140*, 8681−8689.

(345) Platzman, I.; Brener, R.; Haick, H.; Tannenbaum, R. Oxidation of Polycrystalline Copper Thin Films at Ambient Conditions. *J. Phys. Chem. C* **2008**, *112*, 1101−1108.

(346) Lum, Y.; Ager, J. W. Stability of Residual Oxides in Oxide-Derived Copper Catalysts for Electrochemical CO2 Reduction Investigated with 18O Labeling. *Angew. Chem., Int. Ed.* **2018**, *57*, 551−554.

(347) Zhuang, T.-T.; Liang, Z.-Q.; Seifitokaldani, A.; Li, Y.; De Luna, P.; Burdyny, T.; Che, F.; Meng, F.; Min, Y.; Quintero-Bermudez, R.; et al. Steering Post-C-C Coupling Selectivity Enables High Efficiency Electroreduction of Carbon Dioxide to Multi-Carbon Alcohols. *Nat. Catal.* **2018**, *1*, 421−428.

(348) Zhou, Y.; Che, F.; Liu, M.; Zou, C.; Liang, Z.; De Luna, P.; Yuan, H.; Li, J.; Wang, Z.; Xie, H.; et al. Dopant-Induced Electron Localization Drives CO2 Reduction to C2 Hydrocarbons. *Nat. Chem.* **2018**, *10*, 974−980.

(349) Eilert, A.; Cavalca, F.; Roberts, F. S.; Osterwalder, J.; Liu, C.; Favaro, M.; Crumlin, E. J.; Ogasawara, H.; Friebel, D.; Pettersson, L. G. M.; et al. Subsurface Oxygen in Oxide-Derived Copper Electrocatalysts for Carbon Dioxide Reduction. *J. Phys. Chem. Lett.* **2017**, *8*, 285−290.

(350) Kas, R.; Hummadi, K. K.; Kortlever, R.; de Wit, P.; Milbrat, A.; Luiten-Olieman, M. W. J.; Benes, N. E.; Koper, M. T. M.; Mul, G. Three-Dimensional Porous Hollow Fibre Copper Electrodes for Efficient and High-Rate Electrochemical Carbon Dioxide Reduction. *Nat. Commun.* **2016**, *7*, 10748.

(351) Dinh, C.; Burdyny, T.; Kibria, M. G.; Seifitokaldani, A.; Gabardo, C. M.; García de Arquer, F. P.; Kiani, A.; Edwards, J. P.; De Luna, P.; Bushuyev, O. S.; et al. CO2 Electroreduction to Ethylene via Hydroxide-Mediated Copper Catalysis at an Abrupt Interface. *Science* **2018**, *360*, 783−787.

(352) Lv, J.; Jouny, M.; Luc, W.; Zhu, W.; Zhu, J.; Jiao, F. A Highly Porous Copper Electrocatalyst for Carbon Dioxide Reduction. *Adv. Mater.* **2018**, *30*, 1803111.

(353) Han, L.; Zhou, W.; Xiang, C. High-Rate Electrochemical Reduction of Carbon Monoxide to Ethylene Using Cu-Nanoparticle-Based Gas Diffusion Electrodes. *ACS Energy Lett.* **2018**, *3*, 855−860.

(354) Higgins, D.; Hahn, C.; Xiang, C.; Jaramillo, T. F.; Weber, A. Z. Gas-Diffusion Electrodes for Carbon Dioxide Reduction: A New Paradigm. *ACS Energy Lett.* **2019**, *4*, 317−324.

(355) Weekes, D. M.; Salvatore, D. A.; Reyes, A.; Huang, A.; Berlinguette, C. P. Electrolytic CO2 Reduction in a Flow Cell. *Acc. Chem. Res.* **2018**, *51*, 910−918.

(356) Ponec, V. Alloy Catalysts: The Concepts. *Appl. Catal., A* **2001**, *222*, 31−45.

(357) Rodriguez, J. A. Physical and Chemical Properties of Bimetallic Surfaces. *Surf. Sci. Rep.* **1996**, *24*, 223−287.

(358) Sinfelt, J. H.; Carter, J. L.; Yates, D. J. C. Catalytic Hydrogenolysis and Dehydrogenation over Copper-Nickel Alloys. *J. Catal.* **1972**, *24*, 283−296.

(359) Kitchin, J. R.; Nørskov, J. K.; Barteau, M. A.; Chen, J. G. Role of Strain and Ligand Effects in the Modification of the Electronic and Chemical Properties of Bimetallic Surfaces. *Phys. Rev. Lett.* **2004**, *93*, 4−7.

(360) Mavrikakis, M.; Hammer, B.; Nørskov, J. K. Effect of Strain on the Reactivity of Metal Surfaces. *Phys. Rev. Lett.* **1998**, *81*, 2819−2822.

(361) Gsell, M. Effect of Substrate Strain on Adsorption. *Science* **1998**, *280*, 717−720.

(362) Sachtler, W. M. H.; van der Plank, P. The Role of Individual Surface Atoms in Chemisorption and Catalysis by Nickel-Copper Alloys. *Surf. Sci.* **1969**, *18*, 62−79.

(363) Sachtler, J. W. A.; Somorjai, G. A. Influence of Ensemble Size on CO Chemisorption and Catalytic N-Hexane Conversion by Au-Pt(111) Bimetallic Single-Crystal Surfaces. *J. Catal.* **1983**, *81*, 77−94.

(364) Kitchin, J. R.; Nørskov, J. K.; Barteau, M. A.; Chen, J. G. Modification of the Surface Electronic and Chemical Properties of Pt(111) by Subsurface 3d Transition Metals. *J. Chem. Phys.* **2004**, *120*, 10240−10246.

(365) Hansen, H. A.; Shi, C.; Lausche, A. C.; Peterson, A. A.; Nørskov, J. K. Bifunctional Alloys for the Electroreduction of CO2 and CO. *Phys. Chem. Chem. Phys.* **2016**, *18*, 9194−9201.

(366) Karamad, M.; Tripkovic, V.; Rossmeisl, J. Intermetallic Alloys as CO Electroreduction Catalysts − the Role of Isolated Active Sites. *ACS Catal.* **2014**, *4*, 2268−2273.

(367) Cheng, M. J.; Clark, E. L.; Pham, H. H.; Bell, A. T.; Head-Gordon, M. Quantum Mechanical Screening of Single-Atom Bimetallic Alloys for the Selective Reduction of CO2 to C1 Hydrocarbons. *ACS Catal.* **2016**, *6*, 7769−7777.

(368) Hirunsit, P. Electroreduction of Carbon Dioxide to Methane on Copper, Copper-Silver, and Copper-Gold Catalysts: A DFT Study. *J. Phys. Chem. C* **2013**, *117*, 8262−8268.

(369) Hirunsit, P.; Soodsawang, W.; Limtrakul, J. CO2 Electrochemical Reduction to Methane and Methanol on Copper-Based Alloys: Theoretical Insight. *J. Phys. Chem. C* **2015**, *119*, 8238−8249.

(370) Calle-Vallejo, F.; Koper, M. T. M. Accounting for Bifurcating Pathways in the Screening for CO2 Reduction Catalysts. *ACS Catal.* **2017**, *7*, 7346−7351.

(371) Hahn, C.; Abram, D. N.; Hansen, H. A.; Hatsukade, T.; Jackson, A.; Johnson, N. C.; Hellstern, T. R.; Kuhl, K. P.; Cave, E. R.; Feaster, J. T.; et al. Synthesis of Thin Film AuPd Alloys and Their Investigation for Electrocatalytic CO2 Reduction. *J. Mater. Chem. A* **2015**, *3*, 20185−20194.

(372) Kortlever, R.; Peters, I.; Balemans, C.; Kas, R.; Kwon, Y.; Mul, G.; Koper, M. T. M. Palladium−gold Catalyst for the Electrochemical Reduction of CO2 to C1−C5 Hydrocarbons. *Chem. Commun.* **2016**, *52*, 10229−10232.

(373) Jovanov, Z. P.; Hansen, H. A.; Varela, A. S.; Malacrida, P.; Peterson, A. A.; Nørskov, J. K.; Stephens, I. E. L.; Chorkendorff, I. Opportunities and Challenges in the Electrocatalysis of CO2 and CO Reduction Using Bifunctional Surfaces: A Theoretical and Experimental Study of Au−Cd Alloys. *J. Catal.* **2016**, *343*, 215−231.

(374) Torelli, D. A.; Francis, S. A.; Crompton, J. C.; Javier, A.; Thompson, J. R.; Brunschwig, B. S.; Soriaga, M. P.; Lewis, N. S. Nickel-Gallium-Catalyzed Electrochemical Reduction of CO2 to Highly Reduced Products at Low Overpotentials. *ACS Catal.* **2016**, *6*, 2100−2104.

(375) Paris, A. R.; Bocarsly, A. B. Ni−Al Films on Glassy Carbon Electrodes Generate an Array of Oxygenated Organics from CO2. *ACS Catal.* **2017**, *7*, 6815−6820.

(376) Sun, K.; Cheng, T.; Wu, L.; Hu, Y.; Zhou, J.; Maclennan, A.; Jiang, Z.; Gao, Y.; Goddard, W. A.; Wang, Z. Ultrahigh Mass Activity for Carbon Dioxide Reduction Enabled by Gold−Iron Core−Shell Nanoparticles. *J. Am. Chem. Soc.* **2017**, *139*, 15608−15611.

(377) Hori, Y.; Murata, A.; Ito, S.; Yoshinami, Y.; Koga, O. Nickel and Iron Modified Copper Electrode for Electroreduction of CO2 by In-Situ Electrodeposition. *Chem. Lett.* **1989**, *18*, 1567−1570.

(378) Todoroki, N.; Yokota, N.; Nakahata, S.; Nakamura, H.; Wadayama, T. Electrochemical Reduction of CO2 on Ni- and Pt-Epitaxially Grown Cu(111) Surfaces. *Electrocatalysis* **2016**, *7*, 97−103.

(379) Zhao, X.; Luo, B.; Long, R.; Wang, C.; Xiong, Y. Composition-Dependent Activity of Cu−Pt Alloy Nanocubes for Electrocatalytic CO2 Reduction. *J. Mater. Chem. A* **2015**, *3*, 4134−4138.

(380) Guo, X.; Zhang, Y.; Deng, C.; Li, X.; Xue, Y.; Yan, Y.-M.; Sun, K. Composition Dependent Activity of Cu−Pt Nanocrystals for Electrochemical Reduction of CO2. *Chem. Commun.* **2015**, *51*, 1345−1348.

(381) Varela, A. S.; Schlaup, C.; Jovanov, Z. P.; Malacrida, P.; Horch, S.; Stephens, I. E. L.; Chorkendorff, I. CO2 Electroreduction on Well-Defined Bimetallic Surfaces: Cu Overlayers on Pt(111) and Pt(211). *J. Phys. Chem. C* **2013**, *117*, 20500−20508.

(382) Reske, R.; Duca, M.; Oezaslan, M.; Schouten, K. J. P.; Koper, M. T. M.; Strasser, P. Controlling Catalytic Selectivities during CO2 Electroreduction on Thin Cu Metal Overlayers. *J. Phys. Chem. Lett.* **2013**, *4*, 2410−2413.

(383) Watanabe, M.; Shibata, M.; Katoh, A. Design of Alloy Electrocatalysts for CO2 Reduction: Improved Energy Efficiency, Selectivity, and Reaction Rate for the CO2 Electroreduction on Cu Alloy Electrodes. *J. Electroanal. Chem. Interfacial Electrochem.* **1991**, *305*, 319−328.

(384) Watanabe, M. Design of Alloy Electrocatalysts for CO2 Reduction: III. The Selective and Reversible Reduction of CO2 on Cu Alloy Electrodes. *J. Electrochem. Soc.* **1991**, *138*, 3382−3389.

(385) Yoshitake, H.; Takahashi, K.; Ota, K. Electrochemical Reduction of CO2 on Hydrogen-Enriched and Hydrogen-Depleted Surfaces. *J. Chem. Soc., Faraday Trans.* **1994**, *90*, 155−159.

(386) Ohkawa, K.; Noguchi, Y.; Nakayama, S.; Hashimoto, K.; Fujishima, A. Electrochemical Reduction of Carbon Dioxide on Hydrogen-Storing Materials. Part II. Copper-Modified Palladium Electrode. *J. Electroanal. Chem.* **1993**, *348*, 459−464.

(387) Ohkawa, K.; Noguchi, Y.; Nakayama, S.; Hashimoto, K.; Fujishima, A. Electrochemical Reduction of Carbon Dioxide on Hydrogen-Storing Materials. Part 3. The Effect of the Absorption of Hydrogen on the Palladium Electrodes Modified with Copper. *J. Electroanal. Chem.* **1994**, *367*, 165−173.

(388) Chen, C. S.; Wan, J. H.; Yeo, B. S. Electrochemical Reduction of Carbon Dioxide to Ethane Using Nanostructured Cu2O-Derived Copper Catalyst and Palladium(II) Chloride. *J. Phys. Chem. C* **2015**, *119*, 26875−26882.

(389) Yin, Z.; Gao, D.; Yao, S.; Zhao, B.; Cai, F.; Lin, L.; Tang, P.; Zhai, P.; Wang, G.; Ma, D.; et al. Highly Selective Palladium-Copper Bimetallic Electrocatalysts for the Electrochemical Reduction of CO2 to CO. *Nano Energy* **2016**, *27*, 35−43.

(390) Li, M.; Wang, J. J.; Li, P.; Chang, K.; Li, C. L.; Wang, T.; Jiang, B.; Zhang, H. B.; Liu, H. M.; Yamauchi, Y.; et al. Mesoporous Palladium-Copper Bimetallic Electrodes for Selective Electrocatalytic Reduction of Aqueous CO2 to CO. *J. Mater. Chem. A* **2016**, *4*, 4776−4782.

(391) Rochefort, A.; Abon, M.; Delichère, P.; Bertolini, J. C. Alloying Effect on the Adsorption Properties of Pd50Cu50{111} Single Crystal Surface. *Surf. Sci.* **1993**, *294*, 43−52.

(392) Ma, S.; Sadakiyo, M.; Heima, M.; Luo, R.; Haasch, R. T.; Gold, J. I.; Yamauchi, M.; Kenis, P. J. A. Electroreduction of Carbon Dioxide to Hydrocarbons Using Bimetallic Cu-Pd Catalysts with Different Mixing Patterns. *J. Am. Chem. Soc.* **2017**, *139*, 47−50.

(393) Choi, J.; Kim, M.; Ahn, S. H.; Choi, I.; Jang, J. H.; Ham, Y. S.; Kim, J. J.; Kim, S. K. Electrochemical CO2 Reduction to CO on Dendritic Ag-Cu Electrocatalysts Prepared by Electrodeposition. *Chem. Eng. J.* **2016**, *299*, 37−44.

(394) Kyriacou, G.; Anagnostopoulos, A. Electrochemical Reduction of CO2 at Cu + Au Electrodes. *J. Electroanal. Chem.* **1992**, *328*, 233−243.

(395) Roy, C.; Galipaud, J.; Fréchette-Viens, L.; Garbarino, S.; Qiao, J.; Guay, D. CO2 Electroreduction at AuxCu1-x Obtained by Pulsed Laser Deposition in O2 atm. *Electrochim. Acta* **2017**, *246*, 115−122.

(396) Kim, D.; Resasco, J.; Yu, Y.; Asiri, A. M.; Yang, P. Synergistic Geometric and Electronic Effects for Electrochemical Reduction of Carbon Dioxide Using Gold-Copper Bimetallic Nanoparticles. *Nat. Commun.* **2014**, *5*, 4948.

(397) Kim, D.; Xie, C.; Becknell, N.; Yu, Y.; Karamad, M.; Chan, K.; Crumlin, E. J.; Nørskov, J. K.; Yang, P. Electrochemical Activation of CO2 through Atomic Ordering Transformations of AuCu Nanoparticles. *J. Am. Chem. Soc.* **2017**, *139*, 8329−8336.

(398) Jia, F.; Yu, X.; Zhang, L. Enhanced Selectivity for the Electrochemical Reduction of CO2 to Alcohols in Aqueous Solution with Nanostructured Cu-Au Alloy as Catalyst. *J. Power Sources* **2014**, *252*, 85−89.

(399) Morales-Guio, C. G.; Cave, E. R.; Nitopi, S. A.; Feaster, J. T.; Wang, L.; Kuhl, K. P.; Jackson, A.; Johnson, N. C.; Abram, D. N.; Hatsukade, T.; et al. Improved CO2 Reduction Activity towards C2+ Alcohols on a Tandem Au on Cu Electrocatalyst. *Nat. Catal.* **2018**, *1*, 764−771.

(400) Lum, Y.; Ager, J. W. Sequential Catalysis Controls Selectivity in Electrochemical CO2 Reduction on Cu. *Energy Environ. Sci.* **2018**, *11*, 2935−2944.

(401) Higgins, D.; Landers, A. T.; Ji, Y.; Nitopi, S.; Morales-Guio, C. G.; Wang, L.; Chan, K.; Hahn, C.; Jaramillo, T. F. Guiding Electrochemical Carbon Dioxide Reduction toward Carbonyls Using Copper Silver Thin Films with Interphase Miscibility. *ACS Energy Lett.* **2018**, *3*, 2947−2955.

(402) Wang, Y.; Wang, D.; Dares, C. J.; Marquard, S. L.; Sheridan, M. V.; Meyer, T. J. CO2 Reduction to Acetate in Mixtures of Ultrasmall (Cu)n,(Ag)m Bimetallic Nanoparticles. *Proc. Natl. Acad. Sci. U. S. A.* **2018**, *115*, 278−283.

(403) Monzó, J.; Malewski, Y.; Kortlever, R.; Vidal-Iglesias, F. J.; Solla-Gullón, J.; Koper, M. T. M.; Rodriguez, P. Enhanced Electrocatalytic Activity of Au@Cu Core@shell Nanoparticles towards CO2 Reduction. *J. Mater. Chem. A* **2015**, *3*, 23690−23698.

(404) Schlaup, C.; Horch, S.; Chorkendorff, I. On the Stability of Copper Overlayers on Au(111) and Au(100) Electrodes under Low Potential Conditions and in the Presence on CO and CO2. *Surf. Sci.* **2015**, *631*, 155−164.

(405) Friebel, D.; Mbuga, F.; Rajasekaran, S.; Miller, D. J.; Ogasawara, H.; Alonso-Mori, R.; Sokaras, D.; Nordlund, D.; Weng, T. C.; Nilsson, A. Structure, Redox Chemistry, and Interfacial Alloy Formation in Monolayer and Multilayer Cu/Au(111) Model Catalysts for CO2 Electroreduction. *J. Phys. Chem. C* **2014**, *118*, 7954−7961.

(406) Detweiler, Z. M.; White, J. L.; Bernasek, S. L.; Bocarsly, A. B. Anodized Indium Metal Electrodes for Enhanced Carbon Dioxide Reduction in Aqueous Electrolyte. *Langmuir* **2014**, *30*, 7593−7600.

(407) Li, Q.; Fu, J.; Zhu, W.; Chen, Z.; Shen, B.; Wu, L.; Xi, Z.; Wang, T.; Lu, G.; Zhu, J.; et al. Tuning Sn-Catalysis for Electrochemical Reduction of CO2 to CO via the Core/Shell Cu/SnO2 Structure. *J. Am. Chem. Soc.* **2017**, *139*, 4290−4293.

(408) Hoffman, Z. B.; Gray, T. S.; Moraveck, K. B.; Gunnoe, T. B.; Zangari, G. The Electrochemical Reduction of Carbon Dioxide to Syngas and Formate at Dendritic Copper-Indium Electrocatalysts. *ACS Catal.* **2017**, *7*, 5381−5390.

(409) Larrazábal, G. O.; Shinagawa, T.; Martín, A. J.; Pérez-Ramírez, J. Microfabricated Electrodes Unravel the Role of Interfaces in Multicomponent Copper-Based CO2 Reduction Catalysts. *Nat. Commun.* **2018**, *9*, 1477.

(410) Luo, W.; Xie, W.; Mutschler, R.; Oveisi, E.; De Gregorio, G. L.; Buonsanti, R.; Züttel, A. Selective and Stable Electroreduction of CO 2 to CO at the Copper/Indium Interface. *ACS Catal.* **2018**, *8*, 6571−6581.

(411) Zhao, Y.; Wang, C.; Wallace, G. G. Tin Nanoparticles Decorated Copper Oxide Nanowires for Selective Electrochemical Reduction of Aqueous CO2 to CO. *J. Mater. Chem. A* **2016**, *4*, 10710−10718.

(412) Sarfraz, S.; Garcia-Esparza, A. T.; Jedidi, A.; Cavallo, L.; Takanabe, K. Cu-Sn Bimetallic Catalyst for Selective Aqueous Electroreduction of CO2 to CO. *ACS Catal.* **2016**, *6*, 2842−2851.

(413) Rasul, S.; Anjum, D. H.; Jedidi, A.; Minenkov, Y.; Cavallo, L.; Takanabe, K. A Highly Selective Copper-Indium Bimetallic Electrocatalyst for the Electrochemical Reduction of Aqueous CO2 to CO. *Angew. Chem., Int. Ed.* **2015**, *54*, 2146−2150.

(414) Jedidi, A.; Rasul, S.; Masih, D.; Cavallo, L.; Takanabe, K. Generation of Cu−In Alloy Surfaces from CuInO 2 as Selective Catalytic Sites for CO 2 Electroreduction. *J. Mater. Chem. A* **2015**, *3*, 19085−19092.

(415) Larrazábal, G. O.; Martín, A. J.; Mitchell, S.; Hauert, R.; Pérez-Ramírez, J. Enhanced Reduction of CO2 to CO over Cu−In Electrocatalysts: Catalyst Evolution Is the Key. *ACS Catal.* **2016**, *6*, 6265−6274.

(416) He, J.; Dettelbach, K. E.; Salvatore, D. A.; Li, T.; Berlinguette, C. P. High-Throughput Synthesis of Mixed-Metal Electrocatalysts for CO 2 Reduction. *Angew. Chem., Int. Ed.* **2017**, *56*, 6068−6072.

(417) Xie, H.; Chen, S.; Ma, F.; Liang, J.; Miao, Z.; Wang, T.; Wang, H.-L.; Huang, Y.; Li, Q. Boosting Tunable Syngas Formation via Electrochemical CO2 Reduction on Cu/In2O3 Core/Shell Nanoparticles. *ACS Appl. Mater. Interfaces* **2018**, *10*, 36996−37004.

(418) Zeng, J.; Bejtka, K.; Ju, W.; Castellino, M.; Chiodoni, A.; Sacco, A.; Farkhondehfal, M. A.; Hernández, S.; Rentsch, D.; Battaglia, C.; et al. Advanced Cu-Sn Foam for Selectively Converting CO2 to CO in Aqueous Solution. *Appl. Catal., B* **2018**, *236*, 475−482.

(419) Lv, W.; Zhou, J.; Kong, F.; Fang, H.; Wang, W. Porous Tin-Based Film Deposited on Copper Foil for Electrochemical Reduction of Carbon Dioxide to Formate. *Int. J. Hydrogen Energy* **2016**, *41*, 1585−1591.

(420) Wang, Y.; Zhou, J.; Lv, W.; Fang, H.; Wang, W. Electrochemical Reduction of CO2 to Formate Catalyzed by Electroplated Tin Coating on Copper Foam. *Appl. Surf. Sci.* **2016**, *362*, 394−398.

(421) Hori, Y.; Murata, A.; Kikuchi, K.; Suzuki, S. Electrochemical Reduction of Carbon Dioxides to Carbon Monoxide at a Gold Electrode in Aqueous Potassium Hydrogen Carbonate. *J. Chem. Soc., Chem. Commun.* **1987**, *0*, 728.

(422) Chen, Y.; Li, C. W.; Kanan, M. W. Aqueous CO2 Reduction at Very Low Overpotential on Oxide-Derived Au Nanoparticles. *J. Am. Chem. Soc.* **2012**, *134*, 19969−19972.

(423) Soriaga, M. P.; Baricuatro, J. H.; Javier, A. C.; Kim, Y.-G.; Cummins, K. D.; Tsang, C. F.; Hemminger, J. C.; Bui, N. N.; Stickney, J. L. *Electrochemical Surface Science of CO2 Reduction at Well-Defined Cu Electrodes: Surface Characterization by Emersion, Ex Situ, In , In Situ, and Operando Methods*; Elsevier Inc., 2017.

(424) Ulissi, Z. W.; Tang, M. T.; Xiao, J.; Liu, X.; Torelli, D. A.; Karamad, M.; Cummins, K.; Hahn, C.; Lewis, N. S.; Jaramillo, T. F.; et al. Machine-Learning Methods Enable Exhaustive Searches for Active Bimetallic Facets and Reveal New Active Site Motifs for CO2 Reduction. *ACS Catal.* **2017**, *7*, 6600−6608.

(425) Tran, K.; Ulissi, Z. W. Active Learning across Intermetallics to Guide Discovery of Electrocatalysts for CO2 Reduction and H2 Evolution. *Nat. Catal.* **2018**, *1*, 696−703.

(426) Ma, X.; Li, Z.; Achenie, L. E. K.; Xin, H. Machine-Learning-Augmented Chemisorption Model for CO2 Electroreduction Catalyst Screening. *J. Phys. Chem. Lett.* **2015**, *6*, 3528−3533.

(427) Endrődi, B.; Bencsik, G.; Darvas, F.; Jones, R.; Rajeshwar, K.; Janáky, C. Continuous-Flow Electroreduction of Carbon Dioxide. *Prog. Energy Combust. Sci.* **2017**, *62*, 133−154.

(428) Greenblatt, J. B.; Miller, D. J.; Ager, J. W.; Houle, F. A.; Sharp, I. D. The Technical and Energetic Challenges of Separating (Photo)Electrochemical Carbon Dioxide Reduction Products. *Joule* **2018**, *2*, 381−420.

(429) Duan, X.; Xu, J.; Wei, Z.; Ma, J.; Guo, S.; Wang, S.; Liu, H.; Dou, S. Metal-Free Carbon Materials for CO2 Electrochemical Reduction. *Adv. Mater.* **2017**, *29*, 1701784.